Sudan University of Science and Technology

Collage of Engineering

Aeronautical Department

DESIGN & BUILD OF UAV WITH CO-AXIAL PROPELLER

Submitted to the Department of Aeronautical Engineering in partial fulfillment of the requirements for the degree of Bachelor of Science in Aeronautical Engineering

Prepared by:

AHMED HAMD-ALNEEL MADNI SULIMAN

AHMED HASSAN AL-NOOR MOHAMMED

ABDULLAHI AL-ALAMEN EHAMER ALI

MOAWIA ALTOM ISMAEL MOHAMMRD

MOHAMMED MAHMOUD OSMAN AHMED

MOSAB MOHAMMED ALI OMER ALMOBARK

Supervised by:

MR.ABD-ALSAMEE

D.INTSAR ABD-ALFTAH

PROF.ALI ALHASEEN

August, 2014

الآيـــة

قال تعالى :

وَأَعِدُّوا۟ لَهُم مَّا ٱسْتَطَعْتُم مِّن قُوَّةٍ وَمِن رِّبَاطِ ٱلْخَيْلِ
تُرْهِبُونَ بِهِۦ عَدُوَّ ٱللَّهِ وَعَدُوَّكُمْ وَءَاخَرِينَ مِن دُونِهِمْ
لَا تَعْلَمُونَهُمُ ٱللَّهُ يَعْلَمُهُمْ ۚ وَمَا تُنفِقُوا۟ مِن شَىْءٍ فِى سَبِيلِ
ٱللَّهِ يُوَفَّ إِلَيْكُمْ وَأَنتُمْ لَا تُظْلَمُونَ ﴿٦٠﴾

سورة الأنفال

الإهداء

إلى من تعجز الكلمات عن شكرهن.... إلى من ساندننا بالإرشاد والدعاء....!

إلى أمهاتنا العزيزات

إلى من بذلوا لنا أزمانهم الغالية و لم يبخلوا علينا بالعلم...!

إلى معلمينا الأعزاء

إلى كل من وقفوا معنا وقدموا لنا من علمهم أو بأي شكل من أشكال الإسناد.. وكانوا دافعا وحافزا لتقديم الأفضل دوما.......!

نهدى لهم هذا الجهد المتواضع

Dedication

First of all, thanks to ALLAH for all good things that he had done and giving us prescience in our Project

This project is dedicated to the country of our fathers, to the Islam best life religion, to all the humanity and mankind..............

We as Islamic and Arabic nations we suffered the terror and injustice of the other world great nations, but now it is our time to be strong, now it is our time

To be free ……..

شكر وعرفان

ها قد انطوت عنا صفحة مليئة بإشراقات وإسهامات كانت لنا ذخراً ومعينا نستقي منه مجمع الإرشاد والسداد في فيها لواء أمانة كريمة كثر مبتدإ لرحلة طويلة رافعين طلابها واشتكى حاملوها،سائلين الله سبحانه أن يوزعنا على شكره وتحقيق رضوانه. إلى من كانوا لنا سندا ومنعة على أيام مقبلة أضاء الله بهم طريق المعرفة وسخرهم للمنفعة، إلى كل من قاسى حمل الأمانة فصار كلامه لِجَامَهُ ومُلْزِمَ وفائه، إلى من تناسى الأماني ورفع القيم والمعاني، إلى شاحذي الهمم وترجمان العلم الأساتذة والمربين

د.إنتصار عبد الفتاح

أ.عبد السميع

بروف.علي الحسين

إلى الجيل الواعد والموعود بإذن الله بالنجاح والتوفيق، من كان لهم السبق بالعطاء والوفاء فأصدقوا النوايا وكللوا العزائم بطيب الختام، أخواننا ومعلمونا

والشكر موصول إلى مركز أبحاث الطيران متمثلا في:

أ.عبد المنعم بشرى   **أ.محمد مهدي**

إلى صاحب الفعال قبل الأقوال المقبل بالنوال قبل السؤال

د. صخر بابكر

Acknowledgment

It is a pleasure to thank those who have contributed to the realization of this dissertation:

To our families who built us up to face this life…….

To our friends who supported us………

To our teachers who armed us with knowledgement……

To this great university……….

To the best department ever……..

Abstract:

The UAV had been designed in order to meet the specifications required for surveillance and reconnaissance mission. It followed the global UAV designs in this industry where the pusher configuration is dominating over the various other conventional probabilities. A project was undertaken to study & design Co-axial propeller for Small unmanned aerial vehicle UAV .the study started from the comparison between three practical steps ; single propeller , single propeller with forward or rearward cascade & Co-axial propeller. The choice appeared to select a cascade propeller engine to obtain best criteria with less cost. The design had to be compatible with the propeller design work being done concurrently. Of particular interest was comparing the resulting thrust to propel the UAV at a given airspeed.

The entire propeller design process from airfoil selection to final part generation in computer-aided drafting program is mentioned. The Clark-y airfoil defined the propeller cross section.

Design of propeller blades and mechanism to compare the output thrust between them and determine power that required rotating propeller. Modification of the mechanism and the manufacture of propeller from the prototype to the final model will be experimented and discussed throughout the project.

Static and dynamic analysis for a stability model using the digital DATCOM had shown UAV is stable statically and dynamically, and a Simulink model was developed to verify the dynamic modes. A structural analysis was further initiated to assess the loads acting on individual components and whether they can sustain the loads or not.

List of Contents:

Abbreviation:

SUAV	Small unmanned aerial vehicles
WWII	The Second World War
CCRP	Co-axial contra rotating propeller
ISTAR	intelligence ,surveillance and reconnaissance operations
MAV	Micro Air Vehicles
AAA	advance aircraft analysis
DATCOM	Data compendium
CG	Center of Gravity
DCM	Direction Cosine Matrix

List of Tables:

List of Figures:

List of Symbols:

C_D	Drag coefficient of blade section
C_L	Lift coefficient of blade section
C	Blade chord
n	Propeller RPM
B	number of blades
D	propeller diameter
P	power consumed by propeller
C_P	Power coefficient
Q	torque
T	thrust
C_T	Thrust coefficient
V_∞	Free stream velocity
W	local total velocity
α	Angle of attack
β	Blade twist
ρ	Air density
A	propeller disk area
ω	Propeller angular velocity
V_1	Velocity at the outlet of the actuator disk

P_1	Pressure at the inlet of the actuator disk
P_2	Pressure at the outlet of the actuator disk
V_3	Velocity at the outlet of the pipe
V_0	Velocity at the inlet of the pipe
P_o	Atmosphericpressure at the inlet of the pipe
A_o	Area of the inlet of the pipe
A_1	Area of the actuator disk
A_3	Area of the outlet of the pipe
R	Propeller radius
a	Speed of sound
M	$Mach\ number$
a, b	Inflowfactors
λ_r	Veolocity fraction
θ	Flow angle
ΔT	Element thrust
ΔQ	Element torque
C_T	Non − dimensional thrust coefficient
C_Q	Non-dimensional torque coefficient
J	Advance ratio
AF	activity factor

η_{prop} The efficiency of the propeller

AR Aspect Ratio

b Wing Span

B Input Matrix

$\bar{c}$ Mean Aerodynamics Chord

C_M Pitching Moment coefficient

C_N Yawing Moment coefficient

C_l Rolling Moment coefficient

C_L Lift coefficient

C_D Drag coefficient

C_y Side force coefficient

C_{tip}, C_r $root$ Tip and root chords

$C_{L_{\alpha_v}}$ Vertical tails lift curve slope

F_y Body axes aerodynamic force in Y directions

F_x Body axes aerodynamic force in x directions

F_z Body axes aerodynamic force in z directions

H Angular Momentum Vector

H_x, H_y&H_z Angular Momentum x, y, z components

I Inertia tensor

I_{xx},$I_{yy}I_{zz}$ Moment of inertia about x-axis, y-axis, z-axis

I_{xz},$I_{yy}I_{zz}$ Products of inertia

l_t Tail arm

l_v Vertical tail arm

L	Roll moment, Lift Force
N	yaw moment
M	Pitch moment
m	Mass
p	Linear momentum
p	Roll Rate
q	Dynamic pressure or pitch Rate
r	Yaw Rate
S	Reference area, Wing plan area
S_T	Tail area
T	Thrust
Ti	Period
u, u_0	Velocity in X axes, Control input vector
v	Velocity in Y axis
V	Velocity vector
V	Airspeed
V_H	Horizontal tail volume Ratio
w	Velocity in Z axis's
$\boldsymbol{x}$	State vector

Greek letters

α Angle of attack

β Side slip angle (deg)

δ_a Aileron deflection

δ_r Elevator deflection

δ_e Rudder deflection

Φ, φ Roll attitude

Θ, θ Pitch attitude

Ψ, ψ Yaw attitude

λ Taper Ratio, eigenvalue

η Tail Efficiency

ρ Air density

ζ_i Damping ratio

Chapter 1 :

INTRODUCTION & LITRITUREREVIEW

1.2PROBLEM STATEMENT:

Previous UAVs had used conventional propellers which make UAVs suffer from lack of aerodynamics efficiency, caused by the trailing slipstream that creates an opposing torque on the fuselage while rotating. This phenomena has a raised multiple issues such as the extra drag on fuselage, resulting in a lower thrust & reducing stability. The thrust –to-weight ratio in co-axial propeller is much higher than conventional propellers. Other than that, asymmetric effect on propellers can be avoided.

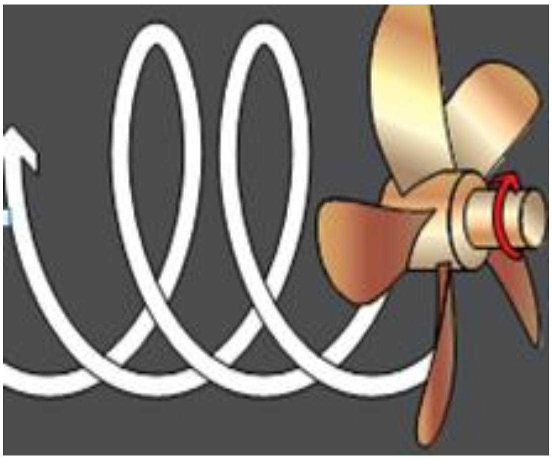

Conventional propulsion

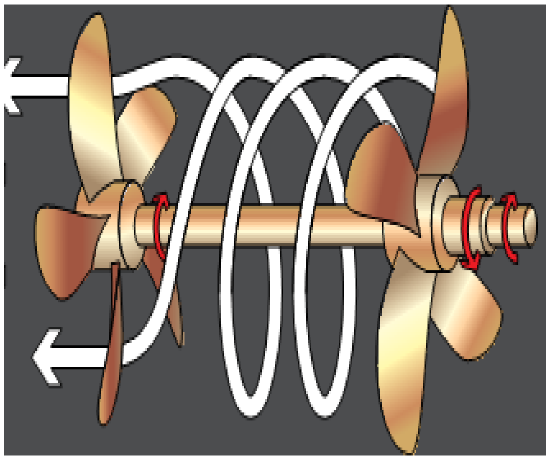

Co-axial propulsion

Figure 1--1: Conventional & coaxial propulsion

1.3PROPOSED SOLUTION:

After extensive research, it's found that the major development can be implement here is use of cascade scheme or co-axial propeller rather than conventional one. Recent research shows that the use of co-axial propeller increase propulsive efficiency as high as 19%.other important advantages is the enhancement of aerodynamic efficiency.

- Design and analysis of cascade & co-axial propeller.
- Maximize aerodynamic efficiency by:

1- Wing lets 2- Landing gear fearing

1.4OBJECTIVES:

The project objectives were specified by the project group very early in the project. These consisted of both primary and extended project goals

- **PRIMARY OBJECTIVES:**

1. Design UAV with level one flying qualities.

2. Developing dynamic model using SIMULINK.

3. Testing of the three schemes of engine (single propeller, single propeller with rearward cascade, coaxial propeller).

- **EXTENDED OBJECTIVES:**

1. Encourage continued undergraduate and postgraduate development of UAVs at the University of Sudan.

2. Development of a surveillance system for a UAV which can stream to a ground based station and allow for autonomous search and identification of ground based targets.

1.5METHODOLOGY:

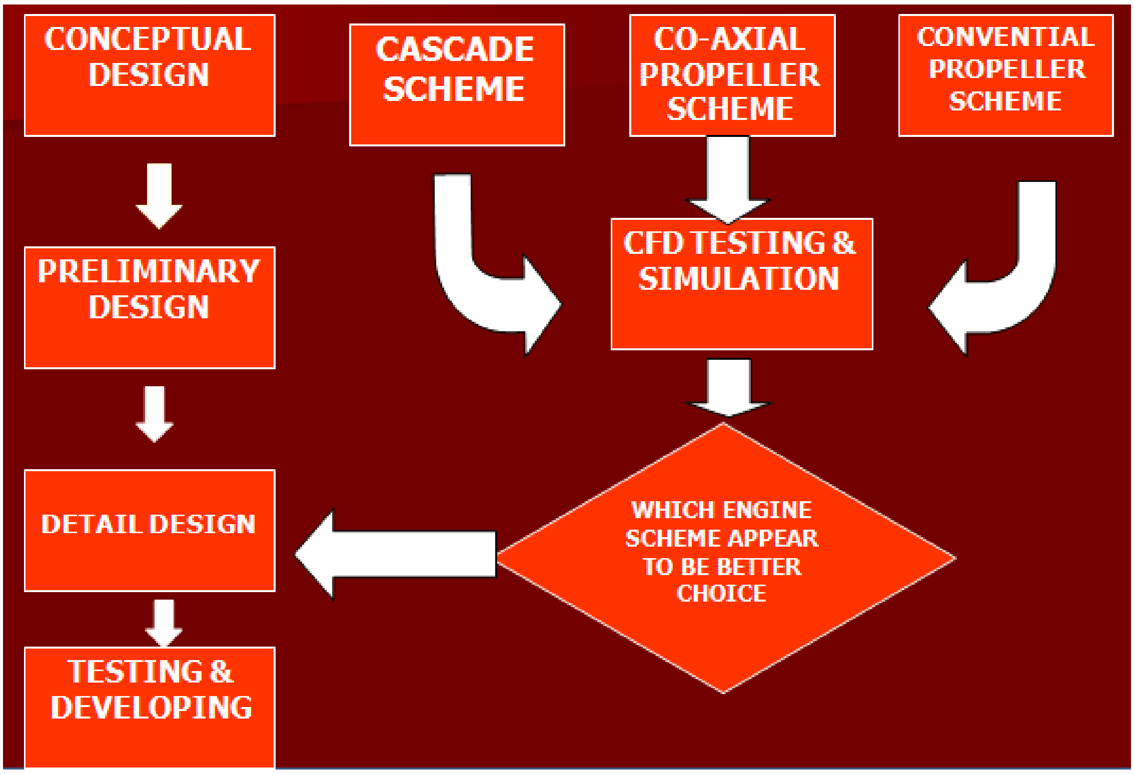

Figure 1-2: methodology

The Gantt chart:

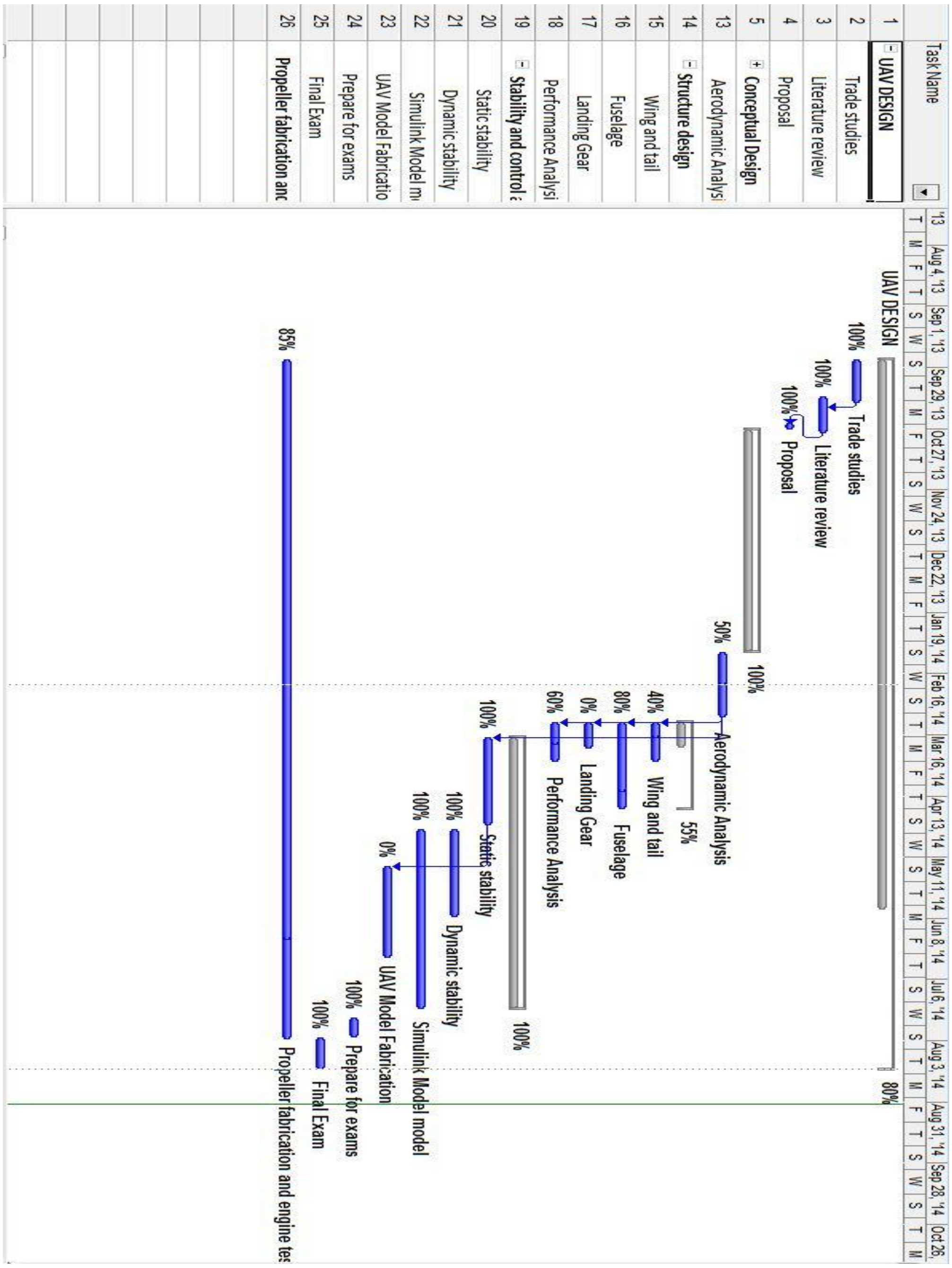

Figure 1-3: Gantt chart

Outlines:

Chapter one includes: introduction, problem statement, proposed solution, objectives, methodology, literature review and feasibility study.

Chapter two include: conceptual design, requirements, weight of the UAV and its first estimate, *estimation* of the critical performance parameters, fuselage configuration, propeller size, landing gear & wing placement, better weight estimate.

Chapter three include preliminary design (aerodynamic , performance and structure analysis)

aerodynamic analyzed by use digital DATCOM aerodynamic program. performance analyses by matlab code programs to calculate wing loading, power loading, rate of climb and climb velocity, time to climb, rang, endurance, take-off distance, landing distance.

structural design include two designs, fuselage design & wing design

Chapter four include stability analysis: static stability, longitudinal static stability, directional static stability, lateral static stability, dynamic stability (modes of vibration), longitudinal modes (steady modes of vibration), flying qualities, longitudinal flying qualities, lateral directional flying qualities, tools to estimate stability derivatives.

Chapter five include mathmatical modeling of uav dynamics, it gives an introduction to aircraft modeling.

Chapter six include UAV dynamics modeling, nonlinear model, aerodynamic model using Matlab simulink.

Chapter seven present propeller design, cascade design, stage with downstream guide vanes, co-axial propeller design, practical calculations.

Chapter eight shows a fabrication of propeller and the experimental that done to the propeller.

Chapter nine shows the results & discussion of all project calculations.

Chapter ten shows the conclusions & recommendations

1.6Literature Review and Feasibility Study:

The following literature review is a brief summary of the extensive investigation into Unmanned Aerial Vehicle technology that was conducted at the beginning of the project. This section has been divided into literature on aircraft design, propulsion systems.

1.6.1Statistical Analysis:

A statistical analysis method was utilized by the project group to design the vehicle. This method was as suggested by both RAYMER and ROSKAM[2, 3].The statistical analysis method involves investigating the performance and designs of existing vehicles and using the information from these designs to construct a baseline design of the vehicle, which can then be optimized for the required technical task. The statistics used for this method were those collected as a result of the market evaluation.

1.6.2Analyzed UAVs:

A number of commercial UAV platforms were analyzed for their design parameters. These included UAVS up to and including 100 kg in takeoff weight, UAVS with both electric internal combustion systems and with an endurance of at least 2hrs.

AEROSKY:

Summary of Design Requirements:

Altitude:

The operational altitude is to be 3km.whiche is a balance between image clarity and covered area.

Cruise Speed:

As a result from literature cruise speed of 47m/s seems reasonable. While the main constraint of the cruise speed is performance of the camera, the cruise speed may be revised after the design of imaging system and selection of the camera.

Takeoff and Landing:

Is the length of the field required for takeoff and landing For this aircraft the maximum takeoff field length was 150m, which was deemed to be short enough to maintain application flexibility and long enough to reduce power requirements. The landing distance should be no more than 250m.

Endurance:

The UAV's minimum endurance will be 4 hour of continuous flight in accordance with the maximum mission time from literature survey result.

Propulsion system:

Contra-rotating propellers have been studied for over 60 years as a more fuel efficient method of aircraft propulsion. A CRP consists of 2 sets of propeller blades, one directly behind the other in the axial direction, spinning in opposite directions. Counter-rotating propellers spin in opposite directions.[4]

The fundamental premise behind CRPs is the elimination of the tangential velocity, which is considered to be a loss in performance and efficiency. Contra-rotating propellers can significantly reduce or even eliminate the tangential velocity of the propelled air, or swirl losses, and also the torque produced by the engine. This leads to a more efficient and economical engine and less torsional loading on the wings. [4]

There has been renewed interest in finding a more efficient replacement for current Aircraft propulsion systems, with one such approach utilizing a counter-rotating propeller Configuration. An initial theory regarding the mechanics of counter-rotating propellers was developed by Locks in 1941 Since then, many investigations into the advantages of Counter-rotating propellers have been conducted. For example, Bergmann and Gray conducted full scale wind tunnel tests on counter-rotating propellers in both tractor and pusher configurations. It was found that an 8 to 16% increase in propeller efficiency could be gained depending upon installation position. In a later test, Bergmann and Hartman found that the performance of counter-rotating propellers was significantly improved at lower advance ratios. McHugh and Pepper have shown that the counter-rotating propeller configuration is highly receptive to the use of aerodynamically improved airfoil designs. Other investigations into the performance of counter-rotating propellers conducted by Gray have indicated that the overall efficiency o f a counter-rotating propeller is not seriously affected by changes in rotational speed

Small changes in blade angle of the aft propeller disk. These changes did, however, have moderate effect when the propeller was operated at peak efficiency. In an experimental study, Mille found that the vibration of counter-rotating propellers caused by mutual blade passage or by blade passage through the wake o f a wing was not significant. Bartlett has shown that locking or wind milling one of the propeller components o f a counter-rotating configuration has a detrimental effect on total propeller efficiency. For example, a counter rotating propeller with one propeller disk disabled results in a total propeller efficiency that is lower than the individual efficiency of the rotating propeller.[5]

The increase in peak efficiency and improved off-design performance of counter-rotating systems allow for smaller propulsion units to be installed on the aircraft. The disadvantages Of counter-rotating propeller configurations include gearbox Complexity and an increased vibration state caused by the periodic blade passage. Research conducted by Strake. al. has shown that with current improvements of present day technology, lightweight and reliable counter-rotating propeller gearboxes can be built. Thus, it is evident that counter- rotating propellers can indeed offer a more efficient means of propulsion.[5]

This brief literature survey has indicated that counter-rotating propellers exhibit many advantages over single rotation propellers such as higher peak efficiency, better off- design performance, and a reduced total torque of the system.[5]

Design Development:

The main advantage of counter-rotating propellers stems from the swirl velocity losses of the front propeller disk being recovered by the aft propeller disk. The front disk imparts a tangential velocity to the air as it passes through the front propeller disk plane. This swirl velocity acts as an additional angular velocity for the aft disk, without the power plant having to drive the aft disk at a higher angular velocity. It may be noted that a tangential interference velocity is recognized by the front disk, but is typically an order-of-magnitude smaller than other interference velocities and therefore neglected, resulting in a first-order theory for the design and analysis of counter-rotating propellers. Airfoil data , such as lift, drag, and angle of attack are specified for each radial location along the propeller blade. This is done through the use of airfoil data banks, utilizing either tabulated data or empirical formulations that yield airfoil lift and drag as functions of angle of attack and Mach number.

The airfoil data used in the calculations during the design process was selected to maximize the lift-to-drag ratio of the airfoil used at each radial location along the blade. In regions near the hub, where the propeller blade quickly transitions from an airfoil to a right circular cylinder, a different approach has been taken. To accommodate this transition, the chord length is linearly interpolated from that calculated to a structurally feasible cylinder at the hub. The design procedure involves calculations, which include division by the lift coefficient, to determine chord length. Since the lift coefficient of a circular cylinder is zero, it may be noted in the development of the theoretical model that it is necessary to maintain a finite- lift coefficient to insure arriving at positive values of the blade chord. [5]

Co-axial contra rotating propeller (CCRP) systems promise a light weight, fuel efficient means for propulsion for the aerospace industry. The only drawback is its high level aerodynamic noise.[6]

The research is study about flow around propeller to increase endurance and thrust by increase the efficiency. The study is decomposing to tasks that’s CFD task, experimental task. The study is a compare between single propeller alone, single propeller with rearward cascade & dual acting propeller (CO-AXIAL PROPELLER).

Chapter 2 :
CONCEPTUAL DESIGN

2.2Weight of the UAV and its first estimate[2]:

There are various ways to categorize the weight of the UAV. The following is a common choice:

1- Payload weight $W_{payload}$: the payload is what the UAV intended to transport (camera & sensors for our case). If the UAV is intended for military combat use, the payload may include missiles, bombs or other disposable weapons.
2- Fuel weight W_{fuel}: this is the weight of the fuel in the fuel tanks. Since fuel is consumed during the course of the flight, W_{fuel} is variable, decreasing with time during the flight.
3- Empty weight W_{empty}: this is the weight of every else (the structure, engines with all accessory equipment, electronic equipment, landing gears, fixed equipment and anything else that is not payload or fuel).

The sum of these weights is the total weight of the UAV (W_{total}). Again W_{total} is varying throughout the flight because fuel is being consumed. The design take-off weight is the gross weight of the UAV at the instance it begins its mission. It includes the weight of all the fuel on board at the beginning of the flight. Hence:

$$W_0 = W_p + W_f + W_e \qquad (2\text{-}1)$$

W_f: is the fuel weight at the beginning of the flight.

W_0: is the first estimate of the total weight of the UAV. To make this estimate, equation (2-1) must be rearranged as follows:

$$W_0 = W_p + W_f + W_e \qquad (2\text{-}2)$$

$$W_0 = W_p + W_f * \frac{W_0}{W_0} + W_e * \frac{W_0}{W_0} \text{ .... (2-3)}$$

Solving equation (2-3) for W_0:

$$W_O = \frac{W_P}{1 - \frac{W_f}{W_O} - \frac{W_e}{W_O}} \text{ .... (2-4)}$$

Although at this stage, we do not have a value ofW_0, we can fairly readily obtain values of ratios of $\frac{W_f}{W_O}$ and $\frac{W_e}{W_O}$ as it can see next. Then equation (2-4) provides a relation from which W_0 can be obtained in an iterative fashion.

Estimation of the value$\frac{W_e}{W_O}$:

A new design is usually an evolutionary change of an existing design. For this reason, historical, statistical data on previous UAVs provide a starting point for the conceptual design of new UAV. In particular, fig () is a plot of $\frac{W_e}{W_O}$ versus W_e for a number of similar UAVs.

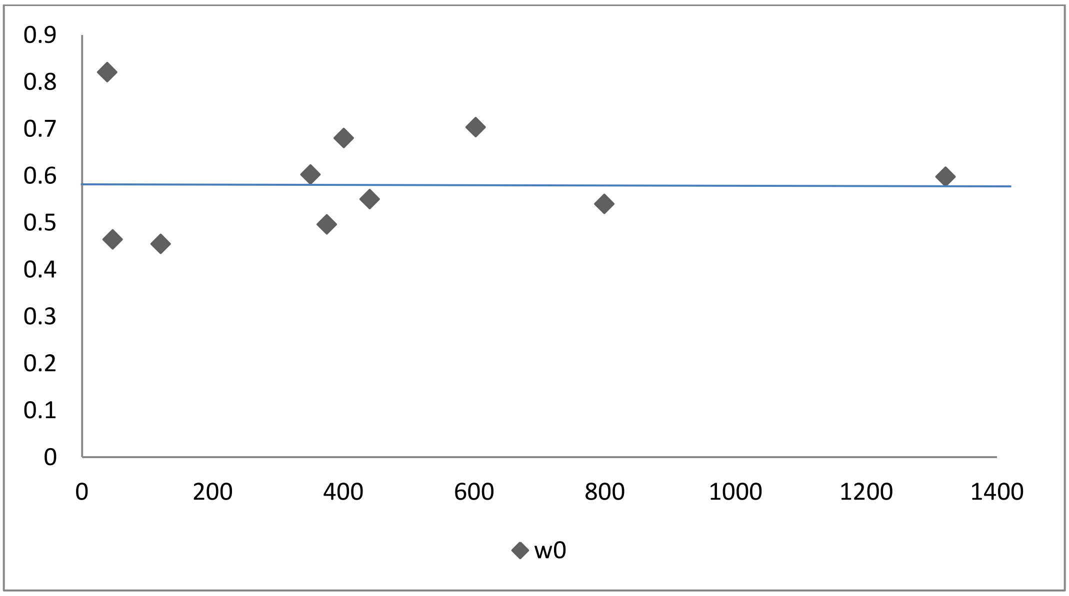

Figure 2-1: empty weight fraction

That's to say, $\frac{W_e}{W_O} = 0.58$

Estimation of $\frac{\mathbf{W_f}}{\mathbf{W_0}}$:

The amount of fuel required to carry out the mission depends critically on the efficiency of the propulsive device (the engine specific fuel consumption & the efficiency of the propellers). It also depends critically on the aerodynamic efficiency (the lift to drag ratio). These factors are the principal player-s at the Brequet range equation given below:

$$R = \frac{\eta}{C} . \frac{L}{D} . \ln \frac{w_0}{w_1} \qquad (2\text{-}5)$$

The total fuel consumed during the mission is that consumed from the moment the engine is turned on to the moment they are shut down at the end of the flight. Between these times, the flight of the UAV can be described by a mission profile, a conceptual sketch of altitude versus time such as the one shown in fig(2-2). As stated in the specifications, the mission of our UAV is that of a recognizance & surveillance type, because of that the mission profile for a simple cruise with loitering at the required location had been selected. It starts at the point labeled 0 when the engine is turned on. The take-off segment is denoted by the segment 0-1, which includes taxing & take-off. Segment 1-2 denotes the climb to cruise altitude (the use of straight line here is only schematic & is not meant to imply a constant rate of climb to altitude). Segment 2-3 & segment 4-5 denote the cruise condition with loiter time at segment 3-4 to fulfill the mission requirements. Segment 5-6 denotes descent. Segment 6-7 represents landing. The mission profile is shown below:

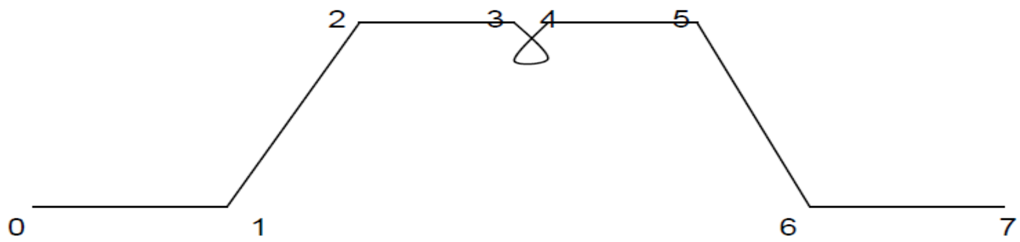

Figure 1-2: mission profile

Each segment of the mission is associated with a weight fraction, defined as the UAV weight at the end of the segment divided by the weight at the beginning of the segment. Hence, the first thing for calculating $\frac{W_f}{W_O}$ is to define the weight fractions of the mission.

Historical data show that weight fractions of take-off, climb, descent & landing respectively as follow:

$$\frac{W_1}{W_0} = 0.97\,, \frac{W_2}{W_1} = 0.985$$

$$\frac{W_6}{W_5} = 0.998\,, \quad \frac{W_7}{W_6} = 0.995$$

For segments 2-3 & 4-5, Brequet range equation had been used. This requires the estimate of $\frac{L}{D}$. At this stage of design, we cannot carryout a detailed aerodynamic analysis to predict $\frac{L}{D}$, we have not even laid out the shape of the UAV yet. Therefore, we can only make a crude approximation based on the data from the previous UAVs. Hence, a reasonable first approximation for our UAV:

$$\frac{L}{D} = 13.5$$

Also, we need in the range equation the specific fuel consumption c & the propeller efficiency η. A typical value of specific fuel consumption for current UAV reciprocating engines is 0.52 lb of fuel consumed per horsepower per hour:

$$c = 0.52 \frac{lb}{hp.h} = 2.63 * 10^{-7} \frac{lb}{ft.lb/s}$$

A reasonable value for the propeller efficiency η for coaxial propellers engine is 0.8:

$$\eta_{pr} = 0.8$$

From Brequet equation, the ratio $\frac{w_0}{w_1}$ is replaced for the mission segment 2-3 by $\frac{w_2}{w_3}$. Hence, eq become:

$$R = \frac{\eta}{C} . \frac{L}{D} . \ln \frac{w_2}{w_3} \qquad (2\text{-}6)$$

$$\ln \frac{w_2}{w_3} = \frac{c}{\eta} . \frac{R}{L/D}$$

$$\frac{w_2}{w_3} = e^{R.C/\eta.\frac{L}{D}} \qquad (2\text{-}7)$$

$$\frac{W_2}{W_3} = e^{\frac{328085*2.63*10^{-7}}{0.8*13.5}} = 1.00801$$

$$\therefore \frac{W_3}{W_2} = 0.99205$$

For cruise, $\frac{W3}{W2} = \frac{W5}{W4} = 0.99205$

3-4 is a loiter flight where:

Endurance=2h;

V_{loiter}= 115.65ft/sec (assumed roughly as (0.75).V_{cr} Based on competitor study)

Propeller Efficiency (η_p)=0.7 (a lower efficiency compared to cruise is used)

(C_{bhp})=$2.63 * 10^{-7}\,\frac{\text{lb}}{\text{ft.lb/s}}$(same as the cruise SFC)

$$\frac{L}{D_{\text{loiter}}} = (0.866).\left(\frac{L}{D}\right) = 11.691$$

$$\frac{W_3}{W_4} = e^{\frac{E.C.Vloiter}{\eta .L/D}} = e^{\frac{7200*2.63*10^{-7}*115.65}{0.8*11.621}} = 1.02366$$

$$\frac{W_4}{W_3} = 0.97689$$

Collecting the various segment weight fractions & getting the product of them to obtain the ratio of the weight at the end of the mission to the initial gross weight:

$$\frac{W_7}{W_0} = \frac{W_1}{W_0} * \frac{W_2}{W_1} * \frac{W_3}{W_2} * \frac{W_4}{W_3} * \frac{W_5}{W_4} * \frac{W_6}{W_5} * \frac{W_7}{W_6} = 0.93375$$

The change in weight is due to the consumption of fuel. If at the end of the flight, the fuel tanks were completely empty, then:

$$W_f = W_0 - W_7$$

$$\frac{W_f}{W_0} = 1 - \frac{W_7}{W_0} \quad \text{(2-8)}$$

However, at the end of the mission, fuel tanks are not completely empty by design. There should be some fuel left in reserve at the end of the mission in case weather conditions or spend a longer than normal time in loiter condition. Also, the geometric design of the fuel tanks & fuel system leads to some trapped fuel that is unavailable at the end of the flight. Typically, 6% allowance is made for reserve and trapped fuel. Modifying previous equation for this allowance, we have:

$$\frac{W_f}{W_0} = 1.06\left(1 - \frac{W_7}{W_0}\right)$$

$$\frac{W_f}{W_O} = 1.06 * \left(1 - \frac{W_0}{W_7}\right) = 1.06 * (1 - 0.93375) = 0.07022$$

Calculation of $\mathbf{W_0}$:

We obtain the values of the ratios $\frac{W_f}{W_0}$&$\frac{W_e}{W_O}$ which are required to obtain the initial design take-off weightW_0. Since our UAV is for recognizance & surveillance, the payload here is a camera in order to survey a prescribed location. The total weight of the payload is 33.1 lbs. inserting the values above into the equation of W_0:

$$W_O = \frac{W_P}{1 - \frac{W_f}{W_O} - \frac{W_e}{W_O}} = \frac{33.07}{1 - 0.07022 - 0.58} = 94.6315\ lb$$

This is our first estimate of the gross weight of the UAV.

Finally, the weight of the fuel in tanks is calculated. This will become important later in sizing the fuel tanks.

$$\frac{W_f}{W_O} = 0.07022$$

Hence:

$$W_f = \frac{W_f}{W_O}.W_O = 0.07022 * 94.6315 = 6.64522 \text{ lb}$$

2.3*Estimation* of the critical performance parameters:

Estimation for the critical performance parameters[2] is needed to determine such aspects as maximum speed, range, ceiling, rate of climb, stalling speed, landing distance & take-off distance. These parameters namely are$(C_L)_{max}$, $L/_D$, $W/_S$ and $T/_W$.

Constrain diagram:

The wing loading and power loading are calculated depending upon design requirements[7]. These requirements are as follows:

Stall speed:

The minimum speed that an aircraft can fly

$$\left(\frac{W}{S}\right)_{V_S} = \frac{1}{2}\rho {V_S}^2 S C_{L_{max}}$$

Maximum speed:

The power loading (W/P) is a non-linear function of the wing loading (W/S) in terms of maximum speed, and may be simplified as:

$$\left(\frac{W}{p}\right) = \frac{\eta_p}{\frac{aV_{max}{}^3}{\left(\frac{W}{S}\right) + \frac{b}{V_{max}}\left(\frac{W}{S}\right)}}$$

$a = \frac{\rho_0 C_{D_0}}{2}$, $b = \frac{2K}{\rho\sigma}$&$\sigma = \frac{\rho_{altitude}}{\rho}$

Take-off distance:

The take-off distance is in the variation of W/Pas a function of W/S based on STO for a prop-driven aircraft can be sketched using Equation ()

$$\left(\frac{W}{P}\right)_{S_{TO}} = \frac{1 - exp\left(0.6\rho g C_{D_G} S_{TO} \frac{1}{W/S}\right)}{\mu - \left(\mu + \frac{C_{D_G}}{C_{L_R}}\right)\left[exp\left(0.6\rho g C_{D_G} S_{TO} \frac{1}{W/S}\right)\right]} \frac{\eta_P}{V_{TO}}$$

The above equations use to contract the constrain diagram shown in appendix

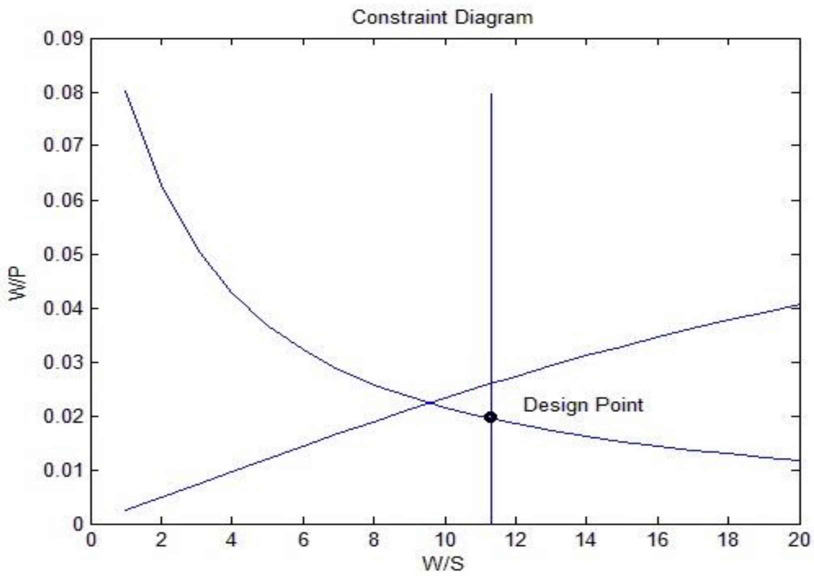

Figure 1-3: constrain diagram

Configuration layout:

There are some basic configuration decisions to make up front. Do we use one or two engines? Do we use a tractor (propeller in front) or a pusher (propeller in back) arrangement (or both)? Will the wing position be low-wing, mid-wing, or high-wing? Indeed, do we have two wings, i.e., a biplane configuration?

First, let us consider the number of engines. The weight of 103.57 lb puts our UAV somewhat on the borderline of single- and twin-engine UAVs. Since the common is to adapt a single engine from the existing UAVs designs, thus a single one is adequate. We need 16.5 hp from the constraint diagram of the statistical data can we get that from a single, existing piston engine. (We have to deal with an existing engine; rarely is enough incentive for the small engine manufacturers to go to the time and expense of designing a new engine.) Examining the available piston engines at the time of writing, we find that the DA-150is rated at 16.4 hp. This appears to be the engine for us. It is only 1 hp.more than our calculations show is required based on the rate-of-climb specification. We could tweak the airplane design, say, by slightly increasing the weight or slightly decreasing the aspect ratio, both of which would increase the power required for climb and would allow us to meet the performance specification with this engine. The free-stream density ratio between 3km and sea level is $1.225/0.90926 = 1.347$. Hence, the engine power at 3km will be $(16.4\ hp)(1.347) = 22.095\ hp$. This is more than enough to meet the calculated requirement of 15.4 hp for V_{max}

at3km. Therefore, we choose a single-engine configuration, using the following engine with the following characteristics:

- **DA-150 piston engine:-**

Rated power output at sea level: 16.4H0p

Length: 0.637ft

Dry weight: 7.96Ib(3.61 kilos)

Diameter of the base: 122mm

E.C.D: 98mm

Bore: 1.9291 in (49 mm)

Stroke: 1.5748 in (40 mm)

RPM Range: 1,000 to 8,500

RPM Max: 11,000

Fuel Consumption: 3.3 oz/min @ 6,000 RPM

Warranty: Three year

Question*:* Do we adopt a tractor or a pusher configuration?

Some of the advantages and disadvantages of these configurations are itemized below:

- **Tractor Configuration Advantages:-**

  1. The heavy engine is at the front, which helps to move the center of gravity forward and therefore allows a smaller tail for stability considerations.
  2. The propeller is working in an undisturbed free stream.
  3. There is a more effective flow of cooling air for the engine.

  Disadvantages:

  1. The propeller slipstream disturbs the quality of the airflow over the fuselage and wing root.
  2. The increased velocity and flow turbulence over the fuselage due to the propeller slipstream increase the local skin friction on the fuselage.

- **Pusher Configuration Advantages:-**

  1. Higher-quality (clean) airflow prevails over the wing and fuselage.
  2. The inflow to the rear propeller induces a favorable pressure gradient at the rear of the fuselage, allowing the fuselage to close at a steeper angle without flow separation. This in turn allows a shorter fuselage, hence smaller wetted surface area.
  3. Engine noise in the cabin area is reduced.

  Disadvantages:

  1. The heavy engine is at the back, which shifts the centre of gravity rearward,hence reducing longitudinal stability.

2. Propeller is more likely to be damaged by flying debris at landing.
3. Engine cooling problems are more severe.

2.4Fuselage configuration:

Once the take-off gross weight has been estimated, the fuselage, wing, and tails can be sized. Many methods exist to initially estimate the required fuselage size. Fuselage length is empirically related to the gross weight by Equation (2-9) given by Raymer where for a home-built aircraft:

$l_{a/c} = aW_0{}^c$.. (2-9)

$a = 1.28$; $C = 0.23$, that gives$l_{a/c} = 3.03894\ m$

However, the empirical formula above is valid for UAV with conventional tail. In our case, as the UAV tail has a boom for connection, the tail is not considered in the fuselage length. Taking the value above as the total length of the UAV, a factor of 0.55 is used for fuselage to total length fraction, suggested by Raymer for pusher configuration keeping the fuselage slightly longer than the half length of the UAV as is common along the competitor UAVs. Then the fuselage length becomes:

$$l_f = 1.67142\ m$$

The height and width of the fuselage are also initially guessed. The design of the fuselage is based on payload requirements, aerodynamics, and structures. The overall dimensions of the fuselage affect the drag through several factors. Hemida, Hassan and Krajnovic, Siniša (2010)Stated that fuselages with smaller fineness ratios have less wetted area to enclose a given volume, but more wetted area when the diameter and length of the cabin are fixed.

The higher Reynolds number and increased tail length generally lead to improved aerodynamics for long, thin fuselages, at the expense of structural weight. Selection of the best layout requires a detailed study of these trade-offs, but to start the design process, something must be chosen. This is generally done by selecting a value not too different from existing aircraft with similar requirements, for which such a detailed study has presumably been done. In the absence of such guidance, one selects an initial layout that satisfies the payload requirements.

In this UAV fuselage design, the payload requires a fuselage being able to hold a camera, batteries, servo, and targeting ball. Except the payload requirement, other considerations are:

1. Low aerodynamic drag
2. Minimum aerodynamic instability
3. ease of assembly and disassembly of fuselage
4. Structural support for wing and tail forces acting in flight, which involves simple stress analysis for the entire fuselage .

- **UAV Shape and Aerodynamics of Fuselage:**

UAV Nose and Tail Cone Design:

The fuselage shape must be such that separation is avoided when possible. This requires that the nose and tail cone fineness ratios be sufficiently large so that excessive flow accelerations are avoided.

The aircraft fineness ratios are defined as length divided by diameter, which including nose fineness ratios and tail cone fineness ratios.

In all of the following nose cone shape equations, *L* is the overall length of the nose cone and *R* is the radius of the base of the nose cone. *y*is the radius at any point *x*, as *x* varies from 0, at the tip of the nose cone, to *L*. The equations define the 2-dimensional profile of the nose shape. The full body of revolution of the nose cone is formed by rotating the profile around the centerline *(C/L)*. Note that the equations describe the 'perfect' shape; practical nose cones are often blunted or truncated for manufacturing or aerodynamic reasons.

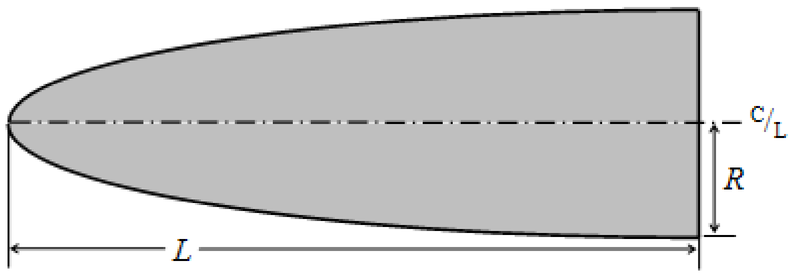

Figure 1-4: elliptical nose cone

There are several shapes available: 3/4 Power, Cone, 1/2 Power, Tangent give, parabolic, ellipsoid, etc.

Liu Tang-Hong, Tian Hong-qi and Wang Cheng-Yao (2006) wrote in journal "Aerodynamic performance comparison of several kind of nose shapes" that as speed of the plane increases, the drag coefficient increase as well. Different type of fuselage shape can give different drag coefficient as well. But as shown above, below Mach number 0.5, the shape of the airplane does not give too much difference.

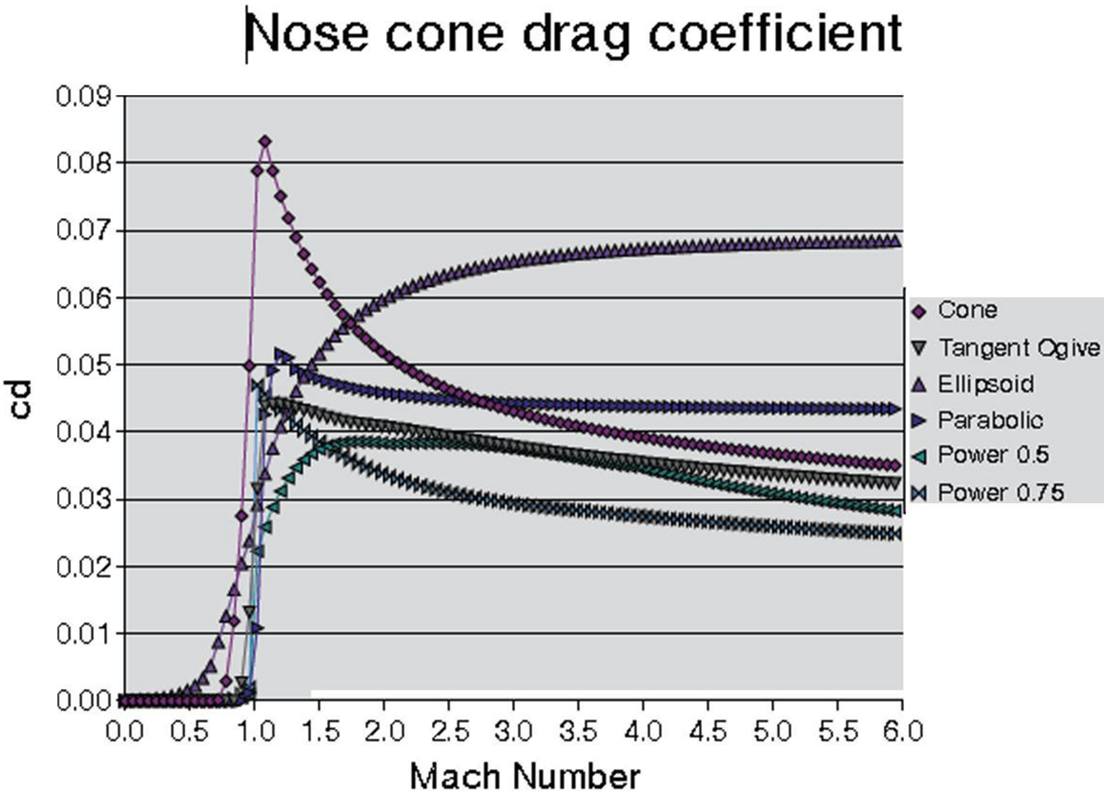

Figure 1-5: nose cone drag coefficient

In this UAV design, one of key factors in UAV fuselage shape design is the payload. According to the payloads weights, centre of gravity as well as the attribution of the different parts, the width, namely the aircraft lateral diameter is **no less than 0.83571.**In order to make sure the Centre of Gravity is behind the aerodynamic centre, which is design to make sure of the aircraft stability and easily maneuverability, and based on the fact that the tail of the plane is relatively high, the batteries and camera should be put into the very front to counter the weight. As such, the nose should be designed so as to have enough space to hold the payloads at the very front. That’s the main reason of this design.

- **Payload sizing:**

The payload here is EO/IR standard .It was selected the ultra 7000 camera setup, with forward and sideways looking camera options and varying lenses. The pixel pitch of the camera is approximately 3-5µm.Power required to operate the camera is 28VDC, 450 Watts. The speed needed to focus on objects of interest will not be an issue with this gimbals', which has 2-Axis, 3 Fiber-Optic gyros Stabilization. The diameter of the camera is about 9 inches; with height 15.2inches.it weighs about 26 lbs. Total system weight less than 40 lbs.

Figure 1-6: ultra 7000 camera

Except the shape of the fuselage, the nose and tail cone fineness ratio play an important role in fuselage design as well. Below is a simulation graph: drag loss VS fineness.

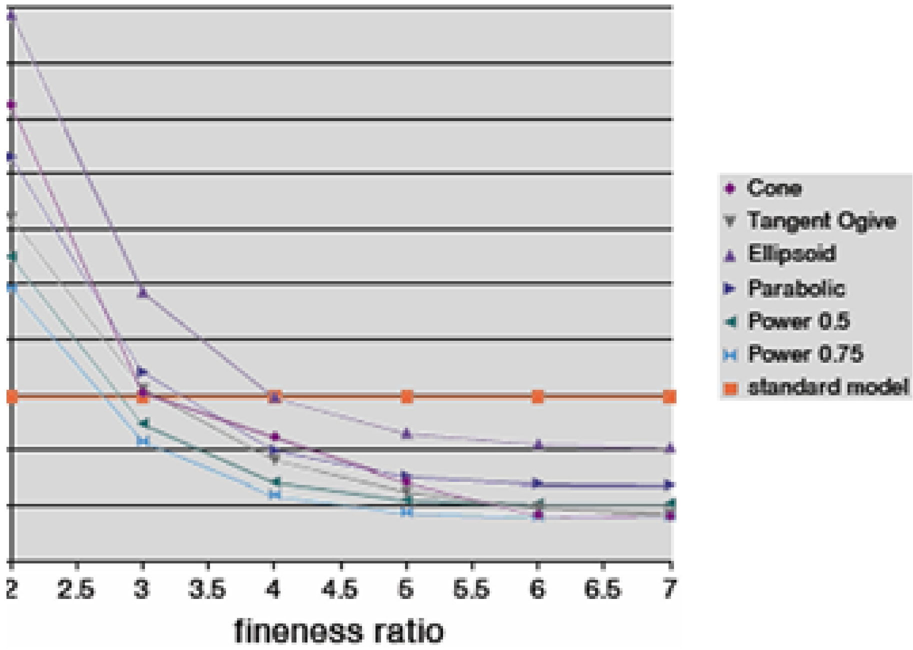

Figure 1-7: configuration drag loss

A square fuselage section with filleted edges, since our UAV is categorized as subsonic, based on the dimensions of the engine and the payload, 0.30952m wide and 0.30952m high is adopted. The fineness ratio of our UAV is then 5.4, which reveals different possibilities for the shape of the nose cone. However, the manufacturing an elliptic shape is more common because of its ease & simplicity, therefore an elliptic nose is preferred. Considering the fuel fraction and total weight, the fuel weight can be calculated:

$W_f = W_{f0} * W_0$, that is $W_f = 6.64522\ lb$

$\rho_{gasoline} = 5.6\ lb/gal$, and considering the 2% oil additive to 2-stroke engines:

$fuel\ capacity = 1.18665\ gal$

$fuel\ volume = 0.161 * 1.18665 = 0.19105\ ft^3$

Considering the wings with a high aspect ratio, there is significant number of beam and rib structure within the wings. Also considering the thickness of the wings being relatively small, placing the fuel tanks inside the wings will be unfeasible. Therefore, a separate fuel tank is placed inside the fuselage.

To size the fuselage, we recall that the engine length, width, and height are 0.637ft, 122mm, and 122mm, respectively. The layout shown in Fig. is a fuselage where the engine fits easily into the backward portion. Also, the length of the fuselage behind the centre of gravity should be long enough to provide a sufficient moment arm for both the horizontal and vertical tails. At this stage of our design, we have not yet determined the location of the centre of gravity or the tail moment arm. The pusher location is now seeing wider use because of its advantages. Most importantly, it can reduce UAV skin friction drag because the pusher location allows the UAV to fly in undisturbed air. With a tractor propeller the UAV flies in the turbulence from the propeller wake.

The fuselage-mounted pusher propeller can allow a reduction in UAV wetted area by shortening the fuselage. The inflow caused by the propeller allows a much steeper fuselage closure angle without flow separation than otherwise possible. Caution must be taken not to taper the back section of the fuselage at too large an angle, or else flow separation will occur. For subsonic UAV, the taper angle should be no larger than about 15°.The pusher propeller may require longer landing gear because the aft location causes the propeller to dip closer to the runway as the nose is lifted for take-off. The propeller should have at least 9 in. of clearance in all attitudes.

Depending on the dimensions of the engine & payload for a pusher configuration, the side view of our UAV is as shown below:

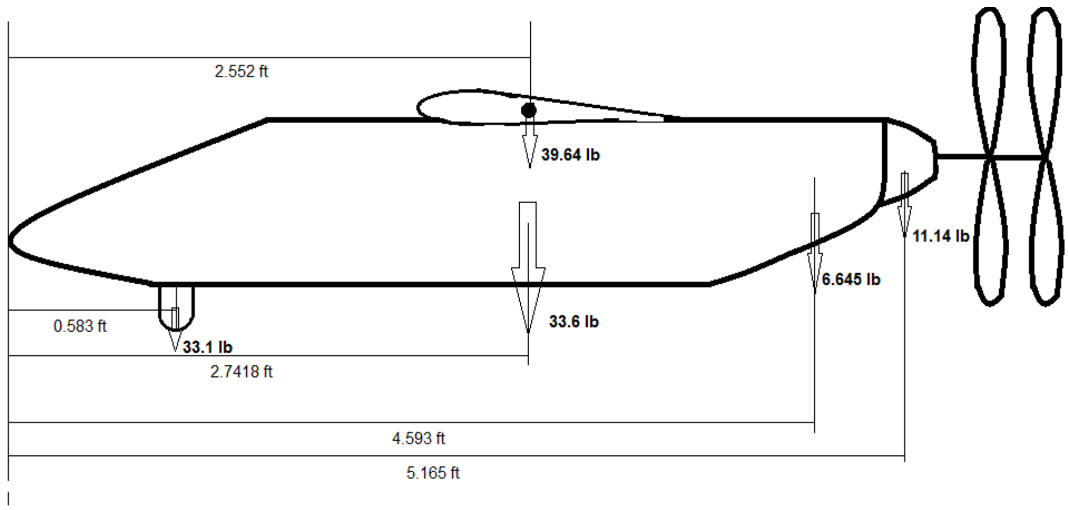

Figure 1-8: distribution of load along UAV

First estimation of center of gravity:

The major weight components for which we have some idea of their location are the engine, the payload and the fuel. Using this information, we can make a very preliminary estimate of the location of the center of gravity, hereafter denoted by C.G[2]. The tail, fuselage, and wing also contribute to the C.G. location; however, as yet we do not know the size and location of the vertical and horizontal tails. We can take into account the wing and fuselage, but again in only an approximate fashion, as we will see. The weights of (engine, payload, and fuel are shown in Fig(2-7), along with the locations of their respective individual C.G locations measured relative to the nose of the UAV. The effective C.G of these the weights, located by *x* in fig(2-8), is calculated by summing moments about the nose and dividing by the sum of the weights. Depending on the assumptions of Raymer, the weight of the major components as follow:

1. Fuselage:

As defined before, the fuselage has a square cross-section, thus

$S_{wet,f} = (4 * w_f * l_f + 2 * w_f * w_f) = 2.539m2$

$W_f = (1.4) * S_{wet,f} = 33.6lb\ where\ X_f = \frac{l_f}{2} = 2.7418\ ft$

2. Wing:

$W_w = (2.5) * S_{ref} = 39.63675\ lb\ where\ X_w$

$= 40\%MAC\ of\ the\ wing\ commonly = 2.552\ ft$

3. Engine:

$W_{dry} = 7.96\ lb\ where\ X_e$

$= 0.95\ of\ l_f\ due\ to\ the\ engine\ location = 5.165\ ft$

$W_e = 1.4 * W_{dry} = 11.144\ lb$

4. Payload:

$W_p = 33.1\ lb\ where\ x_p = 0.10\ of\ l_f = 0.583\ ft$ (As the camera system will be at the front of the aircraft)

The result is:

$$X_{C.Gi} = \frac{W_e \times X_e + W_p \times x_p + W_f \times X_f + W_{fuel} \times X_{fuel}}{W_e + W_p + W_f + W_{fuel}}$$

$$= \frac{11.144 \times 5.165 + 33.1 \times 0.583 + 33.6 \times 2.7418 + 6.645 \times 4.593}{11.144 + 33.1 + 33.6 + 6.645}$$

$$= 2.3699\ ft$$

With including the wing:

$$X_{C.G} = \frac{W_e \times X_e + W_p \times X_p + W_f \times X_f + W_{fuel} \times X_{fuel} + W_w \times X_w}{W_e + W_p + W_f + W_{fuel} + W_w}$$

$$= \frac{199.501025 + 39.63675 \times 2.552}{84.489 + 39.63675} = 2.4281\ ft$$

Under these assumptions, note that the addition of the wing has shifted the C.G only a small amount rearward, from x = 2.3699 ftto2.4281 ft.For the time being, measured from the nose, we will assume the UAV C.G to be at Centre-of-gravity location 2.4281 ft as shown:

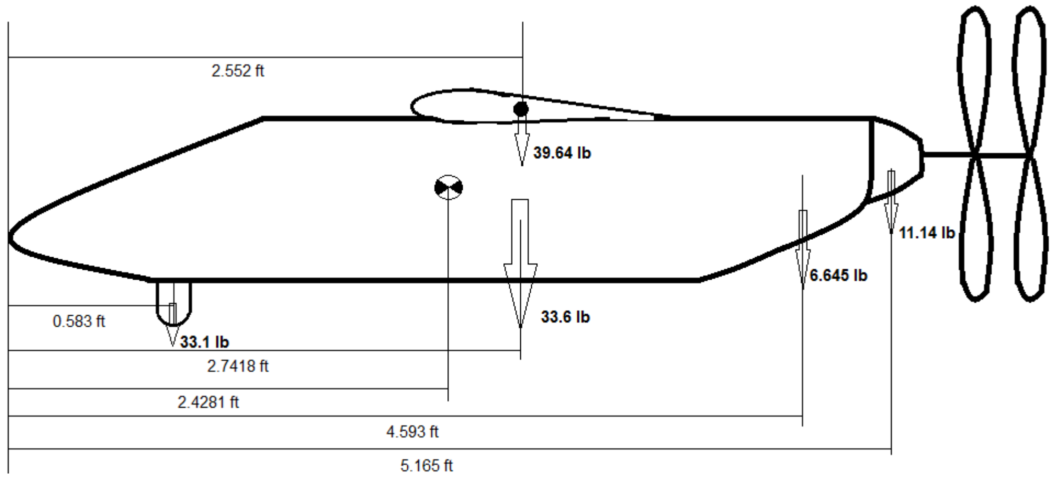

Figure 2-9: C.G. position

2.5Propeller size:

At this stage, we are not concerned with the details of the propeller design—the blade shape, twist, airfoil section, etc. Indeed, for a general aviation airplane of our design type, the propeller would be bought off the shelf from a propeller manufacturer. However, for the configuration layout, we need to establish the propeller diameter, because that will dictate the length (hence weight) of the landing gear.

Propeller efficiency is improved as the diameter of the propeller gets larger. The reason for this can be found in the discussion of propulsive efficiency. Essentially, the larger the propeller diameter, the larger the mass flow of air processed by the propeller. Therefore, for the same thrust, the larger propeller requires a smaller flow velocity increase across the propeller disk.

Decreasing the inflow velocity across any propulsive device will increase the propulsive efficiency.

There are two practical constraints on propeller diameter:

1. The propeller tips must clear the ground when the airplane is on the ground.
2. The propeller tip speed should be less than the speed of sound, or else severe compressibility effects will occur that ruin the propeller performance.

At the same time, the propeller must be large enough to absorb the engine power. The power absorption by the propeller is enhanced by increasing the diameter and/or increasing the number of blades on the propeller. Two-blade propellers are common on UAV designs. For the purpose of initial sizing, Raymer gives an empirical relation for propeller diameter D as a function of engine horsepower, as follows:

Two-blade: $D = 22(HP)^{1/4}$.. (2-10)

Three-blade: $D = 18(HP)]^{1/4}$.. (2-11)

Where D is in inches. For our UAV design, we choose a two-blade, constant-speed propeller. The propeller diameter is approximated as

Two-blade: $D = 22(16.5)^{1/4} = 44.34\ in = 3.695\ ft$

Question: Is this diameter too large to avoid adverse compressibility effects at the tip? Let us check the tip speed. The rated RPM (revolutions per minute) for our chosen DA-150 piston engine is 8,500. The tip speed of the propeller when the UAV is standing still, Denoted by $\left(V_{tip}\right)_0$ is:

$$\left(V_{tip}\right)_0 = \Pi n D \text{.. (2-12)}$$

$$\left(V_{tip}\right)_0 = \Pi * \frac{6500}{60} * 3.695 = 1257.553 ft/sec$$

When the maximum forward velocity of the UAV is vectorally added to $\left(V_{tip}\right)_0$, we have the actual tip velocity relative to the airflow V_∞:

$$V = \sqrt{\left(V_{tip}\right)_0^{\ 2} + V_\infty^{\ 2}} \text{.. (2-13)}$$

The specified $V_{\infty max}$ is 56.4 m/sec=185.039 ft/sec. Hence:

$V = \sqrt{1257.553^2 + 185.039^2} = 1271.094\ ft/sec$

The speed of sound at standard sea level is 1,117 ft/s; our propeller tip speed exceeds the speed of sound, which is not desirable.
So we have to change our initial choice of a two-blade propeller to a Three-blade propeller:

$D = 18(HP)]^{\frac{1}{4}}$.. (2-14)

$= 18(16.5)]^{1/4} = 36.278\ in = 3.023\ ft$

The static tip speed is:

$$\left(V_{tip}\right)_0 \ = \ \Pi nD$$

$$\left(V_{tip}\right)_0 \ = \ \Pi * \frac{6500}{60} * 3.023 = 1028.845\ ft/sec$$

Hence:

$$V = \sqrt{1028.845^{\ 2} + 185.039^2} = 1045.353\ ft/sec$$

Since our engine is designed for two propellers, the tip speed is well below the sound speed.

2.6Landing gear & wing placement:

Of the many internal components that must be defined in an UAV layout, the landing gear will usually cause the most trouble. Landing gear must be placed in the correct down position for landing, and must somehow retract into the UAV without chopping up the structure, obliterating the fuel tanks, or bulging out into the slipstream. The common options for landing-gear arrangement are shown in Fig (2-9).

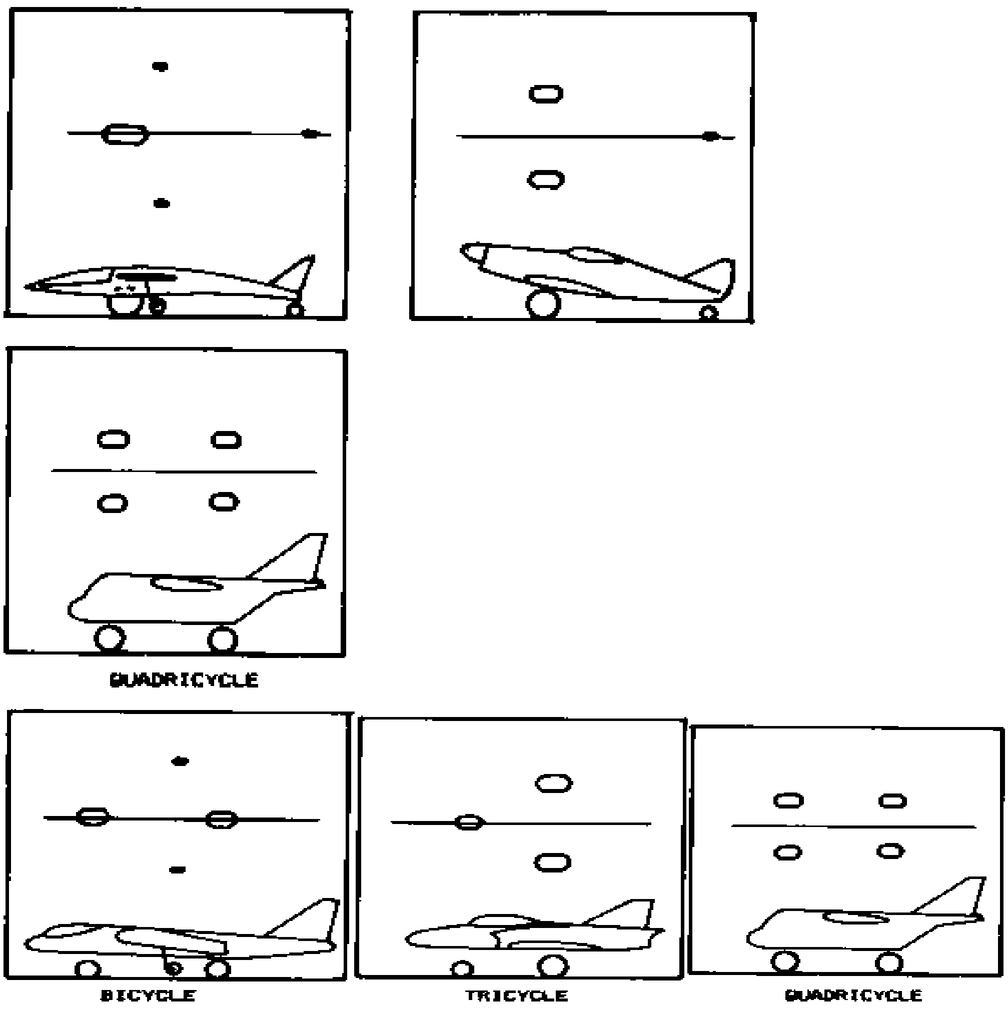

Figure 1-10: landing gear configuration

The most commonly used arrangement today is the “tricycle” gear, with two main wheels aft of the e.g. and an auxiliary wheel forward of the e.g. With a tricycle landing gear, the e.g. is ahead of the main wheels so the UAV is stable on the ground and can be landed at a fairly large “crab” angle (i.e., nose not aligned with the runway). Also, tricycle landing gear improves forward visibility on the ground and permits a flat floor for payload loading.

The engine is at the back of the UAV; therefore the tail dragger configuration is not suitable for our UAV. Furthermore, the bicycle configuration is not stable enough for the ground roll and requires additional wing tip wheels for the sake of stability. Therefore the choice is to adopt the tricycle configuration.

The landing gear should be long enough to give the propeller tip at least 9-in clearance above the ground. We choose a clearance of 1 ft. Since the propeller diameter is 3.023 ft, the radius is 1.5115ft. The landing gear needs to be designed to provide this height above the ground. At this stage we need to estimate the size of the tires. However, the tire size depends on the load carried by each tire. To calculate how the weight of the airplane is distributed over the two main wheels and the nose wheel, we need to locate the wheels relative to the airplane’s center of gravity.

We arbitrarily placed the mean aerodynamic center of the wing at the location of our first estimate for the e.g., namely, at $x = 2.3699\ ft$. Then, with the wing at this location, we recalculated the location of the C.G including the weight of the wing; the result was $x = 2.4281\ ft$.

From considerations of longitudinal stability, the aerodynamic center of the airplane must lie behind the UAV’s center of gravity. The aerodynamic center of the UAV is also called the *neutral point* for the UAV; the neutral point is, by definition, that location of the UAV’s C.G that would result in the pitching moment about the e.g.

being independent of angle of attack. There, the following relation was given between the location of the aerodynamic centre of the wing body $x_{acwb}$and the location of the neutral point $x_n$as

$x_{acwb} = x_n - V_{HT}\frac{a_t}{a}$.. (2-15)

In Equation above, the influence of the downwash angle behind the wing and ahead of the tail is neglected. Furthermore, the *static margin* is defined as:

$static\ margin = \frac{x_n - \bar{x}}{\bar{c}}$... (2-16)

Let us assume the 10% value for our UAV:

$$static\ margin = \frac{x_n - \bar{x}}{\bar{c}} = 0.1$$

Using$x = 2.4281\ ft$ and $\bar{c} = 1.15$ ft as obtained earlier, we find from Eq. above that:

$$x_n = 0.1\bar{c} + \bar{x} = 0.1 * 1.15 + 2.4281 = 2.5431$$

We will assume for simplicity that the aerodynamic canter of the wing- body (wing-fuselage) combination is the same as the aerodynamic centre of the wing, $x_{acwb} = x_{acw}$. Also, we assume for simplicity that the lift slope of the tail and that for the whole airplane are essentially the same, or$a_t = a$. Thus, we obtain for the longitudinal position of the wing aerodynamic centre:

$$x_{acw} = x_n - V_{HT}\frac{a_t}{a} = 2.5431 - 0.7 = 1.8431\ ft$$

Hence, we will locate the wing such that its mean aerodynamic centre is (1.8431) ft behind the nose of the UAV.

With the placement of the wing now established, we return to our consideration of the size and location of the landing gear. The layout of tricycle landing gear is even more complex. The length of the landing gear must be set so that the tail doesn’t hit the ground on landing. This is measured from the wheel in the static position assuming an angle of attack for landing which gives 90% of the maximum lift. This ranges from about 10-15 deg for most types of aircraft.

The “tip back angle” is the maximum UAV nose-up attitude with the tail touching the ground and the strut fully extended. To prevent the UAV from tipping back on its tail, the angle off the vertical from the main wheel position to the C.G should be greater than the tip back angle or 15 deg, whichever is larger.

The “overturn angle” is a measure of the UAV’s tendency to overturn when taxied around a sharp corner. This is measured as the angle from

The C.G to the main wheel, seen from the rear at a location where the main wheel is aligned with the nose wheel, this angle is selected to be 25 deg

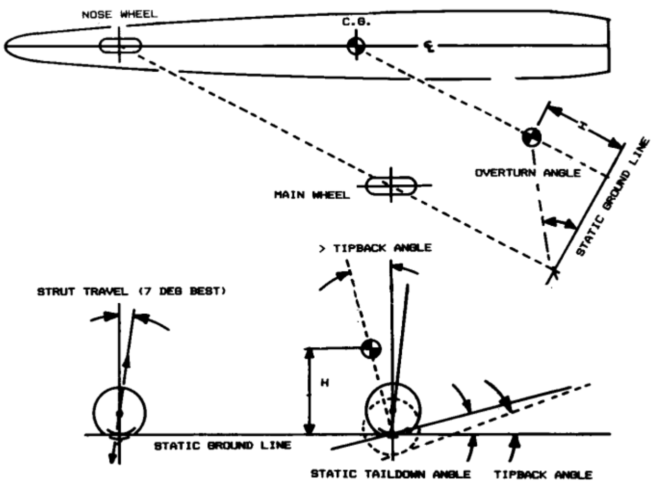

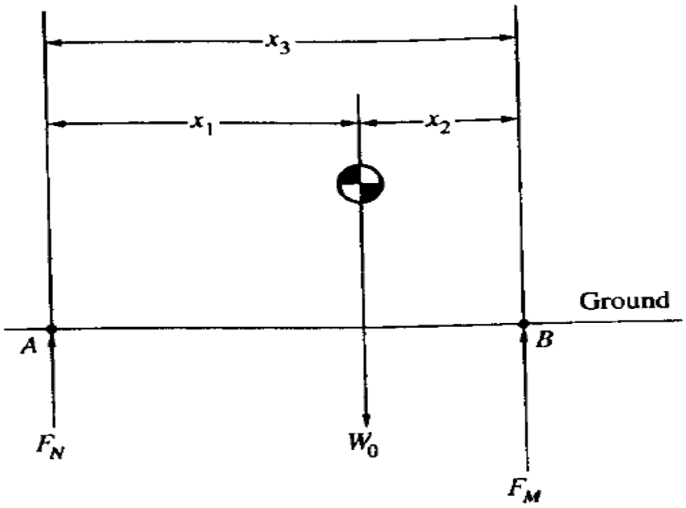

Figure 1-11 : position of main & nose landing gear

The take-off gross weight W_0 acts through the center of gravity. The distance between the line of action of F_N and the C.G is x_1, the distance between the line of action of F_M and the C.G is x_2. The distance between $F_N \& F_M$ is $x_3 = x_1 + x_2$. Taking moments about point *A*, we have

$F_M\, x_3 \; = W_0 x_1$

$F_M = \frac{W_0 x_1}{x_3}$.. (2-17)

Taking moments about point *B*, we have

$F_N\, x_3 \; = W_0 x_2$

Or

$F_N = \frac{W_0 x_2}{x_3}$.. (2-18)

Equations above give the forces carried by the main wheels and the nose wheel, respectively. Comparing Fig. above we find that, for our UAV:

The position of the nose wheel is about 0.6 ft. the main landing gear position depends on the C.G position & the tip back angle as shown:

$$x_1 = 2.4281 - 0.6 = 1.8281\ ft$$

$$H = \frac{dia.of\ propeller}{2} + clearance = \frac{36.278}{2} + 9 = 27.139\ in$$
$$= 2.262\ ft$$

$$x_2 = 2.2615 * tan(15^0) = 0.606\ ft$$

$$x_3 = x_1 + x_2 = 1.8281 + 0.606 = 2.4341\ ft$$

Substituting these values into equations, we obtain

$$F_M = \frac{W_0 x_1}{x_3} = \frac{94.6315 * 1.8281}{2.4341} = 131.8067\ lb$$

$$F_N = \frac{W_0 x_2}{x_3} = \frac{94.6315 * 0.606}{2.4341} = 43.693\ lb$$

Hence, the load on the nose wheel is 43.693 lb, and the load on *each* main wheel is ${F_M}/{2} = {131.8067}/{2} = 65.903\ lb$.

With this information, the tire sizes can be estimated. Raymer gives empirically determined relations for wheel diameter and width in terms of the load on each tire.

$$Wheel\ diameter\ or\ width\ (in) = AW^B$$

Where, for general aviation airplanes, the values of *A* and *B* are as follows:

Table 1: general aviation constant

	A	B
Wheel diameter(in)	1.51	0.349
Wheel width (in)	0.715	0.312

For our design, from Eq. (2-16) we have:

Main wheels:

$Wheel\ diameter =$

$A\left({F_M}/{2}\right)^B$ .... (2-19)

$$= 1.51\left({131.8067}/{2}\right)^{0.349} = 6.513\ in$$

$Wheel\ width =$

$A\left({F_M}/{2}\right)^B$ .... (2-20)

$= 0.715\left({131.8067}/{2}\right)^{0.312} = 2.630\ in$

Nose wheel:

$Wheel\ diameter = A(F_N)^B = 1.51(43.693)^{0.349} = 4.4302\ in$

$Wheel\ width = A(F_N)^B = 0.715(43.693)^{0.312} = 1.864\ in$

As in the case of the propeller, we must use off-the-shelf tires from the manufacturers. From a tire catalogue, we would choose the tires that most closely match the sizes calculated above.

Before we end this section, please note a detail that we did not take into account, namely, the shift in the position of the centre of gravity. In all our previous calculations, we assumed a fixed C.G.

location. However, due to changes in the distribution of payload and fuel during the flight, the C.G. shifts position. In a more detailed analysis, we would estimate the most forward and rearward positions to be expected for the center of gravity. Among other things, this would affect the calculation of the maximum static loads carried by the wheels. For the load on the main wheels, $x_1$would correspond to the most rearward position of the C.G. For the load on the nose wheel, $x_2$would correspond to the most forward position of the centre of gravity. However, we will not account for this effect in our calculations here.

2.7Better Weight Estimate:

Raymer[2] gives an approximate weight buildup as follows:

Wing weight $= 2.5\, S_{exposed\ wing\ plan\ for\ m}$

Horizontal tail weight $= 2\, S_{exposed\ horizontal\ tail\ plan\ form}$

Vertical tail weight $= 2\, S_{exposed\ vertical\ tail\ plan\ form}$

Fuselage weight $= 1\,.4\, S_{wetted\ area}$

Landing gear weight $= 0.057\, W_o$

Installed engine weight = 1.4(Engine weight)

All else empty $= 0.1\, W_o$

Table 2: better weight estimation

W_f	W_{else}	$W_{l.g}$	w_e	w_0
6.64522	9.46315	5.393996	87.62617	127.3714
8.944019	12.73714	7.260169	92.76633	134.8104
9.466383	13.48104	7.68419	93.93425	136.5006
9.585074	13.65006	7.780536	94.19962	136.8847
9.612043	13.68847	7.802428	94.25992	136.972
9.618171	13.6972	7.807402	94.27362	136.9918
9.619564	13.69918	7.808532	94.27674	136.9963
9.61988	13.69963	7.808789	94.27744	136.9973
9.619952	13.69973	7.808847	94.2776	136.9976
9.619968	13.69976	7.808861	94.27764	136.9976
9.619972	13.69976	7.808864	94.27765	136.9976

Chapter 3 : PRELIMINARY DESIGN

3.1Aerodynamics:

3.1.1Introduction:

The initial sizing was based upon rough estimates of the UAV's aerodynamics, weight and propulsion characteristics

Now the UAV design can be analysed "as drawn" to see if It actually meet the required mission range, Also, Varity of trade studies can now be performed to determine the best combination of design parameters (P/W, W/S, Aspect ratio, etc.) to meet the given mission and performance requirements at the min weight and cost.

If the air molecules closest to the aircraft skin are moving with it, there must be slippage (or “shear”) between these molecules and the nonmoving molecules away from the aircraft. “Viscosity” is the honey-like tendency of air to resist shear deformation, which causes additional air near the aircraft skin to be dragged along with the aircraft. The force required to accelerate this “boundary-layer” air in the direction the aircraft is travelling produces skin-friction drag.If the air molecules slide over each other (shear) in an orderly fashion, the flow is said to be “laminar.” If the molecules shear in a disorderly fashion the flow is “turbulent.” This produces a thicker boundary layer, indicating that more air molecules are dragged along with the aircraft, generating more skin-friction drag.
In fact, lift is created by forcing the air that travel over the top of the wing to travel faster than the air which passes under it, this is accomplished by the wing's angle of attack and /or wing camber the resulting difference in air velocity creates a pressure differential

between upper and lower surfaces of the wing, which produces the lift that supports the UAV.

All aerodynamic lift and drag forces result from the combination of the shear and pressure forces.The drag on a wing includes forces variously called airfoil profile drag, skin-friction drag, separation drag, parasite drag, camber drag, drag-due-to-lift, wave drag, wave-drag-due-to-lift, interference drag and so forth .Drag forces not strongly related to lift are usually known as parasite drag or zero-lift drag. Parasite drag consists mostly of skin-friction drag, which depends mostly upon the wetted area. “Scrubbing drag” is eliminated since it is due to the prop wash or jet exhaust impinging upon the aircraft skin. Note that the terms “profile drag” and “form drag” are frequently intermixed, although strictly speaking the profile drag is the sum of the form drag and the skin-friction drag. Also note that the term “profile drag” is sometimes used for the zero-lift drag of an airfoil. Interference drag is the increase in the drag of the various aircraft components due to the change in the airflow caused by other components. For example, the fuselage generally causes an increase in the wing’s drag by encouraging airflow separation at the wing root.

Drag forces that are a strong function of lift are known as “induced drag” or “drag-due-to-lift.” The induced drag is caused by the circulation about the airfoil that, for a three-dimensional wing, produces vortices in the airflow behind the wing. The energy required to produce these vortices is extracted from the wing as a drag force, and is proportional to the square of the lift. Another way of looking at induced drag is that the higher-pressure air under the wing escapes around the wingtip to the wing upper surface, reducing the lift and causing the outer part of the wing to fly in an effective downwash.[2]

3.1.2Aerodynamic coefficients:

-

Lift and drag forces are usually treated as non-dimensional coefficients as defined in equations bellow, the wing reference area, S_{ref}or simply S, is the full trapezoidal area extending to the UAV centreline.[2]

$$L = qsc_l \text{..........} (3\text{-}1)$$

$$C_D = C_{D_{min}} + k\left(C_L - C_{L_{min\,drag}}\right)^2 = 0.896\text{C}$$

($C_{D_{min}}$) Occur at the same positive lift ($C_{L_{\min drag}}$) there is offset in the drag polar.

For wing of moderate camber this offset is usually small which implies that C_{D_0}approximately equal to$C_{D_{min}}$:

$$C_D = C_{D_0} + k(C_L)^2 \text{..........} (3\text{-}2)$$

Subsonic Lift-Curve Slope:

Equation below is a semi-empirical formula from Ref. 36 for the complete wing lift curve slope (per radian). This is accurate up to the drag-divergent Mach number, and reasonably accurate almost to Mach one for a swept wing.

Lift curve slope

$$C_{L_\propto} = \frac{2\pi A}{2+\sqrt{4+\frac{A^2\beta^2}{\eta^2}(1+\frac{\tan\Lambda^2}{\beta^2})}}\left(\frac{S_{exp}}{S_{ref}}\right)(F) \text{..........} (3\text{-}3)$$

$\beta^2 = 1 - M^2$ .... (3-4)

$$= 1 - 0.173^2 = 0.970$$

$\eta = \frac{c_{l_\alpha}}{2\pi\beta}$ .... (3-5)

$$\eta = 0.856$$

$F = 1.07\left(1 + {}^{d}/_{b}\right)^2$ .... (3-6)

$$F = 1.2446$$

$$\therefore C_{L_\propto} = \frac{2\pi * 11.3}{15.154}(1) * 1.2446 = 5.831\, rad$$

Nonlinear Lift Effects:

For a wing of very high sweep or very low aspect ratio (under two or three), the air escaping around the swept leading edge or wing tip will forma strong vortex that creates additional lift at a given angle of attack. This additional lift varies approximately by the square of the angle of attack. This nonlinear increase in the slope of the lift curve is difficult to estimate and can conservatively be ignored during early conceptual design.

(However, the increase in maximum lift due to vortex formation is very important. It will be discussed in the next section.)

Max lift coefficient (clean)

Usually determine the wing area, and is critical in determining the A/C weight, and the max lift coefficient of clean wing (without use of high lift devices) will usually about 90% of the air foil max lift coefficient from 2D aerofoil data

$$C_{L_{max}} = 0.9c_{l_{max}} \cos \Lambda_{0.25c} = 1.296$$

PARASITE (ZERO-LIFT) DRAG:

Equivalent Skin-Friction Method:

A well-designed aircraft in subsonic cruise will have parasite drag that is mostly skin-friction drag plus a small separation pressure drag. The latter is a fairly consistent percentage of the skin-friction drag for different classes of aircraft. This leads to the concept of an “equivalent skin friction coefficient” *(C/e),* which includes both skin-friction and separation drag.

Component Buildup Method

The component buildup method estimates the subsonic parasite drag of each component of the aircraft using a calculated flat-plate skin-friction drag coefficient (C_f) and a component “form factor” *(FF)* that estimates the pressure drag due to viscous separation. Then the interference effects on the component drag are estimated as a factor *“Q”* and the total component drag is determined as the product of the wetted area,C_f, *FF*, and *Q*. Miscellaneous drags (C_{flmisc}) for special features of an aircraft such as flaps, unretract landing gear, an upswept aft fuselage, and base area are then estimated and added to the total, along with estimated contributions[2]

For leakages and protuberances ($C_{flL\&p}$).

$$C_{D,0} = \frac{\sum C_{fc} FF_c Q_c S_{wetc}}{S_{ref}} + C_{Dmisc} + C_{DL\&P} \qquad \text{(3-7)}$$

Flat-Plate Skin Friction Coefficient:

The flat-plate skin friction coefficient *C/* depends upon the Reynolds number, Mach number, and skin roughness. The most important factor affecting skin-friction drag is the extent to which the aircraft has laminar flow over its surfaces. Most current aircraft have turbulent flow over virtually the entire wetted surface, although some laminar flow may be seen towards the front of the wings and tails. A typical current aircraft may have laminar flow over perhaps 10- 20% of the wings and tails, and virtually no laminar flow over the fuselage. For the portion of the aircraft that has laminar flow, the flat-plate skin friction coefficient is expressed by:

$$C_f = \frac{1.328}{\sqrt{R_e}} \text{ ……………………………………………………… (3-8)}$$

Where Reynolds number is:

$$R_e = \frac{\rho_\infty V_\infty \bar{C}}{\mu} \text{ ……………………………………………………... (3-9)}$$

For turbulent flow, which in most cases covers the whole aircraft, the flat-plate skin friction coefficient is determined by*:*

$$C_f = \frac{0.455}{(logR)^{2.58}} \text{ …………………………………………..……… (3-10)}$$

If the surface is relatively rough, the friction coefficient will be higher than indicated by this equation. This is accounted for by the use of a "cut-off Reynolds number," which is determined *by:*

$$R_{cut\ off} = 38.21 \left(\frac{\bar{C}}{K}\right)^{1.053} \text{ …………………..……………….. (3-11)}$$

For fuselage:

$$C_{D,0f} = 0.0003 \left[3 * \frac{l_f}{d_f} + 4.5 * \sqrt{\frac{d_f}{l_f}} + 21 * \left[\frac{d_f}{l_f}\right]^2\right] \text{ ………… (3-12)}$$

$$C_{D,0f} = 0.0003\left[3 * \frac{1.6714}{0.30952} + 4.5 * \sqrt{\frac{0.30952}{1.6714}} + 21 * \left[\frac{0.3095}{1.6714}\right]^2\right]$$

$$= 0.0003 * [16.200 + 4.5 * 0.4303 + 0.0343 * 21]$$

$$= 0.005657$$

Miscellaneous Drags:

The drag of miscellaneous items can be determined separately using a variety of empirical graphs and equations, and then adding the results to the parasite drags determined above.

For wing NACA 4415:

$$\bar{C} = 1.149\,ft = 0.3504\,m$$

$$R_{cut\,off} = 38.21\left(\frac{\bar{C}}{K}\right)^{1.053} = 38.21\left(\frac{1.149}{3.33 * 10^{-5}}\right)^{1.053}$$

$$= 2293824.832$$

$$R_e = \frac{\rho_\infty V_\infty \bar{C}}{\mu} = \frac{0.90926 * 47 * 0.3504}{1.79 * 10^{-5}} = 729124.93$$

The lower Reynolds number is considered⇒$R_e = 729124.93$

For laminar flow:

$$C_f = \frac{1.328}{\sqrt{R_e}} = \frac{1.328}{\sqrt{729124.93}} = 0.001555$$

For turbulence flow:

$$C_f = \frac{0.455}{(logR)^{2.58}} = \frac{0.455}{(log729124.93)^{2.58}} = 0.004746$$

From Raymer assumption, laminar flow is about 10% of the chord and turbulence flow is about 90% of the chord:

$$C_f = 0.1 * C_{flam} + 0.9 * C_{fturb}$$
$$= 0.1 * 0.001555 + 0.9 * 0.004746 = 0.004427$$

$$S_{wet} = S_{exp}\left(1.977 + 0.52\left({}^{t}/_{c}\right)\right) \text{ ……………………….. (3-13)}$$

$$= 14.808\big(1.977 + 0.52(0.15)\big) = 30.430\ ft^2$$

For a high-wing, a mid-wing, or a well-filleted low wing, the interference will be negligible so the *Q* factor will be about 1.0.

$$FF = 1 + \frac{0.6}{({}^{x}/_{c})_m}\left({}^{t}/_{c}\right) + 100\left({}^{t}/_{c}\right)^4 \text{ ………………………. (3-14)}$$

$$= 1 + \frac{0.6}{0.291}(0.15) + 100(0.15)^4 = 1.36$$

For vertical tail:

$$\bar{C} = 0.457 ft = 0.1394\ m$$

$$R_{cut\ off} = 38.21\left(\frac{\bar{C}}{K}\right)^{1.053} = 868830.42$$

$$R_e = \frac{\rho_\infty V_\infty \bar{C}}{\mu} = \frac{0.90926 * 47 * 0.1394}{1.79 * 10^{-5}} = 332809.48$$

The lower Reylonds number is considered$\Rightarrow R_e = 332809.48$

For laminar flow:

$$C_f = \frac{1.328}{\sqrt{R_e}} \text{ ………………………………………………… (3-15)}$$

$$= \frac{1.328}{\sqrt{332809.48}} = 0.002302$$

For turbulence flow:

$$C_f = \frac{0.455}{(logR)^{2.58}} = \frac{0.455}{(log332809.48)^{2.58}} = 0.005538$$

From Raymer assumption, laminar flow is about 10% of the chord and turbulence flow is about 90% of the chord:

$$C_f = 0.1 * C_{flam} + 0.9 * C_{fturb} \quad \text{(3-16)}$$

$$= 0.1 * 0.002302 + 0.9 * 0.005538 = 0.005215$$

$$S_{wet} = S_{exp}\left(1.977 + 0.52\left({}^{t}/_{c}\right)\right) = 1.182\left(1.977 + 0.52(0.12)\right) = 2.4096\ ft^2$$

For H tail, the interference factor from Raymer assumption (Q) is about 1.08:

$$FF = 1 + \frac{0.6}{({}^{x}/_{c})_m}\left({}^{t}/_{c}\right) + 100\left({}^{t}/_{c}\right)^4 \quad \text{(3-17)}$$

$$= 1 + \frac{0.6}{0.291}(0.12) + 100(0.12)^4 = 1.268$$

For horizontal tail:

$$\bar{C} = 0.528\ ft = 0.161\ m$$

$$R_{cut\ off} = 38.21\left(\frac{\bar{C}}{K}\right)^{1.053} = 1011525.37$$

$$R_e = \frac{\rho_\infty V_\infty \bar{C}}{\mu} = \frac{0.90926 * 47 * 0.161}{1.79 * 10^{-5}} = 384378.24$$

The lower Reylonds number is considered $\Rightarrow R_e = 384378.24$

For laminar flow:

$$C_f = \frac{1.328}{\sqrt{R_e}} = \frac{1.328}{\sqrt{384378.24}} = 0.002302$$

For turbulence flow:

$$C_f = \frac{0.455}{(logR)^{2.58}} = \frac{0.455}{(log332809.48)^{2.58}} = 0.00554$$

From Raymer assumption, laminar flow is about 10% of the chord and turbulence flow is about 90% of the chord:

$$C_f = 0.1 * C_{flam} + 0.9 * C_{fturb} = 0.1 * 0.002302 + 0.9 * 0.00554$$
$$= 0.005215$$

$$S_{wet} = S_{exp}\left(1.977 + 0.52\left({}^{t}/_{c}\right)\right) = 2.100\left(1.977 + 0.52(0.12)\right) = 4.283\ ft^2$$

For H tail, the interference factor from Raymer assumption (Q) is about 1.08.

$$FF = 1 + \frac{0.6}{({}^{x}/_{c})_m}\left({}^{t}/_{c}\right) + 100\left({}^{t}/_{c}\right)^4 \quad \text{.......................... (3-18)}$$

$$= 1 + \frac{0.6}{0.291}(0.12) + 100(0.12)^4 = 1.268$$

$$C_{D,0} = \frac{0.004427 * 1.36 * 1 * 30.430}{14.808}$$
$$+ \frac{0.005215 * 1.268 * 1.08 * 2.4096}{1.182}$$
$$+ \frac{0.005215 * 1.268 * 1.08 * 4.283}{2.100}$$
$$= 0.01237 + 0.01456 + 0.01457 = 0.0415$$

Interference drag:

$$C_{Dint}(A_1, A_2) = \left[0.75\left({}^{t}/_{c}\right) - \frac{0.0003}{\left({}^{t}/_{c}\right)^2}\right]\frac{t^2}{A_1 + A_2} \quad \text{……………….. (3-19)}$$

$$C_{Dint}(S_w, A_{f1}) = \left[0.75(0.15) - \frac{0.0003}{(0.15)^2}\right]\frac{0.05255^2}{1.376 + 0.096}$$

$$= 1.298 * 10^{-4}$$

$$C_{Dint}(S_H, S_V) = \left[0.75(0.12) - \frac{0.0003}{(0.12)^2}\right]\frac{0.0193^2}{0.195 + 0.110}$$

$$= 8.447 * 10^{-5}$$

Summation of the components drag:

$$C_{D,0} = 0.0415$$

The total parasite drag:

$$C_{D,0} = 0.0417$$

DRAG DUE TO LIFT (INDUCED DRAG):

The induced-drag coefficient at moderate angles of attack is proportional to the square of the lift coefficient with a proportionality factor called the “drag-due-to-lift factor,” or *“K”*

Oswald Span Efficiency Method:

According to classical wing theory, the induced-drag coefficient of a 3-D wing with an elliptical lift distribution equals the square of the lift coefficient divided by the product of aspect ratio and x. However, few wings actually have an elliptical lift distribution. Also, this doesn’t take into account the wing separation drag.

The extra drag due to the no elliptical lift distribution and the flow separation can be accounted for using *e*, the “Oswald span efficiency factor.”

This effectively reduces the aspect ratio, producing the following equation for *K*.

$$e = 1.78(1 - 0.045A^{0.68}) - 0.64 = 0.723$$

$$k = \frac{1}{\pi A e} = 0.040$$

$$C_{Lideal} = \frac{2W}{\rho_\infty {V_\infty}^2 S} = \frac{2 * 76.046}{0.90926 * 47^2 * 1.376} = 0.055$$

$$\therefore C_D = 0.0417 + 0.040(0.055)^2 = 0.04182$$

3.1.3Digital DATCOM aerodynamic:

The Digital DATCOM program uses aircraft-unique configuration and geometry parameters to predict aircraft performance by utilizing classical aerodynamic equations.

For those speed regimes and configurations where DATCOM methods are available, the Digital DATCOM output provides the longitudinal coefficients C_L, C_d, C_m, C_N, and C_A (body axis), and the derivatives $dC_L/d\alpha$, $dC_m/d\alpha$, $dC_Y/d\beta$, $dC_n/d\beta$, and $dC_l/d\beta$. Output for configurations with a wing and horizontal tail also includes downwash and the local dynamic-pressure ratio in the region of the tail. The pitch, roll, yaw and angle-of-attack rate derivatives dC_L/dq, dC_m/dq, $dC_L/d(\alpha\text{-dot})$, $dC_m/d(\alpha\text{-dot})$, dC_l/dp, dC_Y/dp, dC_n/dp, dC_n/dr, and dC_l/dr are also computed for most configurations. Divided into degree of freedom, the parameters output by the DATCOM program may include:

• Lift Coefficient due to:

- Basic geometry (CL_{α})

- Flap deflection ($CL_{\delta f}$)

- Elevator Deflection ($CL_{\delta e}$)

- Pitch Rate derivative (CL_{q})

- Angle of Attack Rate derivative ($CL_{\alpha dot}$)

• Drag Coefficient due to:

- Basic geometry (Cd_{α})

- Flap deflection ($Cd_{\delta f}$)

- Elevator deflection ($Cd_{\delta e}$)

• Side Force Coefficient due to:

- Sideslip (Cn_{β})

- Roll Rate derivative (Cn_{p})

- Yaw Rate derivative (Cn_{r})

• Pitching Moment Coefficient due to:

- Basic Geometry (Cm_{α})

- Flap Deflection ($Cm_{\delta f}$)

- Elevator Deflection ($Cm_{\delta e}$)

- Pitch Rate derivative (Cm_{q})

- Angle of Attack Rate derivative ($Cm_{\alpha dot}$)

• Rolling Moment Coefficient due to:

- Aileron Deflection ($Cl_{\delta a}$)

- Sideslip (Cl_β)

- Roll Rate derivative (Cl_p)

- Yaw Rate derivative (Cl_r)

• Yawing Moment Coefficient

- Aileron Deflection ($Cy_{\delta a}$)

- Sideslip (Cy_β)

- Roll Rate derivative (Cy_p)

- Yaw Rate derivative (Cy_r)

• Misc

- Horizontal Tail Downwash Angle (ε)

- Derivative of Downwash Angle (δε/δα)

- Elevator-surface hinge-moment derivative with respect to alpha (Ch_α)

- Elevator-surface hinge-moment derivative due to elevator deflection (Ch_δ)

- Normal force coefficient (body axis) (C_N)

- Axial force coefficient (body axis) (C_A)

3.2Performance:

Performance analysis has been conducted to verify that the requirements are met and the next phase of design and manufacturing can be initiated. [8]

3.2.1Wing loading:

Wing loading is calculated using the previously found total weight and reference area calculations as follows:

$$^{W}/_{S} = \frac{W_0}{S_{ref}} \qquad \text{...} (3\text{-}20)$$

With $W_0 = 167.65\ Ib = 76.046\ kg$

And$Sref\ = 14.808\ ft^2\ \ , 1.376\ m^2$

$$W/S = 11.32\ Ib/ft^2$$

$$V_{stall} = \sqrt{\frac{W/S}{0.5\ .\rho_\infty\ .C_{Lmax}}} \text{...} (3\text{-}21)$$

With $CLmax = 1.57$

$$Vstall = 72.861\ m/s$$

3.2.3Power loading:

Using final weight estimation and real engine power value: $\frac{P}{W_0} = 0.194\ \frac{hp}{kg}$which is relatively higher than the aimed value of $0.161\frac{hp}{kg}$

Power required and power available curves:

$$D = D_0 + D_i \text{...} (3\text{-}22)$$

$$D_0\ = \frac{1}{2}\ .\rho_\infty\ .V_\infty{}^2\ .S_{ref}\ .C_{D0} \text{..} (3\text{-}23)$$

$$D_i = \frac{2\ .K\ .S_{ref}}{\rho_\infty\ .V_\infty{}^2} W/S^2 \text{...} (3\text{-}24)$$

Figure 16: is drawn using basic drag equations***Eq (24) and Eq (25) with$C_{D0} = 0.034$,$K = 0.0401$, which were calculated during

conceptual design phase while calculating wing loading. The graph represents the lowest drag value at around 100 ft/s

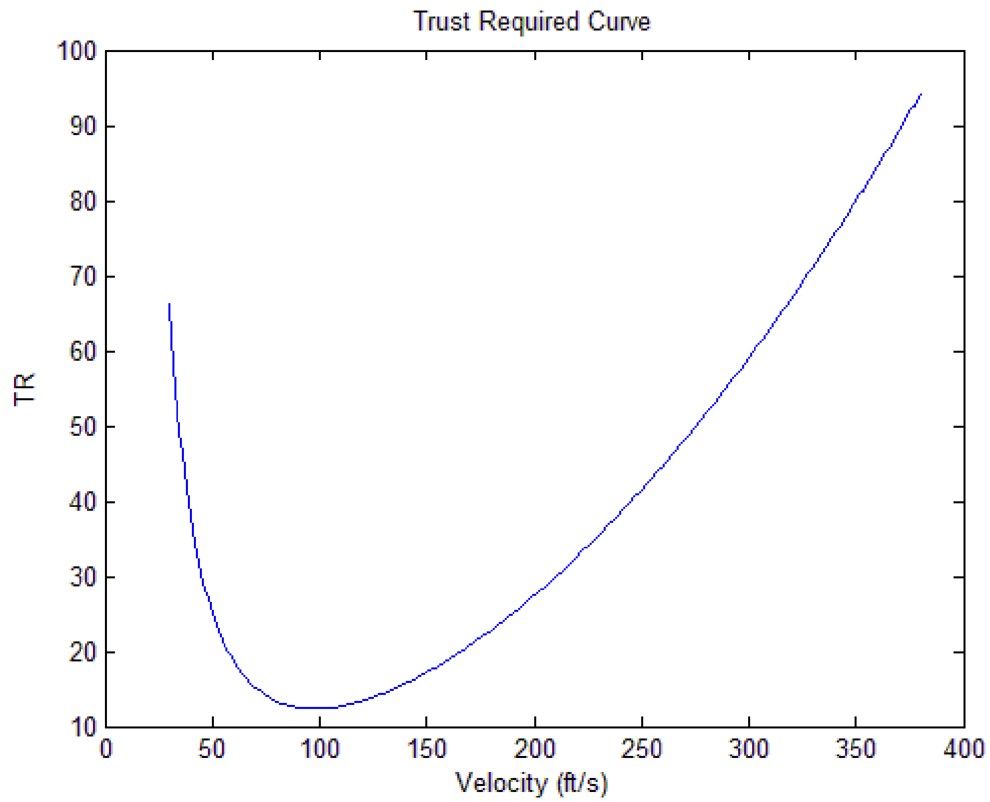

Figure 3-1 : Drag variation graph

Fuel weight is not a major part of the total weight therefore the fuel spent during takeoff and climb is neglected and Wcr is replaced with $W0$ in Eq (26), Eq (27) and Eq (28) which are straightforward formulation of lift to drag ratios. The neglecting also provides a small safety factor to the calculations. The resulting variations are graphed in Figure.

$$\frac{CL}{CD} = \frac{\frac{2 . W_0}{\rho_\infty . S_\infty . V_\infty{}^2}}{C_{D0} + K\left(\frac{2 . W_0}{\rho_\infty . S_{ref} . V_\infty{}^2}\right)^2} \quad \text{...} \ (3\text{-}25)$$

$$\frac{CL^{3/2}}{CD} = \frac{\left(\frac{2 . W_0}{\rho_\infty . S_\infty . V_\infty{}^2}\right)^{3/2}}{C_{D0}+K\left(\frac{2 . W_0}{\rho_\infty . S_{ref} . V_\infty{}^2}\right)^2} \quad \text{(3-26)}$$

$$\frac{CL^{1/2}}{CD} = \frac{\left(\frac{2 . W_0}{\rho_\infty . S_\infty . V_\infty{}^2}\right)^{1/2}}{C_{D0}+K\left(\frac{2 . W_0}{\rho_\infty . S_{ref} . V_\infty{}^2}\right)^2} \quad \text{(3-27)}$$

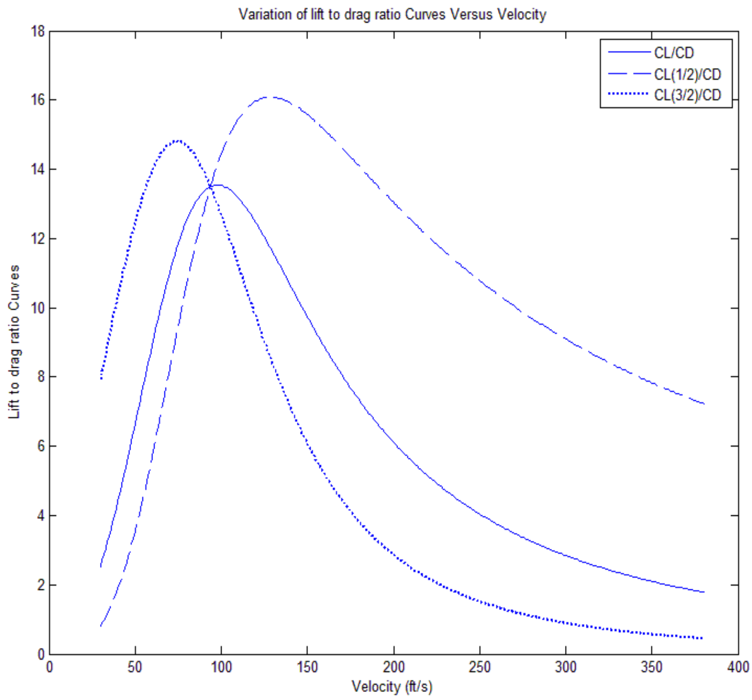

Figure 3-2 : Lift to drag ratios graph

The Lift to Drag Ratios represents different flight conditions. For example:

• When the aircraft flies at its $(CL/CD)max$ velocity, it travels to its maximum range, thus this velocity is used for cruise missions. In **Figure16**, the maximum CL/CD ratio is at around $97.67\ ft/s$

with$CL/CD = 13.5$. The exact value of the cruise velocity is given in Eq (29).

•When the aircraft flies at its $(CL^{3/2}/CD)max$ velocity, it travels for its maximum endurance, thus this velocity is used for loiter missions. In **Figure 17**the maximum $CL^{3/2}/CD$ is at around $128.937\ ft/s$ as is also concluded in **Figure 16**. The lowest $CL/CD3/2$ value is around 16.0837.

• The $({C_L}^{1/2}/CD)max$ value is also used for certain calculations such as required power as a function of velocity, giving a characteristic of the aircraft. In **Figure 17**the maximum $CL/CD1/2$ is at around $47.244\ ft/s$with ${C_L}^{1/2}/CD\ = 14.8099$.

$$V(L/D)_{max} = \sqrt{\frac{2}{\rho_\infty}\sqrt{\frac{K}{C_{D0}}}\frac{W_0}{S_{ref}}} = 97.67\ ft/s \text{.........................} \text{(3-28)}$$

Power required:

Power required and power available varies as in Eq(30) and Eq(31), which are calculated in cruise altitude.

$$P_R = \frac{W_0}{[{C_L}^{1/2}/C_D]}\sqrt{\frac{2\,.W_0}{\rho_\infty\,.S_\infty\,.{V_\infty}^2}} \text{..} \text{(3-29)}$$

$$P_{A,3K} = P.\frac{\rho_{\infty,3K}}{\rho_\infty} = 11\ Hp \qquad \text{...} \text{(3-30)}$$

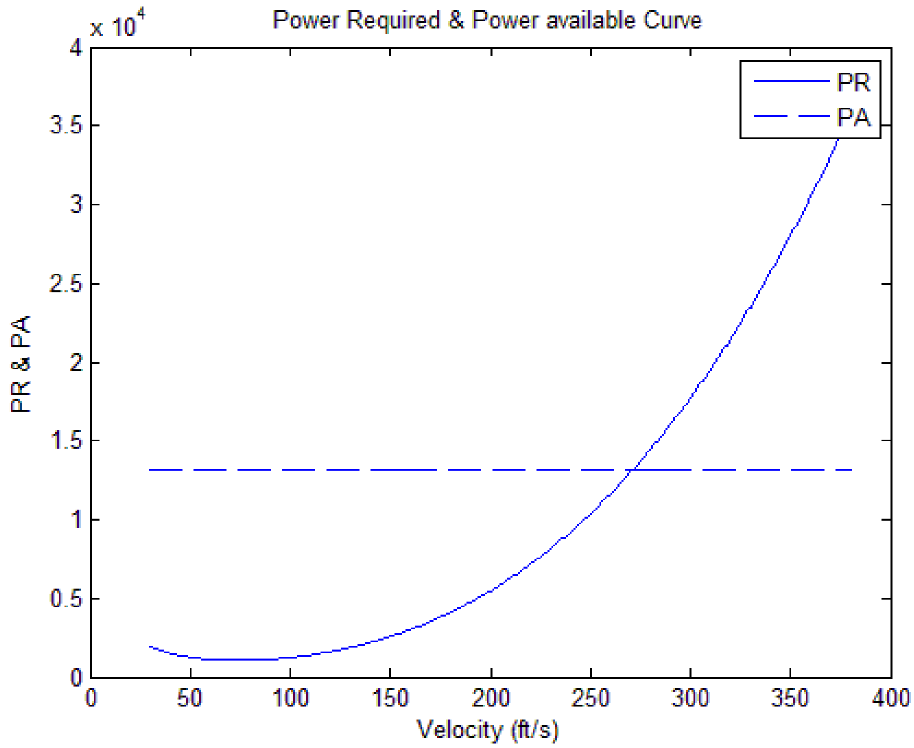

Figure 3-3 : Power required and available graph

The intersection point, where power available and power required curves drawn in **Figure 18**coincide, is the maximum velocity point of the aircraft at $3000m$ altitude after which the power of the engine is not sufficient to sustain the velocity of the aircraft. This maximum velocity at cruise altitude can be read from **Figure 18**which is calculated precisely as Maximum Velocity at $3000m$ is: $Vmax3k = 278.6\ ft/s$

3.2.4Rate of climb and climb velocity:

The following formula is a rough general formula for density variation with altitude

$\boldsymbol{\rho_{\infty,Z} = (6.10).10^{-19}.\ Z^4 - (7.10).10^{-14}.Z^3 + (4.10).10^{-9}.Z^2 - 10^{-4}.Z + 1.225}$ .... (3-31)

Best rate of climb rate is given in Eq(32) which is plotted in **Figure19**. Additionally rate of climb variation with altitude is given in Eq(33) and plotted in **Figure 20.**

$$V_{R/C(altitude)} = \sqrt{\frac{2}{\rho_\infty}\sqrt{\frac{K}{3\,.C_{D0}}}\frac{W_0}{S_{ref}}} \quad \text{(3-32)}$$

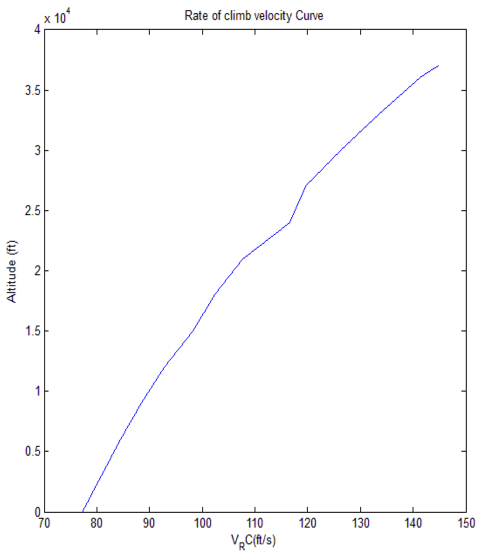

Figure 3-4 : Variation of best rate of climb velocity with altitude graph

$$\mathbf{R/C\,(altitude)} = \frac{\eta_P\,.P\,.\frac{\rho_{inf,altitude}}{\rho_{inf,0}}}{W_0} - \left(\sqrt{\sqrt{\frac{2}{\rho_{inf,altitude}}}\,.\sqrt{\frac{K}{3\,.C_{D0}}\frac{W_0}{S_{ref}}}}\right).\ \frac{1.155}{(L/D)_{max}} \quad \text{... (3-33)}$$

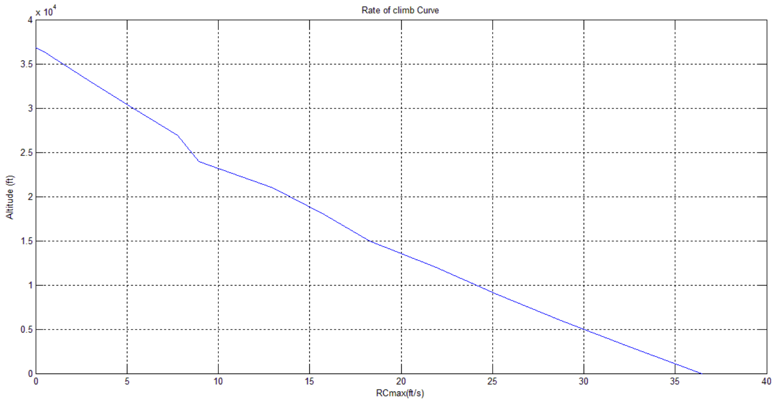

Figure 3-5 : Rate of climb variation with altitude graph

Figure 19represents the best rate of climb velocity which increases with altitude and is higher than the stall velocity at all altitudes. Absolute Ceiling is where Rate of Climb is zero and the service Ceiling is where Rate of Climb is $100 ft/min$; that is $0.508\, m/s$. When the graph in **Figure 20**is considered, the rate of climb is as high as 10m/s at sea level and decreases to $0.508\, m/s$ at $3.58 * 10^4 ft$ which is the service ceiling and a vertical level at $3.7 * 10^4 ft$ is the absolute ceiling of the aircraft. Which are not quite realistic considering the non-linear drop of performance of the reciprocating engine at those altitudes but still as these altitudes are very well above the intended flight altitudes of the aircraft there is a large safety margin for these values.

3.2.5 Time to climb:

$$t_{min} = \int_0^{h_2} \frac{dh}{(R/C)_{max}} = \ 162.16 \text{ sec} = 2.7 \text{ min}$$

By evaluating the **Figure 20,**, which is drawn by integrating the rate of climb over time, the following key times to climb are calculated: t3000=2.7

Best angle and rate of climb:

Vertical velocity is calculated by$V_V = \left(\frac{P \cdot \eta_P}{W_0 \cdot V_\infty} - \frac{D}{W_0}\right)$where D is the total drag at the velocity V_∞calculated previously.

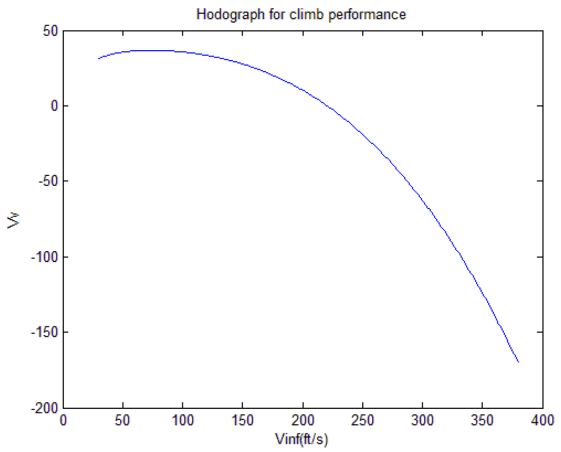

Figure 3-6 : Hodograph for climb performance

$\sin\theta_{max} = \frac{T}{W} - \frac{1}{(L/D)_{max}}$ =0.205

$$\theta_{max} = 11.831^o$$

3.2.6 Range:

Range of the aircraft can be calculated using Eq (34) given in [10].

$R = \frac{\eta_P}{C} \cdot (L/D)_{max} \cdot ln\frac{W_0}{W_0 - W_f}$................................. (3-34)

$= 661.031$ km $(2.1687 * 10^6 ft)$

Where $Cbhp = 1.559 * 10^{-3}$

This is significantly higher than the requirement of $250\ km$

3.2.7 Endurance:

Endurance can be calculated using equation (35) given in [10]

$$E = \frac{\eta_P}{C}\sqrt{2 . \rho_\infty . S_{ref}}\left(\frac{{C_L}^{3/2}}{C_D}\right)_{max}\left(\left(W_0 - W_f\right)^{-0.5} - (W_0)^{-0.5}\right) \ldots \quad (3\text{-}35)$$

At Sea Level: $E = 25200\ s = 7\ hrs$

At Cruise Altitude: $E = 34560\ s = 9.6\ hrs$

The engine has a fixed pitch propeller so its efficiency at endurance speed is lower (taken as 0.7). The endurance value is also way higher than the requirement of 5 hours.

3.2.8 Landing distance:

The parameter in landing distance, j=1.15 for commercial airplanes and 1.1 for military airplanes. The configuration is similar to a commercial airplane so j=1.15

Reaction time $(N) = 3s$as a pilot standard

Friction coefficient $(\mu r) = 0.4$ that is for both dry concrete and hard turf without flap deflection$C_{Lmax} = 1.655$, so as the wing angle is not known. Then L/W at $0.7\ VT$

The parameters are used in equation (41) for evaluation of the landing distance.

$$S_{g,L} = j.N.\sqrt{\frac{2}{\rho_\infty}\frac{W_0}{S_{ref}}\frac{1}{C_{Lmax}}} + \frac{j^2\frac{W_0}{S_{ref}}}{g.\rho_\infty.C_{Lmax}.\mu_r.\left(1-\frac{L}{W_{0.7}V_{TD}}\right)} \quad \ldots\ldots\ldots\ldots\ldots\ldots$$

(3-36)

$$Sg_L = 169.848m(557.2453\,ft)$$

$$L = 470.611m\,(1544ft)$$

The landing distance is relatively low for a tactical size aircraft. The value is low due to the fairly low stall velocity which is the result of relatively high lift coefficient. The low landing distance gives the aircraft more value as it will be operable in small air fields making it more functional. Additionally, during operational necessities, the aircraft is capable of making very short emergency landings.

3.2.9 Take-off distance:

Similar to landing distance calculation, the same parameters are used in evaluation of equation(42).

$$S_{g,T0} = \frac{1.21\frac{W_{0}.g}{S_{ref}}}{g.\rho_\infty.C_{Lmax}.\frac{\frac{P\eta_p}{0.77\times V_{stall}}}{W_{0}.g}} \ldots\ldots\ldots\ldots\ldots\ldots\ldots\ldots\ldots\ldots\ldots\ldots\ldots \text{(3-37)}$$

$$= 141.012\text{m}\ (462.6378\text{ft})$$

The take-off distance is even lower than the landing distance. The key reason for the significantly low take-off distance is the advantageous reciprocating engine which gives fairly high excess power for the aircraft weight and configuration. The relatively low stall velocity due to high lift coefficient is also reducing the take-off distance.

3.3 Structural design:

3.3.1 V-n diagram:

3.3.1.1 Description:

The *V-n* diagram depicts the UAV limit load factor as a function of airspeed. V-n diagram is used primarily in the determination of combination of flight conditions and load factors to which the UAV structure must be designed. V-n diagram precisely gives the structural (maximum load factor) and aerodynamic (maximum CL) boundaries for a particular flight condition. Note that the maximum lift load factor equals 1.0 at level-flight stall speed, as would be expected. The UAV can be stalled at a higher speed by trying to exceed the available load factor, such as in a steep turn.

The point labeled “high A.O.A.” (Angle of attack) is the slowest speed at which the maximum load factor can be reached without stalling. This part of the flight envelope is important because the load on the wing is approximately perpendicular to the flight direction, not the body-axis vertical direction.At high angle of attack the load direction may actually be forward of the aircraft body-axis vertical direction, causing a forward load component on the wing structure. During World War I, several aircraft had a problem with the wings shedding forward due to this unexpected load.The UAV maximum speed, or dive speed, at the right of the *V-n* diagram represents the maximum dynamic pressure q. The point representing maximum q and maximum load factor is clearly important for structural sizing. At this condition the aircraft is at a fairly low angle of attack because of the high dynamic pressure, so the load is approximately vertical in the body axis.

For a subsonic aircraft, maximum or dive speed is typically 50% higher than the level-flight cruise speed. For a supersonic aircraft the maximum speed is typically about Mach 0.2 faster than maximum level-flight speed, although many fighters have enough thrust to accelerate past their maximum structural speed.

Note that UAV speeds for loads calculation are in “equivalent” air-speeds V_e. An aircraft airspeed indicator uses a pitot probe to determine airspeed from the dynamic pressure, so the “airspeed” as measured by a pitot probe is based upon the dynamic pressure at the aircraft’s velocity and altitude, and not the actual velocity. This dynamic pressure-based equivalent airspeed will be less than the actual airspeed at altitude due to the reduction in air density, as this expression describes:

$$V_e = \sqrt{\frac{\rho}{\rho_0}} V_{actual} \sigma V_{actual} \ldots\ldots\ldots\ldots\ldots\ldots\ldots\ldots \text{(3-38)}$$

For loads estimation, V_e is a convenient measure of velocity because it is constant with respect to dynamic pressure regardless of altitude. However, pilots must convert V_e to actual velocity to determine how fast they are really flying. Also, the dynamic pressure as measured by a pitot tube has a compressibility error at higher Mach numbers, so the “indicated” airspeed V_i as displayed to the pilot must be corrected for compressibility to produce the equivalent airspeed V_e, which can then be converted to actual airspeed.

3.3.1.2 Maneuvering Envelope:

In accelerated flight, the lift becomes much more compared to the weight of the aircraft. This implies a net force contributing to the acceleration. This force causes stresses on the aircraft structure. The ratio of the lift experienced to the weight at any instant is defined as the *Load Factor* (n).

$$n = \frac{\frac{1}{2}\rho_\infty V_\infty^2 S C_{Lmax}}{W} \quad (3\text{-}39)$$

Using the above formula, we infer that load factor has a quadratic variation with velocity. However, this is true only up to a certain velocity.

This velocity is determined by simultaneously imposing limiting conditions aerodynamically (C_{Lmax}) as well as structurally (n_{max}). This velocity is called the *Corner Velocity*, and is determined using the following formula[8]:

$$V_A = V_{corner} = \sqrt{\frac{2n_{max}}{\rho_\infty C_{Lmax}} \frac{W}{S}} \quad (3\text{-}40)$$

In this section, we estimate the aerodynamic limits on load factor, and attempt to draw the variation of load factor with velocity, commonly known as the V-n Diagram. The V-n diagram is drawn for Sea level Standard conditions.

Construction of V-n diagram

Curve OA:

Maximum Load Factor:

$n_{max} = 3.8$ (Based onCS-337)

$$n_{max} = \frac{1}{2}\rho_\infty V_\infty^2 \frac{C_{Lmax}}{W/S} \quad (3\text{-}41)$$

Hence, along the curve OA:

$n_{max} = 0.00121 \times V_\infty^2$

Using the above equation, we get:

At A:

$n_A = 3.8$ (Based on CS-337)

$\therefore V^* = 56.04\ m/sec$

Curve AC:

V_C must be more than $2.4\sqrt{\frac{Mg}{S}}$ based on CS-VLA 335:

$$V_C \geq 2.4\sqrt{\frac{Mg}{S}} \quad \text{(3-42)}$$

$= 2.4\sqrt{285.464} = 40.55\ m/sec$

$n_C = n_A = 3.8$ (Based on USAR code)

Along CD:

The velocity at point D is given by:

$V_D = 1.25V_C = 1.25 * 47 = 58.75\ m/sec$

A straight line is used to join the points C and D.

This V_D is the dive velocity or the maximum permissible EAS in which the UAV is at the verge of structural damage due to high dynamic pressure.

Along DE:

E corresponds to zero load factor point i.e.

n= 0

Along EF

The point F corresponds to the velocity:

$V_C = V_F = 47\ m/sec$

Curve OG:

$n_F = -1.5$ (For USAR code)

$n_{max} = \frac{1}{2}\rho_\infty V_\infty^2 \frac{C_{Lmax\,neg}}{W/S}$

Hence along the curve OG:

$n_{OG} = -0.00114V_\infty^2$

Hence we get:

Along GF:

Also$n_G = n_F$, finally join GF by using a straight line.

Nomenclature of curves:

• PHAA – Positive High Angle of Attack

• PSL – Positive Structural Limit

• PLAA – Positive Low Angle of Attack

• HSL –High Speed Limit

• NHAA – Negative High Angle of Attack

• NSL – Negative Structural Limit

• NLAA – Negative Low Angle of Attack

• LSL – Low Speed Limit

Low Speed Limit:

Stall velocity is the maximum speed at which the aircraft can maintain level flight. This implies the intersection of this line at cruise n=1 with OA curve corresponds to stall velocity Vs.

$V_{stall} = 28\, m/sec$

From the V-n diagram, it is observed that the stall curve corresponds to maximum value of C_{Lmax} and any point beyond this curve for a particular velocity is not achievable in flight as it enters the stall region there. The upper horizontal line corresponds to limit load factor as well as ultimate load factor. It shows that there is outright structural failure when the UAV is flown beyond this value of load factor.

$n = -1.5$gives the negative limit load factor and negative ultimate load factor.

From the figure, it is clear that for a particular velocity, it is not possible to fly at a value of C_L higher than the C_{Lmax} corresponding to that velocity. If we wish to increase the lift of the airplane to that value of C_{Lmax}, then we should increase the flying speed of the UAV.

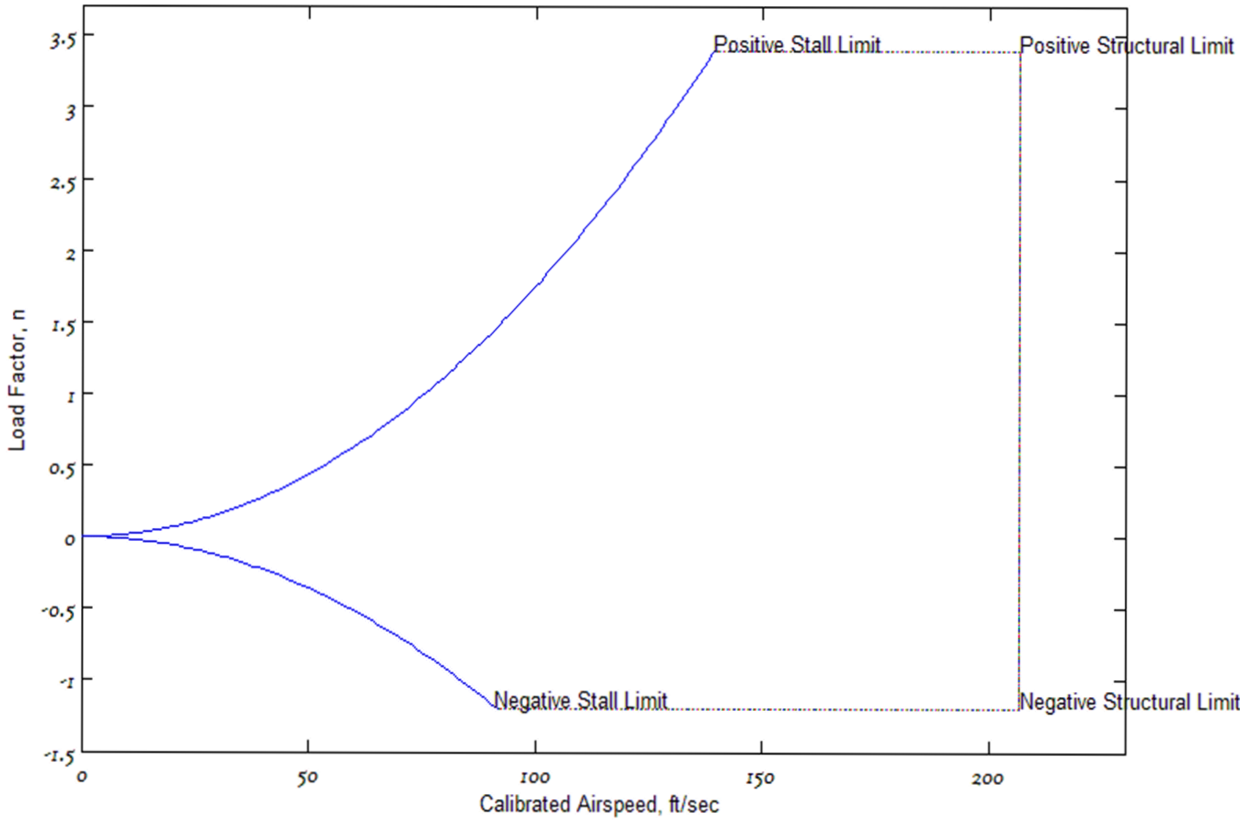

Figure 3-7: V-n diagram

3.3.2 Gust diagram:

Description:

Gust is a sudden, brief increase in the speed of the wind. Generally, winds are least gusty over large water surfaces and most gusty over rough land and near high buildings. With respect to UAV turbulence, a sharp change in wind speed relative to the UAV; a sudden increase in airspeed due to fluctuations in the airflow, resulting in increased structural stresses upon the UAV.

Sharp-edged gust (u) is a wind gust that results in an instantaneous change in direction or speed.

Derived gust velocity ($U \; or \; U_{max}$) is the maximum velocity of a sharp-edged gust that would produce a given acceleration on a particular airplane flown in level flight at the design cruising speed of the airplane and at a given air density. As a result a 25% increase is seen in lift for a longitudinally disturbing gust.

The effect of turbulence gust is to produce a short time change in the effective angle of attack. These changes produce a variation in lift and thereby load factor.

For velocities up to V_{max}, cruise, a gust velocity of 15 m/s at sea level is assumed. ForV_{Div}, a gust velocity of 10 m/s is assumed.

The loads experienced when the UAV encounters a strong gust can exceed the maneuver loads in some cases.

When the UAV experiences a gust, the effect is an increase (or decrease) in angle of attack. The change in angle of attack, as shown in Equation below is approximately *U* divided by *V*, the UAV velocity. The change in UAV lift is shown in Eq. below to be proportional to the gust velocity. The resulting change in load factor is derived in Eq. below:

$$\Delta\alpha = tan^{-1}\left(\frac{U}{V}\right) \cong \frac{U}{V} \quad (3\text{-}43)$$

$$\Delta L = {}^{1}\!/_{2}\,\rho V^2 S(C_{L\alpha}\Delta\alpha) = {}^{1}\!/_{2}\,\rho V S C_{L\alpha} U \quad (3\text{-}44)$$

$$\Delta n = \frac{\Delta L}{W} = \frac{\rho V C_{L\alpha} U}{2W/S} \quad (3\text{-}45)$$

Eq. above assumes that the UAV instantly encounters the gust and that it instantly affects the entire UAV. These assumptions are unrealistic.

Gusts tend to follow a cosine-like intensity increase as the UAV flies through, allowing it more time to react to the gust. This reduces the acceleration experienced by the UAV by as much as 40%. To account for this effect a statistical “gust alleviation factor "K" has been devised and applied to measured gust data (U_{des}). The gust velocity in Eq. below can be defined in the following terms:

$$U = KU_{des} \qquad (3\text{-}46)$$

$$K = \frac{0.88\mu}{5.3+\mu} \qquad (3\text{-}47)$$

The mass ratio term accounts for the fact that a small, light plane encounters the gust more rapidly than a larger plane as Eq. shows:

$$\mu = \frac{2(W/S)}{\rho g \bar{c} C_{L\alpha}} \qquad (3\text{-}48)$$

The design requirements for gust velocities are “derived” from flight-test data and are in “equivalent” airspeed (hence,U_{des}). Actual accelerations experienced in flight have been applied to equations, above to determine what the vertical gust velocities must have been to produce those accelerations in the various flight-research aircraft employed.

The UAV is assumed to be subjected to symmetrical vertical gusts in level flight. The resulting limit load factors must correspond to the conditions determined as follows:

1. Positive (up) and negative (down) gusts of 15.24 m/s at V_C must be considered.
2. Gust load factors vary linearly with speed between V_C and V_D .

Note that the expected gusts are reduced at higher altitude. The maximum turbulence speed V_g may be specified in the design requirements or may be a fallout parameter.

One interesting point concerning gusts is that, as shown in Eq. (3.9), the load factor due to a gust increases if the UAV is lighter. This is counter to the natural assumption that an UAV is more likely to have a structural failure if it is heavily loaded.

In fact, the change in lift due to a gust is unaffected by UAV weight, so the change in wing stress is the same in either case. However, if the UAV is lighter the same lift increase will cause a greater vertical acceleration (load factor) so the rest of the UAV will experience more stress.The *V-n* diagrams are combined to determine the most critical limit load-factor at each speed. Since the gust loads are greater than the assumed limit load, it may be desirable to raise the assumed limit load at all velocities. The structural design load factors will be 50% higher to provide a margin of safety as CS-VLA 303 suggests.

3.3.3 Construction:

The increase in the load factor due to the gust can be calculated by

For curve above V-axis:

$$n_{+ve} = 1 + \frac{KU_{max}\rho Va}{2(\frac{W}{S})} \quad (3\text{-}49)$$

Where

K → Gust Alleviation Factor

U max → Maximum derived Gust Velocity

a → Lift Curve Slope for wing

$$\mu = \frac{2(W/S)}{\rho g \bar{c} C_{L\alpha}} = \frac{2 * 542.2711}{.90926 * 9.81 * 1.149 * 5.218} = 20.28$$

$$K = \frac{0.88\mu}{5.3 + \mu} = \frac{0.88 * 20.28}{5.3 + 20.28} = 0.698$$

For curve below V-axis:

$$n_{-ve} = 1 - \frac{KU_{max}\rho Va}{2\left(\frac{W}{S}\right)}$$

$$= 1 - \left(\frac{0.698 * 15.24 * 0.90926 * 5.218}{2 * 542.2711}\right)V$$

$$\therefore n_{-ve} = 1 - 0.0465V$$

$$\& n_{+ve} = 1 + 0.0465V$$

That goes for the curves of $U_{max} = 10\ m/sec$ & $U_{max} = 5\ m/sec$:

3.3.4 Fuselage design:

Fuselage contributes very little to lift and produces more drag but it is an important structural member/component. It is the connecting member to all load producing components such as wing, horizontal tail, vertical tail, landing gear etc. and thus redistributes the load. It also serves the purpose of housing or accommodating practically all equipment, accessories and systems in addition to carrying the payload. The reactions produced by the wing, tail or landing gear may be considered as concentrated loads at the respective attachment points. The balancing reactions are provided by the inertia forces contributed by the weight of the fuselage structure and the various components inside the fuselage. These reaction forces are distributed all along the length of the fuselage, though need not be uniformly. Unlike the wing, which is subjected to mainly unsymmetrical load, the fuselage is much simpler for structural analysis due to its symmetrical cross-section and symmetrical loading. The main load in the case of fuselage is the shear load because the load acting on the wing is transferred to the fuselage skin in the form of shear only. The structural design of both wing and fuselage begin with shear force and bending moment diagrams for the respective members. The maximum bending stress produced in each of them is checked to be less than the yield stress of the material chosen for the respective member.

3.3.5 Load Determination:

The loading of the UAV was required in order to perform a detailed stress analysis and design a suitable structure. A classical approach has been taken to predict these loads, with detailed hand calculations. This analysis comprised of aerodynamic, weight, inertial and thrust loading resulting in a load distribution throughout the fuselage for bending, shear and torsion loads. From these plots a suitable structure was able to be designed. The largest load the aircraft is actually expected to encounter is called the limit or applied load. To provide a margin of safety, the aircraft structure is always designed to withstand a higher load than the limit load. The highest load the structure is designed to withstand without breaking is the "design" or "ultimate", load. The "factor of safety" is the multiplier used on limit load to determine the design load. In this case, the factor of safety 1.5 will be used based on CS-VLA 303.

Loads and its distribution:

To find out the loads and their distribution, consider the different cases. The main components of the fuselage loading diagram are:

1. Weight of the fuselage.
2. Engine weight.
3. Weight of payload and landing gear.

4. Systems, equipment, accessories.

   Symmetric flight condition, pull down condition: (Downward forces negative) Values for the different component weights are obtained from aerodynamic design calculations.

The force and bending moment calculations:

By collecting the results obtained from the better weight estimation phase, the weights of the major components in the fuselage had been determined:

Table 3: load acting on fuselage

component	Weight (lb)	Load(lb)
Nose	0	0
Nose landing gear	3.8874	14.77212
inertia load	111.2537	1606.504
Fixed equipment	17.05	64.79
Fuselage weight	33.6	127.68
Payload bay	33.1	125.78
Main landing gear	5.8311	22.158
Fuel in fuselage	*6.64522*	*25.252*
engine weight	11.14	42.332
Horizontal stabilizer	2.96	11.248
Vertical Stabilizer	11.329	43.0502
Tail end	0	0

The distribution of the loads through the fuselage when designing for a pull up condition ($n_{max} = 3.8$, Based onCS-337):

$\therefore load = n_{max} W_{component}$, as shown below:

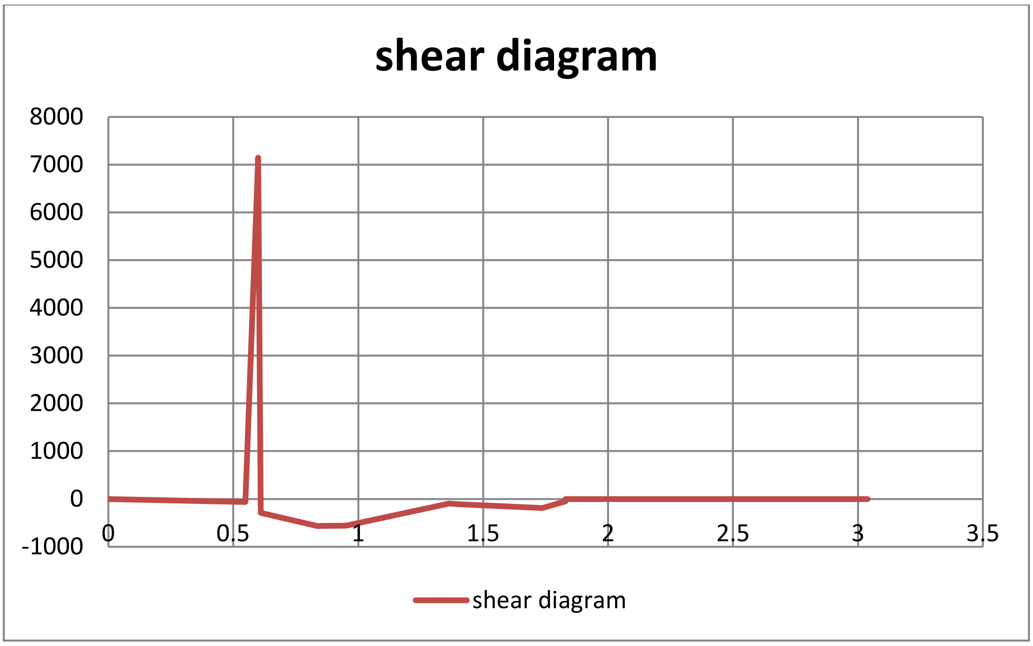

Figure 3-8: shear diagram

nose of the fuselage ($\tau = 1606.504\ lb$).

For the distribution of the moments, the moment arm of the shear loads is shown below:

Table 4: moment about fuselage nose

component	Load(lb)	Distance from nose(m)	Moment(N.m)
Nose	0	0	0
Nose landing gear	14.77212	0.54864	-36.0633
inertia load	1606.504	0.599375	4284.648
Fixed equipment	64.79	0.6096	-175.747
Fuselage weight	127.68	0.835708	-474.802
Payload bay	125.78	0.95189	-532.762
Main landing gear	22.158	1.362761	-134.366
Fuel in fuselage	25.252	1.4	-157.31
engine weight	42.332	1.73736	-327.26
Horizontal stabilizer	11.248	1.8288	-91.5327
Vertical Stabilizer	43.0502	1.8288	0
Tail end	0	3.038938	0

Figure below shows the distribution of the moments about the nose:

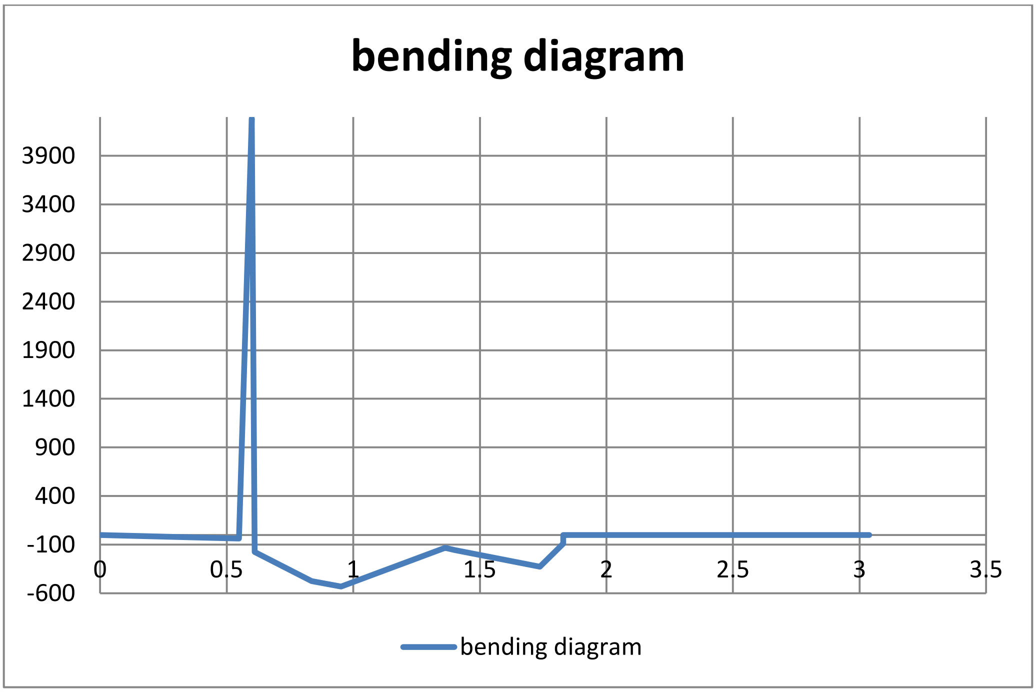

Figure 3-9: bending diagram

Detailed Design of Fuselage:

Stringer Design:

Design of the fuselage can be carried out by considering the maximum bending moment which is taken as the design bending moment. The cross-sectional area required to withstand the bending stress is found out by using the formula for bending stress. This area is divided among several stringers which are spaced evenly. The stringers spacing is calculated by considering the buckling of the portion between adjacent stringers which can be modeled as a plate. Now, the first step is to calculate the required cross-sectional area of the stringers. Use the following formula for bending stress.

$$\sigma = \frac{My}{I} \quad (3\text{-}50)$$

Depending on the historical data collected for number of stringers & their distribution along fuselage section, the section below is taken at maximum bending moment:

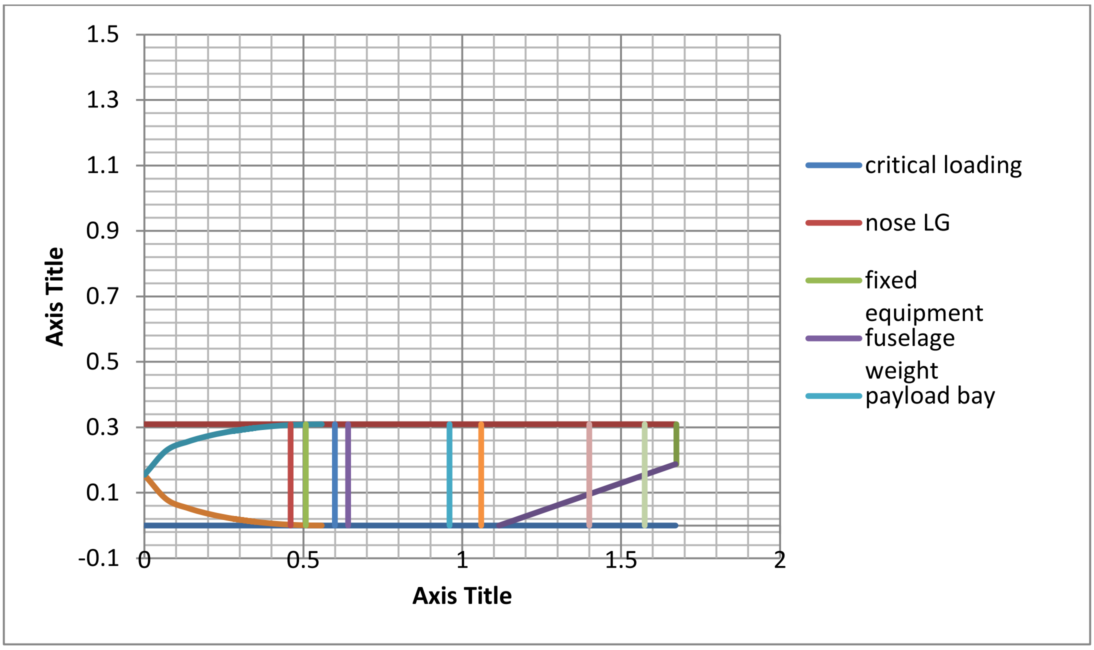

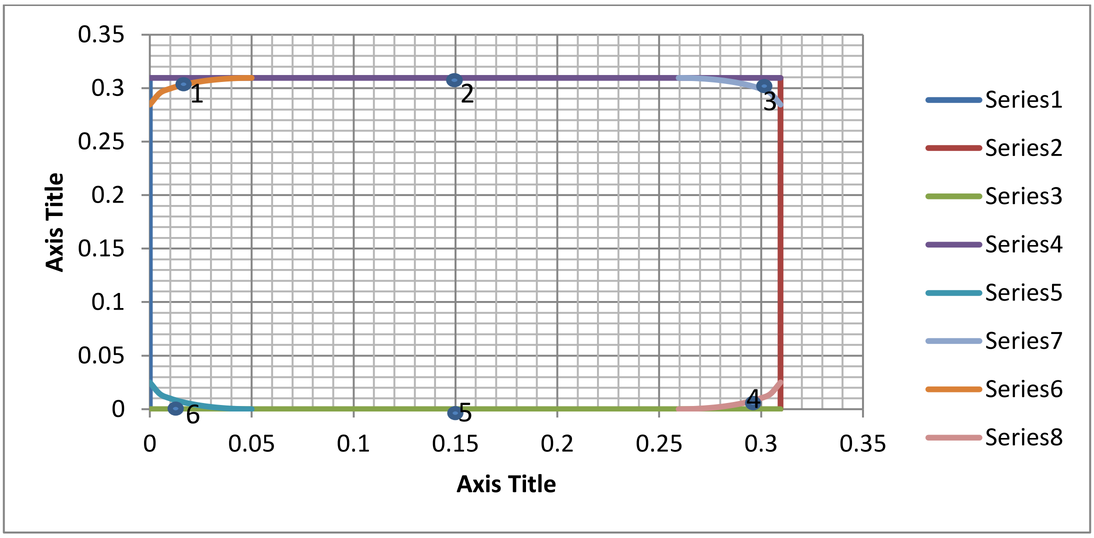

Figure 3-10: critical loaded fuselage section

$$\therefore I_{xx} = \sum By^2 = B[6 * 0.14524^2] = 0.1266B$$

$$\sigma_{mat} = \frac{My}{I} \Rightarrow I_{xx} = \frac{My_{max}}{\sigma_{mat}} \Rightarrow 0.1266B = \frac{4284.648 * 0.14524}{\sigma_{mat}}$$

$$\Rightarrow B = \frac{4915.500}{\sigma_{mat}}$$

The boom's area shall vary according to the material selected.

3.3.6 Material selection:

The actual selection of a material for a particular design application can be an easy one, say, based on previous applications (1020 steel is always a good candidate because of its many positive attributes), or the selection process can be as involved and daunting as any design problem with the evaluation of the many material physical, economical, and processing parameters. There are systematic and optimizing approaches to material selection. One basic technique is to list all the important material properties associated with the design, e.g., strength, stiffness, and cost. This can be prioritized by using a weighting measure depending on what properties are more important than others. Next, for each property, list all available materials and rank them in order beginning with the best material; e.g., for strength, high-strength steel such as 4340 steel should be near the top of the list. For completeness of available materials, this might require a large source of material data. Once the lists are formed, select a manageable amount of materials from the top of each list. From each reduced list select the materials that are contained within every list for further review. The materials in the reduced lists can be graded within the list and then weighted according to the importance of each property. The performance metric P of a structural element depends on the functional requirements (F), the geometry (G), and the material properties of the structure (M). That is:

$$P = [(F).(G).(M)] \quad \text{(3-51)}$$

Since the load is varying along the fuselage, there is no simple approach to adopt for selection of material. By taking candidates of the material used in the previous UAVs, such as aluminum 2017, 2024 T4, 7075 T6, 2024 T4 extrusion, steel 4130, 4130 wrought. By taking the fuselage as a simple beam structure with free edges and the reaction load (maximum load) as a fixed load in its position, we can adopt a crude material selection between the material candidates:

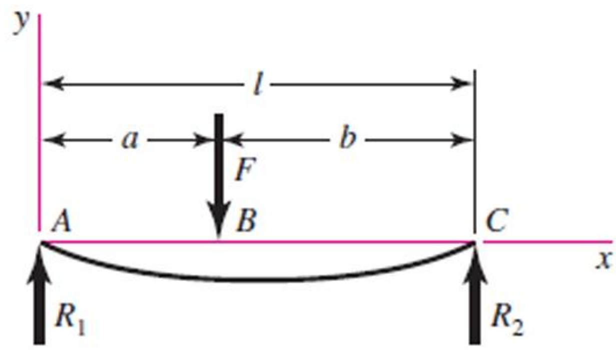

Figure 3-11: fuselage as beam with inertia load

$$y_{AB} = \frac{Fbx}{6ELl}(x^2 + b^2 - l^2) \quad \text{(3-52)}$$

$$y_{BC} = \frac{Fa(l-x)}{6ELl}(x^2 + a^2 - 2lx) \quad \text{(3-53)}$$

$$k_{AB} = \frac{6EIl}{bx(x^2+b^2-l^2)} \quad \text{(3-53)}$$

$$k_{BC} = \frac{6EIl}{a(l-x)(x^2+a^2-2lx)} \quad \text{(3-54)}$$

For optimum design, we desire to maximize or minimize *P*. With regards to material properties alone, this is done by maximizing or minimizing *f* (*M*), called the material efficiency coefficient.

The stiffness of the UAV regarded as a beam is related to its material and geometry. The stiffness of a beam is given by equations above. The mass of the beam is given by:

$m = \rho Al$

$$\therefore k_{AB} = \frac{6El\sum By^2}{bx(x^2+b^2-l^2)} \Rrightarrow B_1 = \frac{k_{AB}bx(x^2+b^2-l^2)}{6El\sum y^2}$$

$$k_{BC} = \frac{6El\sum By^2}{a(l-x)(x^2+a^2-2lx)} \Rrightarrow B_2 = \frac{k_{BC}a(l-x)(x^2+a^2-2lx)}{6El\sum y^2}$$

$\therefore m_1 = \rho \frac{k_{AB}bx(x^2+b^2-l^2)}{6E\sum y^2}$………………………...…...…...……. (3-55)

$m_2 = \rho \frac{k_{BC}a(l-x)(x^2+a^2-2lx)}{6E\sum y^2}$………………………...………. (3-56)

The term ${}^{1}/{}_{6E\sum y^2}$ is simply a constant and can be associated with any function. Thus, the functional requirement, stiffness; the geometric parameter, length; and the material efficiency coefficient as:

$F_1 = \frac{k_{AB}}{6E\sum y^2}$…………………………..………...………...… (3-57)

$F_2 = \frac{k_{BC}}{6E\sum y^2}$…………………………….....………...……… (3-58)

$f(F) = F_1 + F_2$

$G_1 = bx(x^2+b^2-l^2)$……………………………………..… (3-59)

$G_2 = a(l-x)(x^2+a^2-2lx)$…………………...……...… (3-60)

$f(G) = G_1 + G_2$

$M = \frac{E}{\rho}$……………………..…………………......…...……… (3-61)

$$F(M) = \frac{1}{M} \qquad (3\text{-}62)$$

$$\therefore P = \frac{f(F).f(G)}{M}$$

By using the relations above, the material index & performance metric values are shown for the material candidates:

Table 5: Material candidates

Number of material	Name
1	aluminum2017
2	aluminum2024 T4
3	Steel 4130
4	aluminum 7075 T6
5	Steel 4130 wrought
6	aluminum2024 T4 ext.
7	aluminum 7075 T6 ext.

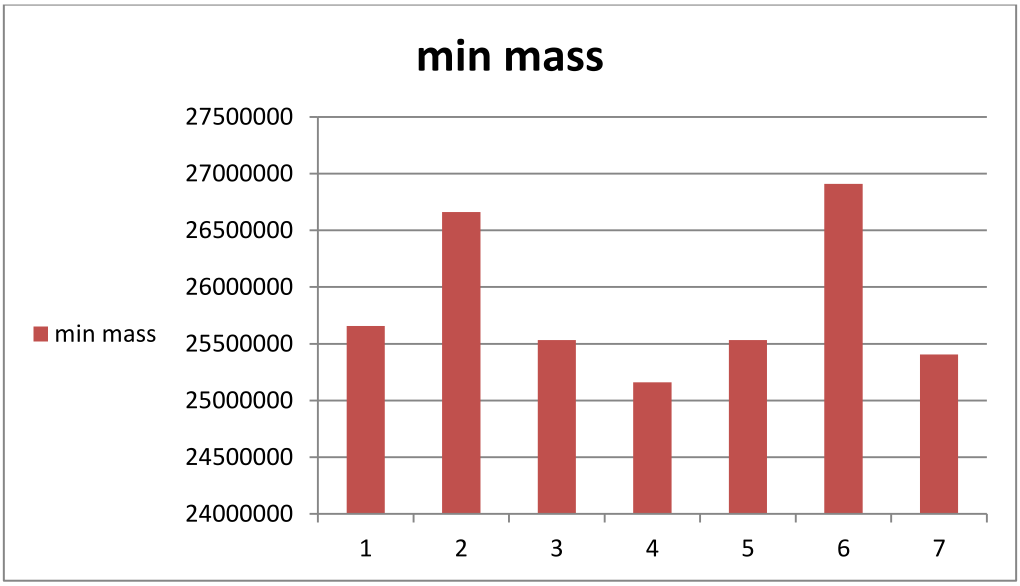

Figure 3-12: minimum mass indicating number

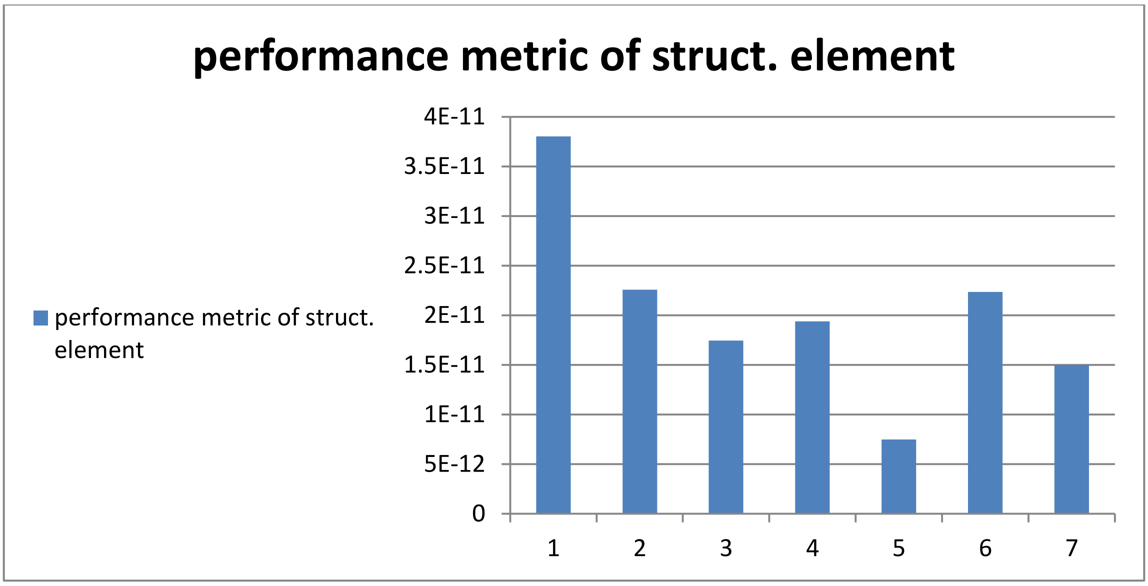

Figure 3-13: performance metric of structure element

From the figures shown above, aluminum 2017 has been selected as the primary material for this UAV.

3.3.7 Stress analysis of fuselage structure:

For aluminum 2017:

Unless otherwise provided, a factor of safety of 1·5 must be used depending upon **CS-VLA 303.**

$$\sigma_{mat} = 220706719.6\frac{N}{m^2} \Rightarrow \sigma_{mat} = \frac{220706719.6}{1.5}$$
$$= 147137816.1\frac{N}{m^2}$$

The boom's area required:

$$B = \frac{4915.500}{\sigma_{mat}} = \frac{4915.500}{147137816.1} = 0.0000334159\, m^2$$

$$I_{xx} = 0.1266B = 0.1266 * 0.0000334159 = 0.00000282m^4$$

Table 6: Stress analysis

No	Boom's area(m^2)	x	y	$\boldsymbol{\sigma_x = \frac{4284.648}{2.82 * 10^{-6}} * y}$
1	0.0000334159	-0.13976	0.14524	
2	0.0000334159	0	0.14524	220674565.8
3	0.0000334159	0.13976	0.14524	220674565.8
4	0.0000334159	0.13976	-0.14524	-220674565.8
5	0.0000334159	0	-0.14524	-220674565.8
6	0.0000334159	-0.13976	-0.14524	-220674565.8

$$\therefore the\ safety\ factor\ for\ our\ UAV = \frac{220706719.6}{220674565.8} = 1.000146$$

Shear flow along skin of fuselage:

$$q_S = -\left[\frac{V_x I_{XX} - V_y I_{xy}}{I_{xx} I_{yy} - {I_{xy}}^2} \sum Ax\right] - \left[\frac{V_y I_{yy} - V_x I_{xy}}{I_{xx} I_{yy} - {I_{xy}}^2} \sum Ay\right] \ldots\ldots\ldots\ldots\ldots \text{(3-63)}$$

Where:

$V_x = 0,\ V_y = 7148.526$ (Max. Shear Force from shear force diagram)

The shear flow equation gets simplified to:

$$q_S = -\left[\frac{V_y}{I_{xx}} \sum By\right] \ldots\ldots\ldots\ldots\ldots\ldots\ldots\ldots\ldots\ldots\ldots\ldots \text{(3-64)}$$

Table 7: shear flow distribution along fuselage skin

Boom's no	Boom's area	Y	$q_{b,n}$
1	0.0000334159	0.14524	-12302.9
2	0.0000334159	0.14524	-24605.8
3	0.0000334159	0.14524	-36908.6
4	0.0000334159	-0.14524	-24605.8
5	0.0000334159	-0.14524	-12302.9
6	0.0000334159	-0.14524	0

$$M_{xx} = \sum q_{b,n}.P.y + q_{s,0}\ .A \ldots\ldots\ldots\ldots\ldots\ldots\ldots\ldots\ldots\ldots\ldots \text{(3-65)}$$

$$\therefore q_{s,0} = \big((q_{s,12} * 0.13976 * 0.14524) + (q_{s,23} * 0.13976 * 0.14524) + (q_{s,34} * 0.27952 * 0.13976) + (q_{s,45} * 0.13976 * -0.14524) + (q_{s,56} * 0.13976 * -0.14524)) - 4284.648\big)/(0.30952^2)$$

$$q_{s,0} = -59.7740\ N/mm$$

$$q_{s,12} 72.0769\ N/mm$$

$$q_{s,23} = -84.3798\ N/mm$$

$$q_{s,34} = -96.6827\ N/mm$$

$$q_{s,45} = -84.3798\ N/mm$$

$$q_{s,56} = -72.0769\ N/mm$$

$$q_{s,61} = -59.7740\ N/mm$$

The critical shear flow is found to occur in elements between 3 and 4. The critical shear flow value is 96.6827 N/mm.

$$\tau = 227603805\ N/m^2$$

$$\tau_{allowable} = \frac{227603805}{1.5} = 151735870\ N/m^2$$

$$\tau_{allowable} = 1.5 * \frac{q}{t} \Rightarrow t = 1.5 * \frac{q}{\tau_{allowable}} = 1.5 * \frac{96687.2}{151735870}$$

$$\Rightarrow t = 0.9558\, mm \approx 1mm$$

The above value of skin thickness is within the standard limits.

3.3.8 Sizing of the main members in fuselage structure:

Stringer design:

In the case of separate Zed-section stringers the width of each of the shorter flanges is often about 40 per cent of stringer height, giving a total cross-section area of $(1.8ht)$ where hand t are the stringer height and thickness, respectively.

The assumption that the total stringer area is 35 per cent of the cover effective area leads to:

$$0.35t_e \times 3.5h_s = 1.8h_s \times t_s$$

So that approximately:

$t_s = 0.68t_e$………………….……………….......…...…… (3-66)

$= 0.68 * 1 = 0.68\, mm$

This suggests that the stringer thickness should be about the same as the cover skin thickness (t). Further the width to thickness ratio of the free flange is typically about 16 to match the local and overall buckling. Thus $0.4h$, is equal to $16t_s$, and:

$h_s = 40t_s$……………………………….……........……… (3-67)

$= 40 * 0.68 = 27.2\, mm$

$w_s = 0.4h_s$……………………...………..…………...…… (3-68)

$= 0.4 * 27.2 = 10.8\, mm$

As the figure of the main section of the UAV shows, the pitch is about 0.13976m between stringer 1-2, 2-3, 4-5, 5-6 & about 0.29048m between 3-4, 6-1.-

The stringer area $= 72{t_s}^2$…………...…...………………… (3-69)

$= 72 * 0.68^2 = 33.2928\ \mathrm{mm}^2 = 0.0000332928\mathrm{m}^2$

3.4 Wing detail design:

Wing layout:

The wing may be considered as the most important component of an aircraft, since a fixed-wing aircraft is not able to fly without it. Thus this section will consider wing geometrical Parameters. The Process of wing design has been adopted from [7], which is showed in the following chart:

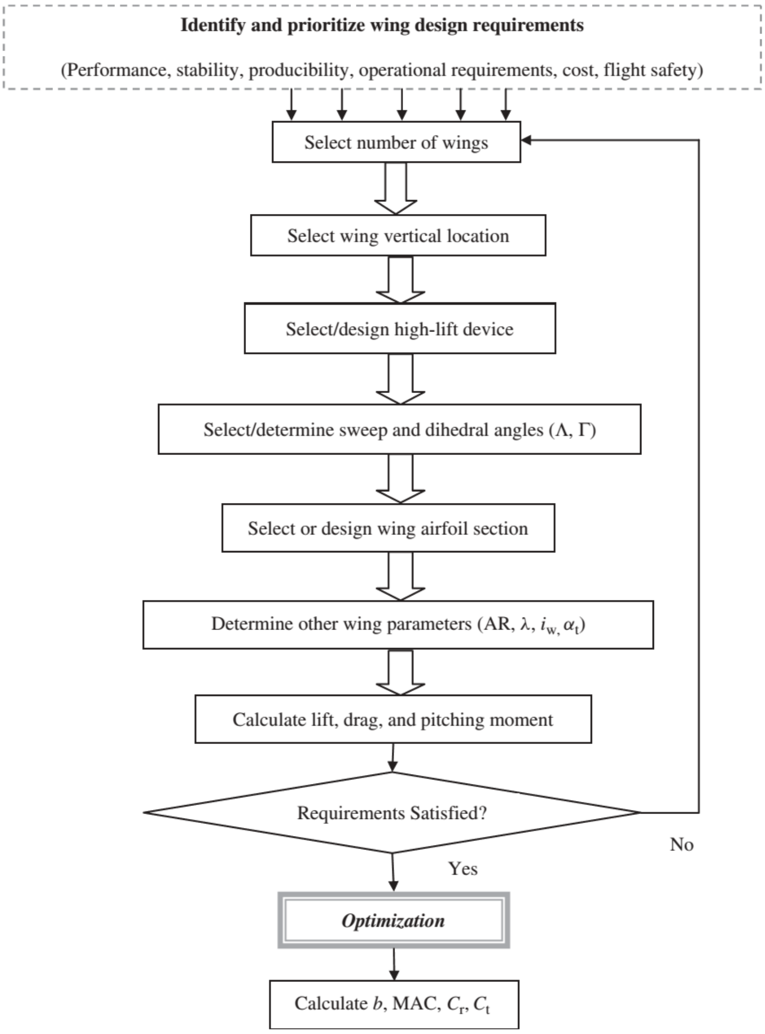

Figure 3-14: wing layout

1-Design requirements

- Performance requirements: major performance requirements are stall speed, maximum speed, take-off run, range, and endurance. these requirements have been already taken in determining wing area in conceptual work.
- Stability and control requirements: include lateral-directional static stability, lateral-directional dynamic stability, and aircraft controllability during probable wing stall. [7],
- Producibility requirements.
- Operational requirements.
- Cost.
- Flight safety.

2-Number of Wings

Tree-wing is not an option (it's not practical at all).in other side bi-plan has disadvantages of being higher weight, lower lift & reduce visibility. [7],

Thus the obvious and the most recently used option in modern aircraft is the mono-plan wing.

3-wing vertical location

This wing parameter will influence the design of other aircraft components directly; including aircraft tail design, landing gear design, and center of gravity.
Since we are incorporating a reconnaissance UAV the visibility is very importance
& as the stability is of major concern (lateral stability) the high wing is the better choice.

4- Airfoil Section

Airfoil section is the most important parameter after wing area; such that the wing depends on its cross section parameter [7], the airfoil selection process has been preceded with concern to the following criterion:

1. The airfoil with the required maximum lift coefficient ($Cl_{max} <= 1.57$).

2. The airfoil with the proper ideal or design lift coefficient (Cld or Cli).

3. The airfoil with the lowest minimum drag coefficient (Cdmin).

4. The airfoil with the highest lift-to-drag ratio ((Cl/Cd)max).

5. The airfoil with the highest lift curve slope (Clαmax).

6. The airfoil with the lowest (closest to zero; negative or positive) pitching moment coefficient (Cm).

7. The proper stall quality in the stall region.

8- Ease of Manufacture.

Airfoil Selection process:

To go on with trends, a similar UAV had been studied (appendix) and the following Airfoil list in considered:

Table 8: airfoil selection parameter

Airfoil	CLmax	CLi	L/D	CM0	$\alpha_{l=0}$	t_{max}
2412	1.411	0.2	102.1	-0.0556	-2.220	0.12
4415	1.565	0.4	123.9678	-0.104	-4.20	0.15
23012	1.508	0.3	94.88889	-0.0115	-1.240	0.12
Fx61147	1.422	-	120	-0.1237	-5.160	0.1476

Thus we will compare this airfoil to get best one suite our design:

❖ Firstly we need to calculate the following:

$$CL_c = \frac{2*W_{avg}}{\rho * V_C * S} = 0.40132$$

$$CL_{cw} = \frac{CL_c}{0.95} = 0.421$$

$$CL_i = \frac{CL_{cw}}{0.9} = 0.467$$

$$CL_{max} = \frac{2 * W_{TO}}{\rho * V_S * S} = 1.67$$

❖ Secondly Compare between Airfoil Sections

- Worttman fx61147 has a very good characteristics, that it give good climb performance, progressive stall, clmax insensitivity to dust or rain contamination, and a small cm,ac/4 that reduces the drag penalty associated with balancing the aircraft.

But its cusp at the trailing edge causes three disadvantages; first of all it gives the airfoil a higher pitching moment coefficient; second, it makes control surface structure weaker; third, harder to manufacture. Thus this airfoil has been eliminated.

- Laminar airfoil likes 23012 had good characteristics, but its sharp stall eliminates it of our consideration.
- Finally we have two airfoils 2412 & 4415, there are two reasons let us take 4415; firstly 2412 has ideal lift of 0.2 that's mean it will need for higher incidence angle to achieve the required cruise lift this will result in a higher cruise drag which degrade performance and increase flight cost; secondly, the thicker the airfoil the easier its manufacture to be.

5-Wing Incidence

The wing incidence is calculated from

$i_w = \frac{CL_c}{a} + \alpha_0$.. (3-70)

$CL_c = 0.4$, a = 0.09436

$i_w = 0.039$ deg

6-Aspect ratio

The AR has been determined in Conceptual Work.

7-Taper ratio

This parameter has direct effect on aerodynamic behavior, that's the larger its value the good stall behavior results (stall from root to tip), also it affect wing structural weight the lower the LAMBDA the lighter the wing structure(Anderson). Thus this value is determined by a compromise between wing structure weights and aerodynamic behavior. We have taken aerodynamic property as upper priority. Thus the value of lambda should give a favorable lift distribution as could be to achieve this and also to insure the required lift during cruise; wing setting angle, aspect ratio & lambda need to be adjusted. Matlab code had been written to compromise between different values of lambda (appendix).the plotting result is as shown below:

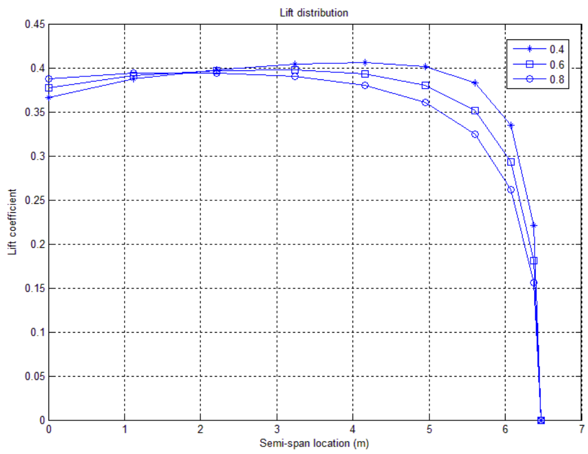

Figure 3-15: lift distribution for different taper ratio

The observation is as follows:

1- Since lambda of one is not considered the nearest elliptic distribution is at lambda = 0.8
2- The m-file also yields the lift coefficient as 0.3396 which is less than the required value of 0.421

Therefore we need to back & change some wing parameters, by trial and error following result is found:

AR = 11.3, λ = 0.8, iw=1.06deg

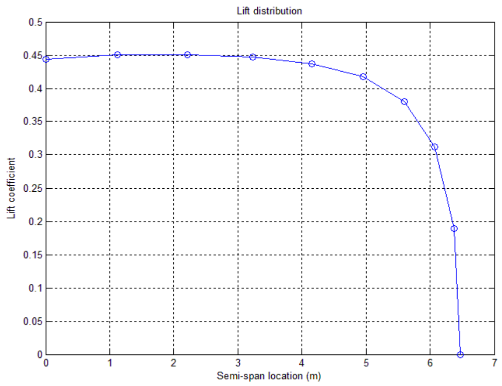

Figure 3-16: lift distribution

CLw = 0.4217

8-sweep angle: for low speed flight sweep angle is not required.

9-twist angle: for ease of manufacturing there is no twist.

10- Dihedral effect: historical value of 2 degree has been selected & it will be revised at stability analysis work.

3.3.9 Wing Structure Design:

Overview:

The structural design of UAV actually begins with the flight envelope or V-n diagram, which clearly limits the maximum load factors that the UAV can withstand at any particular flight velocity. However in normal practice the UAV might experience loads that are much higher than the design loads. Some of the factors that lead to the structural overload of an UAV are high gust velocities, sudden movements of the controls, fatigue load in some cases, bird strikes or lightning strikes. So to add some inherent ability to withstand these rare but large loads, a safety factor of 1.5 is provided during the structural design.

The two major members that need to be considered for the structural design of an airplane are wings and the fuselage. As far as the wing design is concerned, the most significant load is the bending load. So the primary load carrying member in the wing structure is the spar (the front and rear spars) whose cross section is an 'I' section. Apart from the spars to take the bending loads, suitable stringers need to take the shear loads acting on the wings.

3.3.10 Schrenk's Curve:

Description:

Lift varies along the wing span due to the variation in chord length, angle of attack and sweep along the span. Schrenk's curve defines this lift distribution over the wing span of an aircraft, also called simply as Lift Distribution Curve. Schrenk's Curve is given by:

$$y = \frac{y_1 + y_2}{2} \qquad (3\text{-}71)$$

$$a = \frac{b}{2} \qquad (3\text{-}72)$$

Linear Lift Distribution:

Lift at root:

$$L_{root} = 1/2\,\rho V^2 C_L c_{root} \qquad (3\text{-}73)$$

$$L_{root} = 239.932\ N$$

Lift at tip:

$$L_{tip} = 1/2\,\rho V^2 C_L c_{tip} \qquad (3\text{-}74)$$

$$L_{tip} = 132.092\ N$$

By representing this lift at sections of root and tip we can get the equation for the wing.

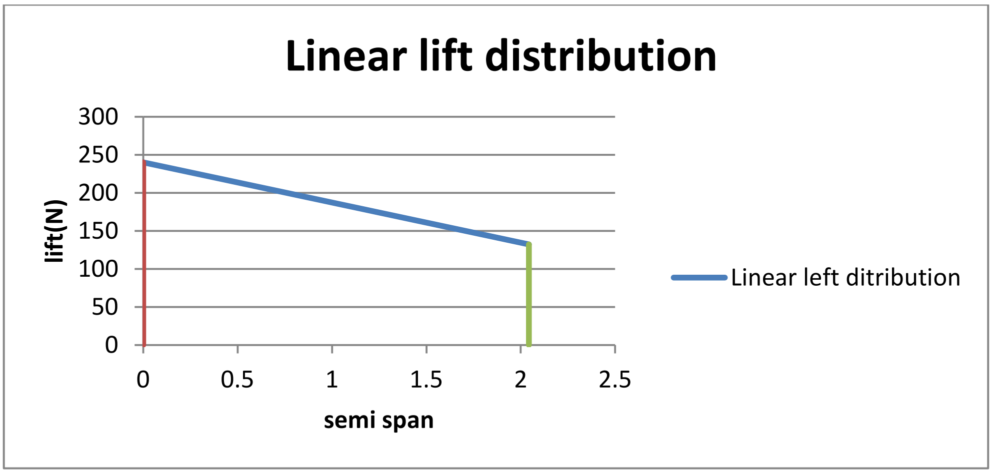

Figure 3-17: linear lift distribution

Equation of linear lift distribution for starboard wing:

$$y_1 = 239.932 - 52.785307x$$

Twice the area under y= Total lift=380.022 N ≈ Take off Gross Weight

For the Schrenk's curve we only consider half of the linear distribution of lift:

$$\frac{y_1}{2} = 119.966 - 26.3926535x$$

Elliptic Lift Distribution:

Twice the area under the curve or line will give the lift which will be required to overcome weight.

Considering an elliptic lift distribution we get:

$$\frac{L}{2} = \frac{W}{2} = \frac{\pi a b_1}{2} \text{ .... } (3\text{-}75)$$

$$A = \frac{\pi a b_1}{2} \text{ .... } (3\text{-}76)$$

Lift at tip:

$$b_1 = \frac{4W}{2\pi a} \text{ .... } (3\text{-}77)$$

$$b_1 = 118.333998\ N/m$$

Equation of elliptic lift distribution:

$$y_2 = 115.843\sqrt{4.174 - x^2}$$

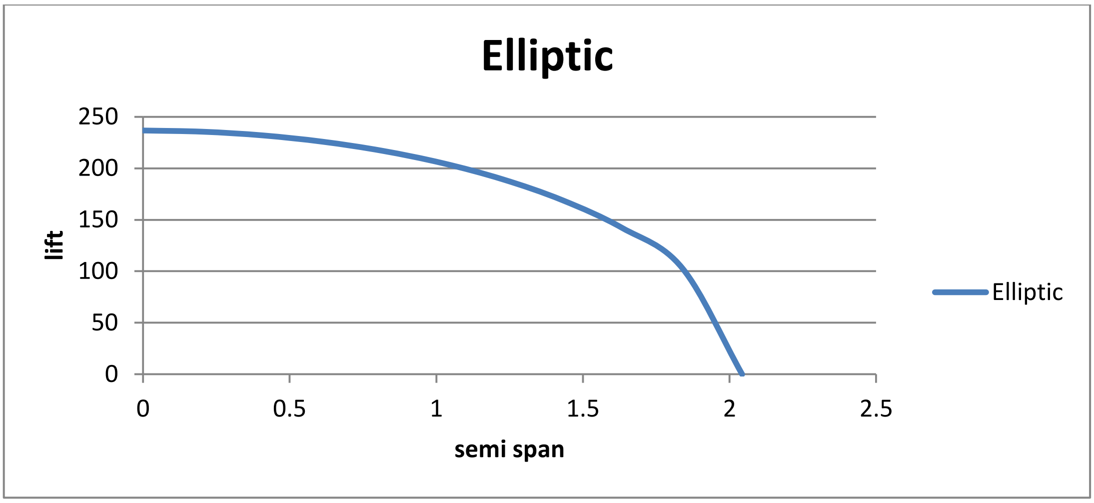

Figure 3-18: elliptical lift distribution

$$\frac{y_2}{2} = 57.9215\sqrt{4.174 - x^2}$$

Construction of Schrenk's Curve:

Schrenk's Curve is given by:

$$y = \frac{y_1 + y_2}{2}$$

$$y = \frac{239.932 \; - 52.785307x + 115.843\sqrt{4.174 - x^2}}{2}$$

$$y = 119.966 - 26.3926535x + 115.843\sqrt{4.174 - x^2}$$

Substituting different values for x we can get the lift distribution for the wing semi span:

Table 9: load acting in wing

X(-)	X(+)	$\frac{y_1}{2}$	$\frac{y_2}{2}$	$\frac{y_1 + y_2}{2}$
0	0	239.932	236.667997	238.299973
-0.2043	0.2043	229.1479	235.481683	232.314798
-	0.4086	218.3639	231.886332	225.125103

0.4086				
-0.6129	0.6129	207.5798	225.76688	216.673358
-0.8172	0.8172	196.7958	216.909802	206.8528
-1.0215	1.0215	186.0118	204.960497	195.486128
-1.2258	1.2258	175.2277	189.334397	182.281059
-1.4301	1.4301	164.4437	169.014756	166.729219
-1.6344	1.6344	153.6596	142.000798	147.830221
-1.8387	1.8387	142.8756	103.161188	123.018397
-2.043	2.043	132.0916	0	66.0457841

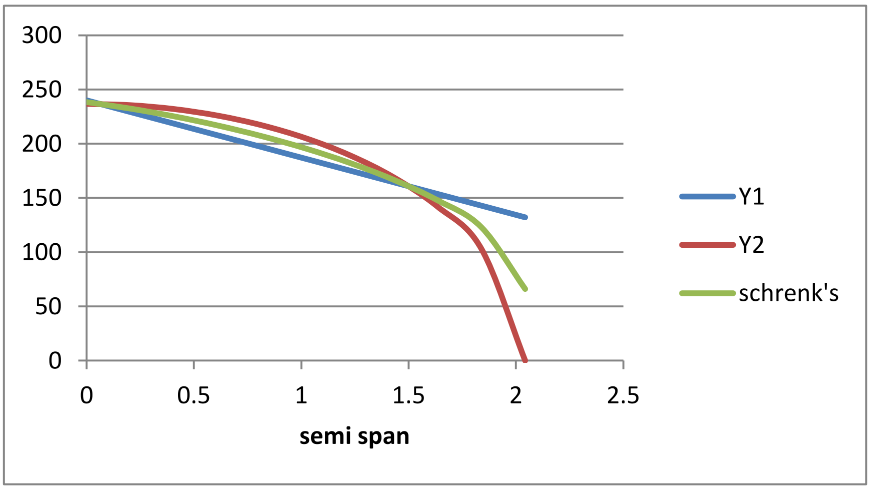

Figure 3-19: shrenk's load distribution for semi span

Replacing x by –x for port wing we can get lift distribution for entire span.

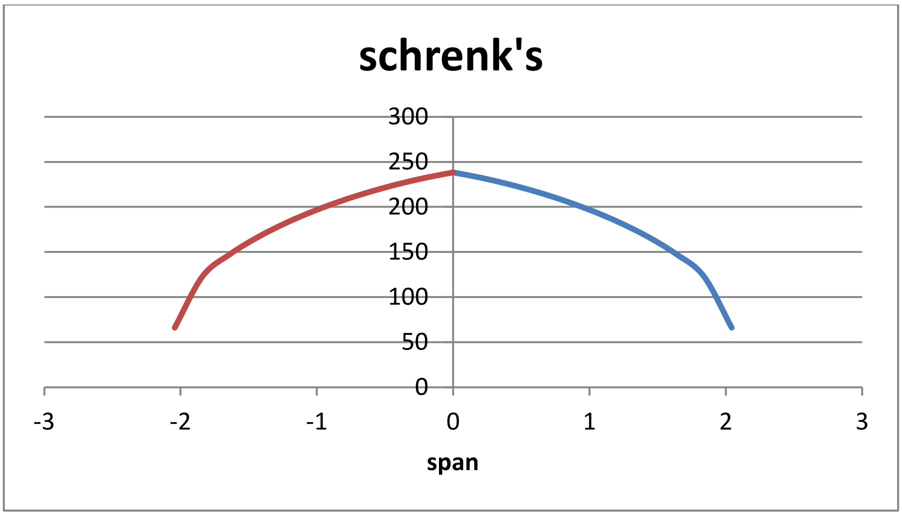

Figure 3-20: shrink's load for the wing

3.3.11 Load Estimation on wings

Description:

The solution methods which follow Euler's beam bending theory (σ/y=M/I=E/R) use the bending moment values to determine the stresses developed at a particular section of the beam due to the combination of aerodynamic and structural loads in the transverse direction. Most engineering solution methods for structural mechanics problems (both exact and approximate methods) use the shear force and bending moment equations to determine the deflection and slope at a particular section of the beam.

Therefore, these equations are to be obtained as analytical expressions in terms of spa wise location. The bending moment produced here is about the longitudinal (x) axis.

Loads acting on wing:

As both the wings are symmetric, let us consider the starboard wing at first. There are three primary loads acting on a wing structure in transverse direction which can cause considerable shear forces and bending moments on it. They are as follows:

- Lift force (given by Schrenk's curve)
- Self-weight of the wing

Shear force and bending moment diagrams due to loads along transverse direction at cruise condition:

Lift Force given by Schrenk's Curve:

$$y = \frac{y_1 + y_2}{2}$$

$$y = 119.966 - 26.3926535x + 115.843\sqrt{4.174 - x^2}$$

Self-weight of the wing:

Self-Weight (y3):

$$W_{wing} = 2.5 * W_{TO} = 3.6825\ kg$$

$$W_{portwing} = 1.84125\ kg$$

$$W_{starwing} = 1.84125\ kg$$

Assuming parabolic weight distribution:

$y_3 = k\left(x - \left(\frac{b}{2}\right)\right)$ .... (3-78)

When we integrate from x=0 (root location) to x=b (tip location) we get the net weight of port wing:

$$\int_0^{2.043} y_3 = \int_0^{2.043} k(x - 2.043)^2$$

$$1.84125 = \frac{k(2.043)^3}{3}$$

$$k = -8.547$$

$$y_3 = -8.547(x - 2.043)^2$$

Substituting various values of x in the above equation we get the self-weight of the wing.

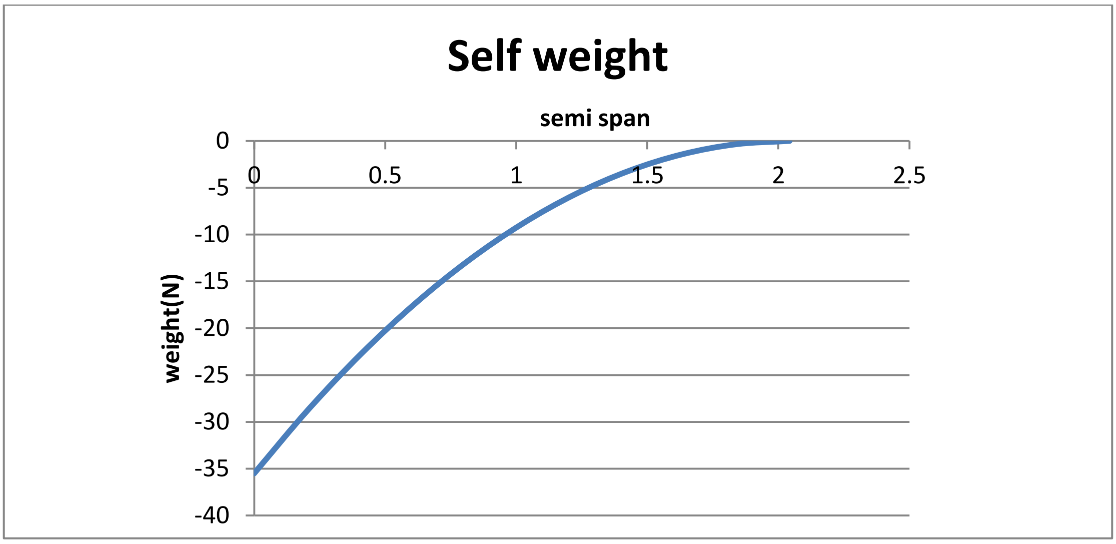

Figure 3-21: self-weight

Shear Force:

$$SF = \int \left\{\frac{y_1 + y_2}{2} + y_3 - V_A\right\} dx \quad \text{(3-79)}$$

$$SF = \int \Big\{119.966 - 26.3926535x + 115.843\sqrt{4.174 - x^2} - 8.547(x - 2.043)^2 - V_A\Big\} dx$$

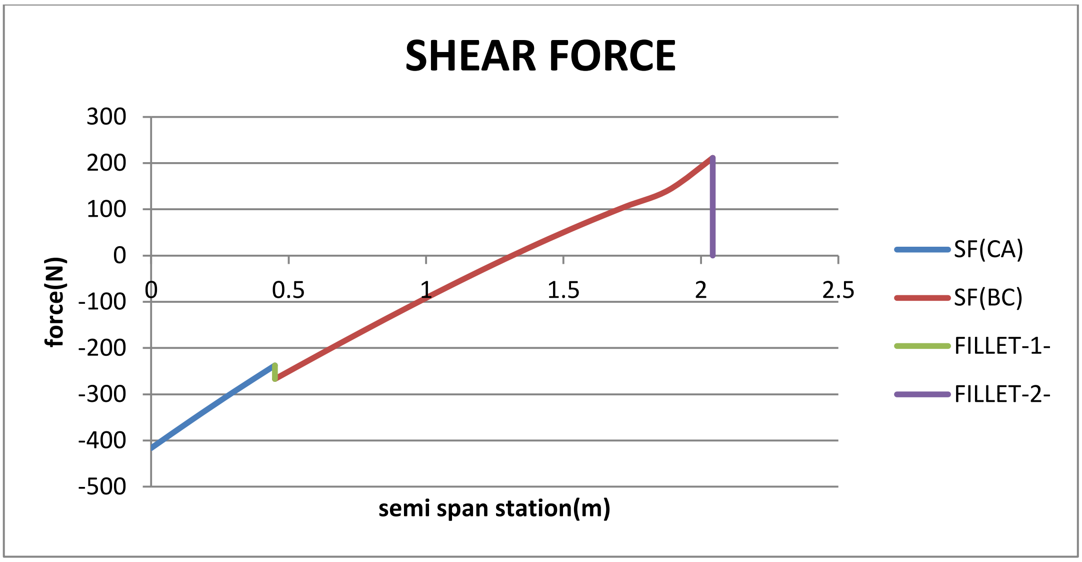

Figure 3-22: shear force diagram for wing

Bending moment:

$$BM = \iint \left\{\frac{y_1+y_2}{2} + y_3 - V_A\right\} dx + M_A \quad \text{(3-80)}$$

$$BM = \iint \left\{119.966 - 26.3926535x + 115.843\sqrt{4.174 - x^2} - 8.547(x - 2.043)^2 - V_A\right\} dx + M_A$$

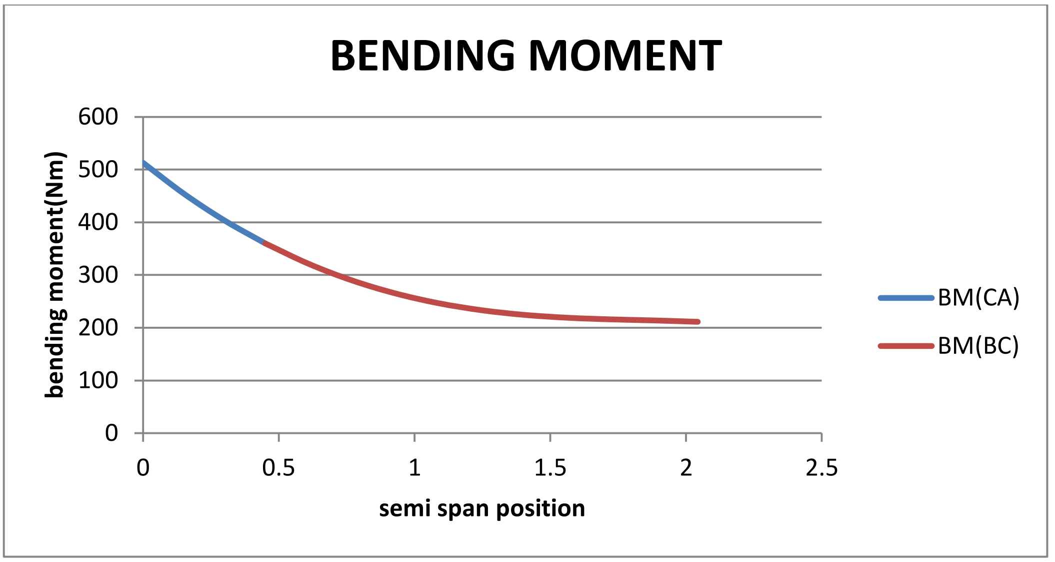

Figure 3-23: bending moment for the wing

Torque at cruise condition:

Torque due to normal force:

$$T_1 = 1/2\, \rho_\infty V_\infty^2 c C_n \left(\frac{x_{sc}}{c} - \frac{x_{ac}}{c}\right) \quad \text{(3-81)}$$

$$C_n = C_{Lmax}\alpha_w + C_{Dcr}\alpha_w = 1.226$$

$$T_1 = 51.443 * 0.031c^2 = 18.020758 * c^2$$

The equation for chord can also be represented in terms of x by taking c= mx +k:

$$c = (0.00456x^3 - 0.053x^2 + 0.2052x)$$

Therefore torque:

$$T_1 = 18.020758 \int c^2\, dx$$

$$T_1 = 18.020758 \int (0.00456x^3 - 0.053x^2 + 0.2052x)^2\, dx$$

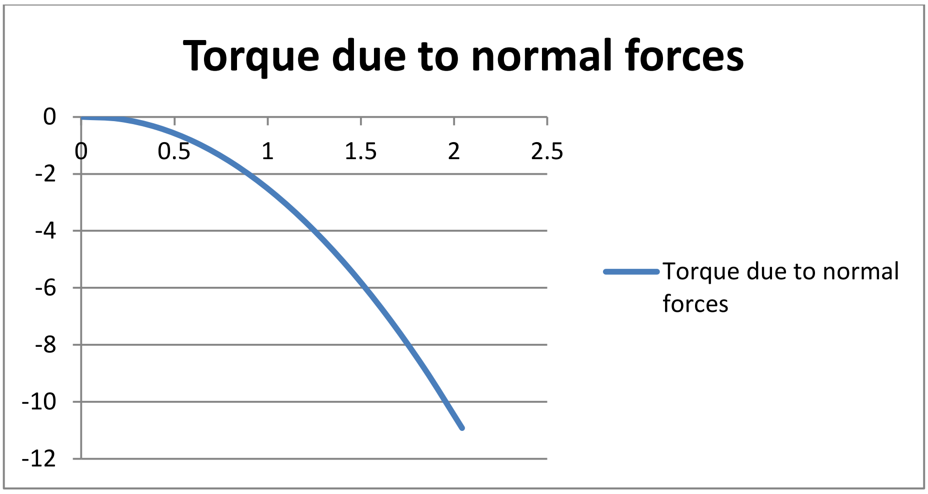

Figure 3-24: torque due to normal forces

Torque due to moment:

$$T_3 = 1/2\, \rho_\infty V_\infty^2 c^2 C_{Mac} \ldots \ldots \ldots \ldots \ldots \ldots \ldots \ldots \ldots \ldots \ldots \ldots \ldots \ldots \ldots \ldots \ldots \ldots \ldots \text{(3-81)}$$

$$C_{Mac} = -0.105$$

$$\therefore T_3 = -142.136c^2$$

$$T_3 = -142.136 \int (0.00456x^3 - 0.053x^2 + 0.2052x)^2\, dx$$

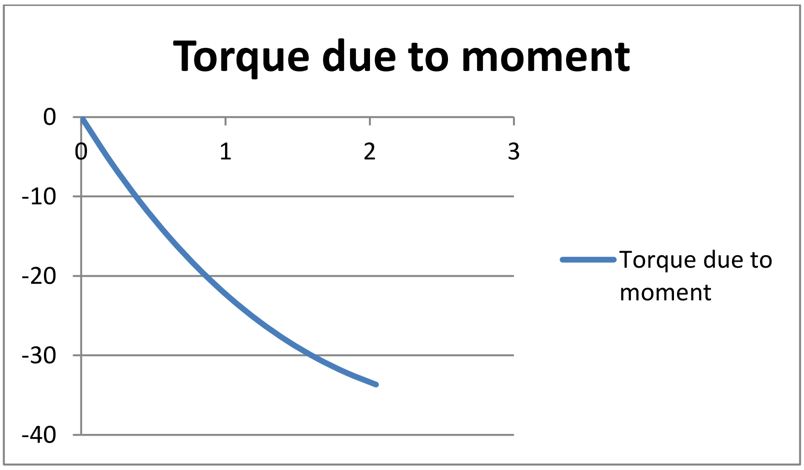

Figure 3-25: torque due to moment

The net torque will be sum of all the above torques:

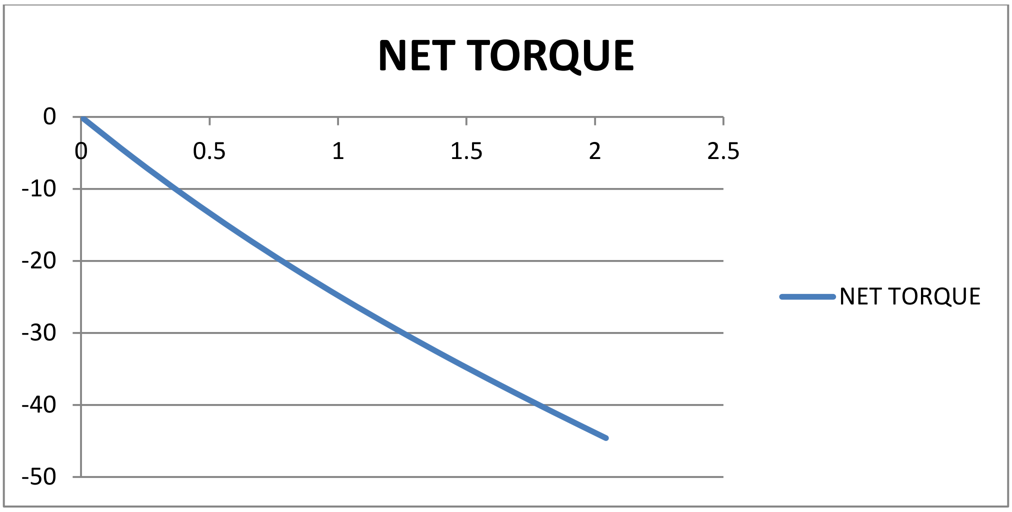

Figure 3-26: net torque

Load at Critical flight condition:

Optimum Wing structural design consists of determining that stiffness distribution which is proportional to the local load distribution. The aerodynamic forces of lift and drag are resolved into components normal and parallel to the wing chord. The distribution of shear force, bending moment and torque over the aircraft wing are considered for wing structural analysis.

By identifying the loads at point A as taken at the preliminary stage of structural design since it has the major load.

$(n_{max} = 3.8)$

$V_A = \frac{2n_{max}W_0}{\rho S C_{Lmax}} = 56.191\ m/sec$).

$$C_{Lcr} = \frac{2n_{max}W_0}{\rho V_D^2 S} = 1.601$$

It is seen that lift has increased by 3.28 times.

So we introduce a constant of proportionality for the lift alone.

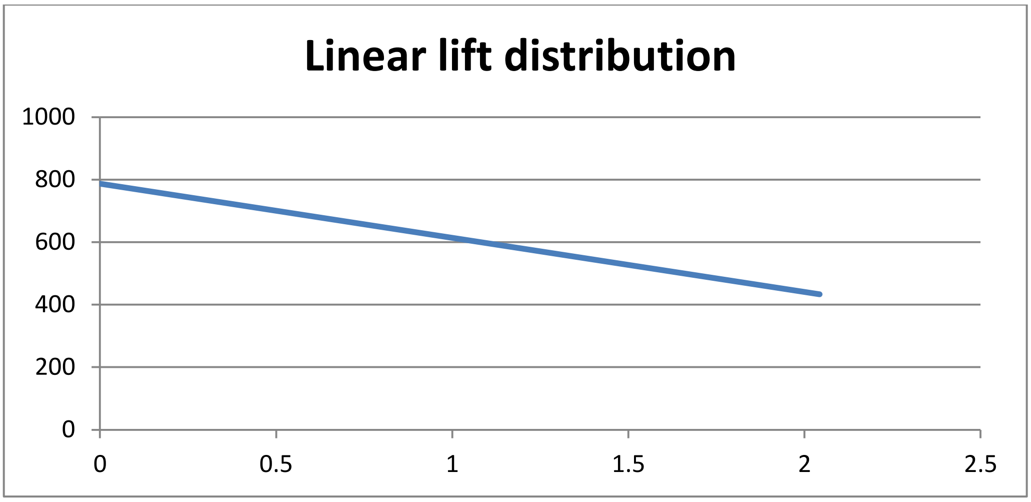

Figure 3-27: Linear lift distribution

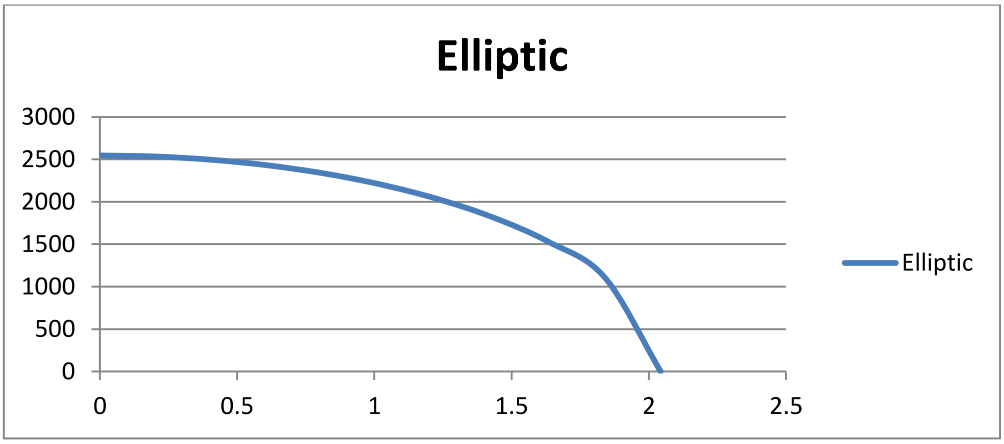

Figure 3-28: elliptical load distribution

The aim is to find the shear forces and bending moments due to normal forces in critical flight condition. There are two primary loads acting on a wing structure in transverse direction which can cause considerable shear forces and bending moments on it. They are as follows:

- Lift force (given by Schrenk's curve)
- Self-weight of the wing

Now, the proportionality constant influences the lift force alone and other factors remain unaffected.

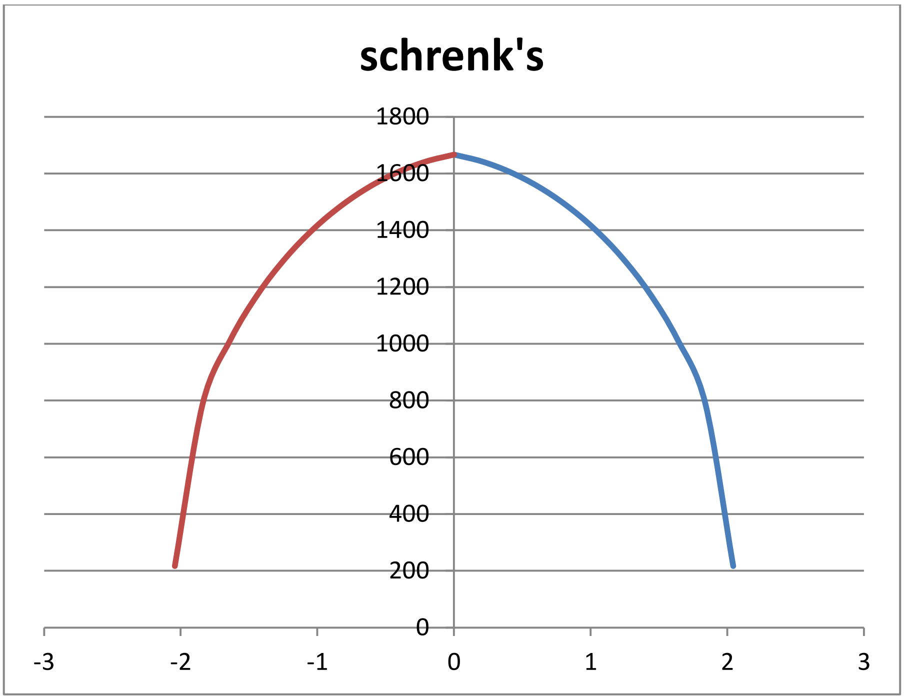

Figure 3-29: shrenk's for critical condition

Shear force and bending moment diagrams due to loads along transverse direction at critical condition:

$$SF = \int \left\{\frac{y_1+y_2}{2} + y_3 - V_A\right\} dx \quad \text{(3-82)}$$

$$SF = 3.28 \int \left\{119.966 - 26.3926535x + 115.843\sqrt{4.174 - x^2} - 8.547(x - 2.043)^2 - V_A\right\} dx$$

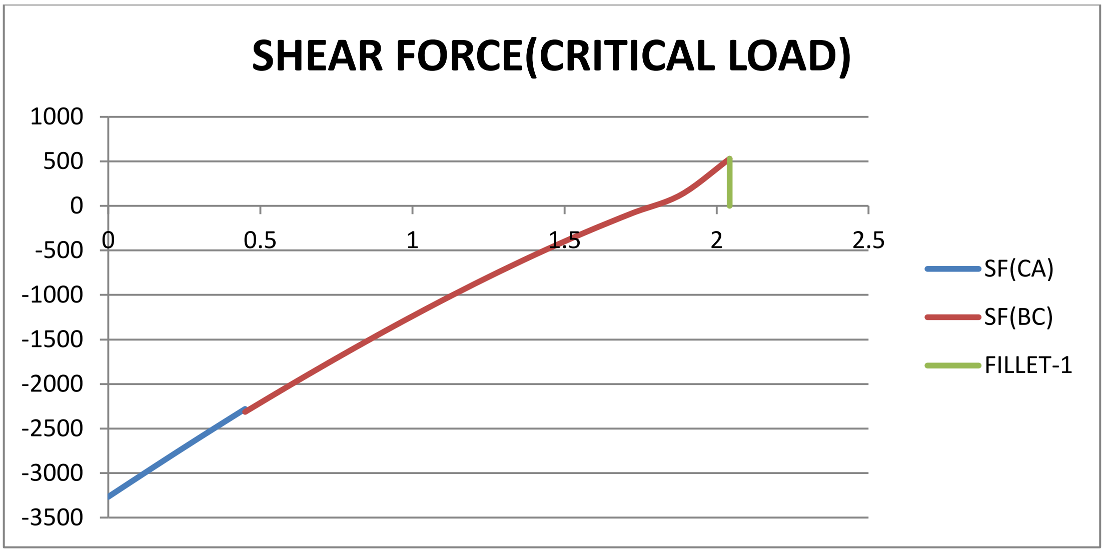

Figure 3-30:shear force

Bending moment:

$$BM = \iint \left\{\frac{y_1+y_2}{2} + y_3 - V_A\right\} dx + M_A \quad \text{(3-84)}$$

$$BM = 3.28 \iint \left\{119.966 - 26.3926535x + 115.843\sqrt{4.174 - x^2} - 8.547(x - 2.043)^2 - V_A\right\} dx + M_A$$

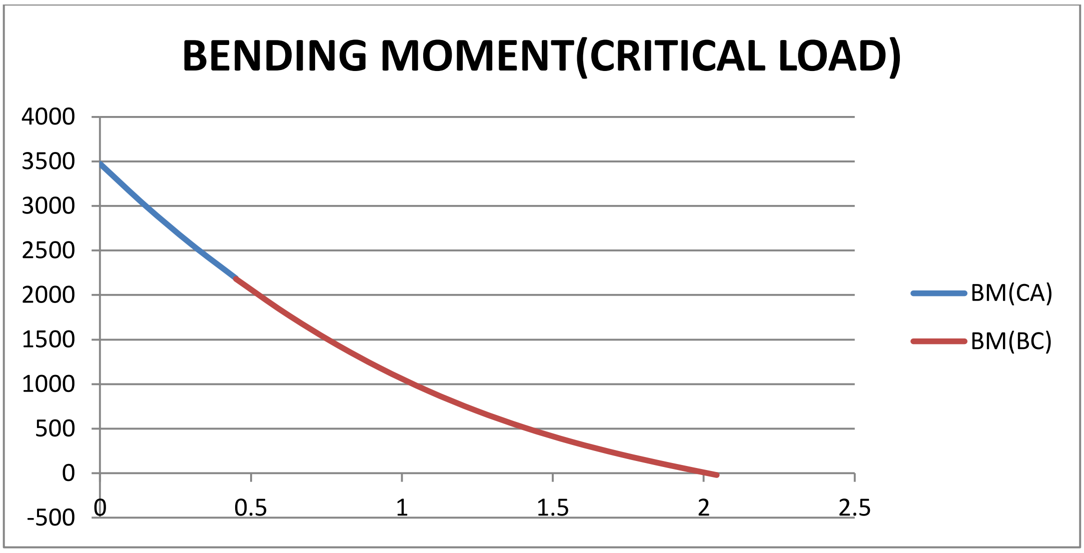

Figure 3-31: bending moment

Torque at critical flight condition:

Torque due to normal force:

$$T_1 = 1/2\,\rho_\infty V_\infty^2 c C_n \left(\frac{x_{sc}}{c} - \frac{x_{ac}}{c}\right) \quad \text{...} \; (3\text{-}85)$$

$$C_n = C_{Lmax}\alpha_w + C_{Dcr}\alpha_w = 1.558$$

$$T_1 = 93.384 * 0.031c^2 = 2.895 * c^2$$

the equation for chord can also be represented in terms of x by taking c= mx +k:

$$c = (0.00456x^3 - 0.053x^2 + 0.2052x)$$

Therefore torque:

$$T_1 = 2.895 \int c^2\,dx$$

$$T_1 = 2.895 \int (0.00456x^3 - 0.053x^2 + 0.2052x)^2\,dx$$

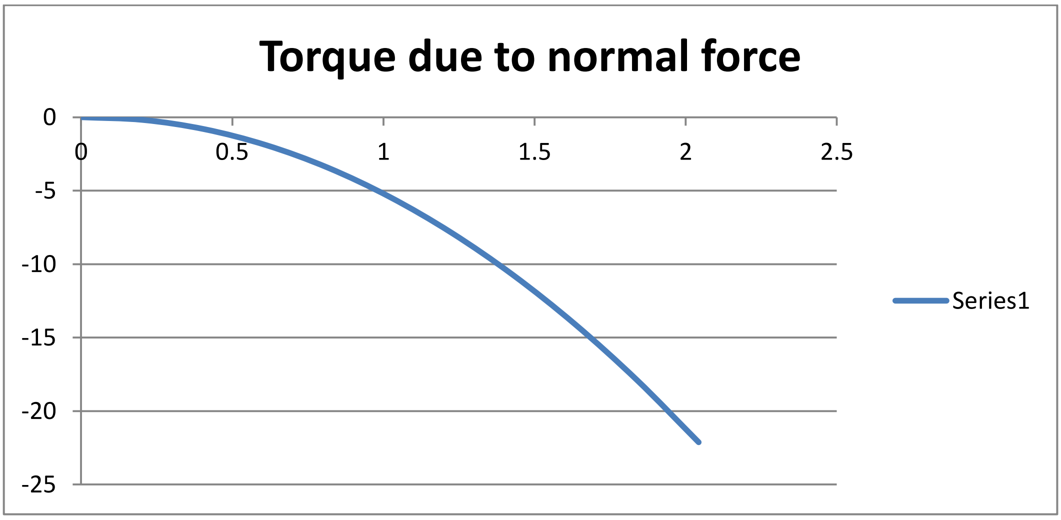

Figure 3-32: torque due to normal force for critical condition

Torque due to moment:

$T_3 = 1/2\,\rho_\infty V_\infty^2 c^2 C_{Mac}$ .... (3-85)

$$C_{Mac} = -0.0416$$

$$\therefore T_3 = -80.4513c^2$$

$$T_3 = -80.4513 \int (0.00456x^3 - 0.053x^2 + 0.2052x)^2\, dx$$

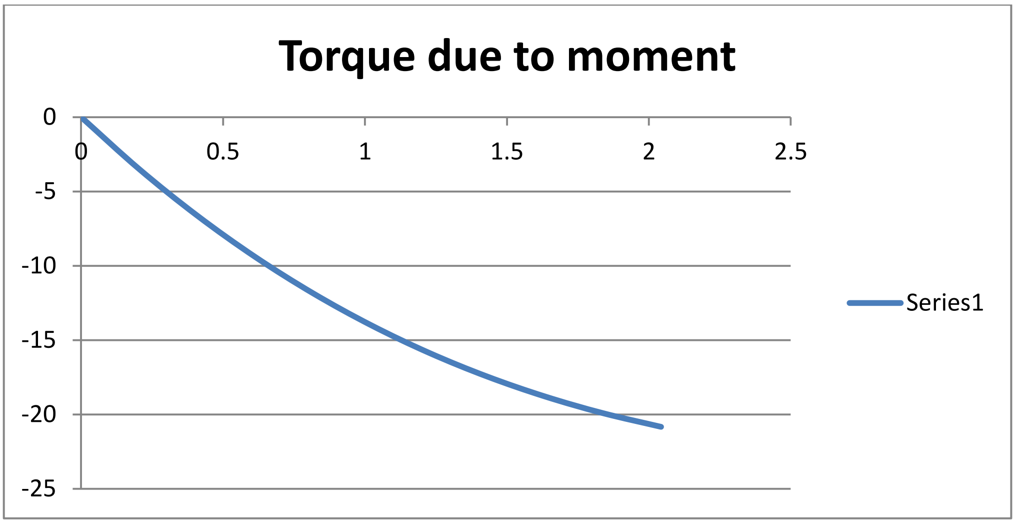

Figure 3-33: torque due to moment for critical condition

Net torque would be:

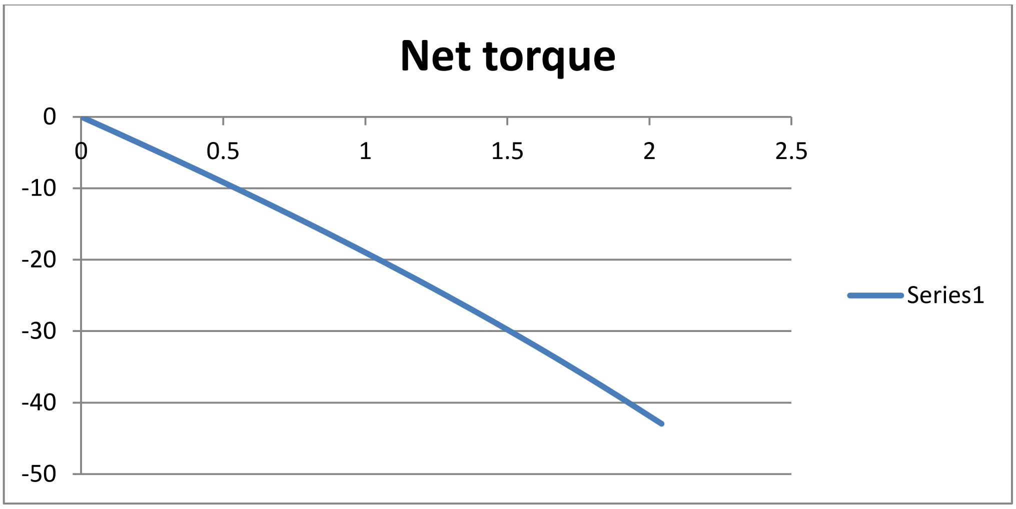

Figure 3-34:net torque for critical condition

Chapter 4 : STABILITY ANALYSIS

4.1 Introduction:

When an aircraft cruises, it is desirable that it do so at constant speed and incidence, so the controls are at a fixed setting. Aircraft stability is the study of how an aircraft responds to small disturbances in flight and how it can be designed so that it remains at a fixed incidence and speed without overworking the pilot. [9]

4.2 Static stability:

The static stability is the initial tendency of the vehicle or aircraft to return to its equilibrium state after a disturbance, so the vehicle must develop a restoring force and/or moment which tends to bring it back to equilibrium condition.

4.2.1 Longitudinal Static stability:

The aircraft trim longitudinally if moment about the center of gravity in Y axis zero, and has static longitudinal stability if any disturbance in pitch direction (vertical direction) develops restoring moment to trim position and that done if the aircraft had positive C_{M_0} and negative $\frac{\partial C_{M,cg}}{\partial \alpha_a}$, the aircraft will response to any disturbance as shown below:

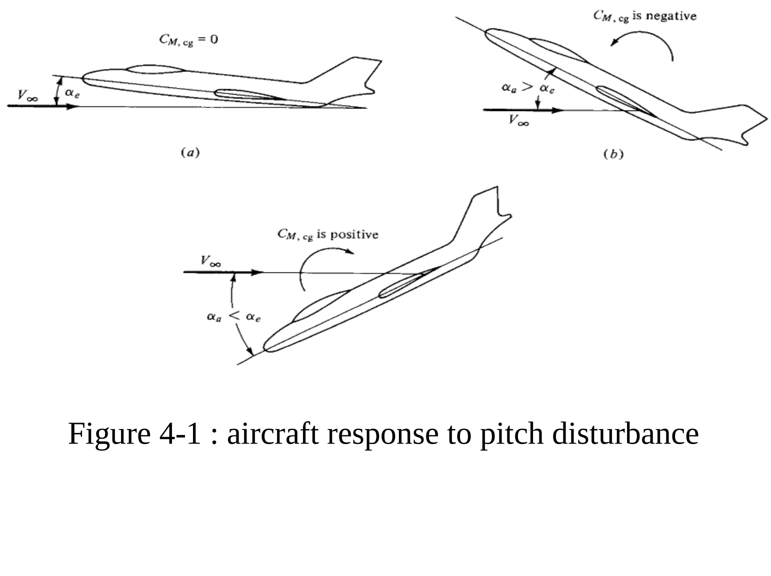

Figure 4-1 : aircraft response to pitch disturbance

The data which result from analysis from the DATCOM show that the trim angle of attack = 4.2° and $C_{M_0} = 0.03116$

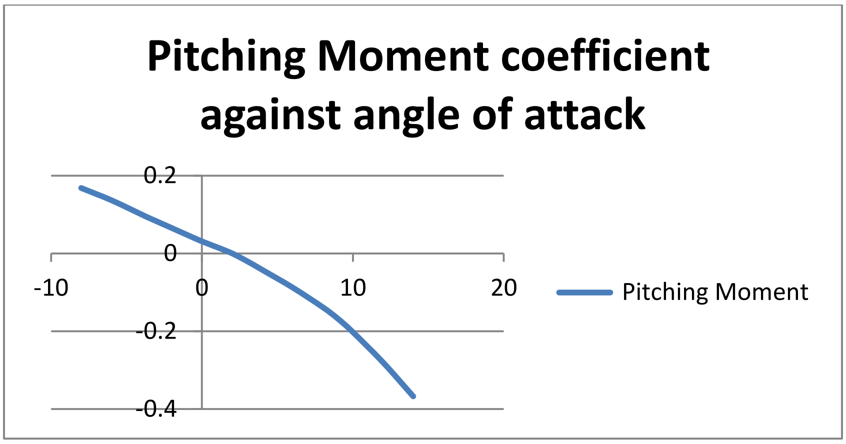

Figure 4-2: Pitching Moment coefficient against angle of attack

4.2.2 Directional static stability:

Static directional stability is a measure of aircraft's ability to realign itself along the direction of the resultant wind so that disturbance in sideslip is effectively eliminated. Therefore, on encountering a disturbance in the horizontal plane, the aircraft orientation in space change but its heading remains the same to the earth as shown in figure 4.3

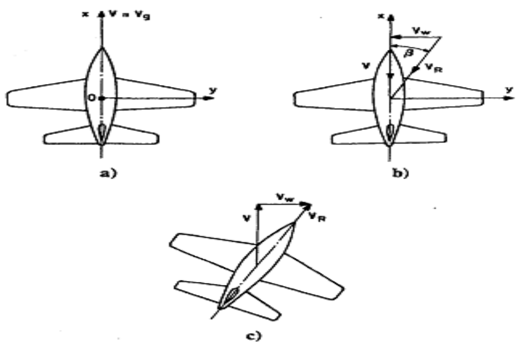

Figure 4-3: aircraft orientation on horizontal plane

An air plane said to be directionally stable if it has positive yaw moment coefficient and positive$\frac{\partial C_n}{\partial \beta}$.

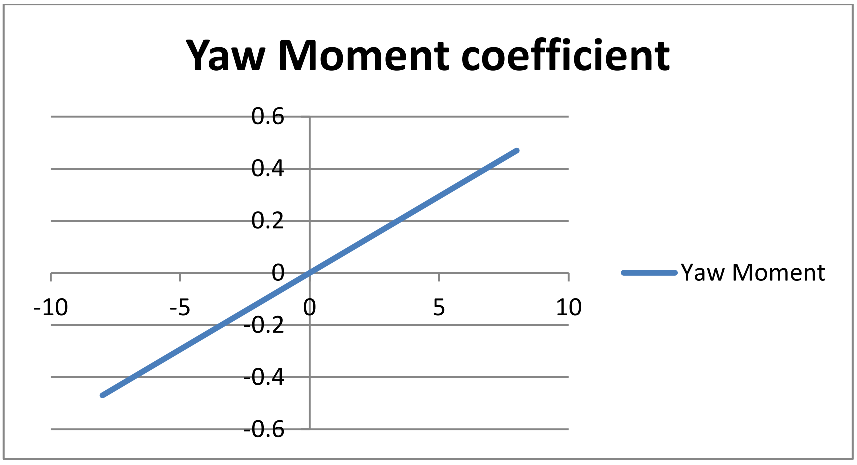

Figure 4-4:yaw moment coefficients against angle of attack

4.2.3 Lateral static stability:

Lateral stability is the inherent capability of the airplane to counter a disturbance in bank; the airplane is neutrally stable with respect to a disturbance in bank without sideslip, the sideslip generate by horizontal weight component. If the sideslip develops restoring moment the airplane said to be laterally stable .The rolling moment that developed by sideslip is known as dihedral effect. The airplane be laterally stable i.e. has positive dihedral effect if has negative slope$\frac{\partial cl}{\partial \beta}$.

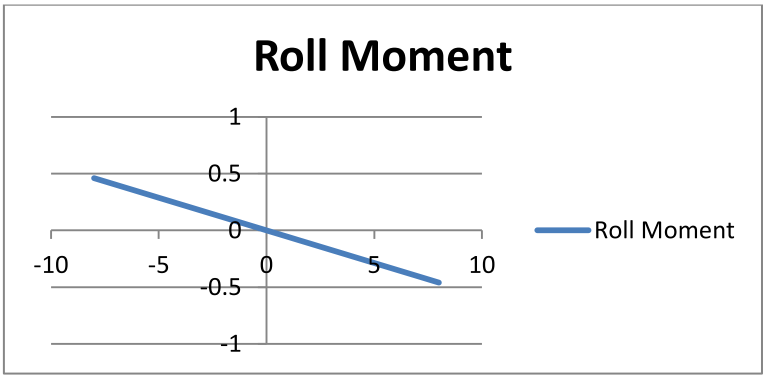

Figure 4-5: rolling moment coefficient against sideslip angle

4.3 Dynamic stability (Modes of Vibration):

In static stability analysis we examined the moments brought about immediately after the disturbance. However a system is said to be dynamically stable if it finally returns to the equilibrium position. Hence to examine the dynamic stability we must analyze the subsequent motion. The motion following an intended control input or a disturbance is called response. Obtaining the response in the case of airplane is an involved task.

4.3.1 Longitudinal Modes (Steady Modes of Vibration):

To examine the dynamic stability of the aircraft, we examine the full longitudinal equations of motion. The longitudinal motion of an airplane (controls fixed) disturbed from its equilibrium flight condition is characterized by two oscillatory modes of motion.Figure 4.6 illustrates these basic modes. We see that one mode is lightly damped and has a long period. This modecalled the long period or phugoid mode. The second basic mode is heavily damped and has a very short period; it is appropriately called the short-period mode.

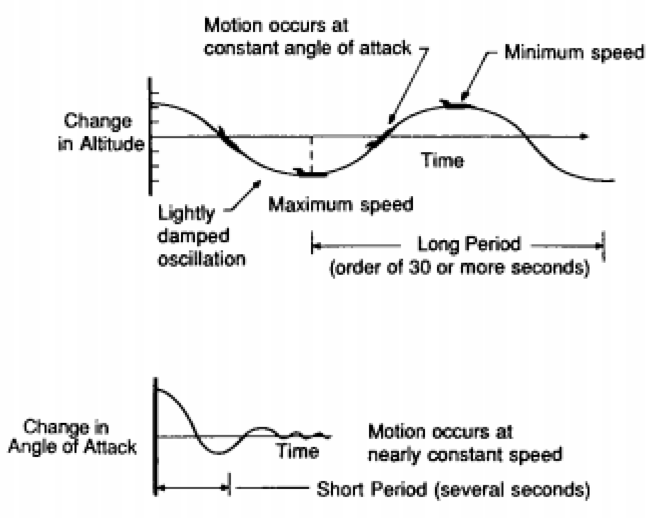

Figure 4-6:phugoid and short period motions

4.3.1.1 Short Period Mode:

This Mode is characterized by change in angle of attack with constant forward speed. It has a relatively big real part $\xi_c$the damping is thereforebig. The complex part $\eta_c$is relatively big as well. So the frequency is high. In other words, we have a highly damped high-frequency oscillation. This motion is known as the short period oscillation.

4.3.1.2 Long Period Mode (Phugoid):

This Mode is characterized by changes in pitch attitude, altitude, and velocity at a nearly constant angle of attack. It has a small real part ξ_c, and therefore a small damping.The complex part $\eta_c$is small as well, so the frequency is low. In other words, we have a lightly dampedlow-frequency oscillation. This motion is known as the phugoid.

4.3.1.3 Longitudinal Modes Excitation:

Since the longitudinal stability modes are usually well separated in frequency, it is Possible to excite the modes more or less independently for the purposes of demonstration or measurement. Indeed, it is a general flying qualities requirement that the modes be well separated in frequency in order to avoid handling problems arising from dynamic mode coupling.

The modes may be excited selectively by the application of a sympathetic elevator input to the trimmed aircraft. The methods developed for in-flight mode excitation reflect an intimate understanding of the dynamics involved and are generally easily adapted to the analytical environment. Because the longitudinal modes are usually well separated in frequency the form of the input disturbance is not, in practice, very critical. However, some consistency in the flight test or analytical procedures adopted is desirable if meaningful comparative studies are to be made.

Short period Excitation:

The short period pitching oscillation may be excited by applying a short duration disturbance in pitch to the trimmed aircraft. This is best achieved with an elevator pulse having duration of a second or less. Analytically this is adequately approximated by a unit impulse applied to the elevator. The essential feature of the disturbance is that it must be sufficiently short so as not to excite the phugoid significantly.

Long period Excitation:

The phugoid mode may be excited by applying a small speed disturbance to the aircraft in trimmed flight. This is best achieved by applying a small step input to the elevator which will cause the aircraft to fly up, or down, according to the sign of the input.

4.3.2.1 Roll Subsidence Mode (periodic roll):

occur when the airplane does not possess directional or weathercock stability. If such an airplane is disturbed from its equilibrium state, it will tend to rotate to ever-increasing angles ofsideslip. Owing to the side force acting on the airplane, it will fly a curved path at large sideslip angles.

4.3.2.2 Spiral Mode:

Spiral divergence is a non-oscillatory divergent motion which can occur when directional stability is large and lateral stability is small. When disturbed from equilibrium, the airplane enters a gradual spiraling motion. Thespiral becomes tighter and steeper as time proceeds and can result in a high-speed spiral dive if corrective action is not taken.

4.3.2.3 Dutch Roll Mode:

The Dutchroll mode is a classical damped oscillation in yaw, about the OZ axisof the aircraft, which couples into roll and, to a lesser extent, into sideslip. Themotion described by the Dutch roll mode is therefore a complex interaction betweenall three lateral–directional degrees of freedom. Its characteristics are described bythe pair of complex roots in the characteristic polynomial. Fundamentally, the Dutchroll mode is the lateral–directional equivalent of the longitudinal short period mode.

Both the damping and stiffness in yaw, which determine the characteristics of themode, are largely determined by the aerodynamic properties of the fin, a large fin beingdesirable for a well behaved stable Dutch roll mode. Unfortunately this contradicts therequirement for a stable spiral mode.

4.3.2.4 Lateral Modes Excitation:

Unlike the longitudinal stability modes the lateral–directional stability modes usually exhibit a significant level of dynamic coupling and as a result it is more difficult to excite the modes independently for the purposes of demonstration or measurement.However, the lateral–directional stability modes may be excited selectively by thecareful application of a sympathetic aileron or rudder input to the trimmed aircraft.

Because the lateral–directional stability modes usually exhibit a degreeof dynamic coupling, the choice and shape of the disturbing input is critical to themode under investigation.

Roll subsidence mode:

The roll subsidence mode may be excited by applying a short duration square pulse to the aileron, the other controls remaining fixed at their trim settings. The magnitude and duration of the pulse must be carefully chosen if the airplane is not to roll too rapidly through a large attitude change and thereby exceed the limit of small perturbation motion. Since the mode involves almost pure rolling motion only no significant motion coupling will be seen in the relatively short time scale of the mode. Therefore, to see the classical characteristics of the roll subsidence mode it is only necessary to observe roll response for a few seconds.

Spiral mode:

The spiral mode may be excited by applying a small step input to rudderζ, the remaining controls being held at their trim settings.

The aero-plane responds by starting to turn, the wing on the inside of the turn starts to drop and sideslip develops in the direction of the turn.

Spiral mode:

Ideally, the Dutch roll mode may be excited by applying a doublet to the rudder pedals with a period matched to that of the mode, all other controls remaining at their trim settings.

4.4 Flying Qualities:

Flight qualities of an airplane are related to the stability and control characteristics and can be defined as those stability and control characteristics that important in forming the pilot's impression of the airplane. The pilot forms subjective opinions about the ease or difficulty of controlling the airplane in steady and maneuvering flight. [10].

The dynamic stability characteristics are used to evaluate the flying qualities of the airplane in the Cooper and Harper rating scale.

The evaluation of flying qualities rates the results in three levels:

• **Level 1:** flying qualities clearly adequate for the mission flight phase

• **Level 2:** flying qualities adequate to accomplish the mission flight phase, but with an increase in pilot workload and, or, degradation in mission effectiveness

• **Level 3:** degraded flying qualities, but such that the aircraft can be controlled, inadequate mission effectiveness and high or limiting pilot workload.

Table 10: Aircraft Class

Class I	Small, light airplanes, such as light utility, primary trainer, and light observation craft
Class II	Medium-weight, low-to-medium maneuverability airplanes, such as heavy utility/search and rescue, lighter medium transport/cargo/tanker, reconnaissance, tactical bomber, heavy attack and trainer for Class II
Class III	Large, heavy, low-to-medium maneuverability airplanes, such as heavy transport/cargo/tanker, heavy bomber and trainer for Class III
Class IV	High-maneuverability airplanes, such as fighter/interceptor, attack, tactical reconnaissance, observation and trainer for Class IV

4.4.1 Longitudinal Flying qualities:

The longitudinal response characteristics of an airplane are related to its stability derivatives. Because the stability derivatives are related to the airplane's geometric and aerodynamic characteristic it is possible for the designer to consider flying qualities in the preliminary design phase.

4.4.1.1 Long Period Mode

Upper and lower values for phugoid frequency are not quantified. However, it is recommended that the phugoid and short period mode frequencies are well separated. It is suggested that handling difficulties may become obtrusive if the frequency ratio of the modes/$\omega s \leq 0.1$. Generally the phugoid dynamics are acceptable provided the mode is stable and damping ratio limits are quantified as shown in Table (4.2).

Table 11: Long Period Mode damping ratio limits

Long period	
Level 1	$\xi > 0.04$
Level 2	$\xi > 0$
Level 3	T > 55s

4.4.1.2 Short Period Mode

Acceptable limits on the stability of the short period mode are quantified in terms of maximum and minimum values of the damping ratio as a function of flight phase category and level of flying qualities as set out in Table 10.4.The maximum values of short period mode damping ratio obviously imply that actable non-oscillatory mode is acceptable, table (4.3).

Table 12: Short period

	Short period	
	ξ	ξ
level	Min.	Max.
1	0.35	1.30
2	0.25	2.00
3	0.15	-

4.4.2 Lateral Directional flying qualities:

4.4.2.1 Spiral mode flying qualities:

A stable spiral mode is acceptable irrespective of its time constant. However, since its time constant is dependent on lateral static stability (dihedral effect) the maximum level of stability is determined by the maximum acceptable roll control force. Because the mode gives rise to very slow dynamic behavior it is not too critical to handling unless it is very unstable.

Table 13: Spiral mode- time to double amplitude

Class	Category	Level 1	Level 2	Level 3
I and IV	**A**	**12 s**	**12 s**	**4 s**
	B and C	**20 s**	**12 s**	**4 s**
II and III	**All**	**20 s**	**12 s**	**4 s**

4.4.2.2 Roll mode flying qualities:

Since the roll subsidence mode describes short term lateral dynamics it is critically important in the determination of lateral handling qualities. For this reason the limiting acceptable values of its time constant are specified precisely as listed in Table 4.5

.

Table 14: Roll mode – time constant

Class	Category	Level 1	Level 2	Level 3
I, IV	**A**	**1.0**	**1.4**	**10**
II, III		**1.4**	**3.0**	
All	**B**	**1.4**	**3.0**	**10**
I, IV	**C**	**1.0**	**1.4**	**10**
II, III		**1.4**	**3.0**	

4.4.2.3 Dutch roll flying qualities:

Since the Dutch roll mode is a short period mode it has an important influence on lateral–directional handling and, as a consequence, its damping and frequency requirements are specified in some detail. It is approximately the lateral–directional equivalent of the longitudinal short period mode and has frequency of the same order since pitch and yaw inertias are usually similar in magnitude.

Table 15: Dutch roll damping at frequency requirement

level	Min ξ	Min $\boldsymbol{\xi_\omega}$	Min $\boldsymbol{\omega_n}$
1	0.19	0.35	1.0
2	0.02	0.05	0.4
3	0.02	-	0.4

4.5 Tools to estimate stability derivatives:

4.5.1 USAF DATCOM

4.5.1.1 Introduction to USAF DATCOM:

In preliminary design operations, rapid and economical estimations of aerodynamic stability and control characteristics are frequently required. The extensive application of complex automated estimation procedures is often prohibitive in terms of time and computer cost in such an environment. Similar inefficiencies accompany hand-calculation procedures, which can require expenditures of significant man-hours, particularly if configuration trade studies are involved, or if estimates are desired over a range of flight conditions. The fundamental purpose of the USAF Stability and Control Dotcom is to provide a systematic summary of methods for estimating stability and control characteristics in preliminary design applications. Consistent with this philosophy, the development of the Digital Dotcom computer program is an approach to provide rapid and economical estimation of aerodynamic stability and control characteristics.

The Digital DATCOM program uses aircraft-unique configuration and geometry parameters to predict aircraft performance by utilizing classical aerodynamic equations. The Digital DATCOM program calculates static stability, high lift and control, and dynamic derivative characteristics, and is applicable to subsonic, transonic, supersonic, and hypersonic vehicles, for traditional body-wing-tail or canard-equipped vehicles.

4.5.1.2 Using DATCOM:

The first step is to generate an input file in text format, its good practice to just modify ready input file. For detail information about input file the manual   is suggested. Second is to execute the input file, there are number of output files but the most important is one with (.OUT) format. This file contains the estimated aerodynamic and stability derivative.

4.5.2 Advance Aircraft Analysis (AAA):

4.5.2.1 Introduction to Advance Aircraft Analysis:

Advanced Aircraft Analysis (AAA) is the industry standard aircraft design, stability, and control analysis software. AAA is installed in over 55 countries and is used by major aeronautical engineering universities, aircraft manufacturers, and military organizations worldwide.

Advanced Aircraft Analysis provides a powerful framework to support the iterative and non-unique process of aircraft preliminary design. The AAA program allows students and preliminary design engineers to take an aircraft configuration from early weight sizing through open loop and closed loop dynamic stability and sensitivity analysis, while working within regulatory and cost constraints.

Chapter 5 : MATHMATICAL MODELING OF UAV DYNAMICS

5.1 Introduction:

This chapter gives an introduction to aircraft modeling. The equations of motion are derived then linearized using small perturbation theory and the final results are state-space models for the longitudinal and lateral motions. The models can be used for aircraft simulation and design of flight control systems**.**

5.2 Definition of coordinate system:

There are mainly three forces that act upon UAV during flight this are aerodynamic, Gravitational, and Thrust forces. This Forces together with linear and angular velocities need to be defined with appropriate coordinate system. Three basic coordinate system often used in UAV modeling it will be defined next.

5.2.1 Inertial Reference Frame:

The inertial reference frame is fixed on a point on the Earth's surface and is aligned so that the positive X axis points to true North and the positive Y axis points to true East. The z axis points down and is normal to the surface of the Earth. This frame is commonly referred to as the North-East-Down, or NED frame. [11]

5.2.2 Body Fixed coordinate Frame:

The aircraft body frame's origin is fixed at the aircraft's center of gravity. The body frame has its X axis aligned with the nose of the aircraft so that the aircraft's nose points in the positive X direction. The positive Y direction points out along the aircraft's starboard wing. The z axis points down to complete a right handed coordinate frame. Figure (5.1) below defines Body Fixed coordinate Frame

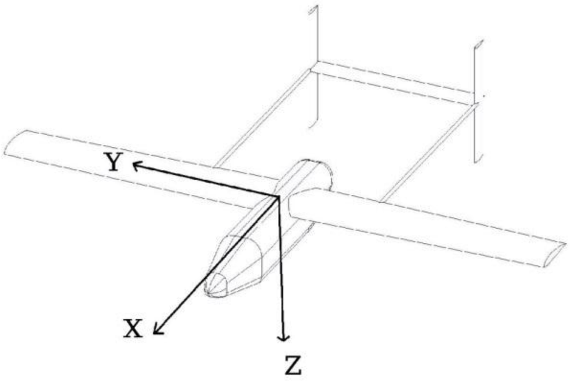

Figure 5-1: Body Fixed coordinate Frame

The body reference frame can assume any orientation with respect to the inertial frame. The orientation of the body frame with respect to the inertial frame is usually described by an Euler sequence of rotations. The ordering of the rotations is critical to the orientation of the body frame. [11]

5.2.3 Wind and Stability Reference Axis:

Wind Axis: This reference frame has origin fixed to the vehicle, usually at the mass center C, and the $O_w z_w$ axis is directed along the velocity vector V o f the vehicle relative to the atmosphere.The axis $O_w z_w$ lies in the plane of symmetry of the vehicle if it has one, otherwise is arbitrary.

Stability axes: are a special set of body axes used primarily in the study of small disturbances from a steady reference flight condition[12]

5.3 Rigid Body Equation of Motion:

The Rigid body equation of motion are obtained from newton's second low of motion, which states that the summation of all eternal forces acting on body is equal to the time rate of change of the momentum of the body; and the summation of the external moments acting on the body is equal to the time rate of change of the moment of momentum. The time rate of change of linear and angular momentum is referred to an absolute or inertial reference frame[10].

$$\sum F = \frac{d}{dt}\,(mV) \quad \text{……(5-1)}$$

$$\sum M = \frac{d}{dt}\,H \quad \text{……(5-2)}$$

The vector equation can be rewritten in scalar form and then consist of three force equation and three moment equation. The force equation can be expressed as follows:

$$F_x = \frac{d}{dt}\,(mu) F_y = \frac{d}{dt}\,(mv) F_z = \frac{d}{dt}\,(mw) \quad \text{……(5-3)}$$

Where F_x,$F_y F_z$and u, v, w are the component of force and velocity along x, y and z axis respectively. The force components are composed of contributions due to the aerodynamic, propulsive and gravitational forces.

The moment equations can be expressed in a similar manner:

$$L = \frac{d}{dt}H_x \;\; M = \frac{d}{dt}H_y \; N = \frac{d}{dt}H_z \quad \text{……(5-4)}$$

Where L, M, N and H_x,H_y,H_z are the component of the moment and moment of momentum along x, y and z axis respectively.

If we take δm as an element of mass of aircraft, v be the velocity of the elemental mass relative to an absolute or inertial frame, and δF be the resulting force acting on the elemental mass then newton's second low yields

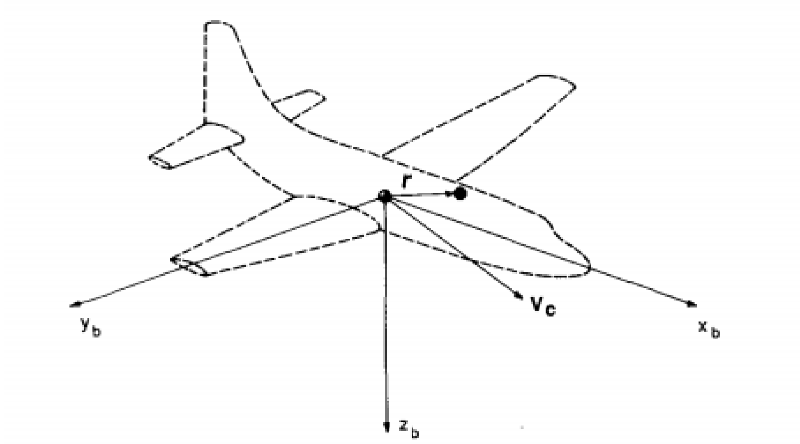

Figure 5-2:Rigid Body Equation of Motion

$\delta F = \delta\text{m} \frac{dv}{dt}$ ……………………………………………………(5-5)

And the total external force acting on the airplane is found by summing all the elements of the airplane

$\delta F = F$ ……………………………………………………(5-6)

The velocity of deferential mass δm is

$v = V_c + \frac{dr}{dt}$ ……………………………………………………(5-7)

where V_c is the velocity of the center of mass of the airplane and dr/dt is the

velocity of the element relative to the center of mass. Substituting this Expression for the velocity into Newton's second law yields

$\sum \delta F = F = d/dt \sum(Vc + dr/dt)\delta m$ ……………………(5-8)

If we assume that the mass of vehicle is constant equation (5-8) can be rewritten as

$$F = m\frac{dV_c}{dt} + \frac{d}{dt}\sum\frac{dr}{dt}\delta m \text{ ....(5-9)}$$

$$F = m\frac{dV_c}{dt} + \frac{d^2}{dt^2}\sum r\,\delta m \text{ .... (5-10)}$$

Because r is measured from the center of mass, the summation $\sum$ r δm is equal to zero. The force equation then becomes

$$F = m\frac{dV_c}{dt} \text{ ....(5-11)}$$

which relates the external force on the airplane to the motion of the vehicle's center of mass. In a similar manner, we can develop the moment equation referred to a moving center of mass. For the differential element of mass, δm, the moment equation can be written as

$$\delta M = d/dt\ \delta H = d/dt\ (r \times v)\ \delta m \text{ ....(5-12)}$$

The velocity of the mass element can be expressed in terms of the velocity of the center of mass and the relative velocity of the mass element to the center of mass:

$$V = V_c + \frac{dr}{dt} = V_c + \omega \times r \text{ ....(5-13)}$$

where ω is the angular velocity of the vehicle and r is the position of the mass element measured from the center of mass. The total moment of momentum can be written as

$$H = \sum\delta H = \sum(r \times V_c)\,\delta m + \sum[r \times (\omega \times r)]\,\delta m \text{ ...(5-14)}$$

The velocity V_c is a constant with respect to the summation and can be taken outside the summation sign

$$H = \sum r\delta\text{m} \times V_c + \sum [r \times (\omega \times r)]\, \delta \ldots\ldots\ldots\ldots\ldots\ldots\ldots\ldots(5\text{-}15)$$

The first term in Eq. (5-15) is zero because the term $\sum r$ δm= 0, as explained previously. If we express the angular velocity and position vector as

$$\omega = p\text{i} + q\text{j} + r\text{κ} \ldots\ldots\ldots\ldots\ldots\ldots\ldots\ldots\ldots\ldots\ldots\ldots\ldots\ldots\ldots\ldots \quad (5\text{-}16)$$

And

$$r = x\text{i} + y\text{j} + z\text{κ} \ldots\ldots\ldots\ldots\ldots\ldots\ldots\ldots\ldots\ldots\ldots\ldots\ldots\ldots\ldots\ldots(5\text{-}17)$$

Then after expanding Eq. (5-15), H can be written as

$$H = (p\text{i} + q\text{j} + rk)\sum(x^2 + y^2 + z^2)\, \delta m - \sum(x\text{i} + y\text{j} + z\text{κ})(px + qy + rz)\delta m \ldots\ldots\ldots\ldots\ldots\ldots\ldots\ldots\ldots\ldots\ldots\ldots\ldots\ldots\ldots\ldots\ldots\ldots\ldots\ldots\ldots \quad (5\text{-}18)$$

The scalar components of H are

$$H_x = p\sum(x^2 + y^2)\delta\text{m} - q\sum xy\, \delta\text{m} - r\sum xz\, \delta\text{m} \ldots\ldots\ldots\ldots\ (5\text{-}19)$$

$$H_y = -p\sum xy\, \delta\text{m} + \text{q}\sum(x^2 + y^2)\delta\text{m} - r\sum yz\, \delta\text{m}(5\text{-}20)$$

$$H_y = -p\sum xz\, \delta\text{m} - q\sum yz\, \delta\text{m} + r\sum(x^2 + y^2)\delta\text{m} \ldots\ldots\ldots(5\text{-}21)$$

The summations in the above equations are the mass moment and products of inertia of the airplane and are defined as follows:

$$I_x = \int\int\int (\,(y^2 + z^2)\, \delta\text{m} I_{xy} = \int\int\int xy\, \delta\text{m} \ldots\ldots\ldots\ldots\ldots(5\text{-}22)$$

$$I_y = \int\int\int (\,(x^2 + z^2)\, \delta\text{m} I_{xz} = \int\int\int xz\, \delta\text{m} \ldots\ldots\ldots\ldots\ldots\ (5\text{-}23)$$

$$I_z = \int\int\int (\,(x^2 + y^2)\, \delta\text{m} I_{yz} = \int\int\int yz\, \delta\text{m} \ldots\ldots\ldots\ldots\ldots(5\text{-}24)$$

The terms I_x, I_y and I_z are the mass moments of inertia of the body about the x, y and z axes, respectively. The terms with the mixed indices are called the products of inertia. Both the moments and products of inertia depend on the shape of the body and the manner in which its mass is distributed. The larger the moments of inertia the greater the resistance the body will have to rotation. The scalar equations for the moment of momentum are given below

$$H_x = pI_x - qI_{xy} - rI_{xz} \quad \ldots\ldots\ldots\ldots\ldots\ldots\ldots\ldots\ldots\ldots\ldots\ldots \text{(5-25)}$$

$$H_y = -pI_{xy} + qI_y - rI_{yz} \ldots\ldots\ldots\ldots\ldots\ldots\ldots\ldots\ldots\ldots\ldots\ldots \text{(5-26)}$$

$$H_z = -pI_{xz} - qI_{yz} + rI_z \quad \ldots\ldots\ldots\ldots\ldots\ldots\ldots\ldots\ldots\ldots\ldots\ldots \text{(5-27)}$$

If the reference frame is not rotating then, as the airplane rotates, the moments and products of inertia will vary with time. To avoid this difficulty we will fix the axis system to the aircraft (body axis system). Now we must determine the derivatives of the vectors v and H referred to the rotating body frame of reference. It can be shown that the derivative of an arbitrary vector A referred to a rotating body frame having an angular velocity ω can be represented by the following vector identity:

$$\left.\frac{dA}{dt}\right|_I = \left.\frac{dA}{dt}\right|_B + \omega \times A \quad \ldots\ldots\ldots\ldots\ldots\ldots\ldots\ldots\ldots\ldots\ldots\ldots \text{(5-28)}$$

where the subscript I and B refer to the inertial and body fixed frames of reference. Applying this identity to the equations derived earlier yields

$$F = m \left.\frac{dV_c}{dt}\right|_B + m\,(\omega \times V_c) \quad \ldots\ldots\ldots\ldots\ldots\ldots\ldots\ldots\ldots\ldots \text{(5-29)}$$

$$M = \left.\frac{dH}{dt}\right|_B + \omega \times H \quad \text{(5-30)}$$

$$F_x = m(\dot{u} + qw + rv)F_y = m(\dot{v} + ru - pw)F_z = m(\dot{w} + pv + qu \quad \text{(5-31)}$$

$$L = \dot{H}_x + qH_z - rH_y M = \dot{H}_y + rH_x - pH_z N = \dot{H}_z + pH_y - qH_x \quad \text{(5-32)}$$

The components of the force and moment acting on the airplane are composed of aerodynamic, gravitational, and propulsive contributions. By proper positioning of the body axis system, one can make the products of inertia $I_{yz} = I_{xy} = I_{xz} = 0$. To do this we are assuming that the XZ plane is a plane of symmetry of the airplane. With this assumption, the moment equations can be written as

$$L = \dot{p}I_x - \dot{r}I_{xz} + qr(I_z - I_y) - I_{xz}pq \quad \text{(5-33)}$$

$$M = \dot{q}I_y + rp(I_x - I_z) + I_{xz}(p^2 - r^2) \quad \text{(5-34)}$$

$$N = -\dot{p}I_{xz} + \dot{r}I_z + pq(I_y - I_x) + I_{xz}\, qr \quad \text{(5-35)}$$

5.4 linearization using Small-perturbation theory:

The equations developed in the previous section can be linearized by using small-disturbance theory. In applying small disturbance theory we are assuming that the motion of the airplane consists of small deviations about a steady flight condition. Obviously, this theory cannot be applied to problems in which large amplitude motions are to be expected (e.g. Spinning or stalled flight).However, in many cases small disturbance theory yields sufficient accuracy for practical engineering purposes.

All the variables in the equations of motion are replaced by a reference value plus a perturbation or disturbance:

$$u = u_0 + \Delta u v = v_0 + \Delta v w = w_0 + \Delta w$$

$$p = p_0 + \Delta p q = q_0 + \Delta q r = r_0 + \Delta r$$

$$X = X_0 + \Delta X Y = Y_0 + \Delta Y Z = Z_0 + \Delta Z$$

$$M = M_0 + \Delta M N = N_0 + \Delta N L = L_0 + \Delta L \ldots\ldots\ldots\ldots\ldots.. (5\text{-}36)$$

$$\delta = \delta_0 + \Delta\delta$$

For convenience, the reference flight condition is assumed to be symmetric and the propulsive forces are assumed to remain constant. This implies that

$$v_0 = p_0 = q_0 = r_0 = \emptyset_0 = \psi_0 = 0 \ldots\ldots\ldots\ldots\ldots\ldots\ldots\ldots (5\text{-}37)$$

Furthermore, if we initially align the x axis so that it is along the direction of the airplane's velocity vector, then w_0 = 0

Now, if we introduce the small disturbance notation into the equations of motion, we can simplify the equations of motion. With appropriate derivation will result in the linearized small disturbance longitudinal Equation:

$$\left(\frac{d}{dt} - X_u\right)\Delta u - X_w \Delta w + (g\cos\theta_0)\Delta\theta = X_{\delta_e}\Delta\delta_e + X_{\delta_T}\Delta\delta_T (5\text{-}38)$$

$$-Z_u\Delta u + ((1 - Z_{\dot{w}})\frac{d}{dt} - Z_w))\Delta w - ((u_0 + Z_q)\frac{d}{dt} - g\sin\theta_0))\Delta\theta = Z_{\delta_e}\Delta\delta_e + Z_{\delta_T}\Delta\delta_T \ldots\ldots\ldots\ldots\ldots\ldots\ldots\ldots\ldots\ldots\ldots\ldots\ldots (5\text{-}39)$$

$-M_u\Delta u - \left(M_{\dot{w}}\frac{d}{dt} + M_w\right)\Delta w + (\frac{d^2}{dt^2} - M_q\frac{d}{dt})\Delta\theta = M_{\delta_e}\Delta\delta_e +$
$M_{\delta_T}\Delta\delta_T$
…………………………………………………………………... (5-40)

The linearized small disturbance Lateral Equation:

$\left(\frac{d}{dt} - Y_v\right)\Delta v - Y_p\Delta p + (u_0 - Y_r)\Delta r + (g\cos\theta_0)\Delta\varphi = X_{\delta_r}\Delta\delta_r$(5-41)

$-L_v\Delta v + \left(\frac{d}{dt} - L_p\right)\Delta p - \left(\frac{I_{xz}}{I_x}\frac{d}{dt} + L_r\right)\Delta r = L_{\delta_a}\Delta\delta_a + Z_{\delta_r}\Delta\delta_r$ ….
(5-42)

$-N_v\Delta v + \left(\frac{I_{xz}}{I_z}\frac{d}{dt} + N_p\right)\Delta p + \left(\frac{d}{dt} - N_r\right)\Delta r = N_{\delta_a}\Delta\delta_a + N_{\delta_r}\Delta\delta_r$
.(5-43)

5.5 Aerodynamic and stability Derivatives

5.5.1Longitudinal Derivatives:

5.5.1.1 Derivative due to change in forward speed, u($\mathbf{CL_u}$, $\mathbf{CD_u}$, $\mathbf{CM_u}$):

The drag, lift and pitching moment vary with changes in the airplane's forward speed. In addition the thrust of the airplane is also a function of the forward speed. The aerodynamic and propulsive forces acting on the airplane along the X body axes are the drag force and the thrust. The change in the X force can be expressed as:

$\Delta X = \frac{\partial X}{\partial u}\Delta u = -\frac{\partial D}{\partial u}\Delta u + \frac{\partial T}{\partial u}\Delta u$ ……................................... (5-44)

$$\frac{\partial X}{\partial u} = -\frac{\partial D}{\partial u} + \frac{\partial T}{\partial u} \text{ ......} \quad (5\text{-}45)$$

The derivative $\frac{\partial X}{\partial u}$ is called the speed damping derivative.

$$\mathrm{CD_u} = \mathrm{M}\frac{\partial CD}{\partial \mathrm{M}} \text{ ......} \quad (5\text{-}46)$$

$$\mathrm{CL_u} = \frac{\mathrm{M}^2}{1-\mathrm{M}^2}\mathrm{CL_0} \text{......} \quad (5\text{-}47)$$

$$\mathrm{CM_u} = \frac{\partial CM}{\partial M} M \text{ ......} \quad (5\text{-}48)$$

Since Our UAV had low Mach number this derivatives have no significant affect.

Derivative due to change in Pitching Velocity, q (C_{z_q},$\mathrm{C_{m_q}}$):

The stability coefficients $C_{z_q}$and $\mathrm{C_{m_q}}$represent the change in the Z force and pitching moment coefficients with respect to the pitching velocity q.

$$\mathrm{C_{z_q}} = -2\, CL_{\alpha_t} \eta\, V_H \text{......} \quad (5\text{-}48)$$

Pitch Damping Derivative C_{m_q}: This derivative is normally negative, and determines the moment that opposes any pitch rate. It provides the most important contribution to the damping of the dynamic behavior in pitch and hence is intimately involved in aircraft handling qualities. The pitch damping is not given by the slope of an aerodynamic coefficient; it must be estimated from oscillatory motion of the aircraft or aircraft model, or calculated.[13]

$$C_{m_q} = -2\, CL_{\alpha_t} \eta\, V_H \frac{l_t}{\bar{c}} \qquad (5\text{-}49)$$

Derivative due to change of $\dot{\alpha}$($C_{z_{\dot{\alpha}}}$,$C_{m_{\dot{\alpha}}}$):

The stability coefficients $C_{z_{\dot{\alpha}}}$ and $C_{m_{\dot{\alpha}}}$ arise because of the lag in the wing downwash getting to the tail. As the wing angle of attack changes, the circulation around the wing will be altered. The change in circulation alters the downwash at the tail; however, it takes a finite time for the alteration to occur.

$$C_{z_{\dot{\alpha}}} = -2CL_{\alpha_t} \eta\, V_H \frac{d\varepsilon}{d\alpha} \qquad (5\text{-}50)$$

$$C_{m_{\dot{\alpha}}} = -2CL_{\alpha_t} \eta\, V_H \frac{d\varepsilon}{d\alpha} \frac{l_t}{\bar{c}} \qquad (5\text{-}51)$$

Equations (5-50) and (5-51) yield only the tail contribution to these stability coefficients. To obtain an estimate for the complete airplane these coefficients are increased by 10 percent.

Derivative due to the Rolling rate, p (C_{y_p},C_{n_p}, C_{l_p}):

The stability coefficientC_{y_p},C_{n_p}, C_{l_p}arise due to the rolling angular velocity,p.When an airplane rolls about its longitudinal axis, the roll rate creates a linear velocity distribution along the vertical, horizontal and wing surfaces. The velocity distribution causes a local change in angle of attack over each of this surfaces that result in a change in the lift distribution and consequently the moment about center of gravity[10]

$$C_{y_p} = CL\ \frac{AR+cos\Lambda}{AR+4cos\Lambda}\ tan\Lambda \quad (5\text{-}52)$$

$$C_{n_p} = -\frac{Cl}{8} \quad (5\text{-}53)$$

$$C_{l_p} = -\frac{CL_\alpha}{12}\frac{1+3\lambda}{1+\lambda} \quad (5\text{-}54)$$

Derivative due to the Yawing rate, r (C_{y_r},C_{n_r}, C_{l_r}): The stability coefficientC_{y_r},C_{n_r}, $C_{l_r}$are caused by yawing angular velocity, r. A yawing rate causes a change in the side force acting on the vertical tail surface.

$$C_{y_r} = -2\ (\frac{l_v}{b})(C_{y_\beta})_{tail} \quad (5\text{-}55)$$

$$C_{n_r} = 2\eta_t V_v(\frac{l_v}{b})\ CL_{\alpha_v} C_{l_r} = -\frac{CL}{4} - 2\,\frac{l_v}{b}\frac{z_v}{b} C_{y_{\beta_{tail}}} \quad (5\text{-}56)$$

5.6 State variable representation of the equations of motion:

The linearized longitudinal equations developed in Chapter 3 are simple, ordinary linear differential equations with constant coefficients. The coefficients in the differential equations are made up of the aerodynamic stability derivatives, mass, and inertia characteristics of the airplane. These equations can be written as a set of first-order differential equations. When the equations are written as a system of first-order differential equations they are called the state-space or state variable equations and are represented mathematically as

$$\dot{\boldsymbol{x}} = \boldsymbol{Ax} + \boldsymbol{B\eta} \quad \text{.........} \quad (5\text{-}57)$$

Where x is the state vector, $\boldsymbol{\eta}$ s the control vector and the matrices **A** and **B** contain the aircraft's dimensional stability derivatives

The linearized longitudinal equations developed earlier are repeated below.

In practice, the force derivatives $\boldsymbol{Z_q}$and $\boldsymbol{Z_{\dot{w}}}$ are usually neglected because they contribute very little to the aircraft response. Therefore, to simplify our presentation of the equations of motion in the state space form we will neglect both $\boldsymbol{Z_q}$and$\boldsymbol{Z_{\dot{w}}}$. Rewriting the equations in the state-space form yields

$$\begin{bmatrix} \Delta\dot{u} \\ \Delta\dot{w} \\ \Delta\dot{q} \\ \Delta\dot{\theta} \end{bmatrix} = \begin{bmatrix} X_u & X_w & 0 & -g \\ Z_u & Z_w & u_0 & 0 \\ M_u + M_{\dot{w}} Z_u & M_w + M_{\dot{w}} Z_w & M_q + M_{\dot{w}} Z u_0 & 0 \\ 0 & 0 & 1 & 0 \end{bmatrix} \begin{bmatrix} \Delta\mathrm{u} \\ \Delta w \\ \Delta q \\ \Delta\theta \end{bmatrix} + \begin{bmatrix} X_\delta & X \\ Z_\delta & Z_{\delta r} \\ M_\delta + M_{\dot{w}} Z_\delta & M_{\delta r} + M_{\dot{w}} Z_{\delta r} \\ 0 & 0 \end{bmatrix} \begin{bmatrix} \Delta\delta \\ \Delta\delta_T \end{bmatrix}$$

where the state vector **x** and control vector $\boldsymbol{\eta}$are given by

$$x = \begin{bmatrix} \Delta\mathrm{u} \\ \Delta w \\ \Delta q \\ \Delta\theta \end{bmatrix} \eta = \begin{bmatrix} \Delta\delta \\ \Delta\delta_T \end{bmatrix}$$

and the matrices **A** and **B** are given by

$$A = \begin{bmatrix} X_u & X_w & 0 & -g \\ Z_u & Z_w & u_0 & 0 \\ M0_u + M_{\dot{w}} Z_u & M_w + M_{\dot{w}} Z_w & M_q + M_{\dot{w}} Z u_0 & 0 \\ 0 & 0 & 1 & 0 \end{bmatrix}$$

$$B = \begin{bmatrix} X_\delta & X \\ Z_\delta & Z_{\delta r} \\ M_\delta + M_{\dot{w}} Z_\delta & M_{\delta r} + M_{\dot{w}} Z_{\delta r} \\ 0 & 0 \end{bmatrix}$$

From [nelson]:

$\lambda^2 + 2\,\xi\,\omega_n + \omega_n{}^2 = 0$ .... (5-58)

$\omega_n = \sqrt{-M_\alpha}$ .... (5-59)

$\xi = \frac{-(M_q + M_{\dot{\alpha}})}{2\sqrt{-M_\alpha}}$ ....(5-60)

$Period = \frac{2\pi}{\omega}$ ....(5-61)

$t_{double} or\ t_{halve} \quad = \frac{0.693}{|\eta|}$ .... (5-62)

Lateral-directional equations of motion:

The lateral-directional equations of motion consist of the side force, rolling moment and yawing moment equations of motion. The lateral equations of motion can be rearranged into the state space form in the following manner. We start with Eq. (5.27) shown below.

$$\left(\frac{d}{dt} - Y_v\right)\Delta v - Y_P\Delta_P + (u_0 - Y_r)\Delta r - g\ cos\theta_0\Delta\emptyset = Y_{\delta r}\Delta\delta_r \quad \ldots\ldots (5\text{-}63)$$

$$-L_v\Delta v + \left(\frac{d}{dt} - L_P\right)\Delta_P - \left(\frac{I_{xz}}{I_x}\frac{d}{dt} + L_r\right)\Delta r = L_{\delta a}\Delta_{\delta a} + L_{\delta r}\Delta\delta_r \ldots\ldots (5\text{-}64)$$

$$-N_v\Delta v - \left(\frac{I_{xz}}{I_x}\frac{d}{dt} + N_P\right)\Delta_P + \left(\frac{d}{dt} - N_r\right)\Delta r = N_{\delta a}\Delta_{\delta a} + N_{\delta r}\Delta\delta_r \ldots (5\text{-}65)$$

Rearranging and collecting terms the above equations can be written in the state variable form:

$$\dot{\boldsymbol{x}} = \boldsymbol{A}\boldsymbol{x} + \boldsymbol{B}\boldsymbol{\eta} \ldots\ldots\ldots\ldots (5\text{-}66)$$

The matrices **A** and **B** are defined as follows:

$$A = \begin{bmatrix} Y_{\upsilon} & Y_P & -(u_0 - Y_r) & g\cos\theta_0 \\ {L_{\upsilon}}^* + \dfrac{I_{xz}}{I_x}{N_{\upsilon}}^* & {L_P}^* + \dfrac{I_{xz}}{I_x}{N_P}^* & {L_r}^* + \dfrac{I_{xz}}{I_x}{N_r}^* & 0 \\ {N_{\upsilon}}^* + \dfrac{I_{xz}}{I_z}{L_{\upsilon}}^* & {N_P}^* + \dfrac{I_{xz}}{I_z}{L_P}^* & {N_r}^* + \dfrac{I_{xz}}{I_z}{L_r}^* & 0 \\ 0 & 1 & 0 & 0 \end{bmatrix}$$

$$B = \begin{bmatrix} 0 & Y_{\delta_r} \\ {L_{\delta_a}}^* + \dfrac{I_{xz}}{I_x}{N_{\delta_a}}^* & {L_{\delta_r}}^* + \dfrac{I_{xz}}{I_x}{N_{\delta_r}}^* \\ {N_{\delta_a}}^* + \dfrac{I_{xz}}{I_z}{L_{\delta_a}}^* & {N_{\delta_r}}^* + \dfrac{I_{xz}}{I_z}{L_{\delta_r}}^* \\ 0 & 0 \end{bmatrix}$$

$$x = \begin{bmatrix} \Delta\upsilon \\ \Delta P \\ \Delta r \\ \Delta\phi \end{bmatrix} \text{And} \eta = \begin{bmatrix} \Delta\delta_a \\ \Delta\delta_r \end{bmatrix}$$

From [nelson]:

$$\omega_n = \sqrt{-\mathrm{N}_{\beta}} \qquad \text{(5-67)}$$

$$\xi = \frac{N_r}{2\sqrt{N_{\beta}}} \qquad \text{(5-68)}$$

Chapter 6 : UAV DYNAMICS MODELING USING SIMULINK

6.1 Introduction:

In Chapter II the full nonlinear equations of motion were developed and in Chapter III the complete set of stability and control derivatives were obtained. Now the next step is to develop the model of the aircraft on a Matlab Simulink.

6.2 UAV Dynamic Modeling:

UAV modeling has been part of the design and modification process for new UAVs and has increasingly been used for rapid testing and verification. Changes and modifications are made to the model, evaluating it for intended function against the requirement. Modeling allows a faster verification and iteration of the design change cycle without having to conduct a flight test with a prototype UAV. It also reduces the cost incurred for each design change.

6.2.1 Nonlinear Model:

Nonlinear aircraft simulations are useful for dynamic analysis, control law design and validation, guidance and trajectory studies, pilot training, and many other tasks. (Nonlinear AC Simulations in MATLAB)

The nonlinear models contain three basic models:

1) Aerodynamic Model: Contains forces and moments that act on aircraft during flight, the equation used to estimate these forces and moments are defined at each model below since it depends on degrees of freedoms of the model.
2) Atmosphere model: since Dynamic pressure is necessary to estimate aerodynamic forces and moment, therefore air density at each altitude is also required. For this purpose, the ‘ISA Atmosphere Model ' model will be used. A description of this idealized model of the earth's atmosphere can, for instance.
3) Engine Model: For simplicity engine thrust is assumed to be constant for all altitude and forward flight speed.
4) Gravity Model: The gravitational force acting on the airplane acts through the center of gravity of the airplane. Because the body axis system is fixed to the center of gravity, the gravitational force will not produce any moments. It will, however,

contribute to the external force acting on the airplane and will have components along the respective body axes.

6.2.1.1 Three Degree of freedom Longitudinal Model:

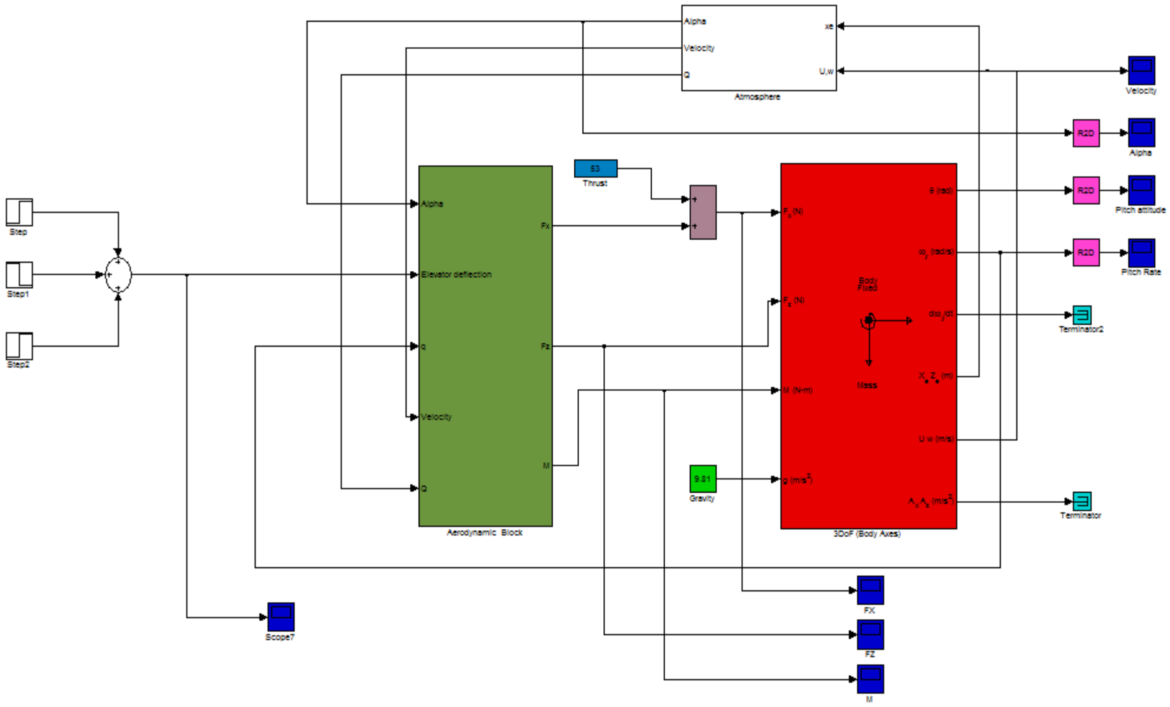

Figure 6-1:Three Degree of freedom Longitudinal Model

The three degree of freedom Longitudinal Model is composed of the following blocks:

Equation of motion Block: this block is taken from aerospace block set and is used to solve three degree of freedom longitudinal equation, the equation is as follows:

$$\dot{U} = \frac{(T+F_x)}{m} - qw - g \sin\theta \quad \ldots\ldots\ldots\ldots\ldots\ldots\ldots\ldots \text{(6-1)}$$

$$\dot{w} = \frac{F_z}{m} + + qu + g \cos\theta \quad \ldots\ldots\ldots\ldots\ldots\ldots\ldots\ldots \text{(6-2)}$$

$$\dot{q} = \frac{M}{I_{yy}} \quad \ldots\ldots\ldots\ldots\ldots\ldots\ldots\ldots\ldots\ldots\ldots\ldots \text{(6-3)}$$

$$\dot{\theta} = q \quad \text{...} \quad (6\text{-}4)$$

Aerodynamic Block:

The aerodynamic block is shown below:

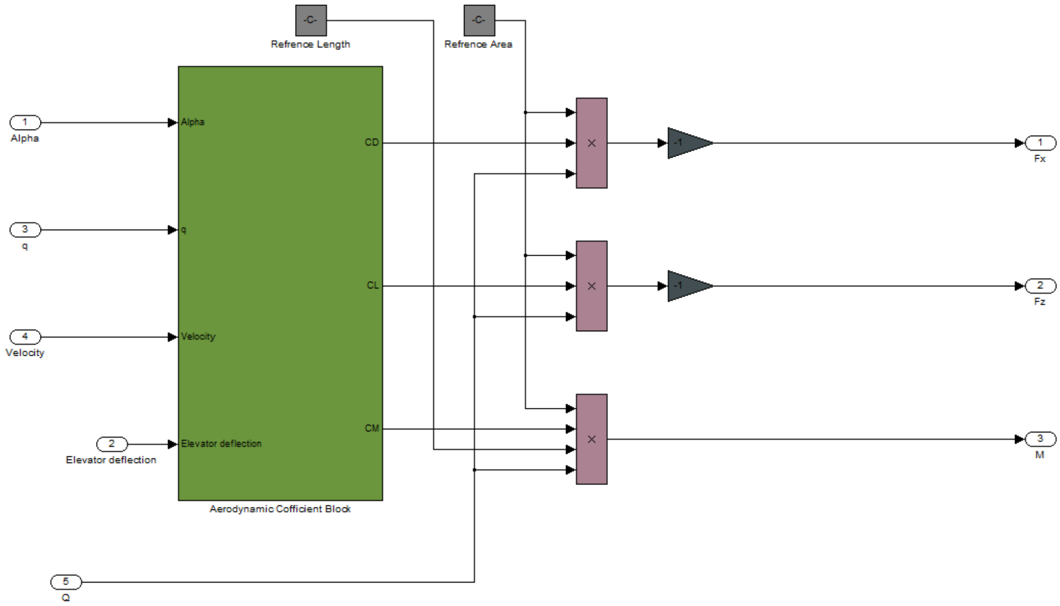

Figure 6-2: aerodynamic block

The component of this block as follows:

Lift coefficient block

$$C_L = C_{L_0} + C_{L_\alpha}\alpha + C_{L_{\delta e}}\delta_e + C_{L_q}\frac{q*\bar{c}}{2V} \quad \text{..................} \quad (6\text{-}5)$$

The lift model is shown in Figure (6-3) below

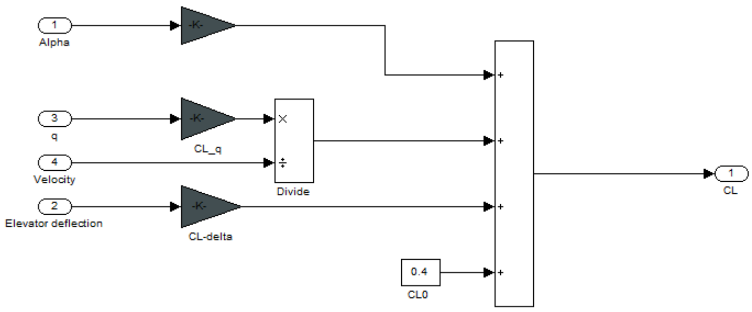

Figure 6-3: Lift coefficient block

The drag coefficient block:

$$C_D = C_{D_0} + C_{D_{\delta e}}\delta_e + k(C_L - C_{L_{min\,drag}})^2 \quad \ldots\ldots\ldots \quad (6\text{-}6)$$

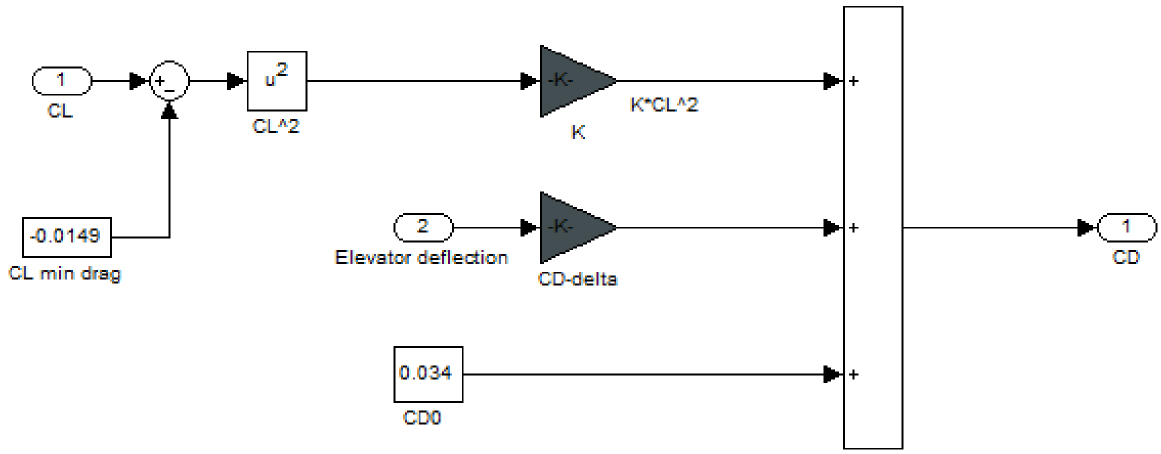

Figure 6-4: Drag coefficient block

Moment Coefficient block:

$$C_m = C_{m_0} + C_{m_\alpha}\alpha + C_{m_{\delta e}}\delta_e + C_{m_q}\frac{q*\bar{c}}{2V} \quad \ldots\ldots\ldots\ldots\ldots \quad (6\text{-}7)$$

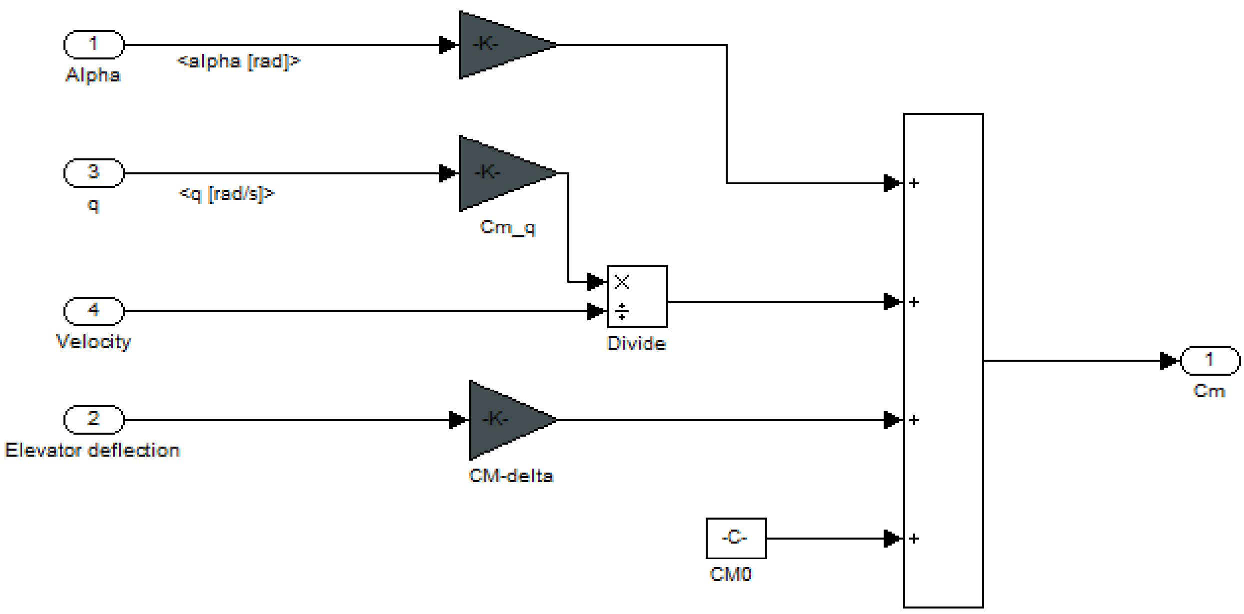

Figure 6-5: Moment Coefficient Block

Atmospheric Model:

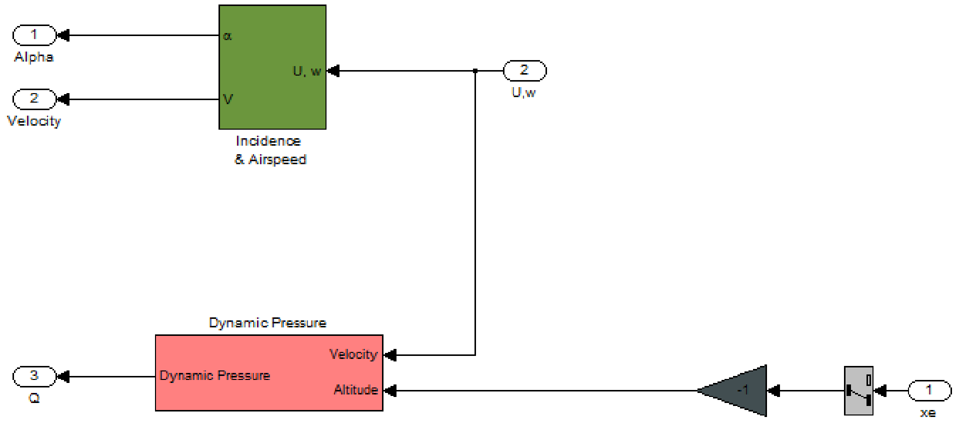

Figure 6-6: Atmospheric Model

The angle of attack is calculated from

$$\alpha = \tan^{-1}\frac{w}{u} \quad \ldots\ldots\ldots\ldots\ldots\ldots\ldots\ldots\ldots\ldots\ldots\ldots\ldots\ldots\ldots\ldots\ldots\ldots\ldots\ldots\ldots\ldots\ldots \text{(6-8)}$$

6.2.1.2 Three Degree of freedom Lateral Model:

In similar manner to longitudinal Model the lateral Model construction is shown:

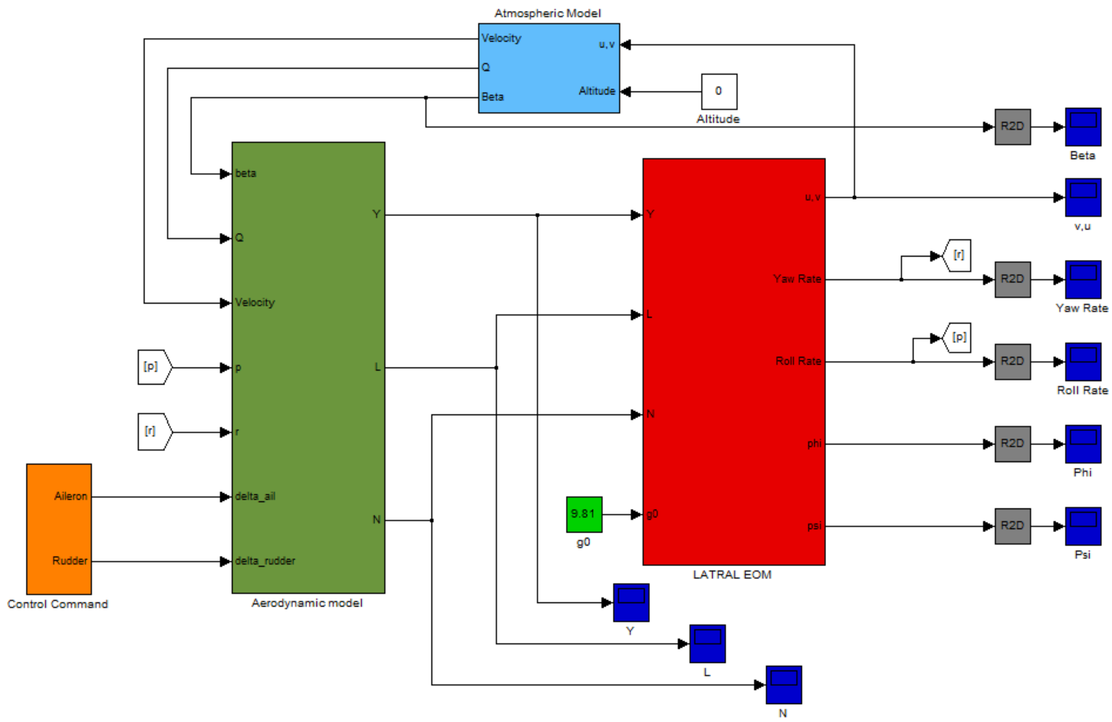

Figure 6-7: Three Degree of freedom Lateral Model

Three Degree of freedom Lateral equation of motion is modeled using Simulink block set, these equation are defined as:

$$\dot{v} = \frac{F_y}{m} - ur + gsin\varphi \quad \text{(6-9)}$$

$$\dot{p} = \frac{L}{I_{xx}} \quad \text{(6-10)}$$

$$\dot{r} = \frac{N}{I_{zz}} \quad \text{(6-11)}$$

$$\dot{p} = \dot{\varphi} \quad \text{(6-12)}$$

$$\dot{r} = \dot{\psi} \quad \text{(6-13)}$$

This equation of motion is modeled as:

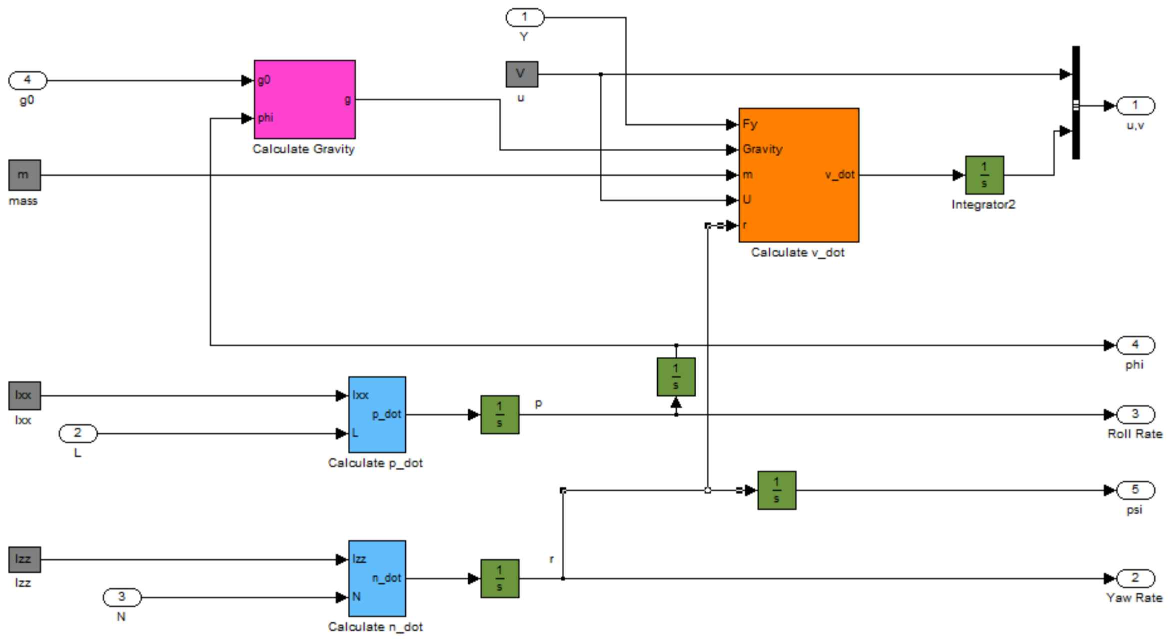

Figure 6-8: Lateral Equation of motion

Aerodynamic Forces and Moments:

$$F_y = qsc_y \quad \text{(6-14)}$$

$$L = qsbc_l \quad \text{(6-15)}$$

$$N = qsbc_n \quad \text{(6-16)}$$

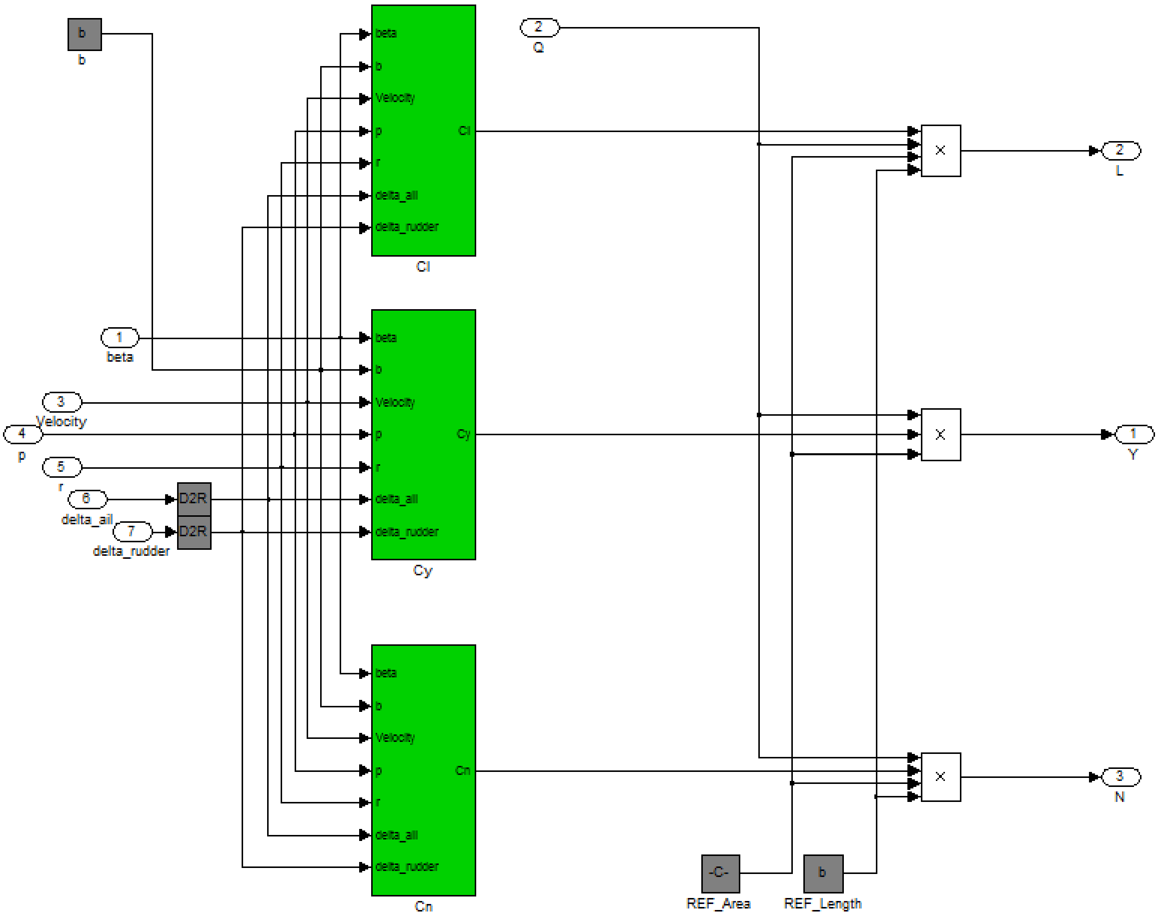

Figure 6-9: Aerodynamic Forces and Moments

Aerodynamic Forces and Moments Coefficient are calculated (a/c from dynamic to simulation)

$$C_y = C_{y\beta}\,\beta + \frac{b}{2V}\left(C_{y_p}p + C_{y_r}r\right) + C_{y_{\delta_a}}\delta_a + C_{y_{\delta_r}}\delta_r \text{..(6-17)}$$

$$C_l = C_{l\beta}\,\beta + \frac{b}{2V}\left(C_{l_p}p + C_{l_r}r\right) + C_{l_{\delta_a}}\delta_a + C_{l_{\delta_r}}\delta_r \text{.... (6-18)}$$

$$C_n = C_{n\beta}\,\beta + \frac{b}{2V}\left(C_{n_p}p + C_{n_r}r\right) + C_{n_{\delta_a}}\delta_a + C_{n_{\delta_r}}\delta_r \text{ (6-19)}$$

For instance, C_y Coefficient is modeled as in Figure (6-10)

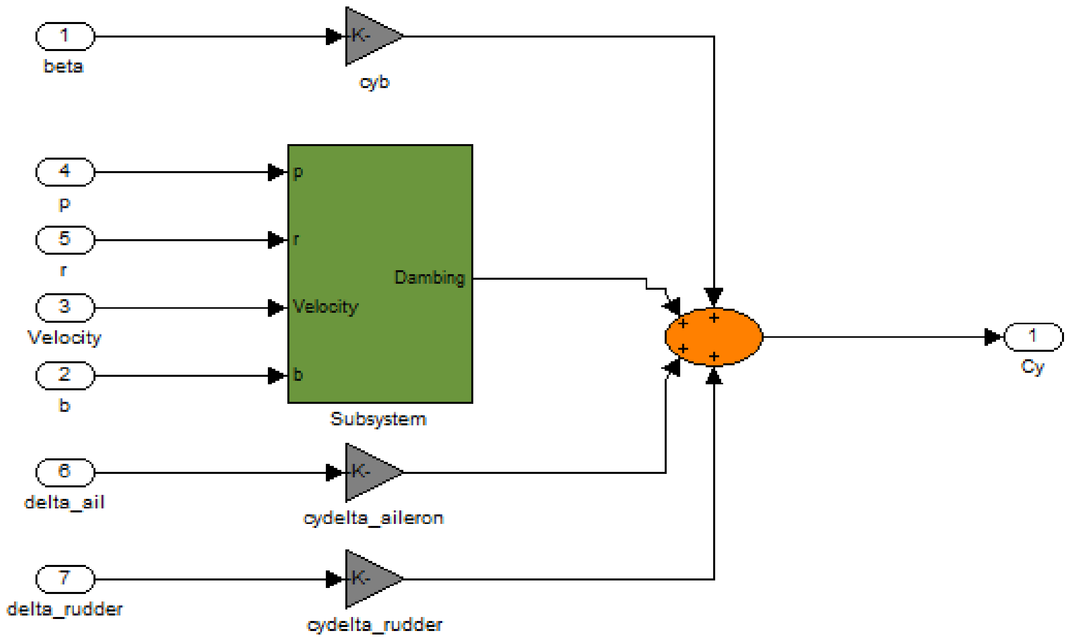

Figure 6-10:C_y Coefficient Block

The other coefficients (C_l, C_n) are modeled in the same manner.

6.2.1.3 Six Degree of freedom Model:

This Model is a result of coupling three degree of freedom longitudinal and lateral models into one six degree of freedom model. The model is shown in Figure (6-11).

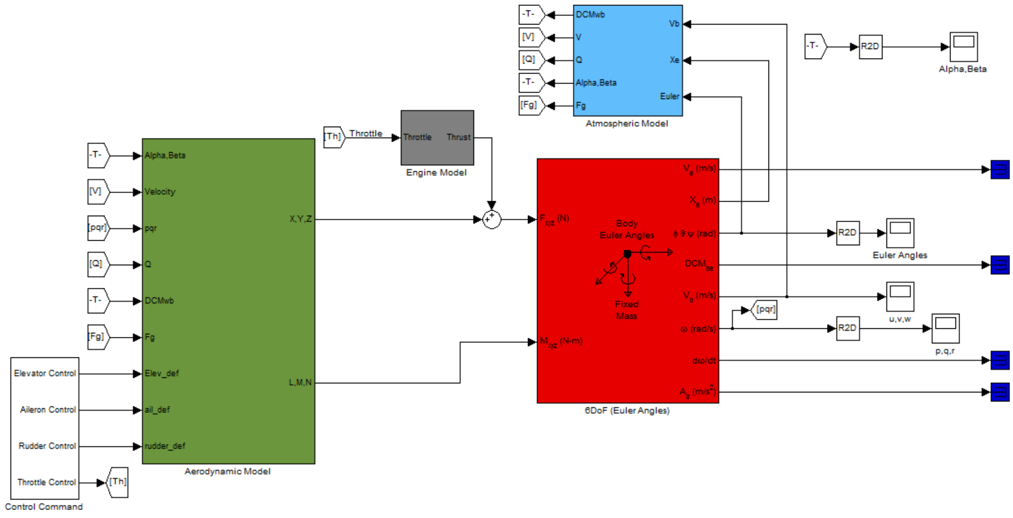

Figure 6-11: Six Degree of freedom Model

Calculation of equation of motion requires the definition of tensor matrix as follows:

$$\mathbf{I} = \begin{bmatrix} I_{xx} & -I_{xy} & -I_{xz} \\ -I_{yx} & I_{yy} & -I_{yz} \\ -I_{zx} & -I_{zy} & I_{zz} \end{bmatrix} \quad (6\text{-}20)$$

Atmospheric Model

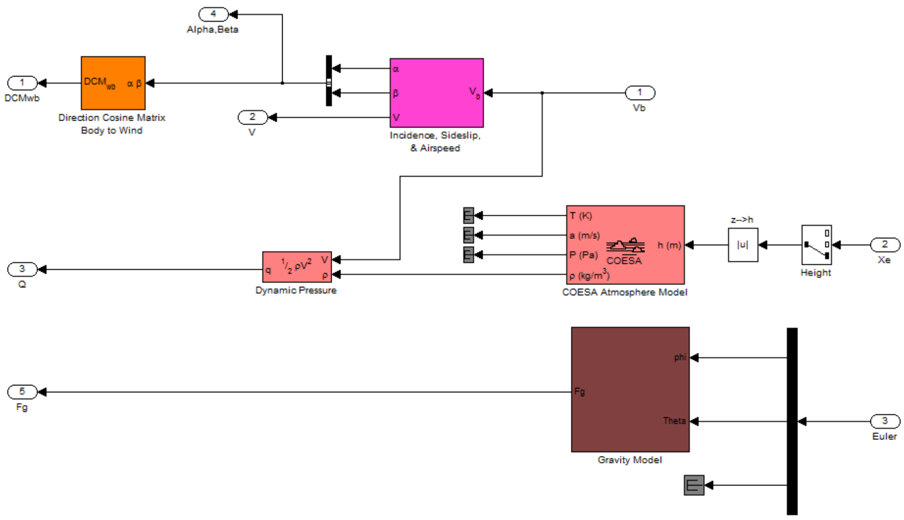

Figure 6-12: eAtmospheric Model

6.3 Aerodynamic Model:

To calculate aerodynamic and moments the following model is constructed.

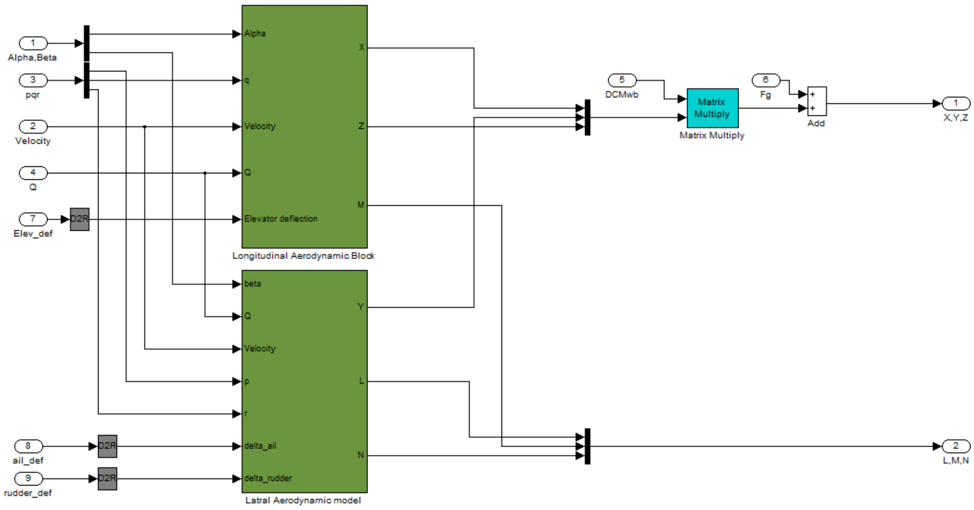

Figure 6-13: Aerodynamic and moment of Six DOF model

The Aerodynamics forces & Moments are in wind axis system to transfer it into body axis system; we will need to the following transformation matrix (DCM):

$$DCM_{WB} = \begin{bmatrix} cos\alpha\ cos\beta & -cos\alpha\ sin\beta & -sin\alpha \\ sin\beta & cos\beta & 0 \\ sin\alpha\ cos\beta & -sin\alpha\ sin\beta & cos\alpha \end{bmatrix} \ldots\ldots\ldots\ldots\ (6\text{-}21)$$

Gravity Model: obtained from reference [nelson].figure (6-14) below

$$F_{gravity} = \begin{bmatrix} -mg\ sin\theta \\ mg\ sin\theta\ sin\varphi \\ mg\ cos\theta\ cos\varphi \end{bmatrix} \ldots\ldots\ldots\ldots\ldots\ldots\ldots\ldots\ (6\text{-}22)$$

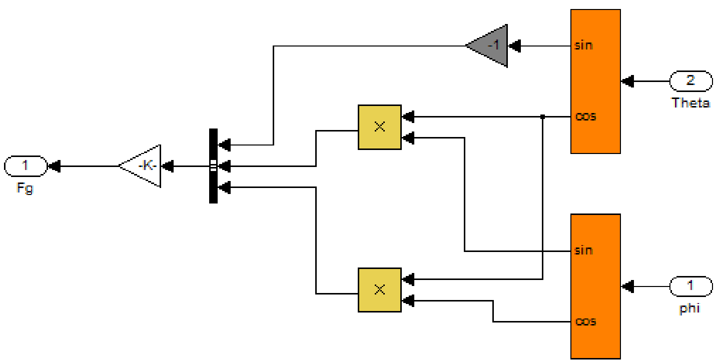

Figure 6-14: Gravity Model

6.2.2 Linear Model:

Linear is constructed using state space models derived in the previous chapter.

6.2.2.1 Three Degree of freedom Longitudinal Model:

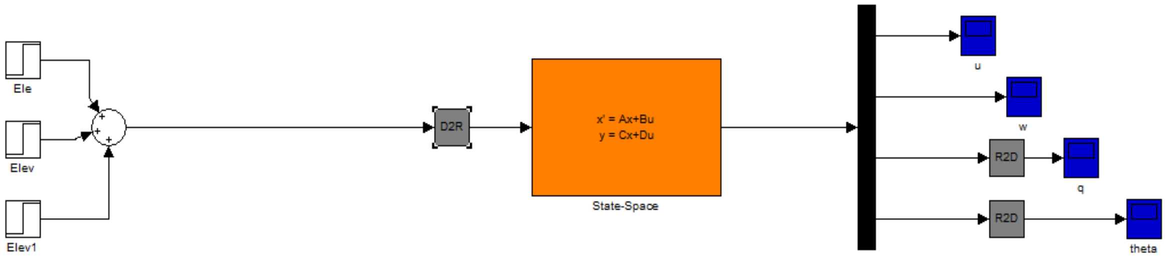

Figure 6-15: Three DOF Linear Longitudinal Model

6.2.2.2 Three Degree of freedom Lateral Model:

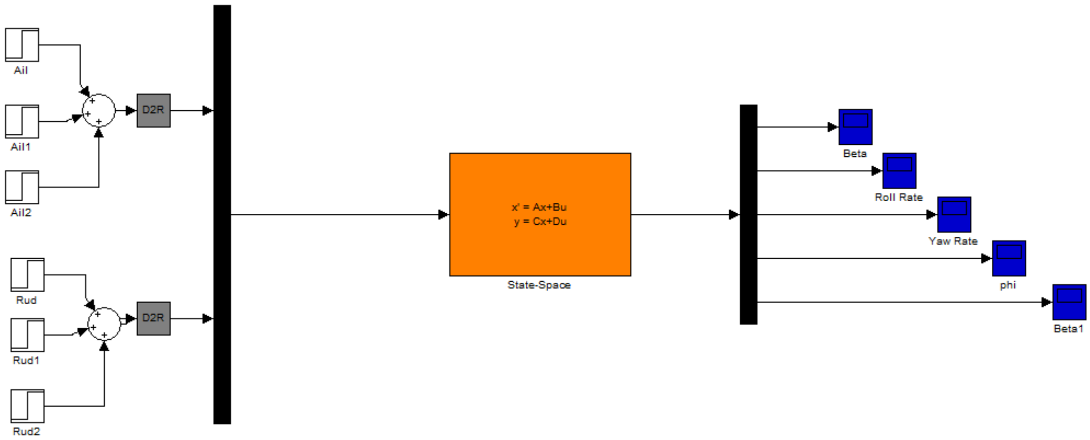

Figure 6-16: Three DOF Linear Lateral Model

Chapter 7 : PROPELLER DESIGN

AERODYNAMIC DESIGN

7.1 Theories comparison

As it was seen before propeller is made of number of blades which made of some airfoils arranged in such manner to compose blade, when this blade rotate it will create lift and drag which lead to create thrust and torque. That blade must be arranged in specific shape according to aerodynamics lows and equations.

In this chapter aerodynamics theories and equations shall be discussed and there comparison between them to choose one of theory for design and then aerodynamics design will be achieved. Those theories are[14]:

1. Momentum theory
2. Blade element theory

7.1.1 Momentum theory:

Momentum theory does not use blade shape or airfoil shape for design, there are many assumptions for this theory like:

a. Propeller assumed to replace by actuator disk energizer.
b. The disk assumes to be very small thickness and is continuous and 100% porous of no mass. With projected frontal area A (swept area) to the annulus of rotating propeller blade.
c. There is no resistance (i.e. drag) of the air pressure through actuator disc (since there are no propeller blade).
d. The axial velocity $\boldsymbol{V_1}$ through the disc is uniform over actuation area and considered to be smooth across the disc, i.e. no abrupt change is experienced.
e. The received energy manifests itself in working medium (i.e. air) finally in form of differential pressure $(\boldsymbol{P_1} - \boldsymbol{P_2})$ a jump change

across the actuator disc uniformly distributed across the disc surface.

f. The fluid medium (air) assumed to be perfect in compressible fluid flow is irrotational in front of and behind disc but not through it.

g. The static pressure far from the disc, i.e. far upstream and downstream, are both assumed equal atmospheric pressure, the corresponding velocity are independent value , to be determine separately.

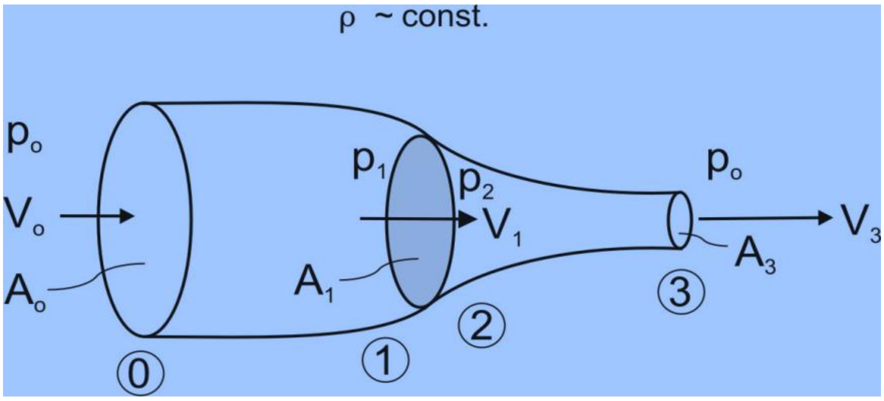

Figure 7-1: Momentum theory

Advantages of the theory:

Easy to calculate.

Disadvantages of the theory:

1. Thrust assumed to be generated by actuator disc not by blade so that there is not consideration of interference between blades, propeller chord, length and angle of the blade.
2. It considers there is not drag generated by the propeller.

3. Velocity through disc assumed to be constant but that is not true because of the appearance of blade sections.

7.1.2 Blade element theory:

A relatively simple method of predicting the performance of a propeller (as well as fans or windmills) is the use of Blade Element Theory. The primary limitation of the momentum theory is that it provides no information as to how the rotor blades should be designed so as to produce a given thrust. Also, profile drag losses are ignored. The blade-element theory is based on the assumption that each element of a propeller or rotor can be considered as an airfoil segment. Lift and drag are then calculated from the resultant velocity acting on the airfoil, each element considered independent of the adjoining elements.

This produces a set of non-linear equations that can be solved by iteration for each blade section. The resulting values of section thrust and torque can be summed to predict the overall performance of the propeller.

Disadvantages of the theory:

The theory does not include secondary effects such as 3-D flow velocities induced on the propeller by the shed tip vortex or radial components of flow induced by angular acceleration due to rotation of the propeller. In comparison with real propeller results this theory will over-predict thrust and under-predict torque with a resulting increase in theoretical efficiency of 5% to 10% over measured performance. Some of the flow assumptions made also breakdown for extreme conditions when the flow on the blades becomes stalled or there is a significant proportion of the propeller blade in wind milling configuration while other parts are still thrust producing.

Advantages of the theory:

The theory has been found very useful for comparative studies such as optimizing blade pitch setting for a given cruise speed or in determining the optimum blade solidity for a propeller. Given the above limitations it is still the best tool available for getting good first order predictions of thrust, torque and efficiency for propeller under a large range of operating conditions. All equations will be explained later.

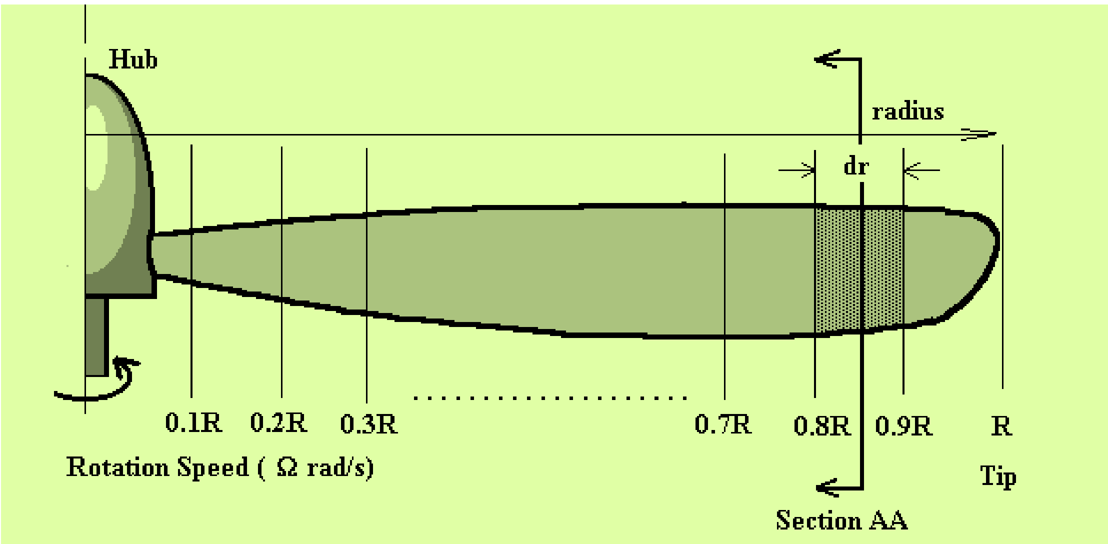

Figure 7-2: propeller blade sections

7.2 Aerodynamic calculations:

In this part, the aerodynamic calculation of the propeller will be achieved.

For the given data of the propeller and engine many parameters must be estimated such as:

Propeller diameter, propeller pitch angle, propeller chord line, thrust produced by propeller, power consumed by propeller and propeller drag.

7.2.1 Propeller diameter

Diameter is the most important parameter of the propeller and it effects directly in propeller performance. As diameter increase, thrust produced by propeller increased and power consumed by propeller will increase also, but the efficiency of the propeller will decrease.

There are many parameters must be taken into consideration in diameter calculation such as:

1. Space between two tail booms.
2. The height of the propeller from the earth.
3. Engine characteristics (such as engine horsepower and engine rpm).

7.2.2 Diameter calculation:

$$n = 11000\,rpm$$

$$\omega = \frac{2\pi n}{60} = \frac{2 \times \pi \times 11000}{60} = 1151.33\,rad/sec$$

To prevent stall propeller tip Mach number must be less than 1

$$\frac{V_{tip}}{a} > 1$$

$$V_{tip} \leq a$$

$$a = V_{tip} = \sqrt{\gamma RT} = \sqrt{1.4} \times 287 \times 288 = 340.174\ \ m/sec$$

$$V_{tip} = \omega R$$

$$R = \frac{V_{tip}}{\omega} = \frac{340.174}{1151.33} = 0.295 \text{ m} \quad , \mathbf{D}=2R = 2\times 0.295 = 0.591m$$

Also, there is many other ways and equations used to calculate aircraft propeller diameter[8] such as:

1. $D = 22\times \sqrt[4]{HP}$ …………………………………………….(7-1)

   $D = 22\times \sqrt[4]{16.4} = 44.27\ in = 1.12\ m$ & r = 0.562 m

2. $D = \frac{a}{\pi n}\sqrt{M_{tip}^2 - M^2}$ …………………………..………(7-2)

   $= \frac{340.174}{3.14\times 183.33}\sqrt{(1-0.14^2)}$ = 0.585 m, r = 0.2925 m

From the above equations it seems , there are many values for aircraft propeller diameter, but value which estimated by equation (7-2) will be taken as a value of aircraft propeller diameter because it takes many parameters into consideration , ensures better strength and satisfy the aircraft design requirements.

Note: this diameter is equivalent to the length of wing span, as the propeller rotates an induced roll moment is generated. We further explore the possibility of using counter-rotating blades. Counter-rotating blades have mainly two advantages: they are more efficient at high Mach numbers than a single propeller configuration and they allow a smaller diameter blade, allowing them to spin at higher rpm without a loss in aerodynamic efficiency. By having counter-rotating blades, our propeller diameter will be decreased considerably while maintaining the same efficiency.

7.3 Design envelops:

In this section, design of aircraft propeller will be done depending on the engine characteristics such as engine rpm and horsepower, and aircraft Specifications like aircraft cruise speed, Maximum speed and distance between the tail booms. Propeller design includes calculation of the length of chord line at each section, drag and lift generated at each section and power consumed by aircraft propeller[15].

To fulfill these objectives there are many parameters should be known previously.

7.3.1 Airfoil selection:

Due to the high Mach number, compressibility effects (recompression shocks, causing additional drag) reduce the efficiency of the propeller. A practical way to keep the drag of an airfoil at acceptable levels is the use of thinner and less cambered airfoils, to avoid excessive drag.

The airfoils selected were the CLARK–Y, NACA6412, MH 114 and NACA9412 because the characteristics that met the design constraints.

The first step while carrying out a propeller design to choosing an airfoil is looking into the airfoil characteristics such as the L/D ratio, the maximum CL, stall angle depending on the desired thickness as well.

Table16: airfoil characteristics comparisons

	CLARK-Y	NACA 6412	NACA 9412	MH 114
Thickness	0.117c	0.12 c	0.12c	0.13c
Camber	0.034c	0.06c	0.09c	0.6c
Trailing edge angle	15.3deg	14.2deg	13.7deg	11.8deg
Lower flatness	.718c	.812c	.381c	.808c
Max CL	1.295	1.785	2.148	1.981
Max CL angle	8.5	12.0	12.0	12.0
Leading edge radius	.12c	.17c	.17c	.27c
Max L/D	51.61	60.34	58.12	46.291
Max L/D angle	7.0	4.0	0.5	6.5
Max L/D CL	1.18	1.268	1.229	1.676
Stall angle	8.5deg	4.0deg	12.0deg	12.0deg
Zero-lift angle	-3.5deg	-6.0deg	-9.5deg	-8.0deg

The proper airfoil selected is Clark-y

Figure 7-3: Clark-y airfoil

There are many types of airfoil used for propeller design like NACA 16 series and Clark-Y airfoils, NACA 16 series usually use in designing of propeller with engines which have horse power greater than 700 hp so that Clark-Y

Airfoil was selected for this project. The airfoil has a maximum thickness of 11.7 percent of the chord at 30 percent of chord back and is flat on the lower surface .The flat bottom simplifies angle measurements on propellers, for many applications the Clark Y has been adequate; it gives reasonable overall performance in respect of its lift-to- drag ratio, and has gentle and relatively benign stall characteristics .But the flat lower surface is sub-optimal from an aerodynamic perspective, and it is rarely used in new designs.

From lift and drag curve (fig 7.3) below which plotted against of attack it is found that (α=10 degree) is the best angle of attack for Clark-Y airfoil which gives maximum lift to drag ratio (CL/CD=14.667).

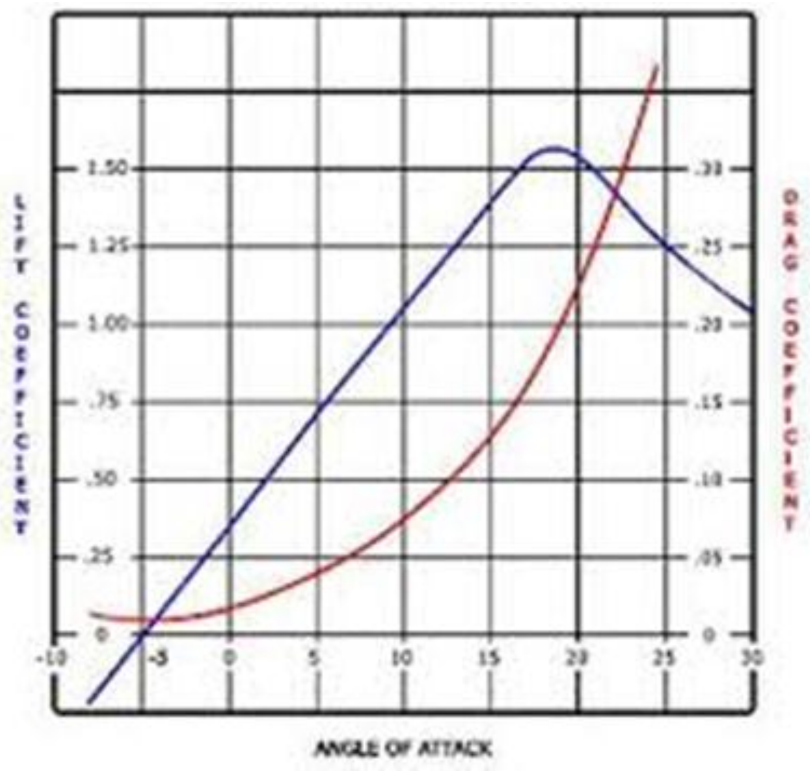

Figure 7-4: Clark-y lifte and drag curve

7.3.2 Number of Blades, *B:*

There are many parameters must be taken in consideration at the number of blade selection, like engine horsepower, diameter of the propeller and chord length of the propeller. The most efficient propellers are two bladed. Because the diameter of propellers is so s mall, multiple blade propellers disturb the air that the trailing blade is entering. Therefore, 3 and 4 blade propellers are less efficient.

7.4 Calculation method and iteration:

In this section of the project, calculation method and iteration will be discussed, all calculations and iteration will be achieved according to the blade element theory with iteration method because there are many parameters need initial guessed values, and the last value will be obtained from iteration as explained below :

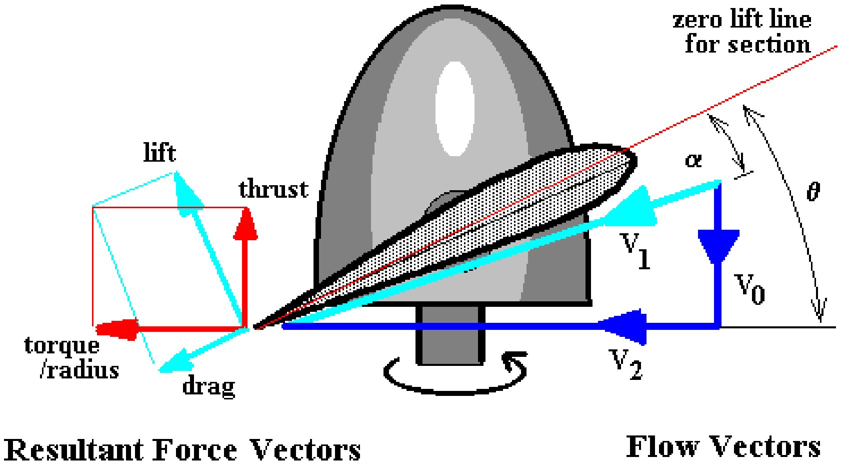

Figure 7-5: Blade element theory parameters

Iteration method

1. Firstly, solution will start with some initial guessed values of inflow factors (a) and (b) , apply this guessed values on equations ((7-3) to (7-7)) to find the flow angle on the blade.

$$V_0 = V_\infty(1 + \mathrm{a}) \quad \text{(7-3)}$$

$$V_2 = \omega\mathrm{r}(1 - \mathrm{b}) \quad \text{(7-4)}$$

$$V_1 = \sqrt{V_0 + V_2} \quad \text{(7-5)}$$

$$\varphi = \tan^{-1}\frac{V_0}{V_2} \quad \text{(7-6)}$$

$$\theta = (\alpha + \varphi) \quad \text{(7-7)}$$

2. The second step: chord length can be calculated by using equation (7-9)

$$\lambda_\mathrm{r} = \frac{\mathrm{V}_2}{\mathrm{V}_0} \quad \text{(7-8)}$$

$C = \frac{8\pi r sin\varphi}{3B\lambda_r}$……………………………………………………….. (7-9)

3. Then use blade section properties to estimate the element thrust and torque from equation (7-10) and (7-11))

$\Delta T = \frac{1}{2}\rho V_1^2 C\,(C_L \cos\varphi - C_D \sin\varphi).B.dr$………………...…..... (7-10)

$\Delta Q = \frac{1}{2}\rho V_1^2 c(C_L \sin\varphi + C_D \cos\varphi(\varphi)\,).B.r.dr$…………. (7-11)

4. With these approximate values of thrust and torque equations (7-12) and (7-13) can be used to give improved estimates of the inflow factors (a) and (b).

$\Delta T = 4\pi\rho r V_\infty^2 (1+a)a.dr$……………………………………………… (7-12)

$\Delta Q = 4\pi\rho r^3 V_\infty^2 (1+a)b.\omega.dr$…………….…………………………. (7-13)

5. This process can be repeated until values for (a) and (b) have converged to within a specified tolerance; this process must be used for blade sections separated from each other.

For the final values of inflow factor (a) and (b) an accurate prediction of element thrust and torque will be obtained from equations (7-10) and (7-11).

$\Delta T = \frac{1}{2}\rho V_1^2 C\,(C_L \cos\varphi - C_D \sin\varphi).B.dr$…………..…..….. (7-10)

$\Delta Q = \frac{1}{2}\rho V_1^2 c(C_L \sin\varphi + C_D \cos\varphi(\varphi)\,).B.r.dr$…………. (7-11)

6. The overall propeller thrust and torque will be obtained by summing the results of all the radial blade element values.

The non-dimensional thrust and torque coefficients can then be calculated along with the advance ratio at which they have been calculated.

$C_{\mathrm{T}} = T/(\rho n^2 D^4)$……………………………………………….……….. (7-14)

And

$C_{\mathrm{Q}} = Q/(\rho n^2 D^5)$……………………………………………………… (7-15)

For

$J = V_{\infty}/(nD)$…………………….…………………………………….. (7-16)

Where n is the rotation speed of propeller in revs per second and D is the propeller diameter.

The efficiency of the propeller under these flight conditions will then be:

$\eta_{prop} = J/(2\pi).(C_{\mathrm{T}}/C_{\mathrm{Q}})$…………………………………….. (7-17)

Design condition and assumption:

In this part of project many assumption and values of parameter will be explained. This value taken from the aircraft specification engines description and airfoil characteristics and will take as constant values it will not change through this project.

Table17: Design condition and assumption

NO	Parameter	symbol	Dimension	Value
1	Angle of attack	α	Degree	10
2	Lift coefficient	C_L	-	1.1
3	Drag coefficient	C_D	-	0.075
4	Maximum aircraft speed	V_∞	m/sec	47
5	Maximum revolution per minute	N	Rpm	2980
6	Engine power	HP	Hp	16.4
7	Propeller diameter	D	M	0.585
8	Design condition	Sea level		

The equations states above from (7-3) to (7-15) were programmed in MATLAB Software code.

The result of this code are reasonable and realistic, at the root of the propeller the chord length is 0.1443 m and the pitch angle is 1.1369 RAD (65.14 deg).at the tip of the propeller the chord length 0.0295 m and the pitch angle is 0.3294 RAD(18.87 deg).All the results are scheduled in the tables below:

Symbol for iteration :

Section 1 r = 0.02925 m

NO	C	φ	θ	ΔT	ΔQ	An	b_n
1	0.1454	0.9649	1.1394	10.0811	0.4497	0.0238	0.01
2	0.1445	0.9627	1.1372	9.8161	0.4356	0.01	0.0188
3	0.1443	0.9624	1.1369	9.8129	0.4351	0.0098	0.014

Table18: Results of iteration for all sections of propeller

NO	C	φ	θ	ΔT	ΔQ	An	b_n	R
1	0.1443	0.9624	1.1369	9.8129	0.4351	0.0098	0.014	0.02925
2	0.1020	0.6210	0.7956	21.1474	0.8419	0.0208	0.0044	0.0585
3	0.0767	0.4484	0.6229	32.9721	1.2351	0.0321	0.0019	0.08775
4	0.0612	0.3495	0.5241	45.3174	1.6111	0.0437	0.0010	0.117
5	0.0511	0.2866	0.4612	58.2064	1.9683	0.0554	0.00063640	0.14625
6	0.0440	0.2435	0.4180	71.6892	2.3063	0.0675	0.00042759	0.1755
7	0.0339	0.1982	0.3727	74.6897	2.0567	0.0702	0.00025452	0.20475
8	0.0342	0.1862	0.3608	98.2262	2.7994	0.0906	0.00021644	0.234
9	0.0319	0.1697	0.3443	115.8586	3.1848	0.1054	0.00016900	0.26325
10	0.0295	0.1548	0.3294	131.9649	3.4294	0.1186	0.00013109	0.2925

$T = \sum \Delta T(for all elements) = 659.8848 \quad N$

$Q = \sum \Delta Q(for all elements) = 19.8681 \quad N.m$

$C_{\mathrm{T}} = \frac{T}{\rho n^2 D^4} = 659.8848 \quad /(1.225 \times 183.33^2 \times 0.585^4) = 0.137$

$C_{\mathrm{Q}} = Q/(\rho n^2 D^5) = 19.8681/(1.225 \times 183.33^2 \times 0.585^5) = 0.00704$

$J = V_\infty/(nD) = 47/(183.33 \times 0.585) = 0.438$

$\eta_{prop} = J/(2\pi).(C_{\mathrm{T}}/C_{\mathrm{Q}}) = 0.438/2\pi \times (0.137 / 0.00704) = 1.36\%$

The total torque required to drive propeller, power required and activity factor can be calculated by equations (7-18),(7-19) and (7-20) as shown below:

$$C \equiv C_{mean} = 0.06088\, m$$

$Q_{\mathrm{r}} = 2\pi^2 \rho C_{\mathrm{D}} \mathrm{Bn}^2 \int_{root}^{\mathrm{tip}} \mathrm{Cr}^3.\mathrm{dr}$ …………………………….. (7-18)

$$Q_{\mathrm{r}} = 2\pi^2 \times 1.225 \times 0.075 \times 2 \times 183.33^2 \int_{0.02925}^{0.2925} \mathrm{Cr}^3.\mathrm{dr}$$

$$= 13.5799\ \mathrm{N.m}$$

$\mathrm{P_r} = 4\pi^3 \rho C_{\mathrm{D}}\ \mathrm{Bn}^3 \int_{0.02925}^{0.2925} \mathrm{Cr}^3.\mathrm{dr}$…………….…………………… (7-19)

$$\mathrm{P_r} = 4\pi^3 \times 1.225 \times 0.075 \times 2 \times 183.33^3 \int_{0.02925}^{0.2925} \mathrm{Cr}^3.\mathrm{dr}$$

=15.64 KW

Activity factor (AF) is a design parameter associated with the propeller blades geometry

$$AF=\frac{10^5}{16}\int_{0.02925}^{0.2925}\frac{C}{d}r^3\,.\,dr. \ldots\ldots\ldots\ldots\ldots\ldots\ldots\ldots\ldots\ldots\ldots \text{(7-20)}$$

$$AF=\frac{10^5}{16}\int_{0.02925}^{0.2925}\frac{C}{0.585}r^3.dr = 19$$

The more slender the blade (larger radius, smaller chord), the lower the AF value

JAVAPROP is a simple tool for the design and the analysis of propellers and wind turbines .Within its limits, it is applicable to aeronautical as well as to marine applications. The implemented classical blade element design and analysis methods are based on a coupling of momentum considerations with two-dimensional airfoil characteristics. It is therefore possible to consider different airfoil sections and the impact of their characteristics on rotor performance.

JAVAPROP contains a powerful direct inverse design module. Inverse design means that specify only a few basic parameters and Java Foil produces a geometry which automatically has the maximum efficiency for the selected design parameters. The beautiful thing is that JAVAPROP creates an optimum propeller with just 5 design parameters plus a selection of airfoil operating points along the radius.

7.5 Cascade design:

7.5.1 Stage with downstream guide vanes:

This arrangement is shown in figure (7.5) below. The rotor blades receive air in the axial direction. The absolute velocity vector C_2 at the rotor exit has swirl component C_{y2} which is removed by the downstream guide vanes (DGVs) and the flow is finally discharged axially from the stage.

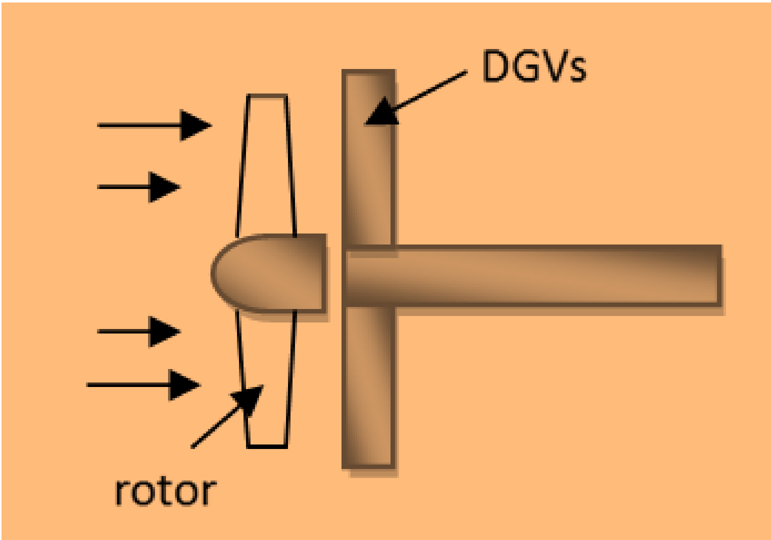

Figure 7-6: Axial propeller stage with downstream guide vanes

The design start firstly by estimate the propeller stage parameters: stage work, stage reaction, stage pressure rise.

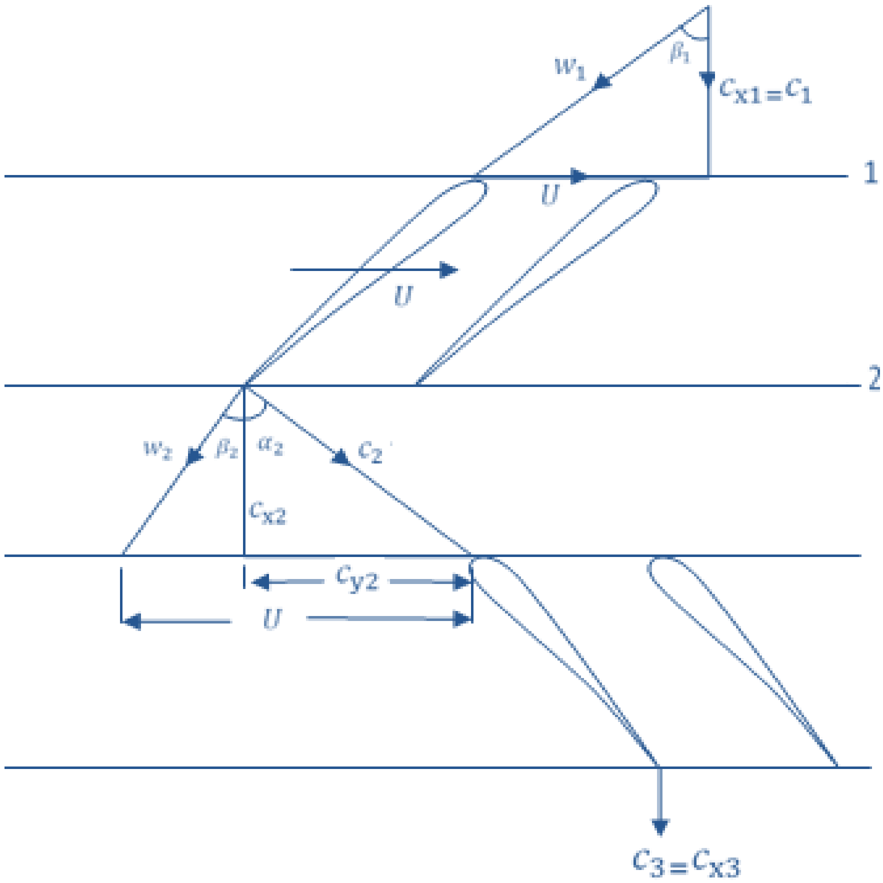

Figure 7-7: Axial propeller stage with downstream guide vanes (velocity triangles for R<1)

The swirl at the entry to the rotor is zero (C_{y1}=0).

The work done in the stage:

$W_{st}=U^2(1-\emptyset\tan B_2)$

The stage pressure rise:

$$(\Delta P_o)_{st}=\rho U^2(1-\emptyset\tan B_2)$$

Therefore the stage pressure coefficient:

$\psi=2(1-\emptyset\tan B_2)$

The pressure rise in the rotor:

$$(\Delta P)_r = \rho U C_{y2} - \frac{1}{2}\rho C_{y2}^2$$

Stage reaction:

$$R = \frac{1}{2}(1 + \emptyset \tan B_2)$$

As the propeller rotation speed is 2100 rpm so,$U = \frac{\pi N D}{60} = \pi \times 2100 \times \frac{0.585}{60} = 64.29\ m/s$

$\emptyset = 0.156$, $B_2 = 10\ deg$, $C_{y2} = 62.53\ m/s$

$W_{st} = U^2(1 - \emptyset \tan B_2)$

$= 64.29\ ^2(1 - 0.156 \times \tan 10) = 4019.51\ \ J/Kg$

$$(\Delta P_o)_{st} = \rho U^2(1 - \emptyset \tan B_2)$$
$$= 1.225 \times 64.29\ ^2(1 - 0.156 \tan 10) = 4923.90\ N/m^2$$

ψ=$2(1 - \emptyset \tan B_2) = 2(1 - 0.156 \times \tan 10) = 1.945$

$(\Delta P)_r = \rho U C_{y2} - \frac{1}{2}\rho C_{y2}^2$=$1.225\times 64.29 \times 62.53 - \frac{1}{2} \times 1.225 \times 62.53^2 = 2529.69 N/m^2$

$R = \frac{1}{2}(1 + \emptyset \tan B_2)$= $\frac{1}{2} \times (1 + 0.156 \times \tan 10) = 0.514$

Secondly, by take these parameters in consideration.

The cascade system is a number of guide vanes (2 to 8), the choice of guide vanes depending on the number of rotor blades and the area of actuation.

In this procedure, the best choice for 2-rotor blades is 4 guide vanes has the same of some of the specifications of the blade such as, airfoil selection is Clark-y ,each two guide vanes with the hub diameter like propeller diameter. This arrangement is shown in figure (7.7) below:

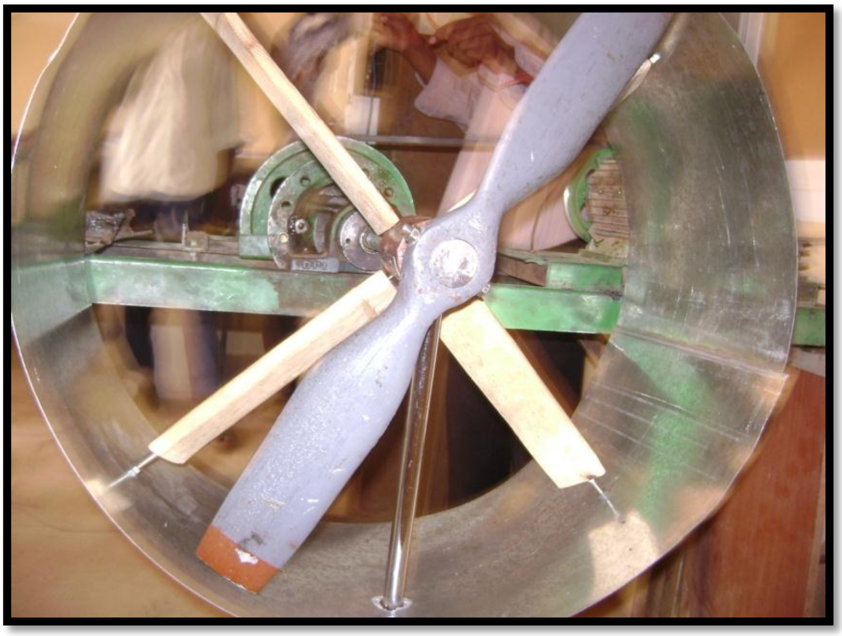

Figure7-8: Cascade arrangement

7.6 Co-axial propeller design:

In this section, the coaxial propeller system is made by using the same procedure of the above design to design the lower rotor (the second propeller), by take in consideration the opposite setting angle of the propeller. The critical distance between the two propellers assume to be as the chord length at tip

The coaxial rotor design offers many advantageous attributes over singular rotor systems.

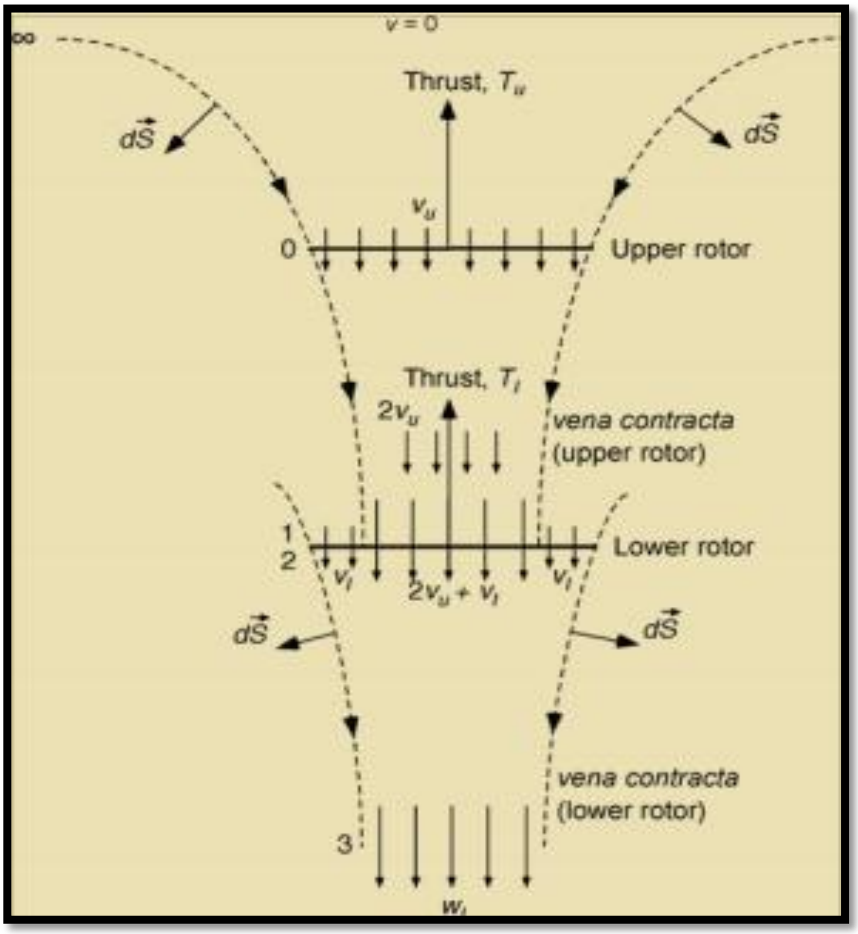

Figure 7-9: Flow Model of a Co - Axial Rotor System

Co-axial advantages:

1. Directional stability through cancellation of torque moment (Yaw torque reaction)
2. Compact size through use of concentric shafts.
3. Increased pressure differential over rotor system; increased thrust, higher efficiency for increase in thrust, which translates into a reduction in rotor diameter for a given thrust.
4. High thrust to weight ratio
5. Absence of torque transfer
6. Precession load are balanced
7. Freedom from propeller size limitations.

8. Complete symmetry of rotor system.
9. Simplified rotor system.
10. Freedom from control cross-coupling
11. Optimal transmission design

Disadvantages:

1. They can be very noisy, with increases in noise in the axial (forward and aft) direction of up to 30 dB, and tangentially 10 dB.
2. Inter- rotor wash interference. Reduced efficiency of the lower rotor due to the upper rotor swirling the air in the opposite direction of the lower rotor which requires the lower rotor to run at higher speed to produce the same lift as the upper rotor.
3. Importance of flow interaction, requirement for rotor spacing. To ensure sufficiently clean flow for the lower disc, the spacing must be wide enough to allow as little interaction of the swirl of the upper rotor to impinge on the retreating component of the lower disc.

7.7 Practical calculations:

To evaluate the value of static thrust on each case, practical experiments were done. By running the motor, the propeller started to suck the air. The manometer used to estimate the value of dynamic pressure.

Figure 7-10: Pitot-tube and the manometer

As the K.E = $\frac{1}{2}\rho_{air}v^2$... (7-21)

The pressure from the manometer:

P=$\rho_m gh$... (7-22)

As p is a K.E (dynamic pressure), h is the height of water inside the manometer

$$\frac{1}{2}\rho_{air}V^2 = \rho_m gh$$

So;

$$V = \sqrt{\frac{2\rho_m gh}{\rho_{air}}} \quad \text{...} \quad (7\text{-}23)$$

$\rho_{air} = 1.11 kg/m^3$, $\rho_m = 1000\ kg/m^3$

T = $m^{\circ}(V_{exit} - V_{in})$... (7-24)

For static thrust $V_{in} = 0$, T =$\rho_{air} \times V^2 \times A$,

$A = \frac{\pi}{4} d^2 = \frac{\pi}{4} (0.585)^2$=0.269 m^2

$\eta_{prop} = \frac{T_{static} \times V_{static}}{P_{engine}}$, $P_{motor} \equiv P_{engine}$ =1864 watt

FOR SIGLE PROPELLER:

The manometer measure h=11 mm =0.011m

$$V = \sqrt{\frac{2 \times 1000 \times 9.81 \times 0.011}{1.11}} = 13.94\ m/s$$

T= $1.11 \times 13.94^2 \times 0.269 = 58.02\ N$

η_{prop}= 43.39 %

FOR SIGLE PROPELLER WITH REARWARD CASCADE:

By setting the cascade blade at **5 deg,** the manometer measure h=14.5 mm =0.0145m

$$V = \sqrt{\frac{2 \times 1000 \times 9.81 \times 0.0145}{1.11}} = 16.01\ m/s$$

T= $1.11 \times 16.01^2 \times 0.269 = 76.53\ \ N$

η_{prop}= 65.74 %

By setting the cascade blade at **10 deg,** the manometer measure h=18 mm =0.018m

$$V = \sqrt{\frac{2 \times 1000 \times 9.81 \times 0.018}{1.11}} = 17.829\ m/s$$

T= $1.11 \times 17.829^2 \times 0.269 = 95.0\ N$

η_{prop}= 90.87 %

By setting the cascade blade at **15 deg,** the manometer measure h=16.5mm =0.0165m

$$V = \sqrt{\frac{2 \times 1000 \times 9.81 \times 0.0165}{1.11}} = 17.08\, m/s$$

T= $1.11 \times 17.08^2 \times 0.269 = 87.11\ N$

η_{prop}= 79.82 %

FOR COAXIAL PROPELLER: the manometer measure h=18.7 mm =0.0187m

$$V = \sqrt{\frac{2 \times 1000 \times 9.81 \times 0.0187}{1.11}} = 18.18\, m/s$$

T= $1.11 \times 18.18^2 \times 0.269 = 98.69N$

η_{prop}= 96.259 %

Chapter 8 : FABRICATION

Propeller fabrication method:

One of the key goals of this work was to automate as much of the fabrication process as possible.

The needed to fabrication start when propeller needed to run experiment aims to reduce the effect of swirl flow.

The needed propeller chosen to made by casting but first must make wood model to prepare the cast.

The wooded propeller was made by method of carving propellers with helical pitch [16]as showing in the blow picture:

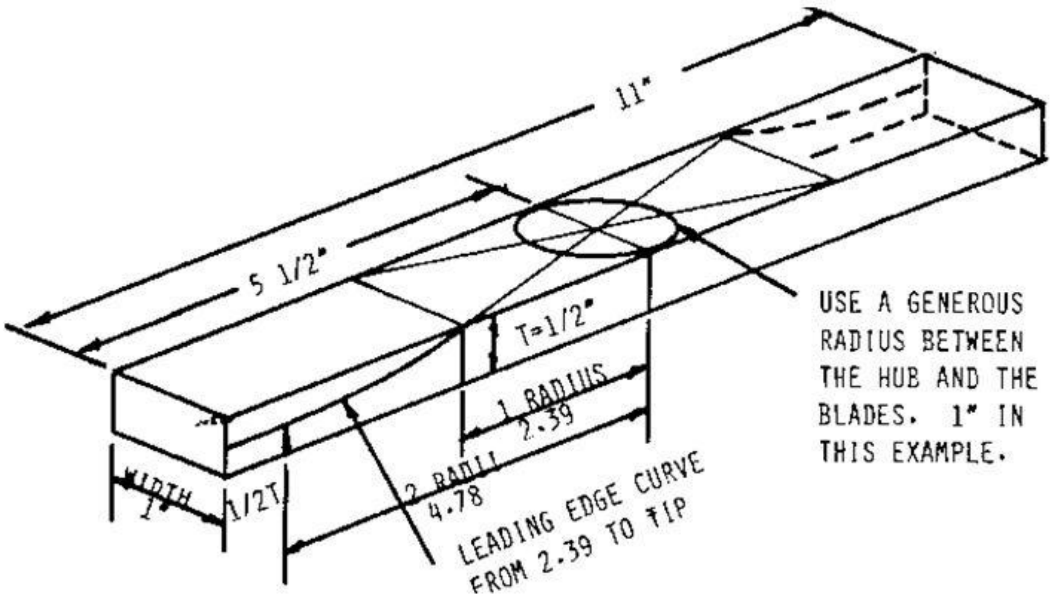

Figure 8-1: propeller layout

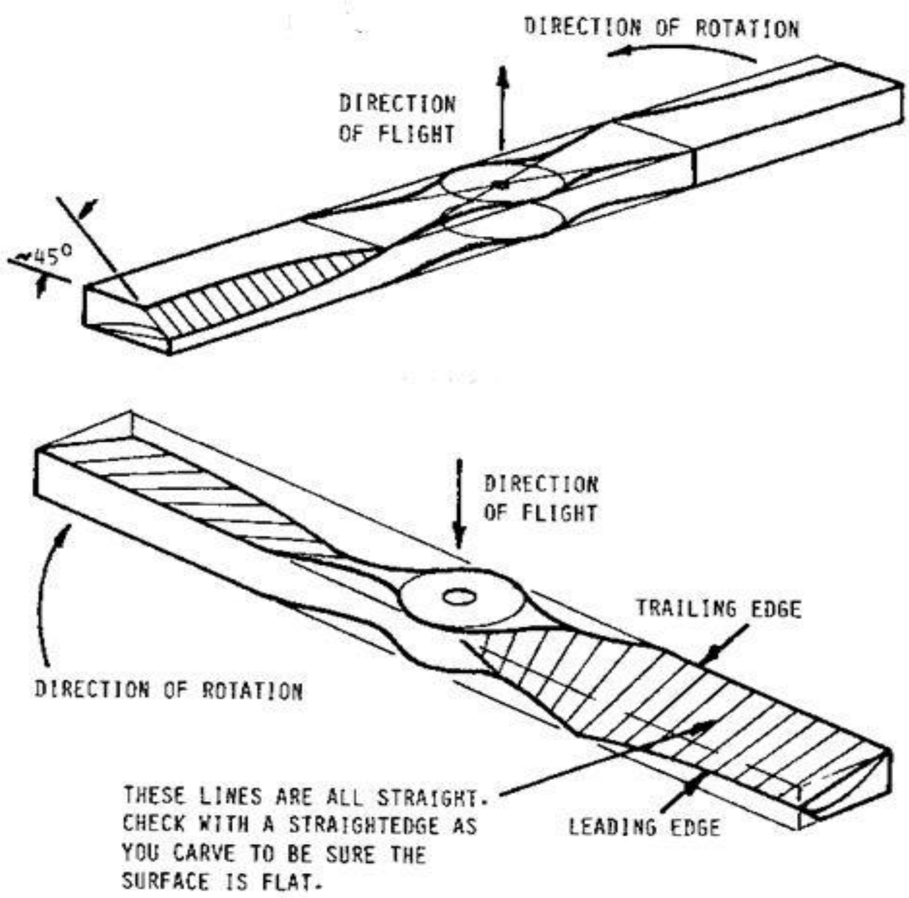

Figure 8-2: Propeller curving

And by using sample carpentry tools as show below:

Figure 8-3: carpentry tools

Figure 8-4: Propeller wooden model

Then the propeller had been casted and surface finished as showing below:

Figure 8-5: Propeller casting

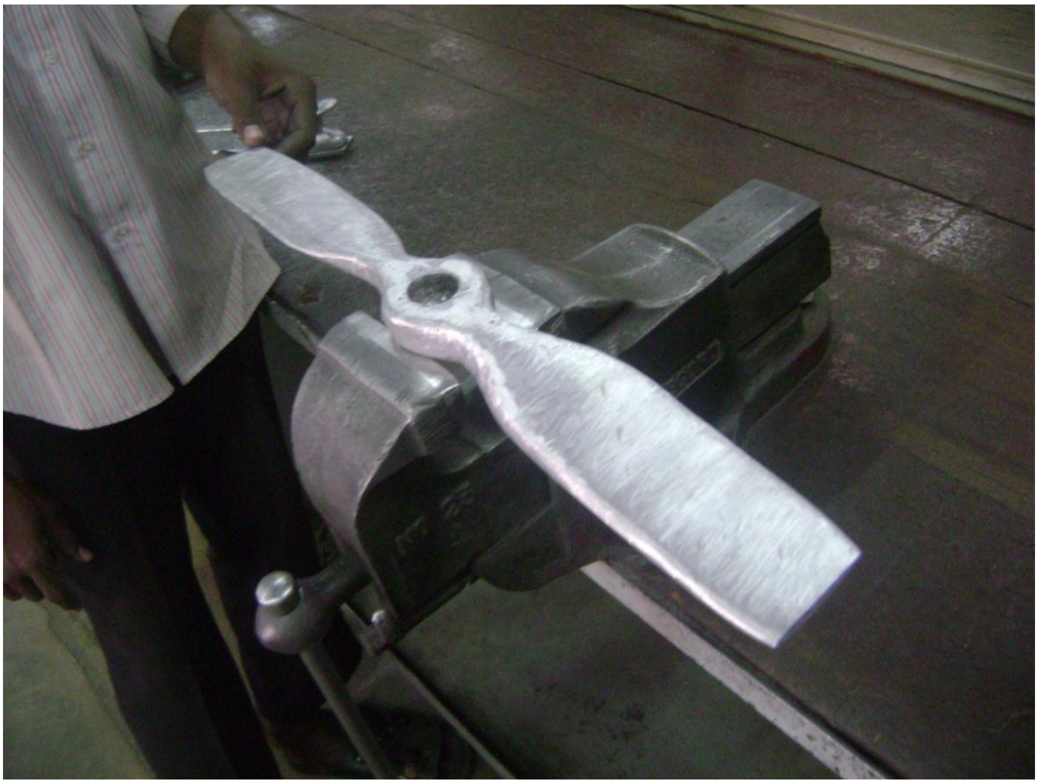

Figure 8-6: Surface finishing

Figure 8-7: Final product

After that there was need to test section to collect the air flow and its made from sheet of alminium rolled as a duct, the duct also used to support the fixed cascade, and to get continous test section with high unformity flow with minimum disturbance, to achieve that the shaft should extend, but the long shaft lead to high vibrations and bending loads this need front bearig support as showing in figure below:

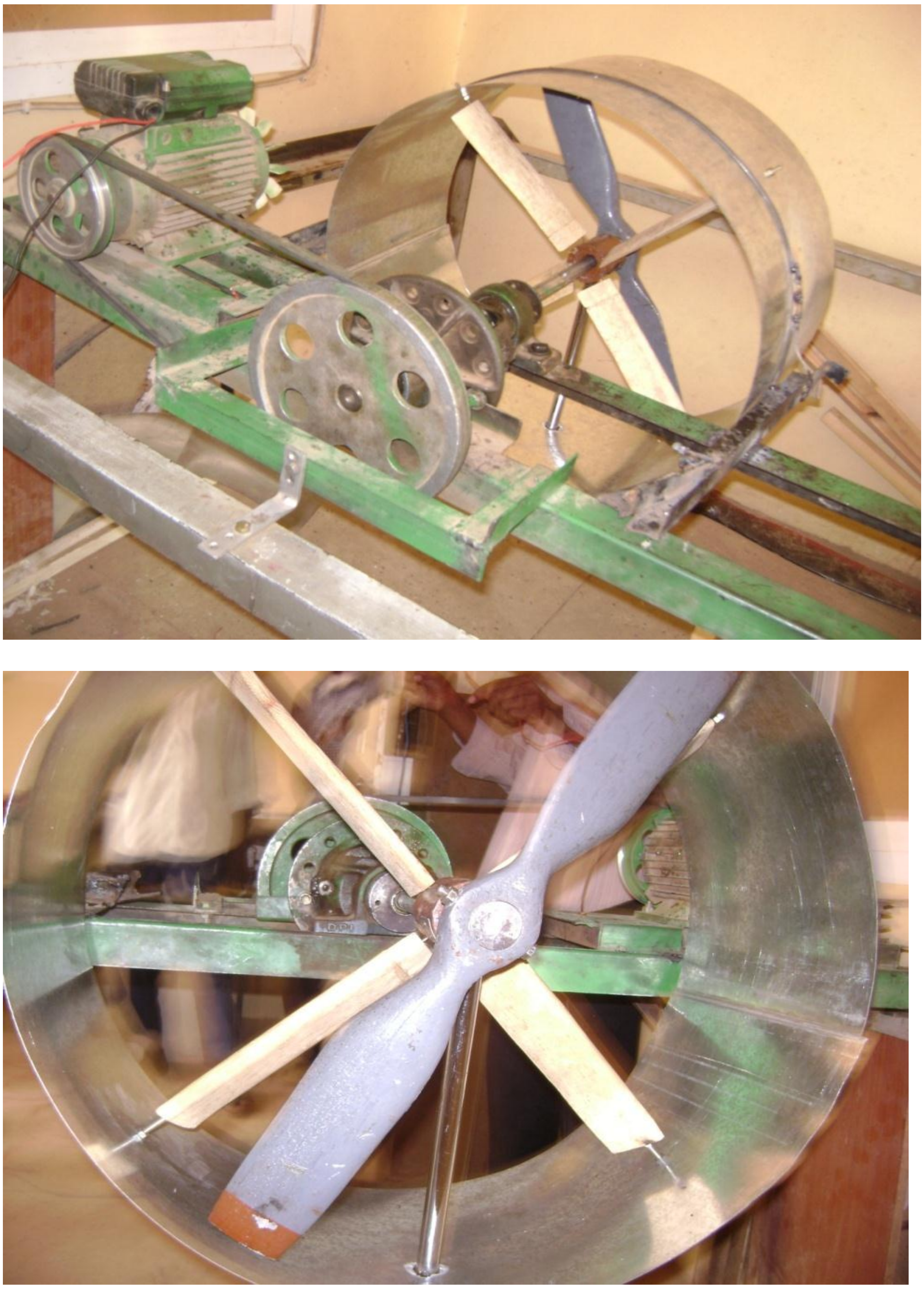

Figure 8-8: System modifications

The cascade is the first method of reduceing swirl generated by the propeller and made from four wooden blade and used screw and nuts to judging the blade angle.

Figure 8-9: Cascade blades

The last step was to use coaxial propellers and this required additional propeller with opposite pitch relative to the first one and fabricated by wood due to the load acting on the electrical motor by propeller weight and friction load from the gear box.

Figure 8-10: Coaxial system

The tools which used to measure the motor and propeller RPM & the flow velocity is optical digital tachometer and pitot tube with manometer respectively.

Figure 8-11: Optical digital tachometer

Figure 8-12: Pitot tube with manometer

Chapter 9 : RESULTS & DISCUSION

Aerodynamics:

The approach conducted to calculate the aerodynamic coefficients is a crude mean to follow. It assumes that the laminar flow is about 10% of the total flow and turbulent flow is about 90%.

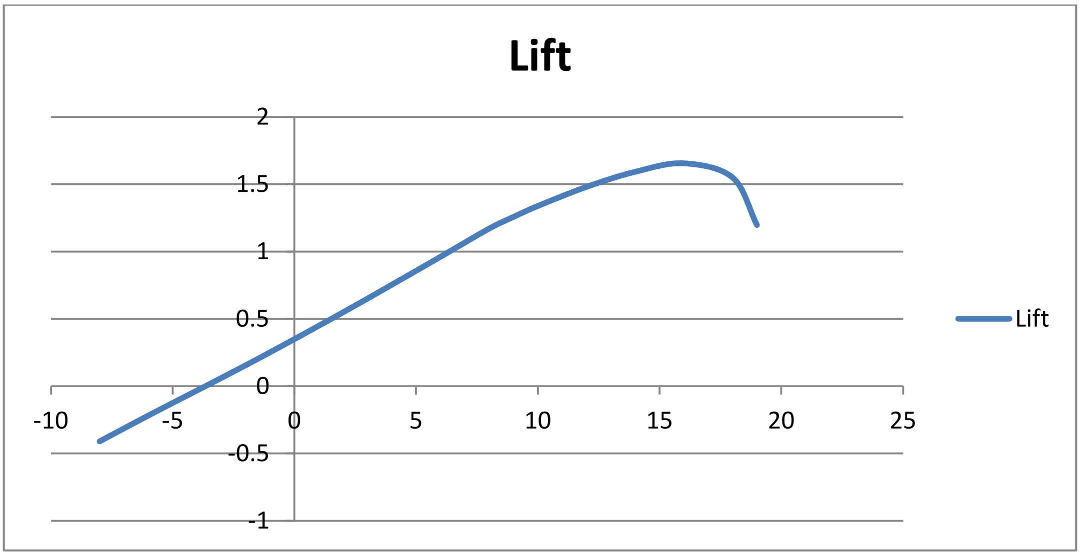

Figure 9-1: lift curve slope

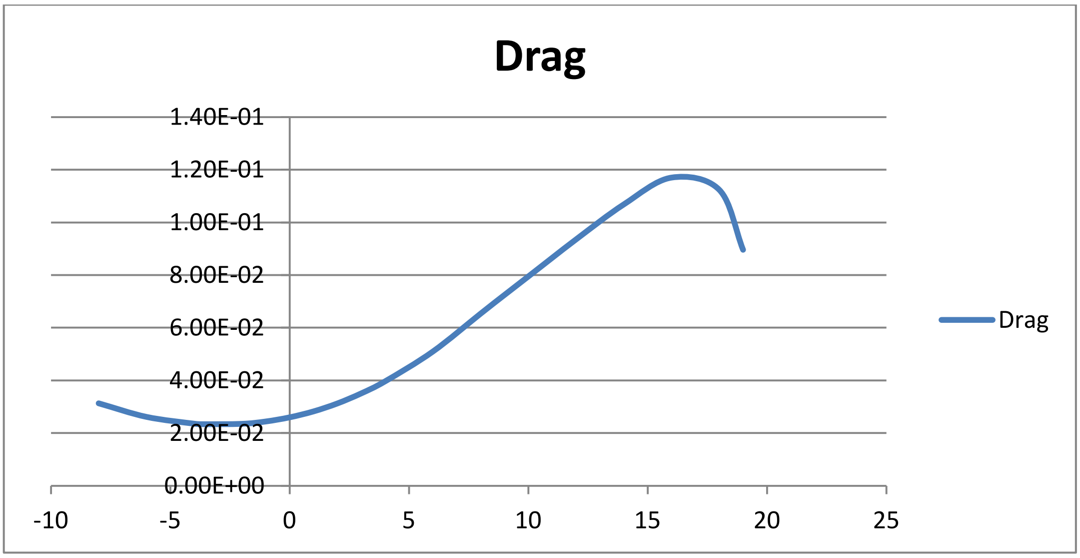

Figure 9-2: drag against angle of attack

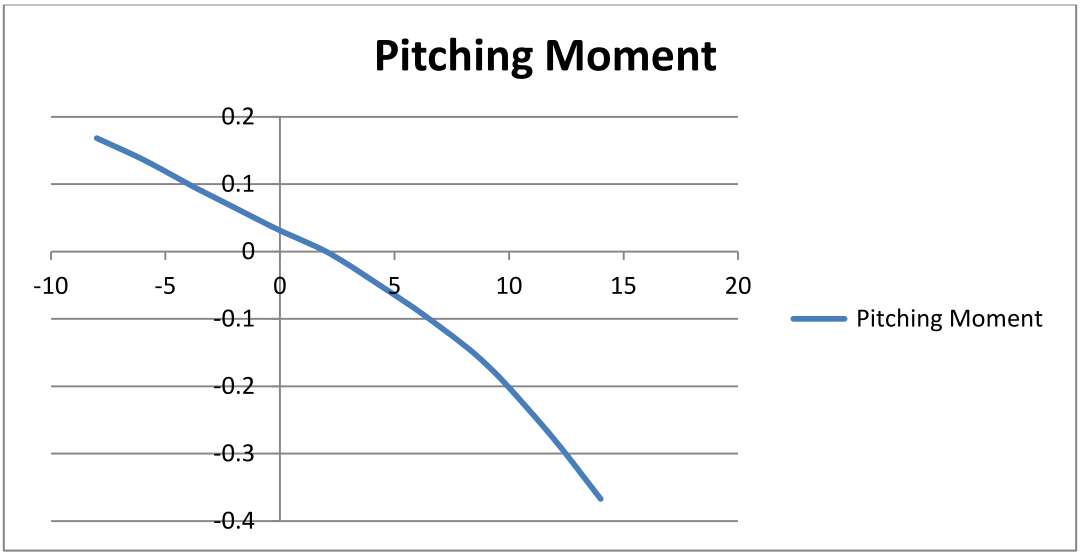

Figure 9-3: Pitching Moment

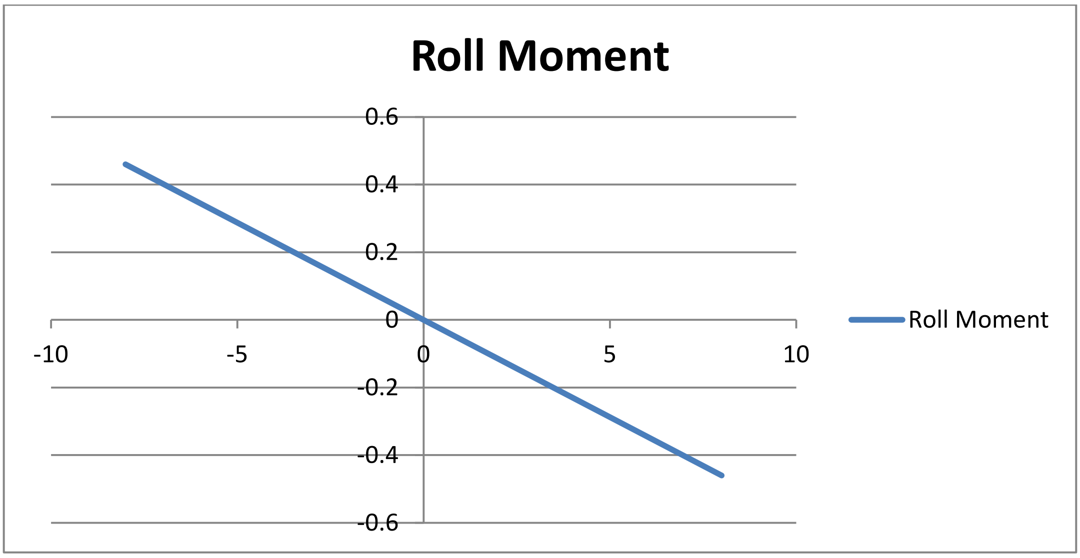

Figure 9-4: Roll Moment

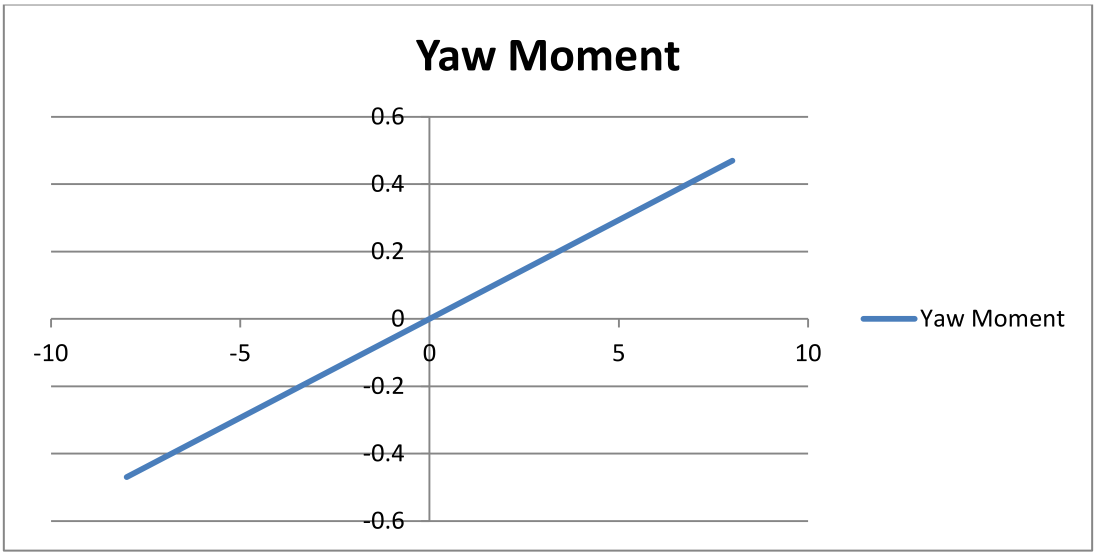

Figure 9-5: aw Moment

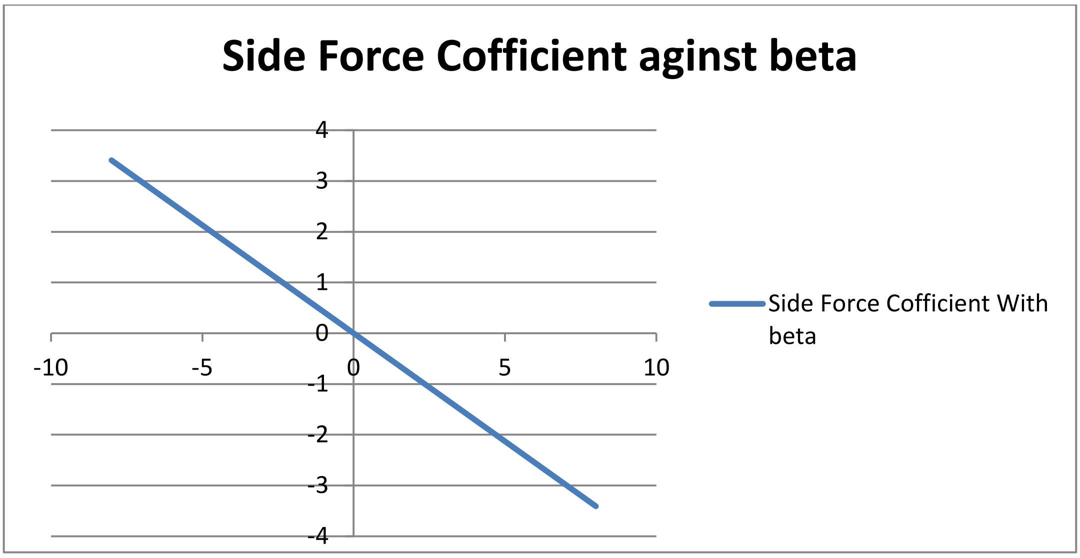

Figure 9-6: side force coefficient against beta

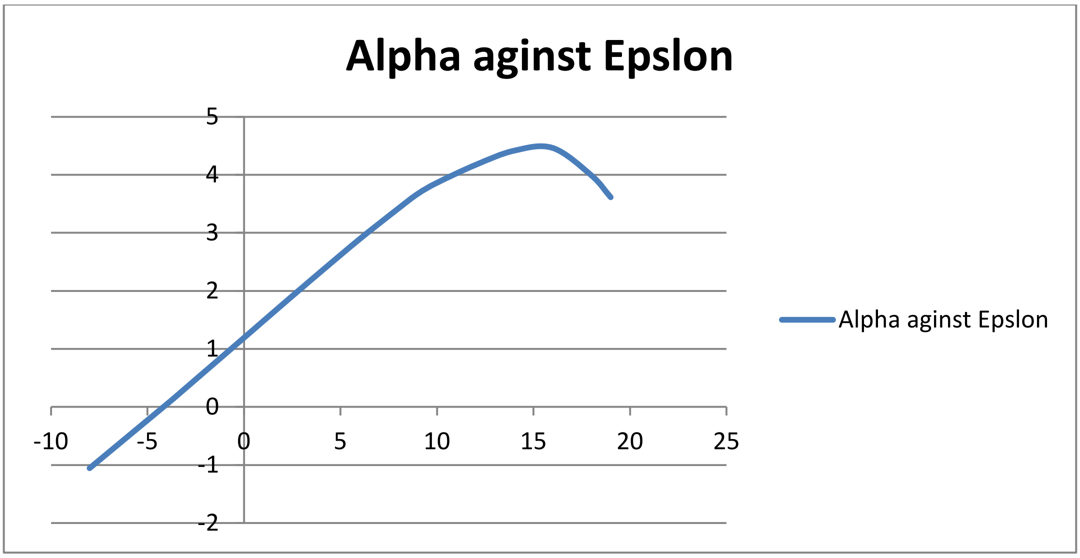

Figure 9-7: alpha against Epslon

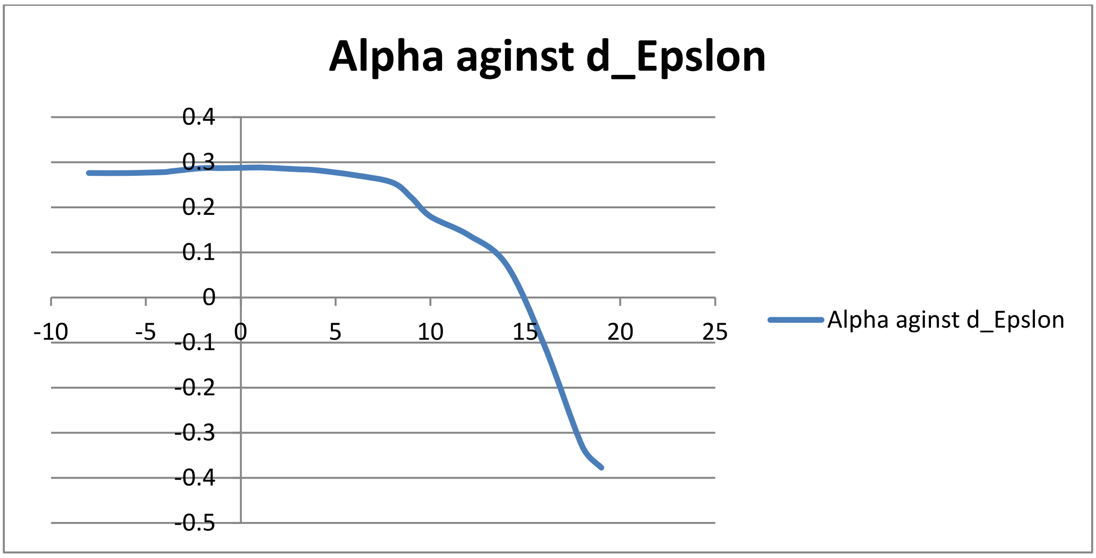

Figure 9-8: alpha against d_Epslon

Performance analysis:

The power required &power available curve define the maximum & minimum speeds. The maximum speed is about $278.6\frac{ft}{s} = 84.917\,m/s$ which exceeds the required maximum speed. This is considered as a positive indication to the performance of UAV.

The stall speed is found to be5 26.6 m/s while the required stall speed is about 28 m/s which is beyond the required speed. The landing distance is about $169.848m$ which is beyond the required landing distance. The take-off distance is about 141.02m as seen to be less than the required take-off distance. These characteristics serve to optimize performance characteristics.

Structure analysis of fuselage:

V-n diagram has been drawn based on CS-VLA (UAV standard requirements) as considered the first step to initialize structural design. The maximum load factor for positive angle of attack is 3.8 and for negative angle of attack is -1.5, while the maximum dive speed as $1.25 * V_C$ The gust diagram which defines the loads originating from sudden increase of speed winds has been constructed with gust speed of 15.24 m/s for V_C. Loads on the fuselage have been regarded as inertia loads exerted by the various weights on the fuselage (payload, landing gear, fuel, fixed equipment & fuselage weight itself), where a pull down condition is taken to be our design condition since the major loads are likely to occur there. By constructing the shear & bending moments diagrams depending on the loads and their distribution, a design position along the fuselage is selected as the maximum value of each ($\tau = 1606.504\ lb, M = 4284.648\ at\ x = 1.966453\ ft$). Structure layout has been selected from previous UAVs noticing that the stringer distribution happened to be at the edges of the cross section of the maximum load, in order to assist in reacting the direct stressing on the skin of the structure. The simple bending moment theory has been adopted for analytical calculation of stress and shear flow. The results obtained from these calculations as shown in table (6).

$$q_{s,12} 72.0769\ N/mm$$

$$q_{s,23} = -84.3798\ N/mm$$
$$q_{s,34} = -96.6827\ N/mm$$
$$q_{s,45} = -84.3798\ N/mm$$
$$q_{s,56} = -72.0769\ N/mm$$
$$q_{s,61} = -59.7740\ N/mm$$

Depending on these values, the required skin thickness happened to be 1mm. Zed-section stringers has been selected and the results of sizing them have shown that:

$$t_s = 0.68mm$$
$$h_s = 27.2mm$$
$$w_s = 10.8mm$$

Structure analysis of wing:

The structural design of the wing is followed according to the Shrenk's load distribution along span which is a combined approach of linear and elliptic load distribution on the wing as shown in figure (34).

In addition to the shrenk's load, self-weight of the wing is regarded. It is the parabolic distribution of the weight of the wing itself as shown in figure (36).

Depending on the summation of the shrenk's load and self weight distribution, the shear and bending diagrams were obtained as first integral & second integral with respect to position along span as shown in figure (45), &figure (46).

The torque on the wing is also considered. It originates on this project from two sources (normal force and moment), which are dependent on the angle of attack as shown in figure (47) & figure (48).

The critical loading is assigned for point A as it's considered at the preliminary stage of structural design. The lift & drag coefficient were increased by 3.28. This shall absolutely affect the shrenk's and self-weight loads & consequently the shear & bending moment diagrams. The load resulted from the torque is affected due to variation with normal force and the moment as shown in fig(49).

Stability analysis:

Static stability results:

The static stability analysis is estimated with DATCOM the output together with the discussion is as follows:

Longitudinal static stability:

From DATCOM results in figure (51)

- $Cm_{\alpha}$are negative and equal to -0.8
- Trim angle of attack equal to 2°

Directional Stability:

From figure (53) :

- The slop $C_{n_{\beta}}$ is Positive hence the UAV is directionally stable

Lateral Static Stability from figure (54)

- The slop $C_{l_{\beta}}$ is negative as required hence the UAV is directionally stable.

- **Complete Definition of stability& control derivatives:**
- The stability derivatives estimated using two software tools DATCOM & AAA, The result is shown on table below:

Table 20: Stability derivatives

Coefficients	DATCOM	AAA
Cd_0	0.024	0.02304
$\mathbf{CL_0}$	0.344	0.3789
$\mathbf{Cm_0}$	0.1034	0.1139
$\mathbf{CL_\alpha}$	5.6149	5.2181
$\mathbf{Cd_\alpha}$	0.17188	0.1607
$\mathbf{Cm_\alpha}$	-0.7563	-0.8281
$\boldsymbol{\alpha_0}$	-3.655	-4.2
CYB	-0.4262	-0.8575
CNB	0.05872	0.3178
CLB	-0.0575	-0.0785
CLP	-0.4878	-0.0105
CYP	-0.01994	-0.0013
$\mathbf{CL_q}$	6.383	6.8487
$\mathbf{Cm_q}$	-31.16	-33.6478
$\mathbf{Cd_q}$	-	0
CNR	-0.0965	-0.2814
CLR	0.191	0.1266
CYR	-	0.6121
Cdαdot	-	0
Clαdot	-	1.4698
Cybeta dot	-	-0.2297
Clbeta dot	-	-0.0006
Clu	-	**0.0078**
Cmu	-	**0.0001**
Cdu	-	**0.0**

Verification:

Table 1 has a summary of stability coefficients and aerodynamic characteristics of the UAV calculated by both AAA & DATCOM.

In general, the longitudinal aerodynamics coefficients computed by DATCOM agree well with these ones estimated by AAA. Excellent correlations are achieved for the lift, Drag & Moment at zero angle of attack.

The Longitudinal stability coefficients ($\mathbf{Cm_{\alpha}}$,$\mathbf{Cm_{q}}$&$\mathbf{CL_{q}}$) agree well with the two method. But Lateral derivatives are very different, the reason of this might be:

1. As the DATCOM can't take twin boom configuration, we were urgency to assume one vertical tail. This will strongly affect lateral directional stability derivatives.
2. After literature survey on lateral stability estimation and verification, we found that lateral directional derivatives are always different and harder to correlate with different estimation methods.
3.

State space results

Using Matlab code in appendix ().the state space of both longitudinal and lateral equation of motion are solved. The eigenvalues of the state matrix are as follows:

Eigenvalues of the longitudinal states:

$$\lambda_{1,2} = -1.8994 \pm 4.0858i$$

$\lambda_{1,2} = \ -0.0012 \ \pm 0.0482i$

By examining theeigenvalues:

- There are two pairs of complex conjugate eigenvalues.
- Both pairs of eigenvalues have negative real parts. This means that the UAV is stable.

Parameter	Short period	Long period
$\boldsymbol{\eta}$	-1.8994	-0.0012
$\boldsymbol{\omega}$	4.0858	0.0482
$\boldsymbol{t_{halve}}$	0.363	575
period	1.537s	130.356
Number of cycles to half-amplitude	0.2366 cycles	4.418

Eigenvalues of the lateral states:

$\lambda_{1,2} = -0.7336 \pm 4.5649\text{i}$

$\lambda_{1,2} = -46.3409$

$\lambda_{1,2} = 0.0205$

By examining the eigenvalues:

- There are two real eigenvalues and one pair of complex conjugate eigenvalues.
- The UAV thus has three modes of vibration.
- There is a positive eigenvalue. The aircraft is thus unstable. But since the eigenvalue is small the UAV will diverge slowly.

$$\eta_{dutch} = -0.7336$$

$$\omega_{dutch} = 4.5649$$

$$t_{halve} = 0.9405s$$

Period = 1.376s

Number of cycles to half-amplitude = 0.684cycles

Flying Qualities:

The dynamic stability characteristics are used to evaluate the flying qualities of the airplane in the Cooper and Harper rating scale. The flying qualities for all the modes of motion are excellent, rating in Level 1 for the Cooper and Harper scale.

Lateral Directional flying qualities:

Roll subsidence flying qualities:

From AAA the Roll mode time constant is equal to:

$$T_R = 0.325$$

Thus UAV achieved level one flying quality in Roll.

Spiral mode flying qualities:

From AAA software tool the time to half amplitude is found to be (3.85) this approximately gives level three flying qualities.

Dutch roll flying qualities:

From Matlab code appendix ().the Dutch roll frequency and damping is found as follows:

$\xi = \ 2.3198$

$$\omega_n = 4.06$$

Thus from table () the Dutch roll is achieved level one flying qualities.

Mode EXCITATION:

Each mode is excited using appropriate control input. Table () shows how to excite each mode:

Table21: Model Excitation

Longitudinal Modes	
Long Period (**Phugoid**)	Elevator step
Short Period	Elevator Impulse
Lateral Modes	
a periodic roll	Aileron square pulse
Spiral	Rudder Step
Dutch Roll	Rudder doublet

Nonlinear model:

Three Degree of freedom longitudinal model:

Initial condition:

m = 76.6532 kg

Initial velocity = 47 m/s

Initial body attitude (θ) = 0

Initial incidence (α)= 0

Initial body rotation rate (q) = 0

δ_e = 0

Response to Elevator Impulse:

As from above table elevator impulse used to excite short period mode, it's difficult to separate short period from long period modes. The short period is appearing in the first three second, while the long period mode which is now is not of our interest appeared at 400 sec. The elevator impulse is shown in figure () below

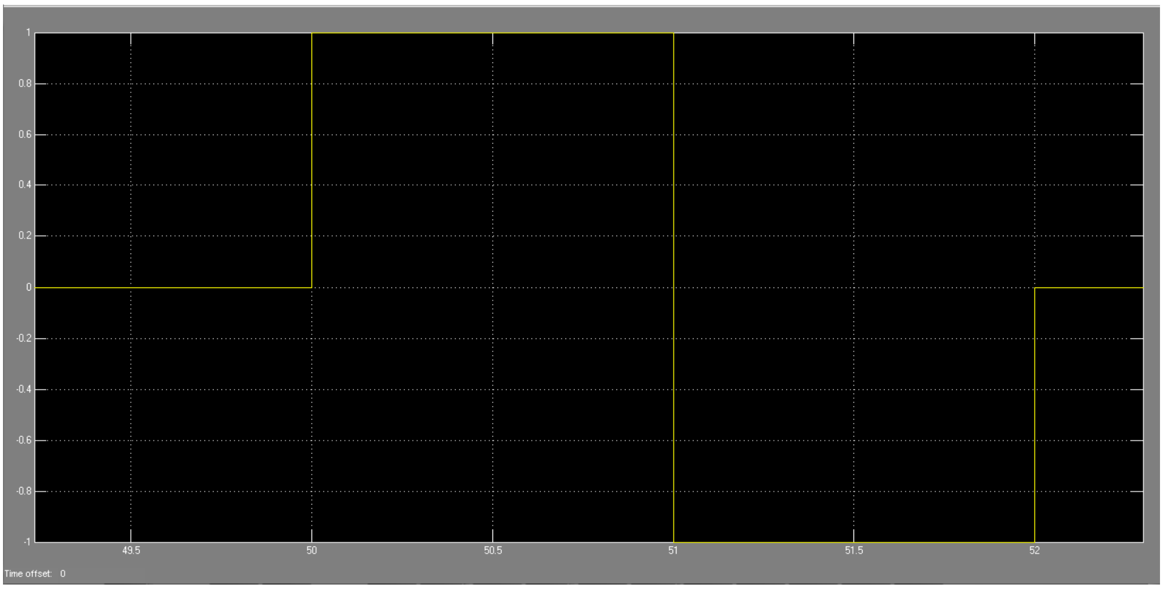

Figure 9-9: Response to Elevator Impulse

Alpha:

The Short period is obvious at first 3sec.

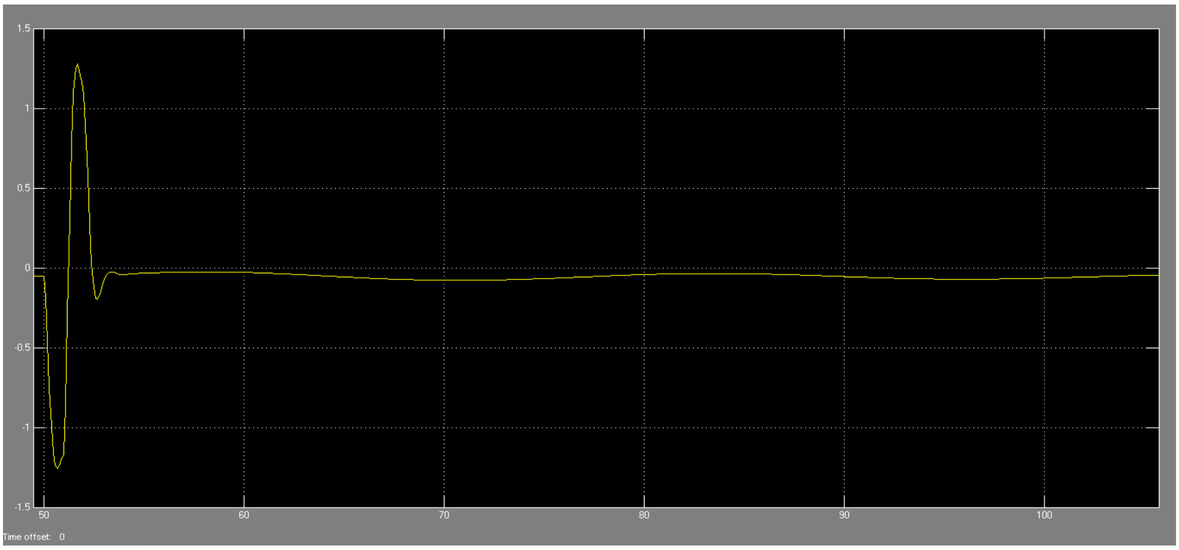

Figure 9-10: angle of attack

Pitch attitude:

The long period is obvious at pitch, and is running from 53sec till it damped out at 400 sec. figure () show this discussion.

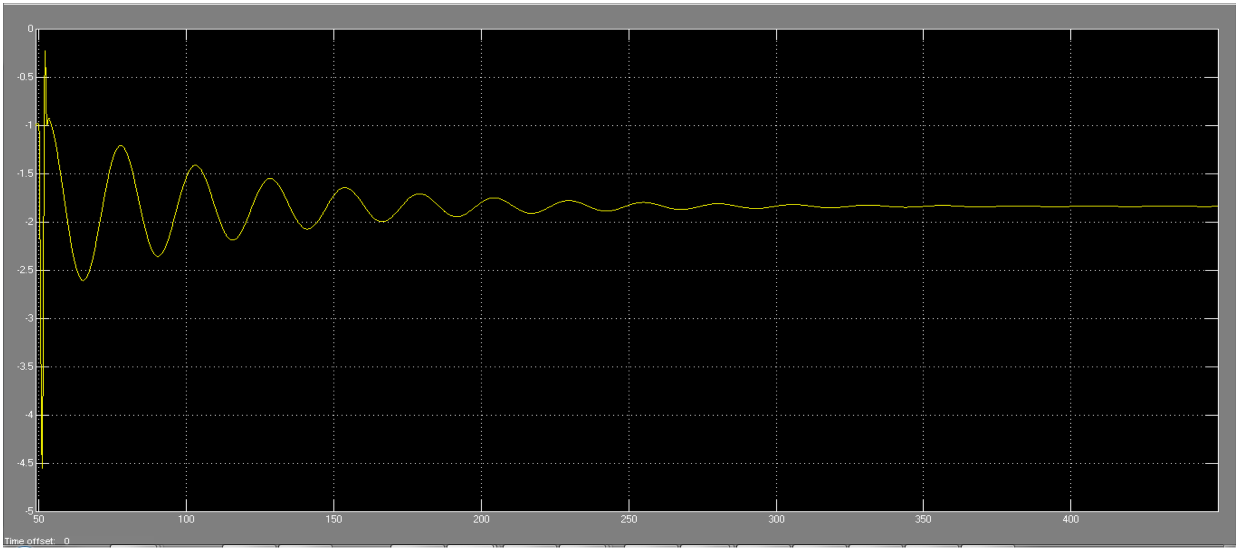

Figure 9-11: Pitch attitude

Pitch Rate:

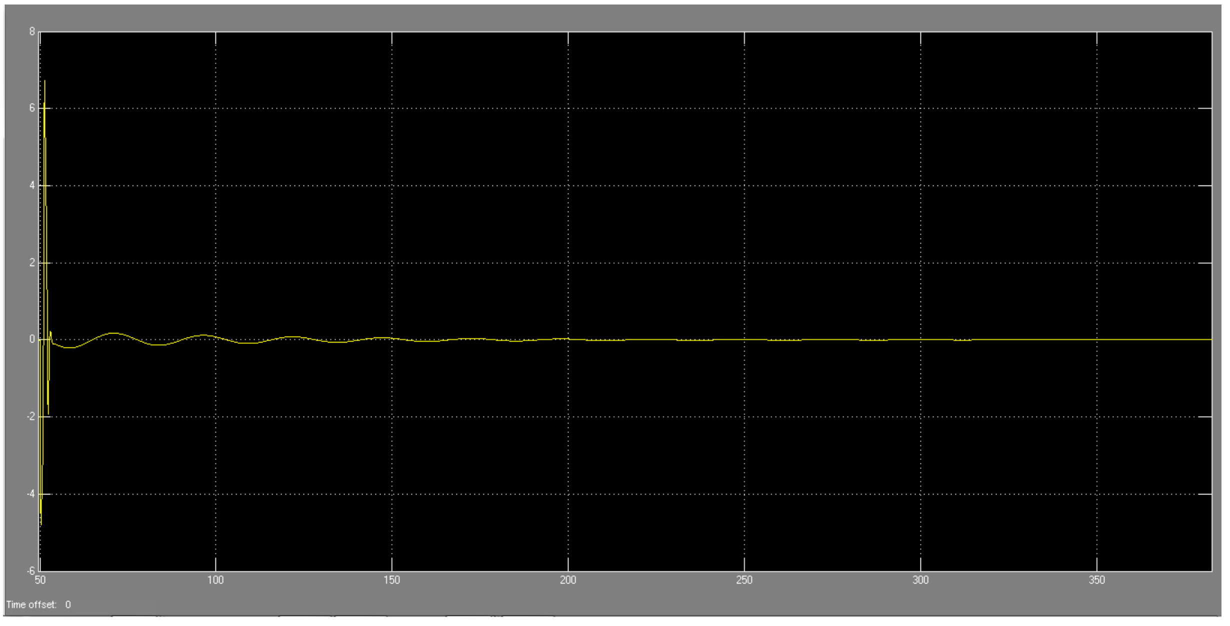

Figure 9-12: Pitch Rate

Forward Speed (u):

Forward Speed varies as the pitch attitude the long period is visible.

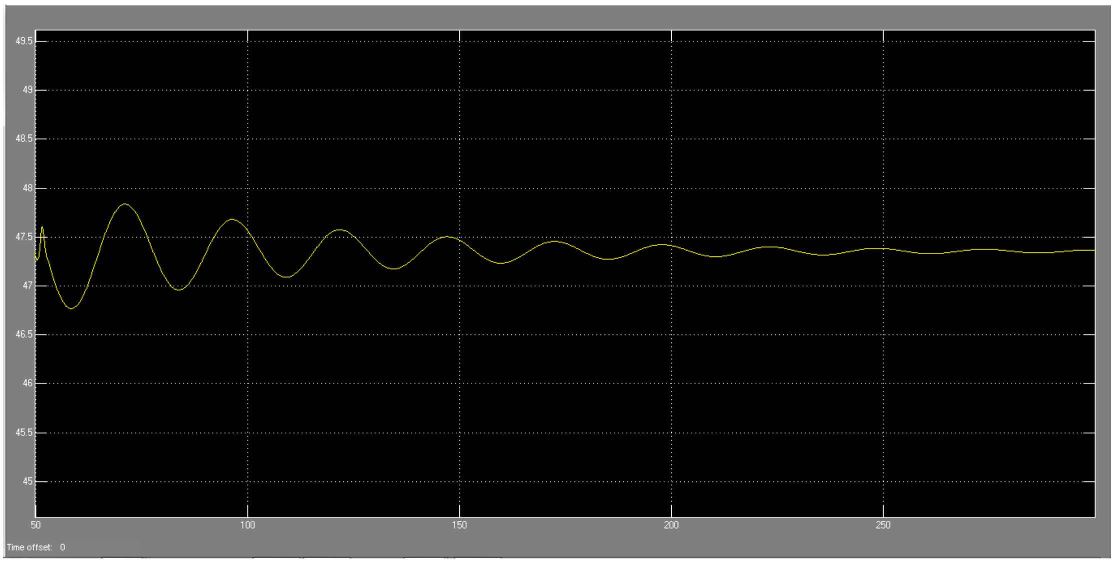

Figure 9-13: Forward Speed (u)

Speed (W):

The (w) is same as angle of attack (Alpha**).**

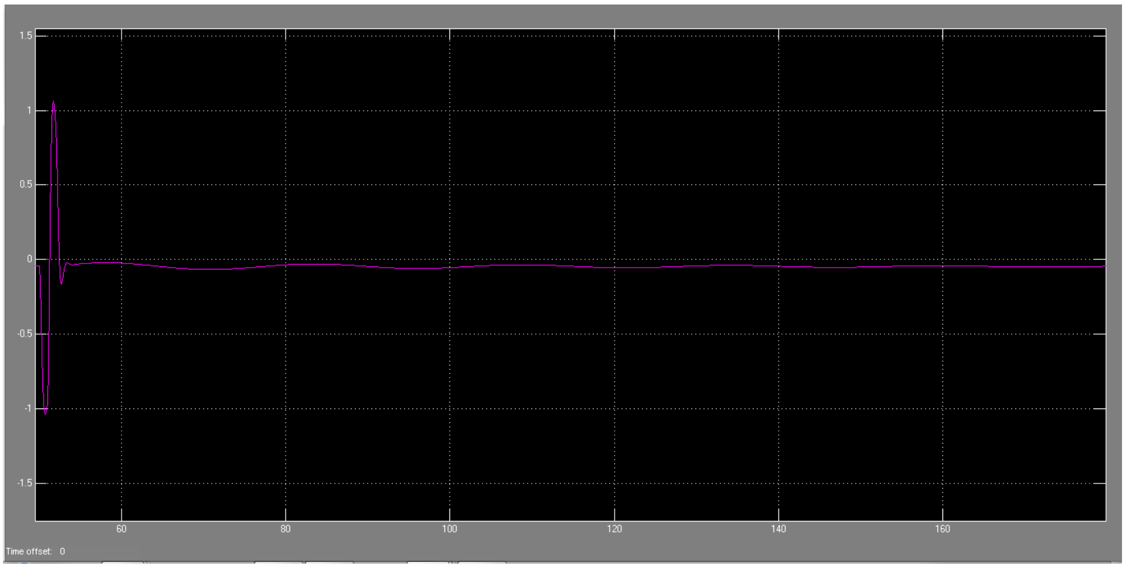

Figure 9-14: Upward Speed (w)

Response to Elevator Step:

As from table is used to excite Long period, the short period is characterized by change in angle of attack with constant forward speed. The elevator step is shown in figure (110) below:

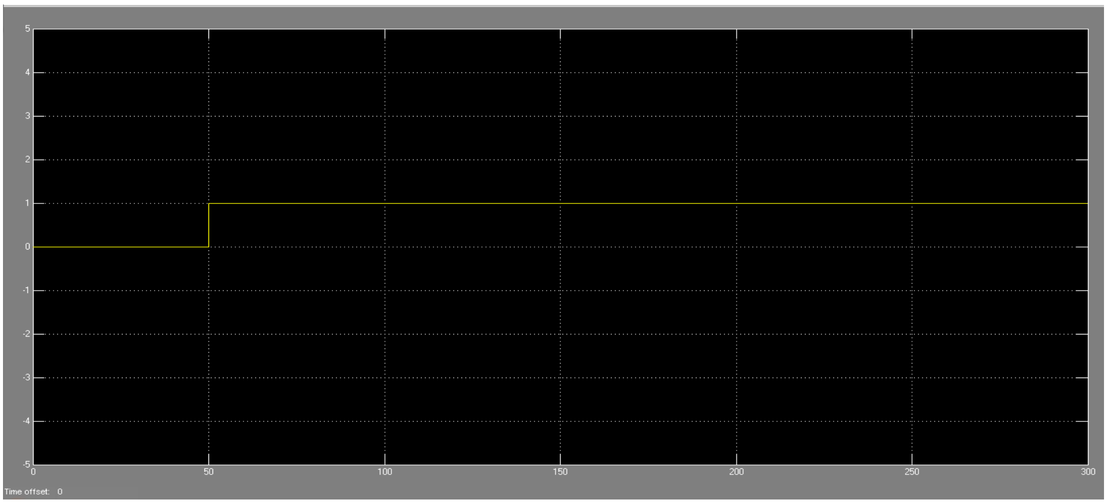

Figure 9-15: Elevator Step of one degree

Alpha: from figure (111) the disturbance is damped at 250sec.

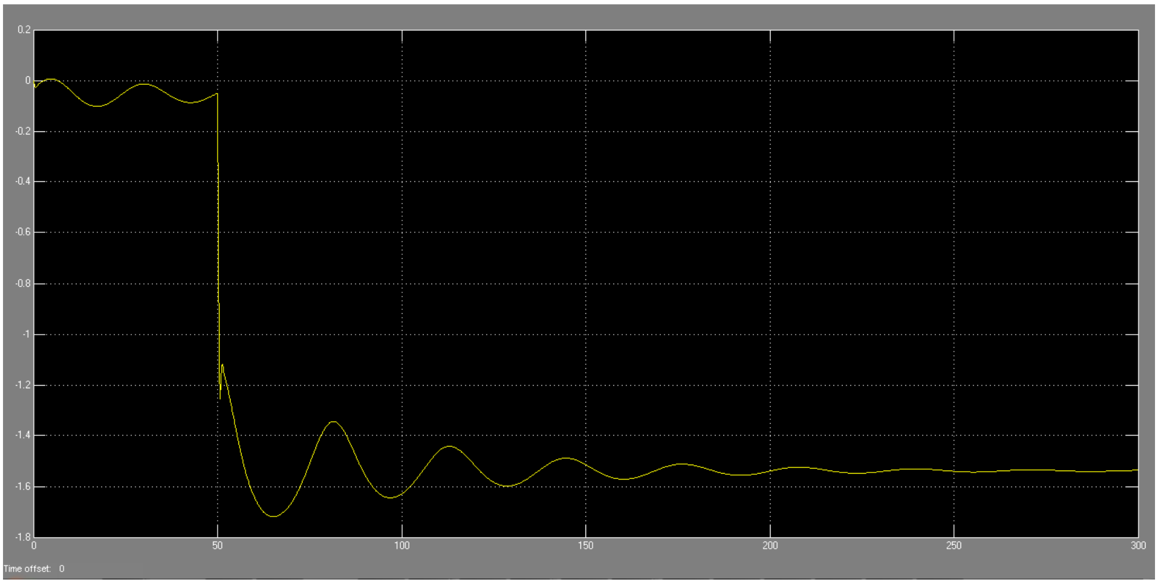

Figure 9-16: Alpha

Pitch attitude:

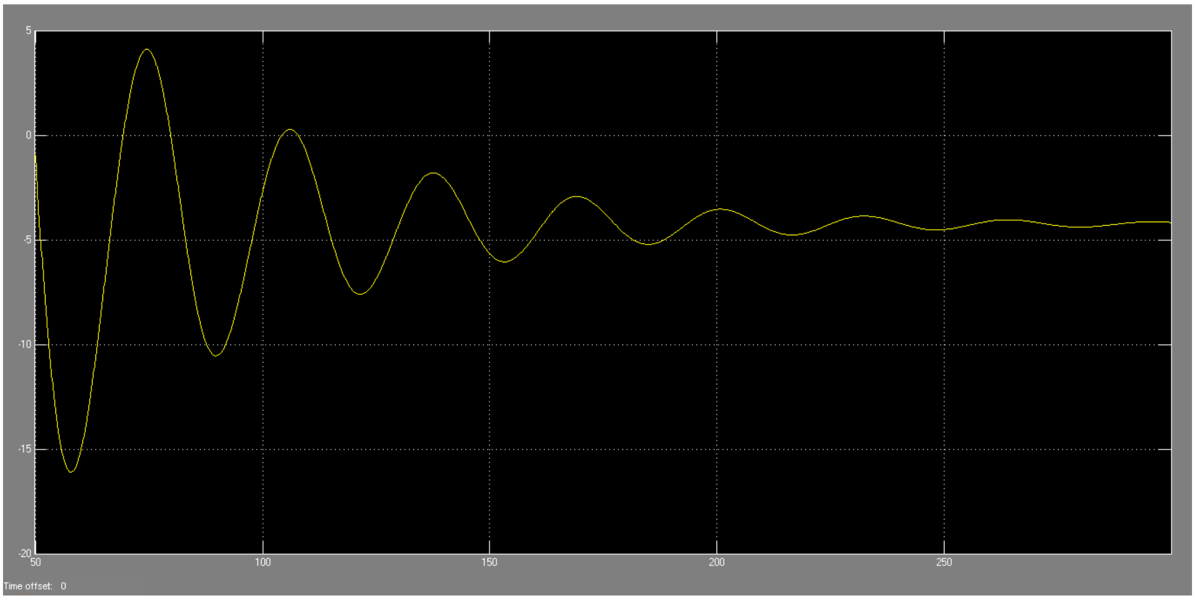

Figure 9-17: Pitch attitude

Pitch Rate:

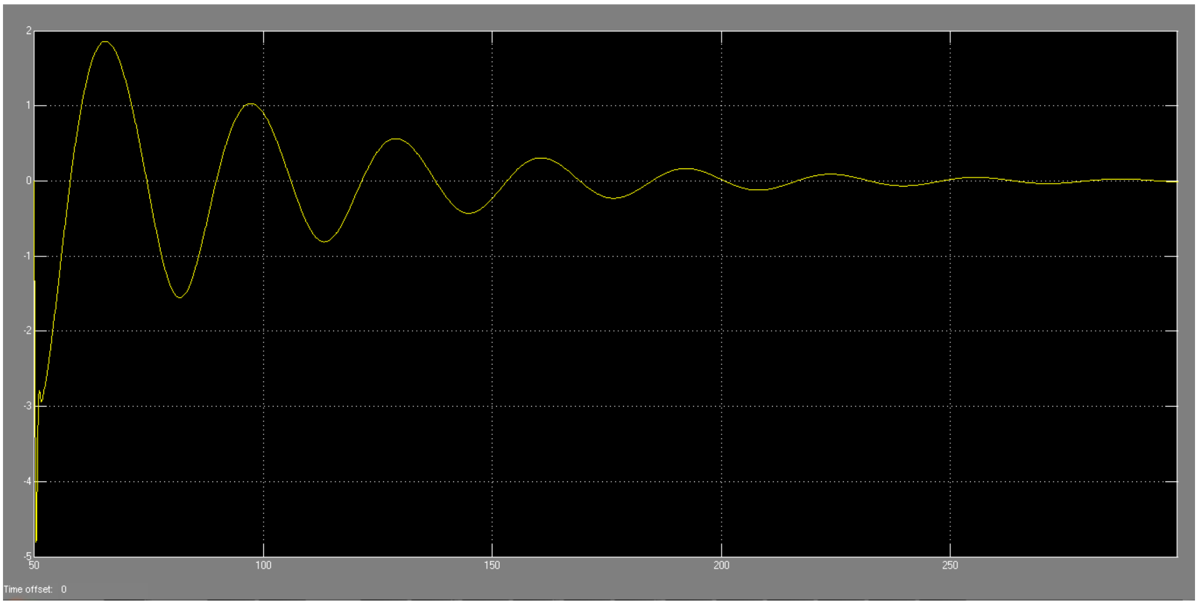

Figure 9-18: Pitch Rate

U, W

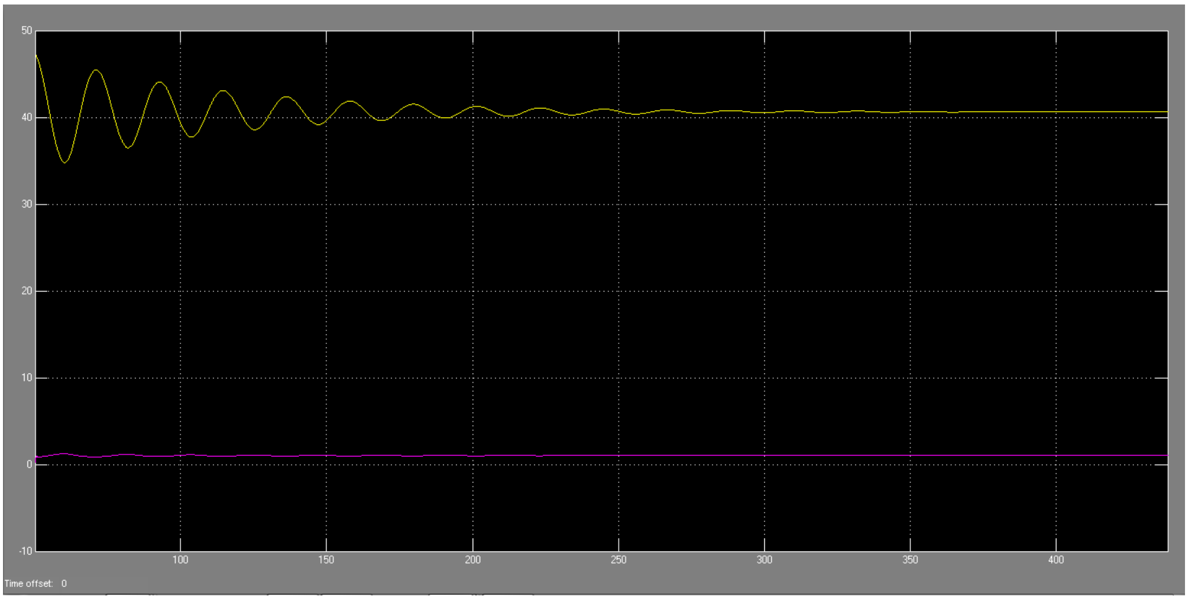

Figure 9-19: U, W

From above result the following is noticed:

- The short period and long period's modes are both stable.

9.4.2 Three Degree of freedom Lateral model:

Initial Conditions:

U = 47 m/s

φ_0 = 0

β_0= 0

q = 0

δ_r = 0

δ_e = 0

Aileron Step:

The aileron step is used to excite Roll subsidence.

Beta:

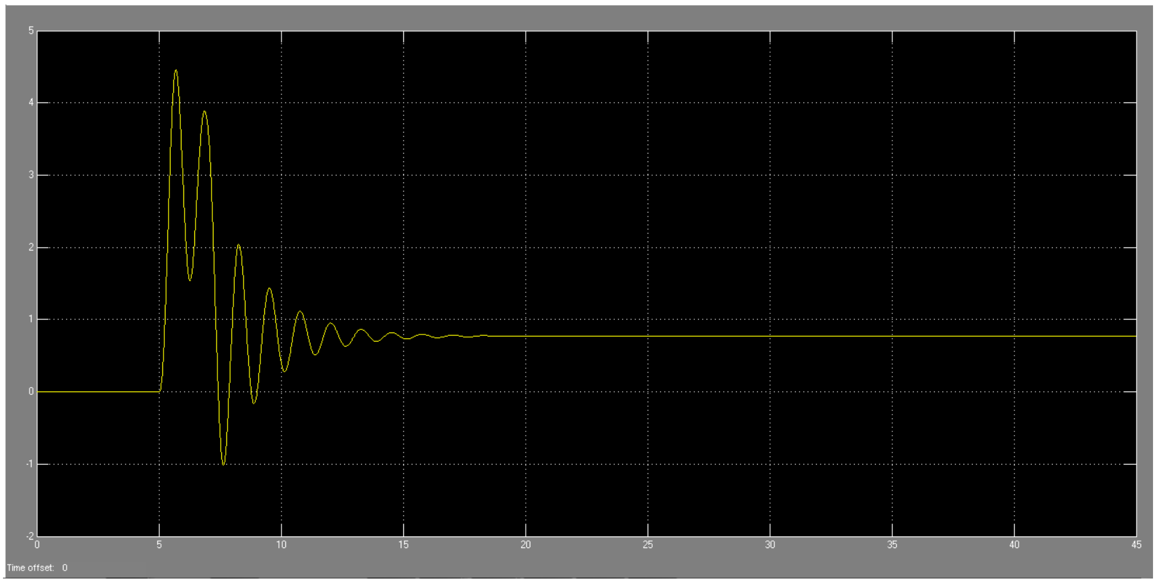

Figure 9-20: Beta

Phi

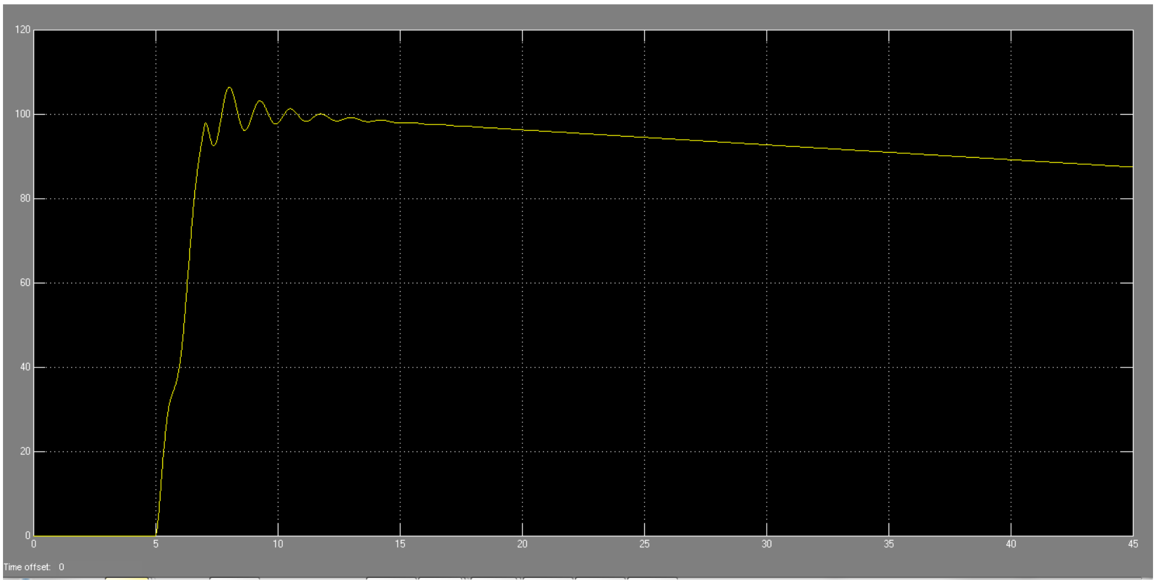

Figure 9-21: Phi

Psi

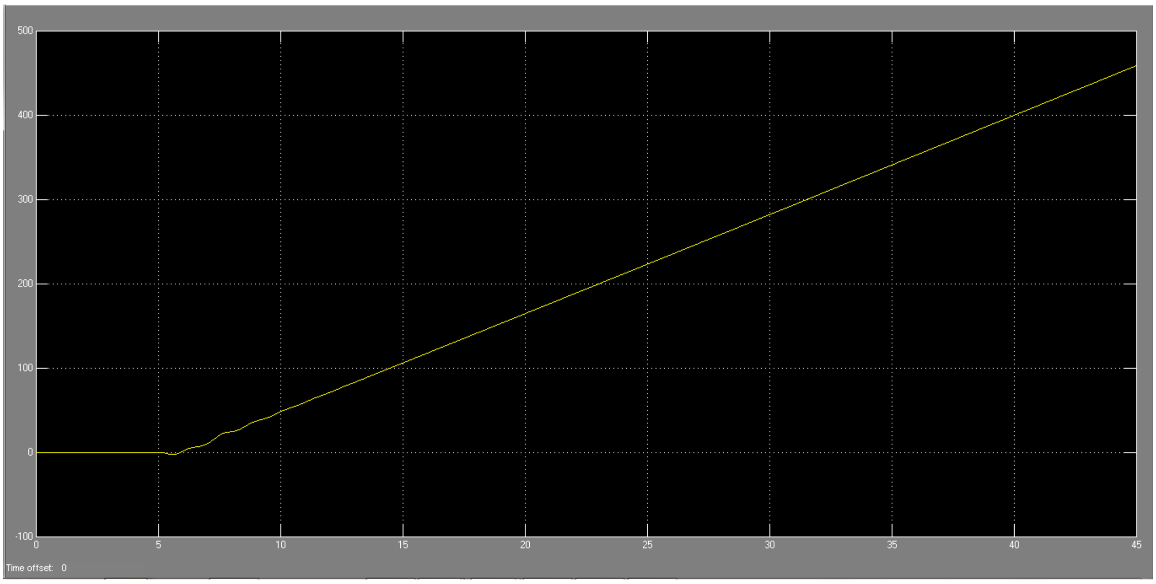

Figure 9-22: Psi

Roll Rate:

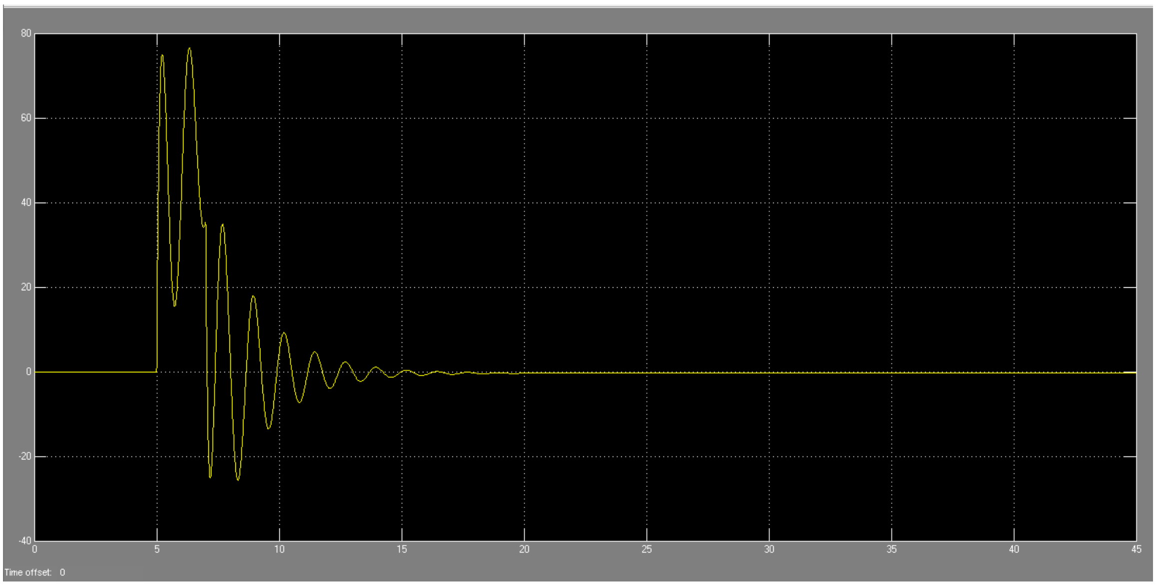

Figure 9-23: Roll Rate

V:

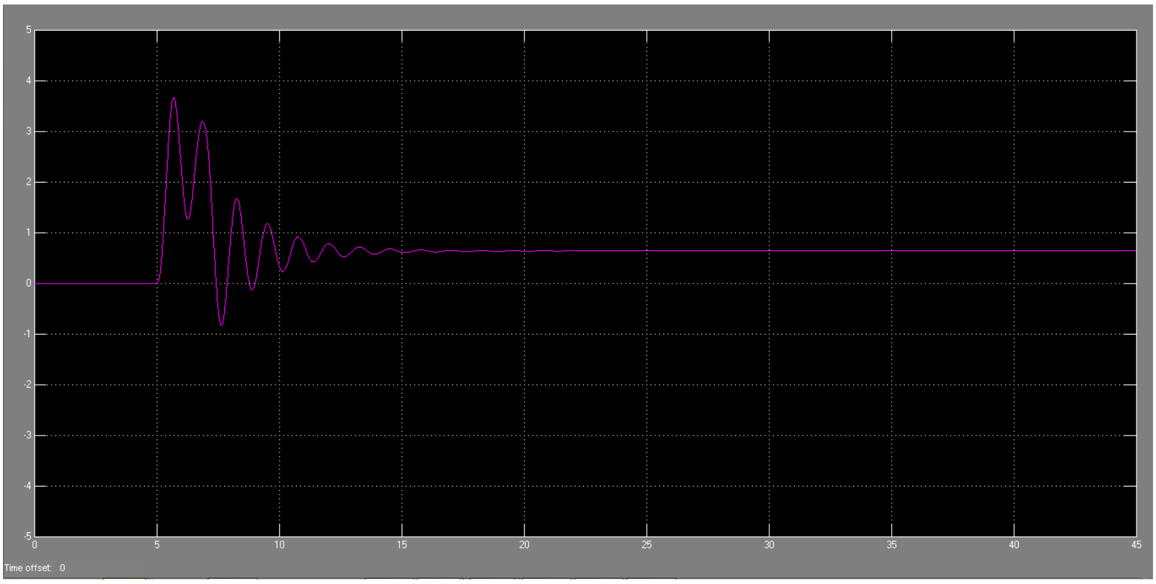

Figure 9-24: V

Yaw Rate:

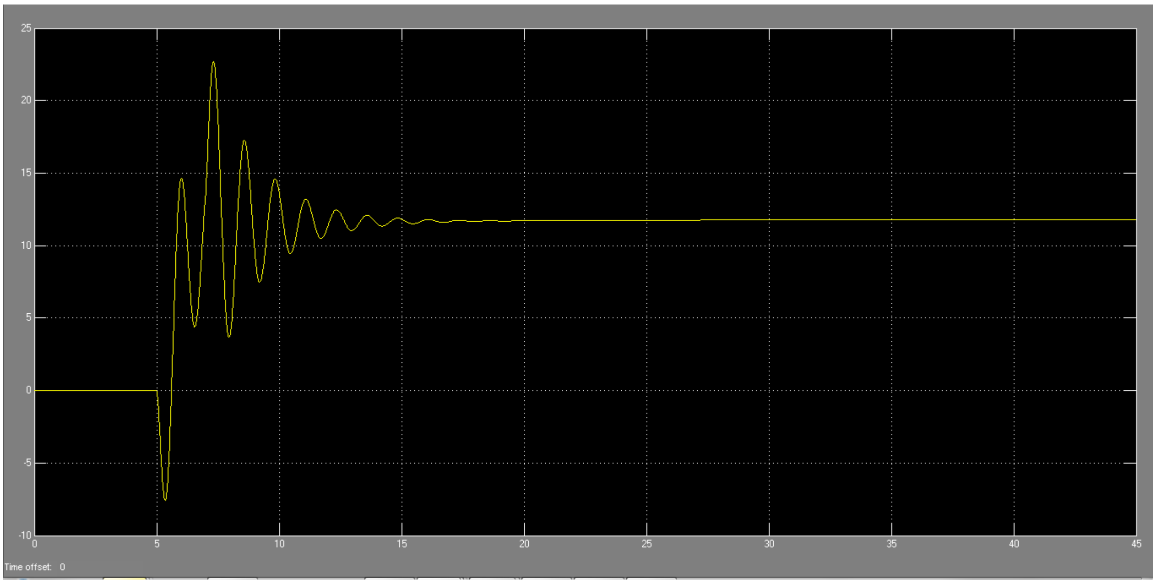

Figure 9-25: Yaw Rate

Rudder Step:

Beta

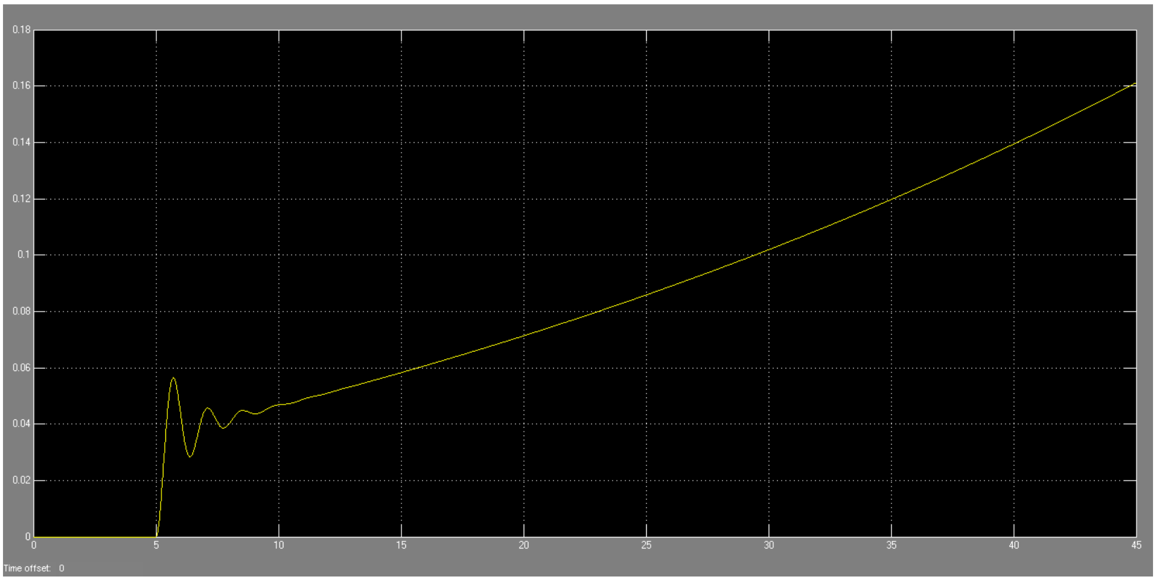

Figure 9-26: Beta

Phi:

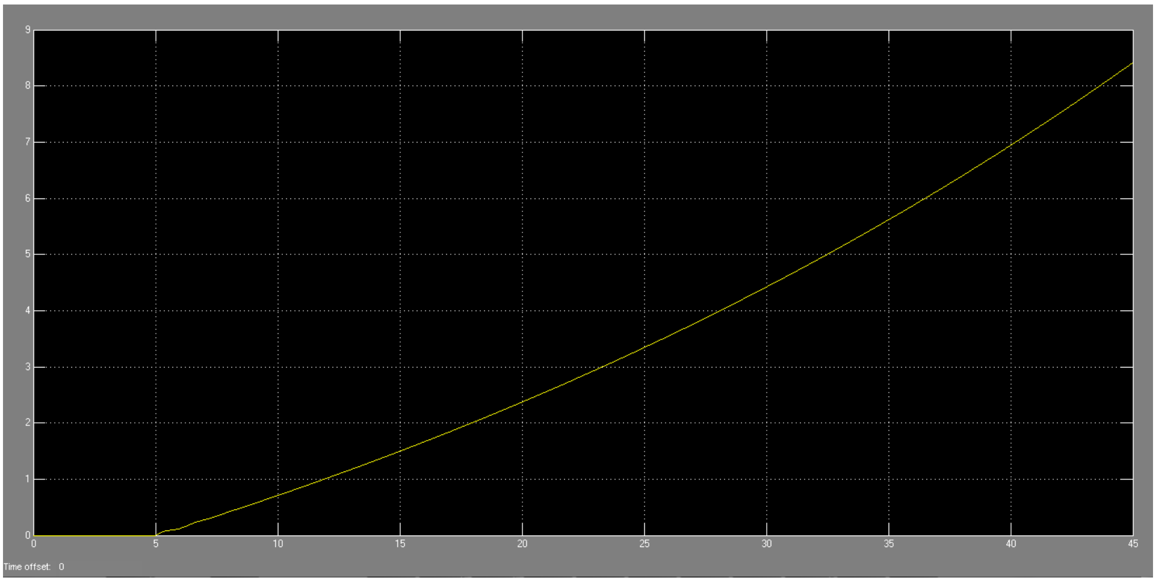

Figure 9-27: Phi

Psi:

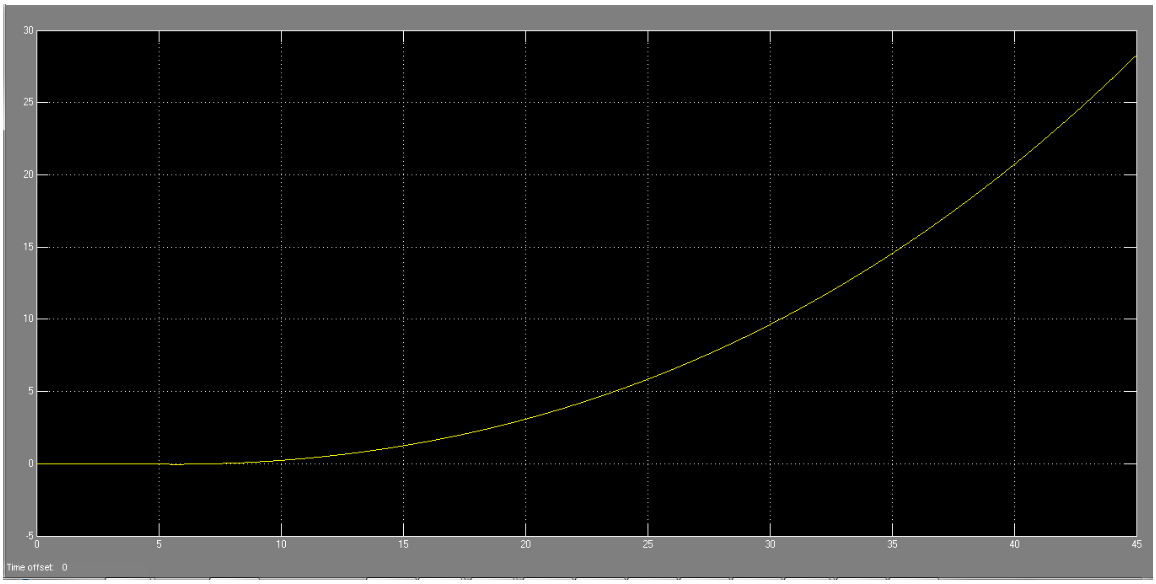

Figure 9-28: Psi

Roll Rate:

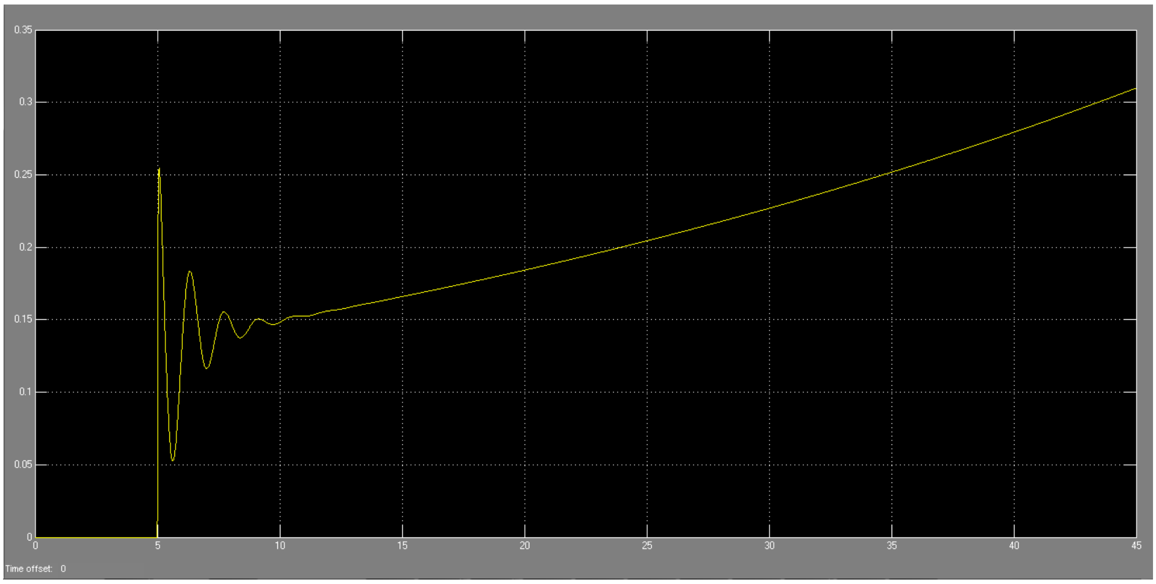

Figure 9-29: Roll Rate

Yaw Rate

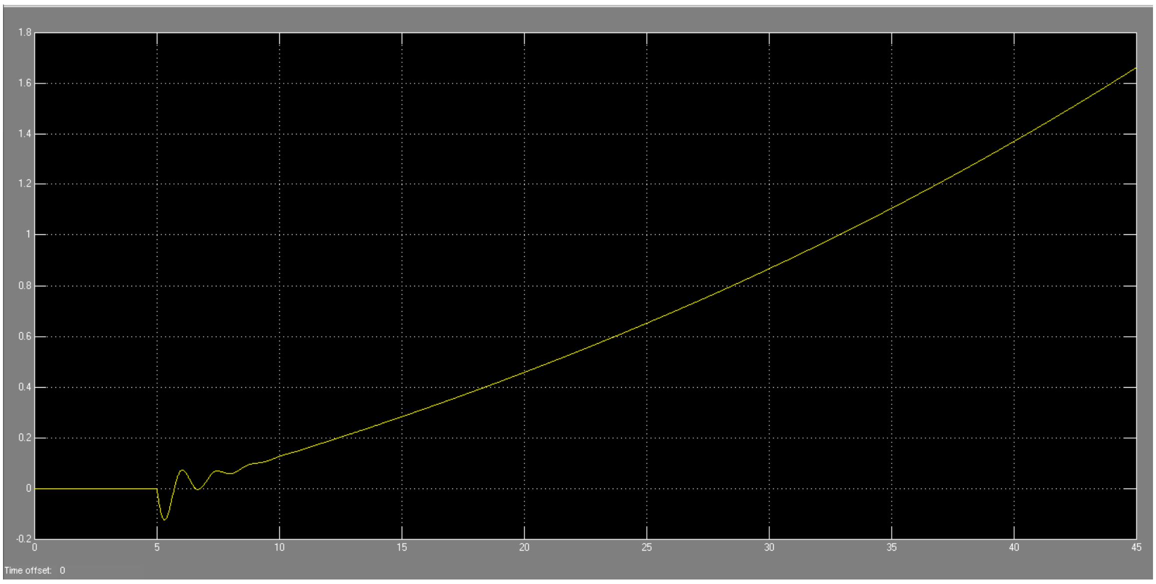

Figure 9-30: Yaw Rate

Rudder Impulse

Beta

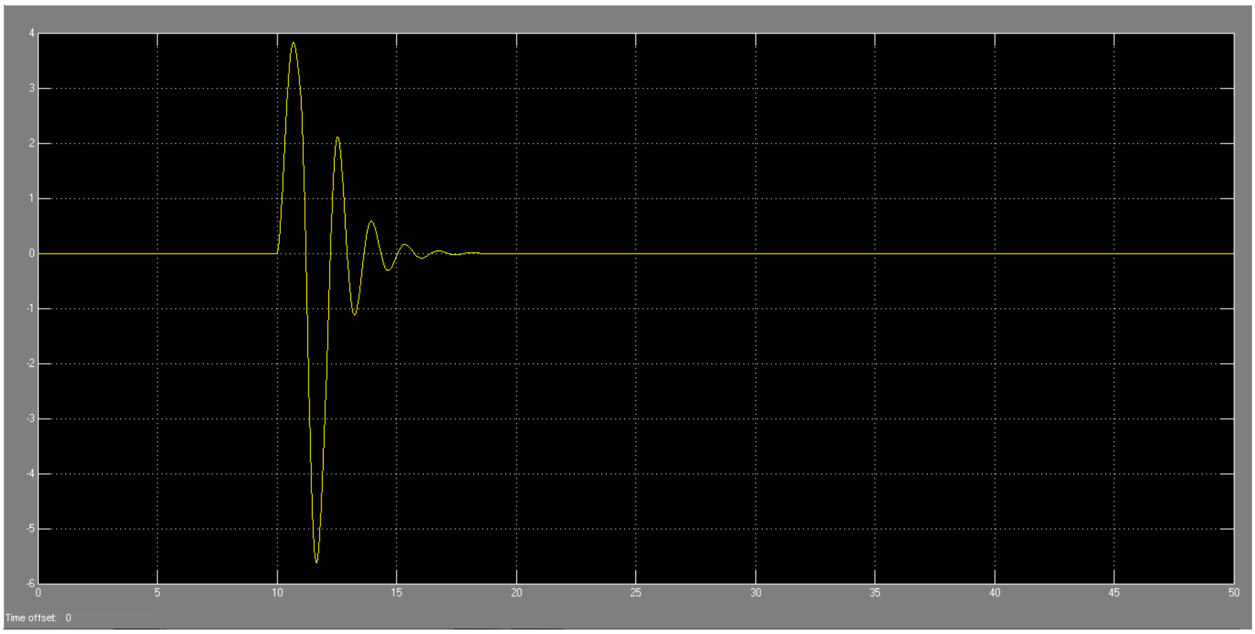

Figure 9-31: Beta

PHI

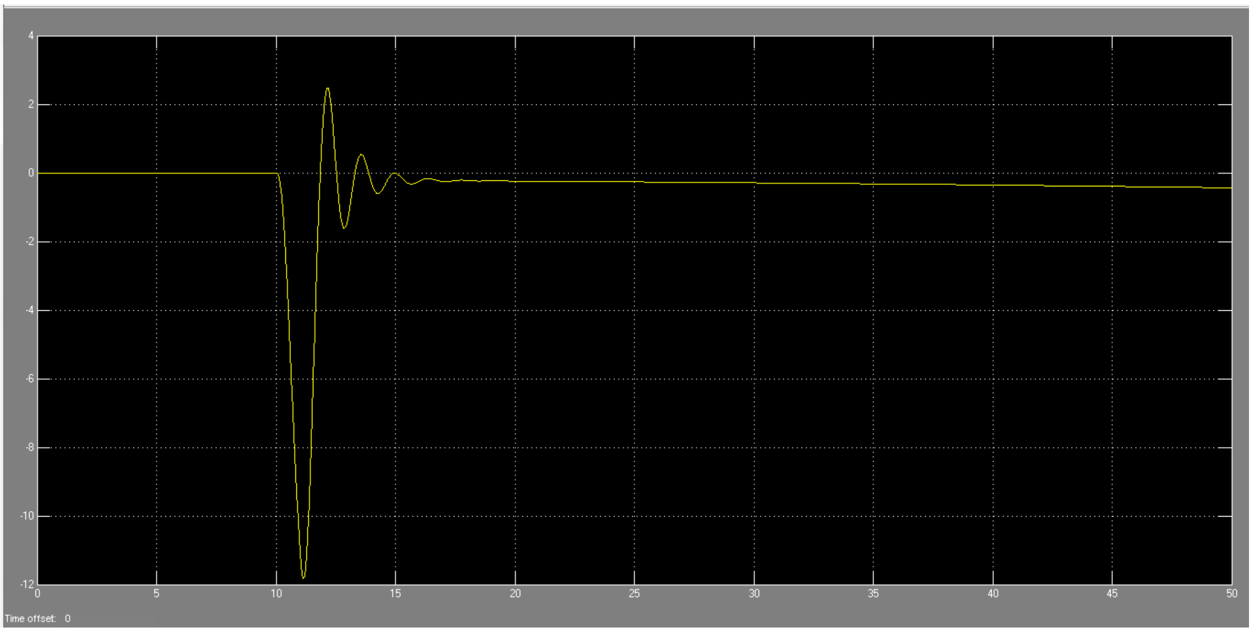

Figure 9-32: PHI

Psi

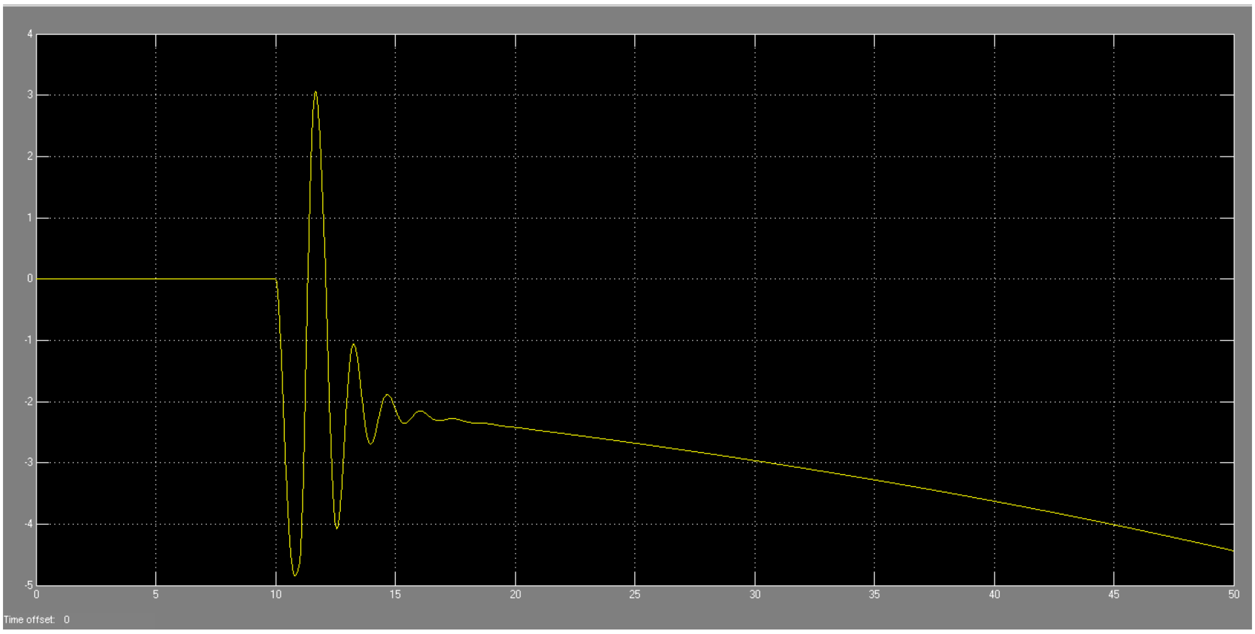

Figure 9-33: Psi

Roll Rate

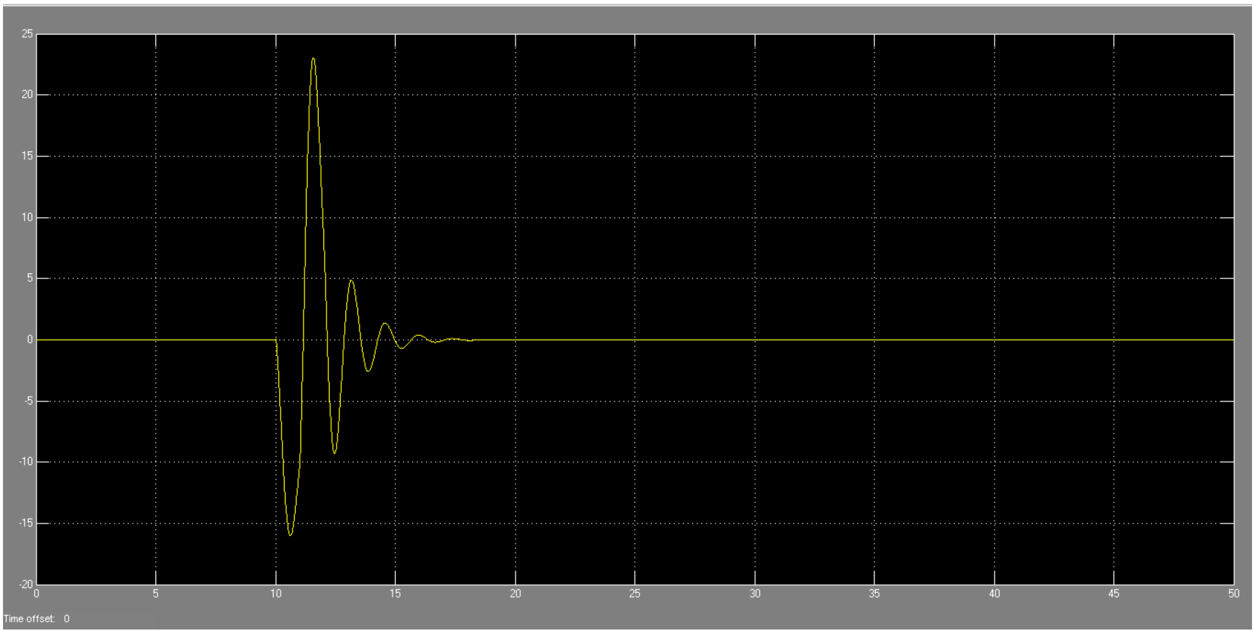

Figure 9-34: Roll Rate

Yaw Rate

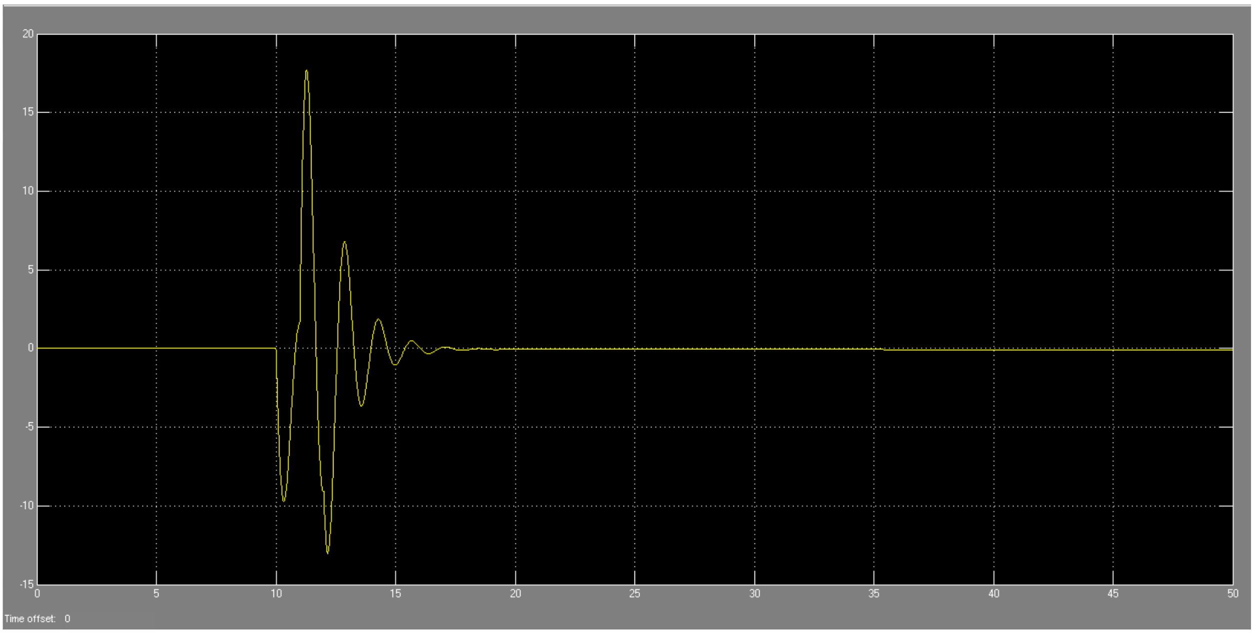

Figure 9-35: Yaw Rate

V

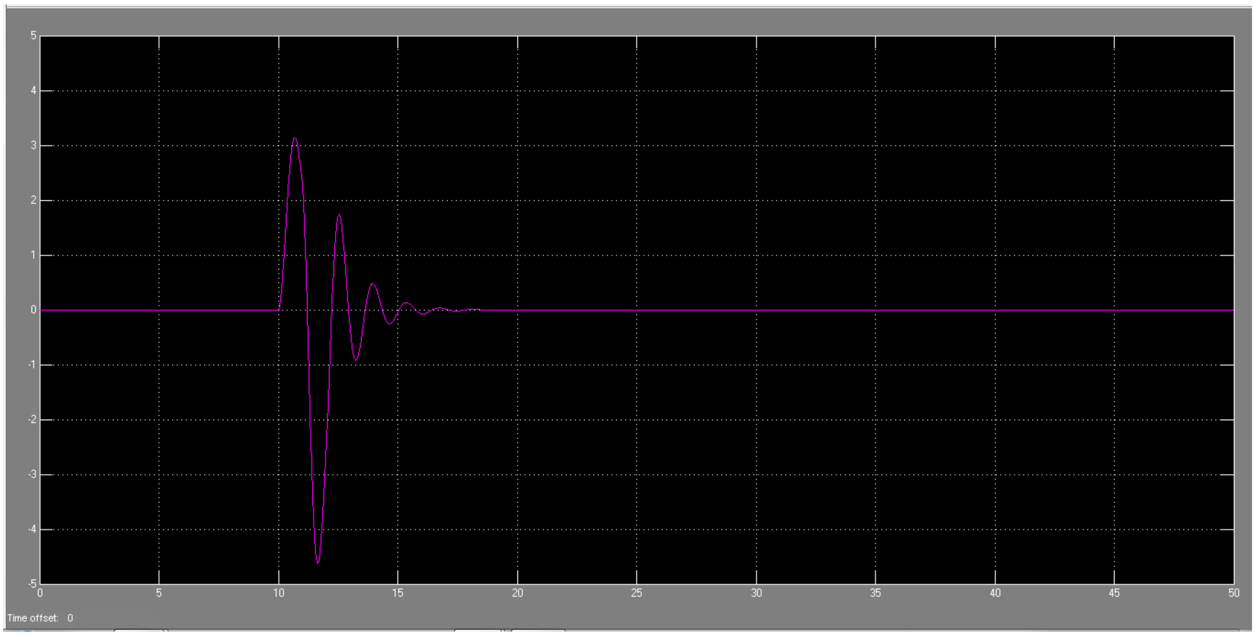

Figure 9-36: V

General discussion of Lateral model results:

- The Roll mode is stable
- The spiral Mode is stable

Six degree of freedom Model:

Elevator Impulse

Alpha

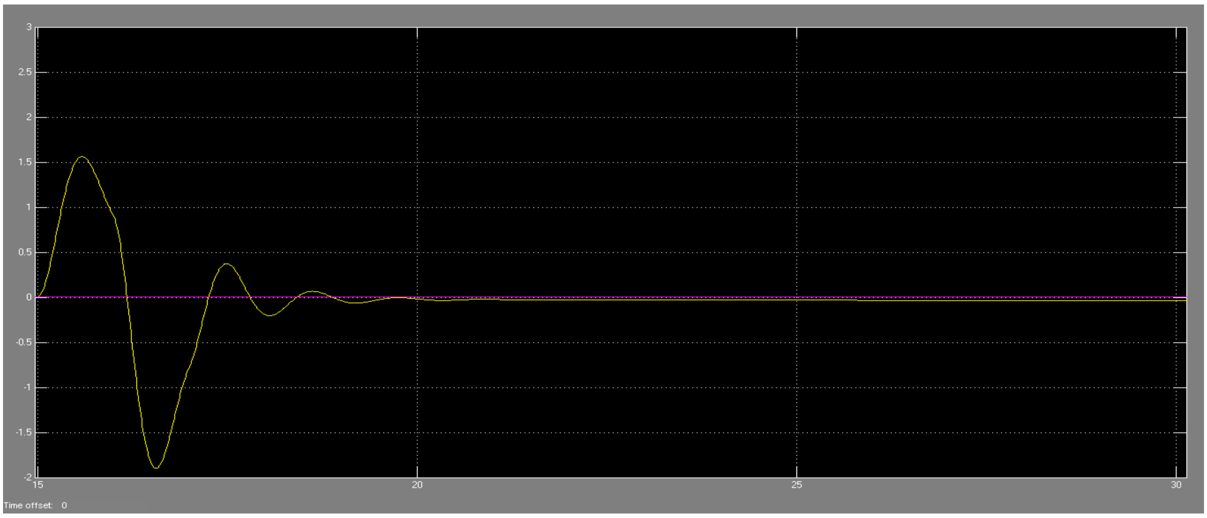

Figure 9-37: Alp

Euler Angles

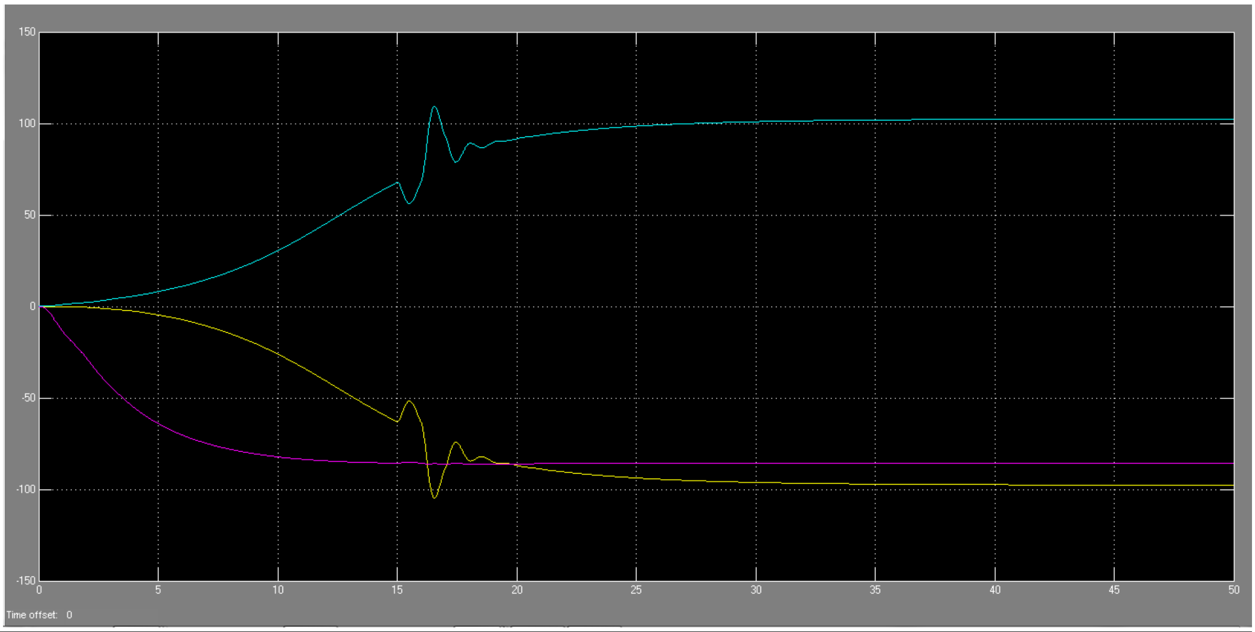

Figure 9-38: Euler Angles

p , q , r

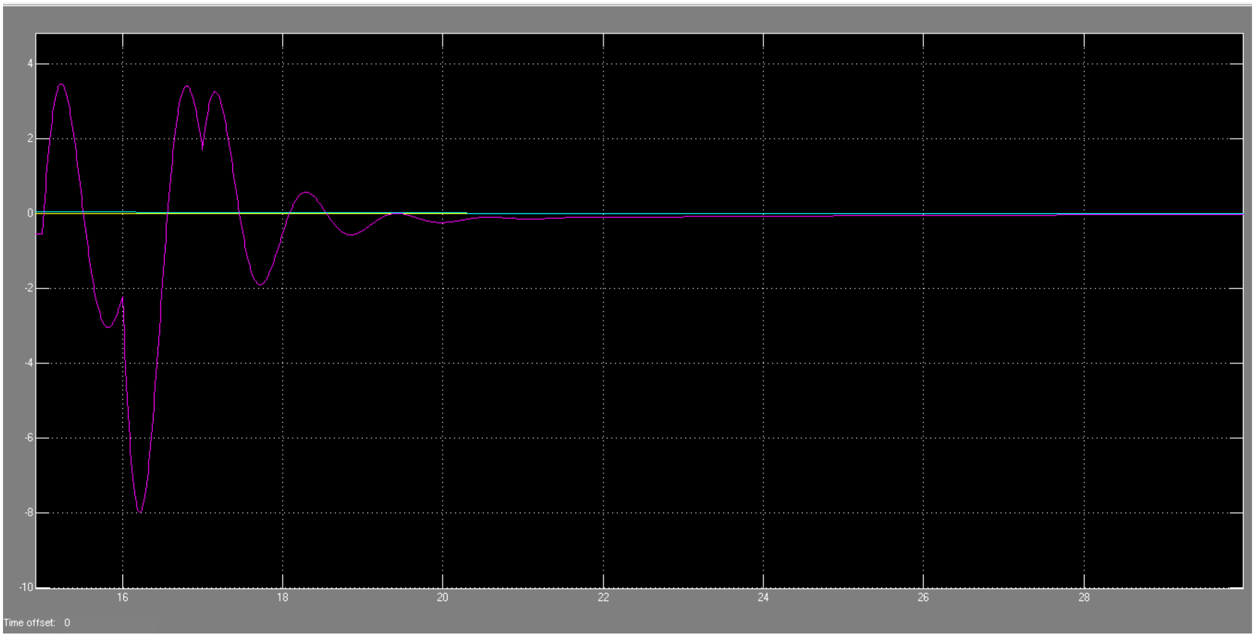

Figure 9-39: p , q , r

U , V , W

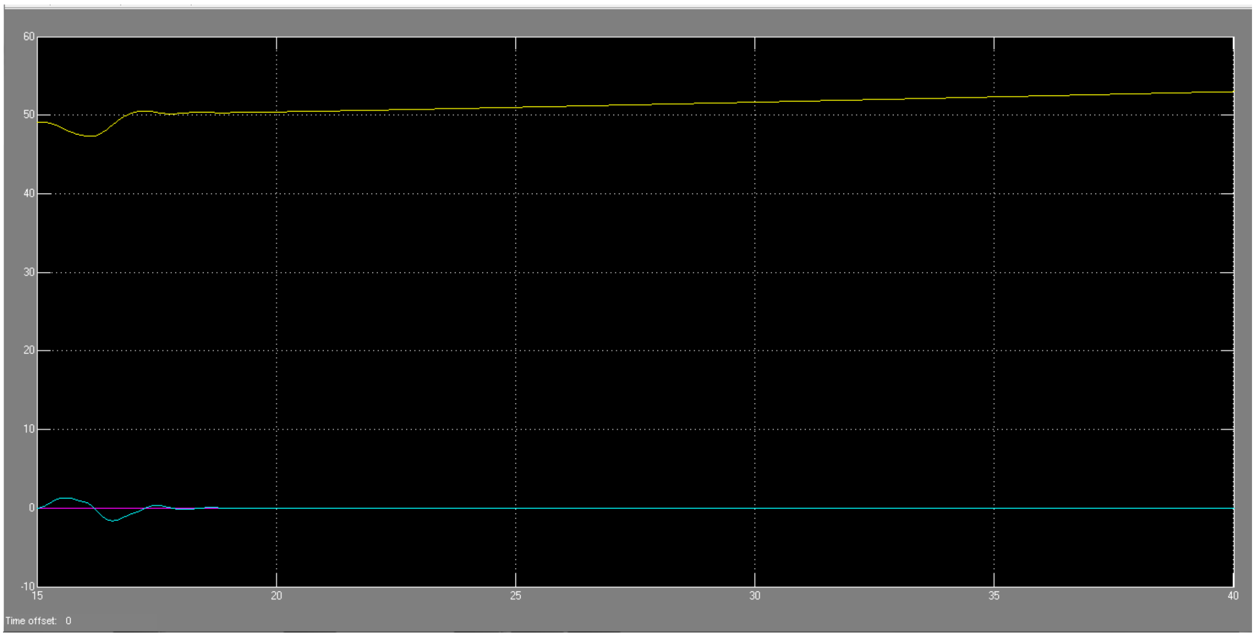

Figure 9-40: U , V , W

Linear Model:

Three degree of freedom Longitudinal:

Elevator Impulse

q

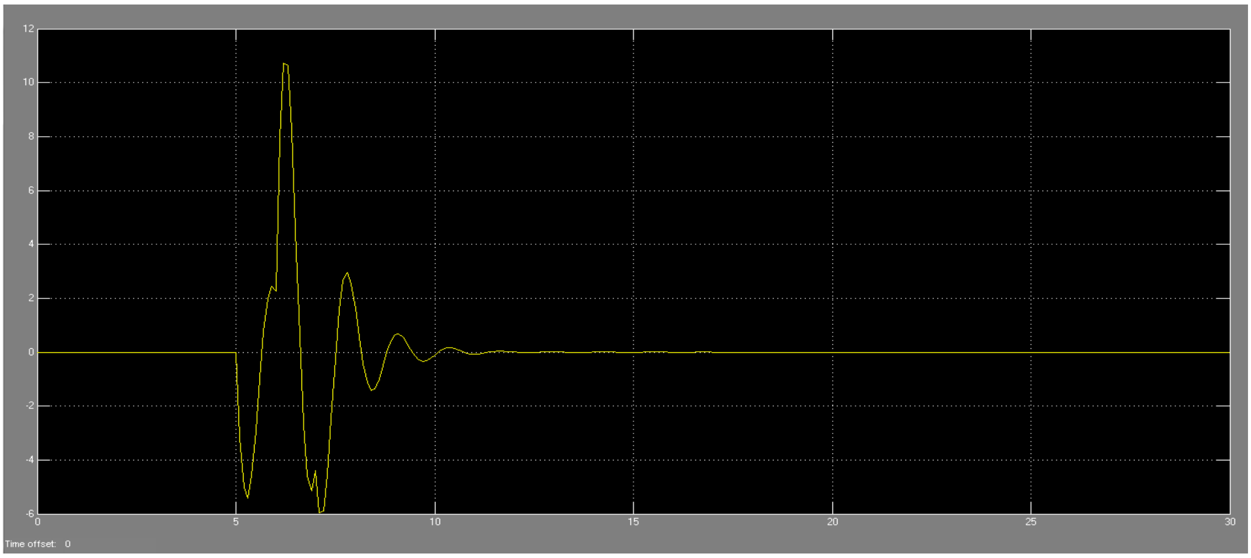

Figure 9-41: q

Theta

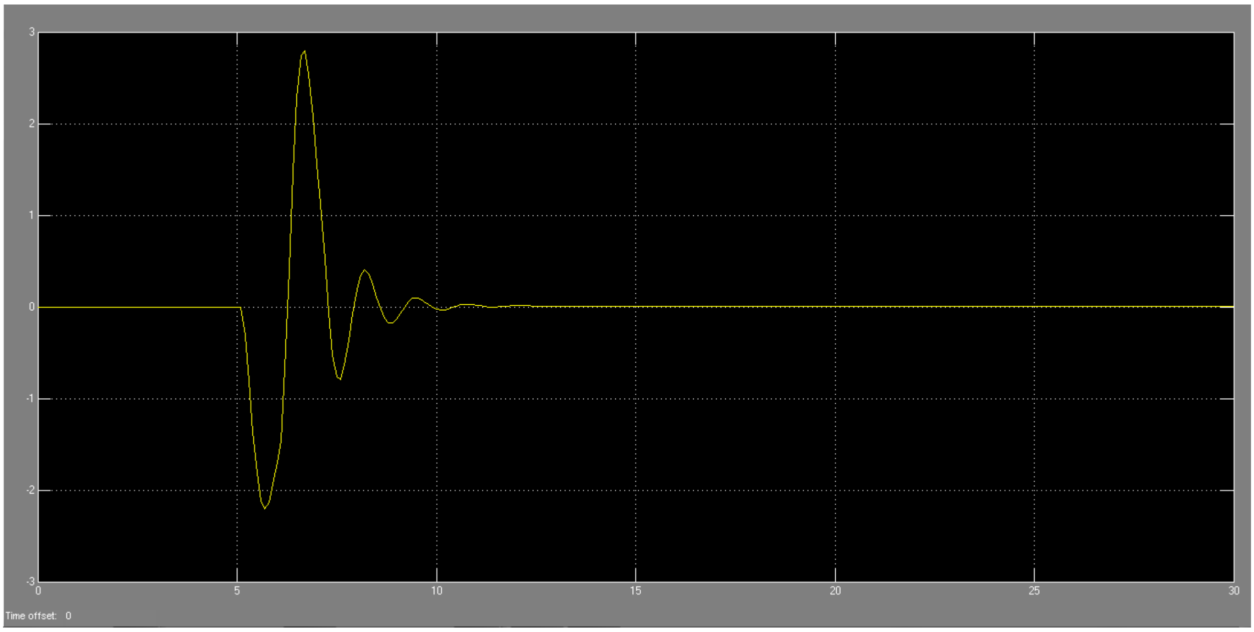

Figure 9-42: Theta

u

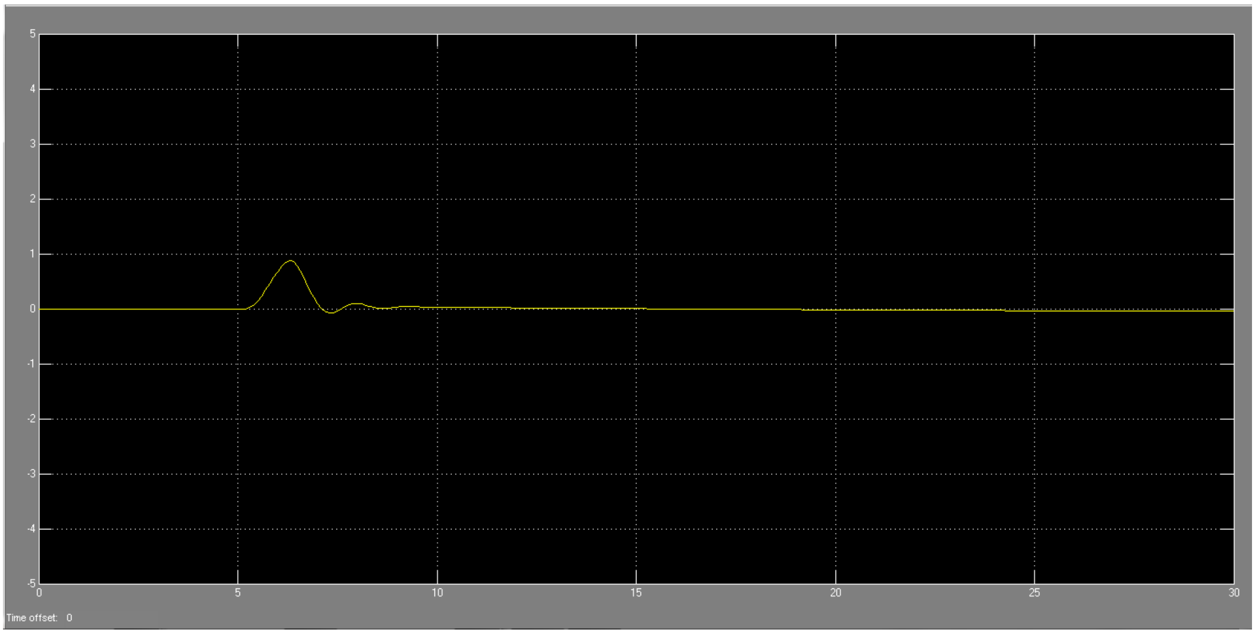

Figure 9-43: u

w

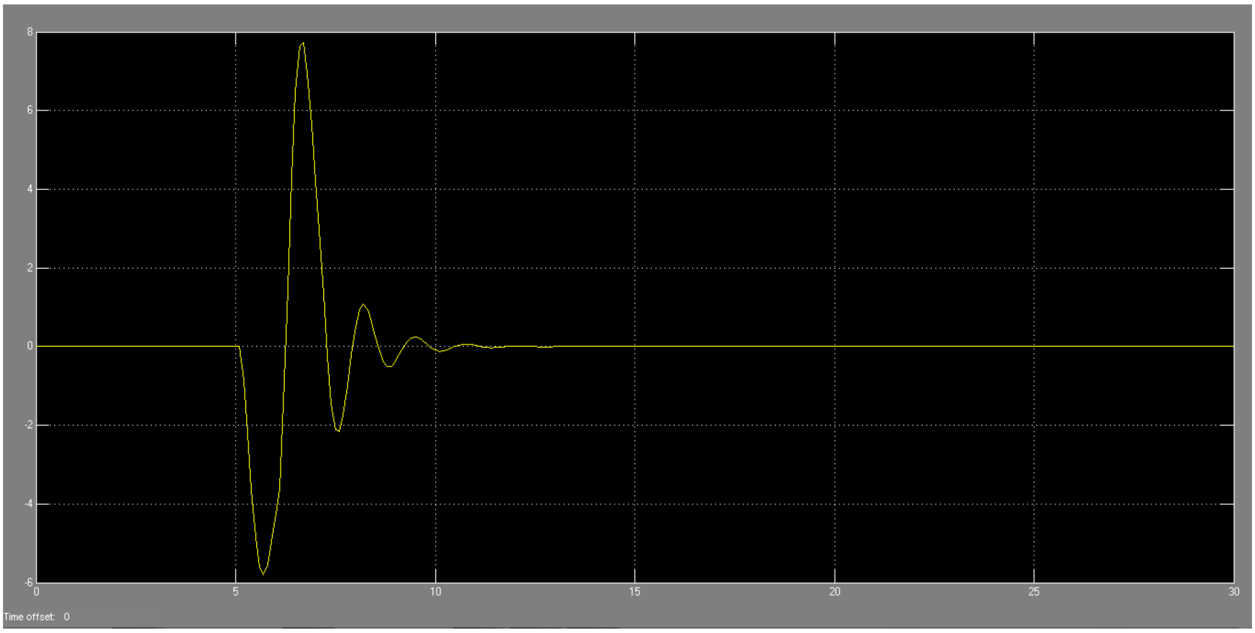

Figure 9-44: w

Elevator Step

q

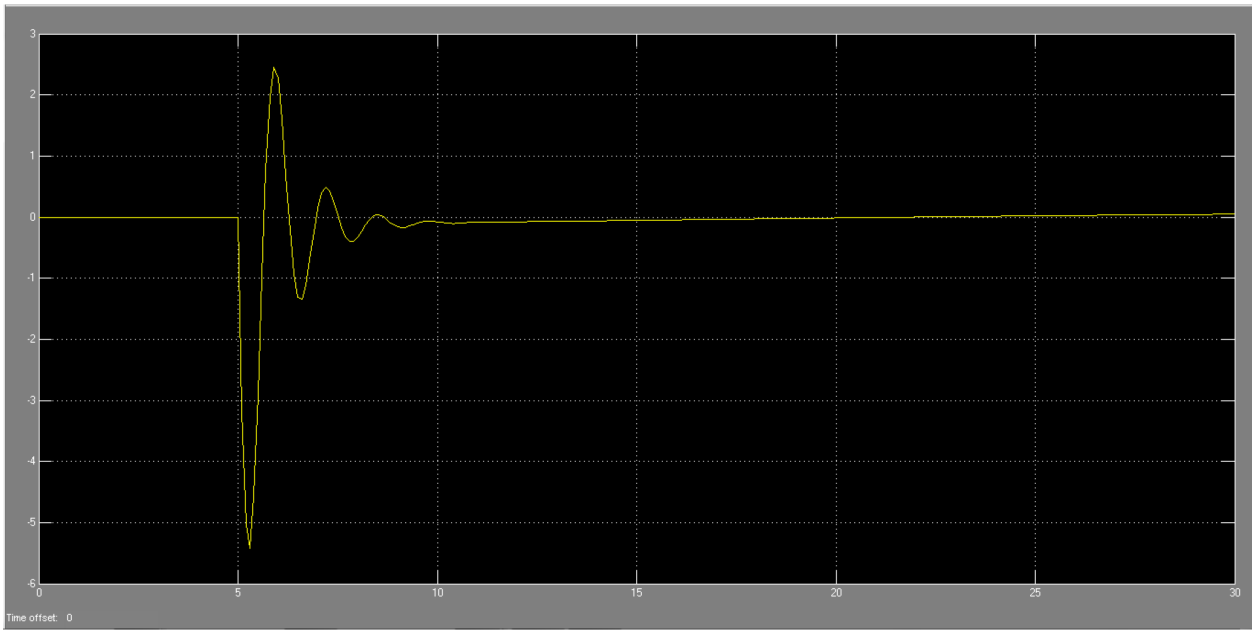

Figure 9-45: q

Theta

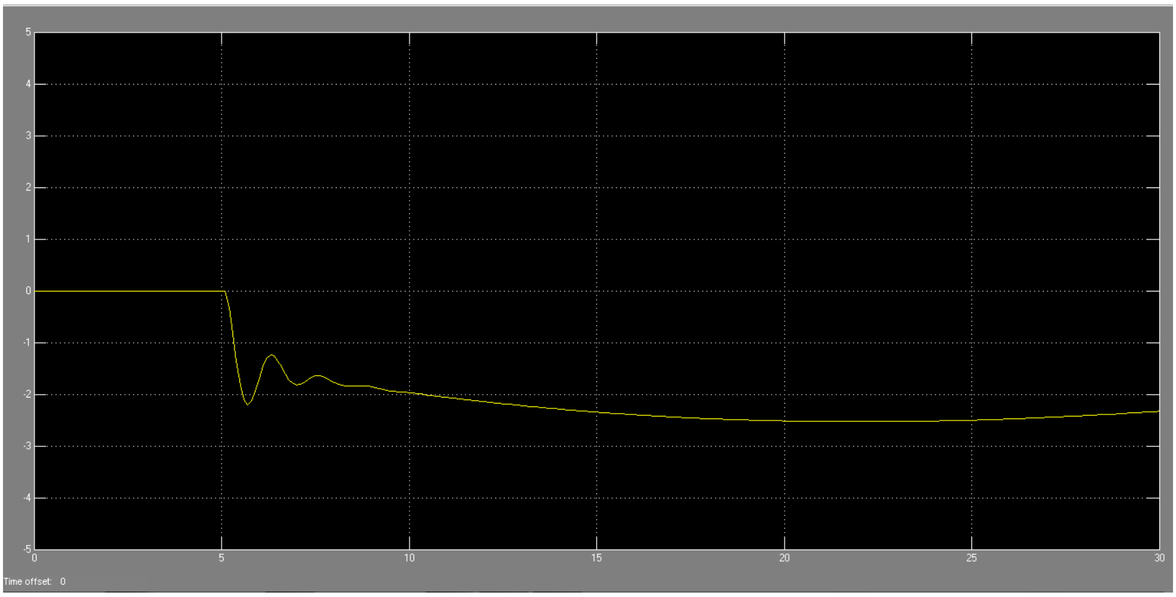

Figure 9-46: Theta

u

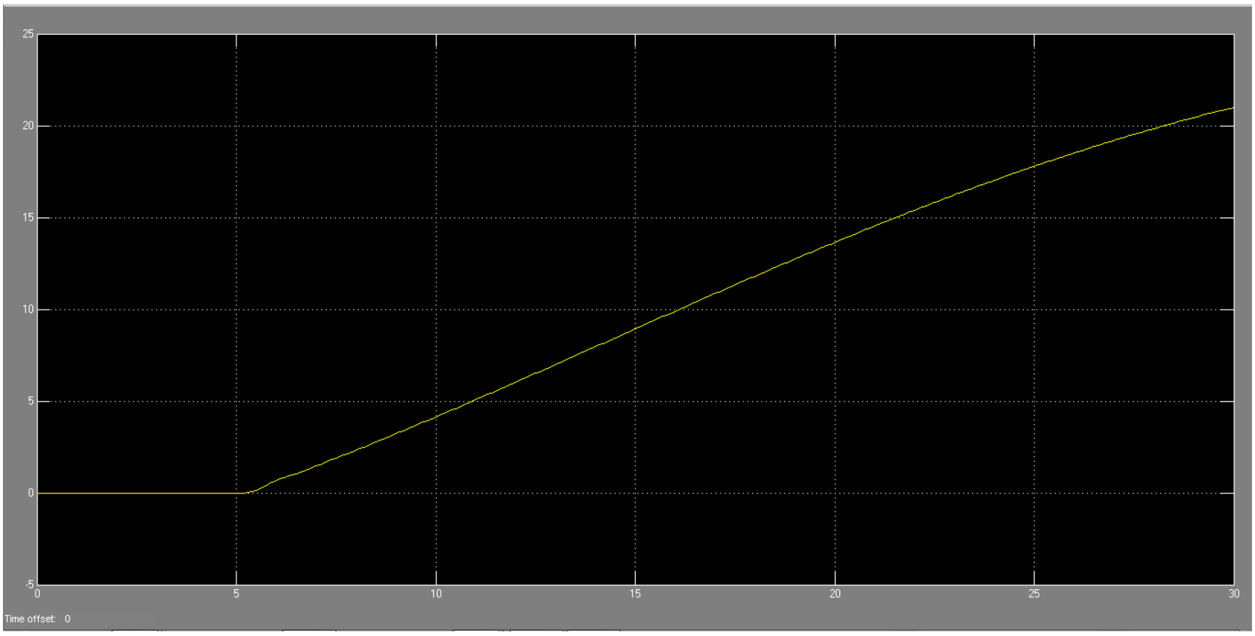

Figure 9-47: u

w

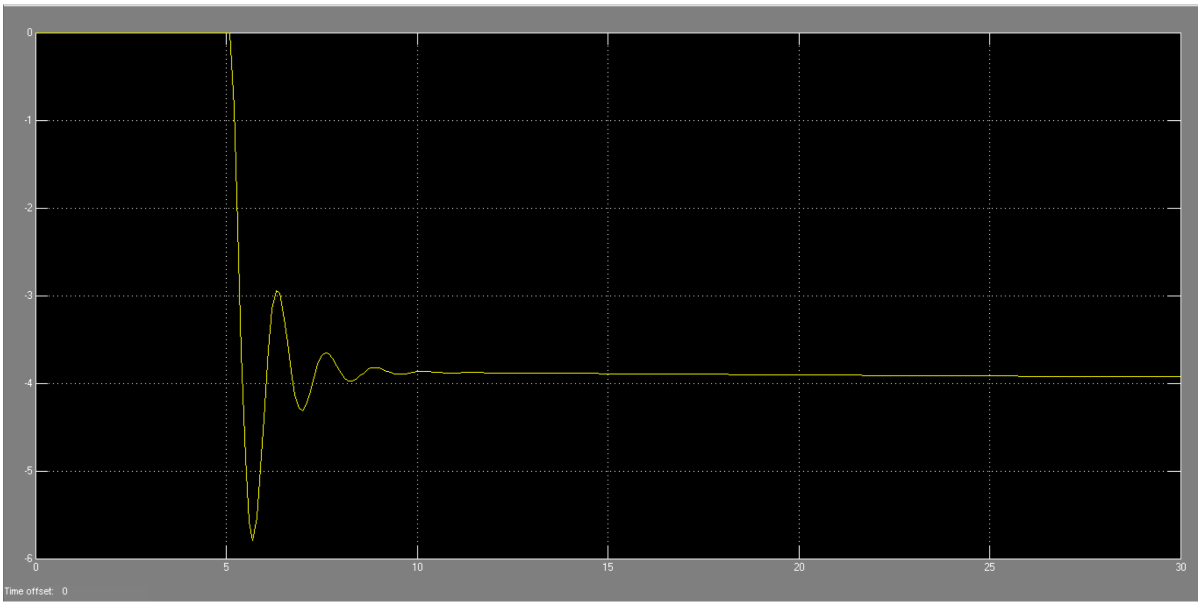

Figure 9-48: w

Three Degree of Freedom Lateral Model:

Aileron Step

Beta

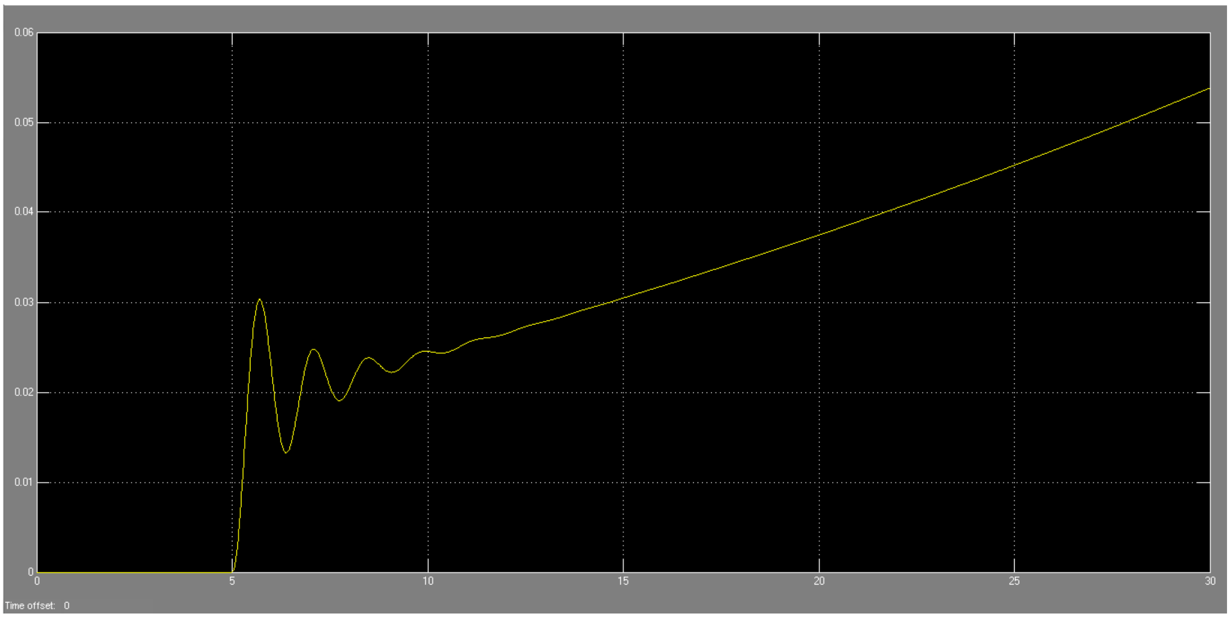

Figure 9-49: Beta

PHI

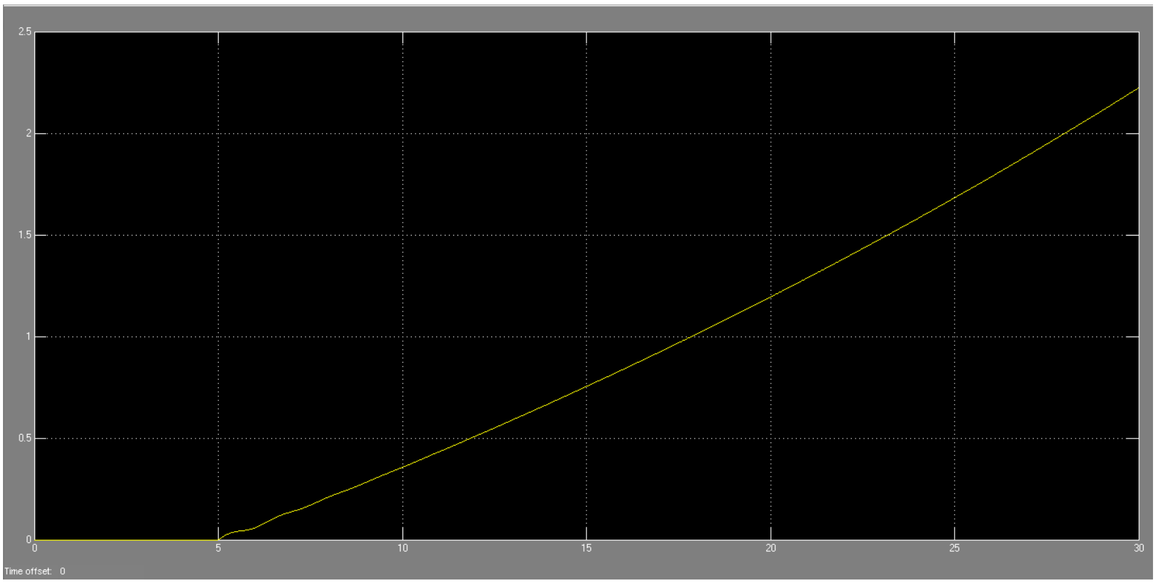

Figure 9-50: phi

Roll Rate

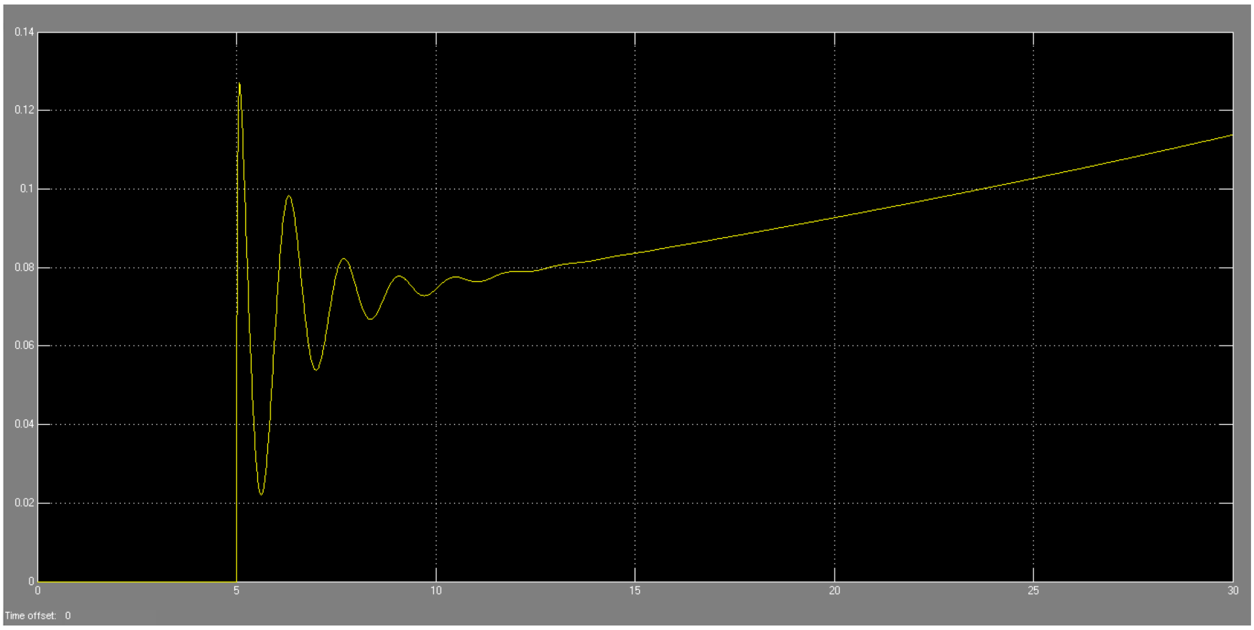

Figure 9-51: Roll Rate

Yaw Rate

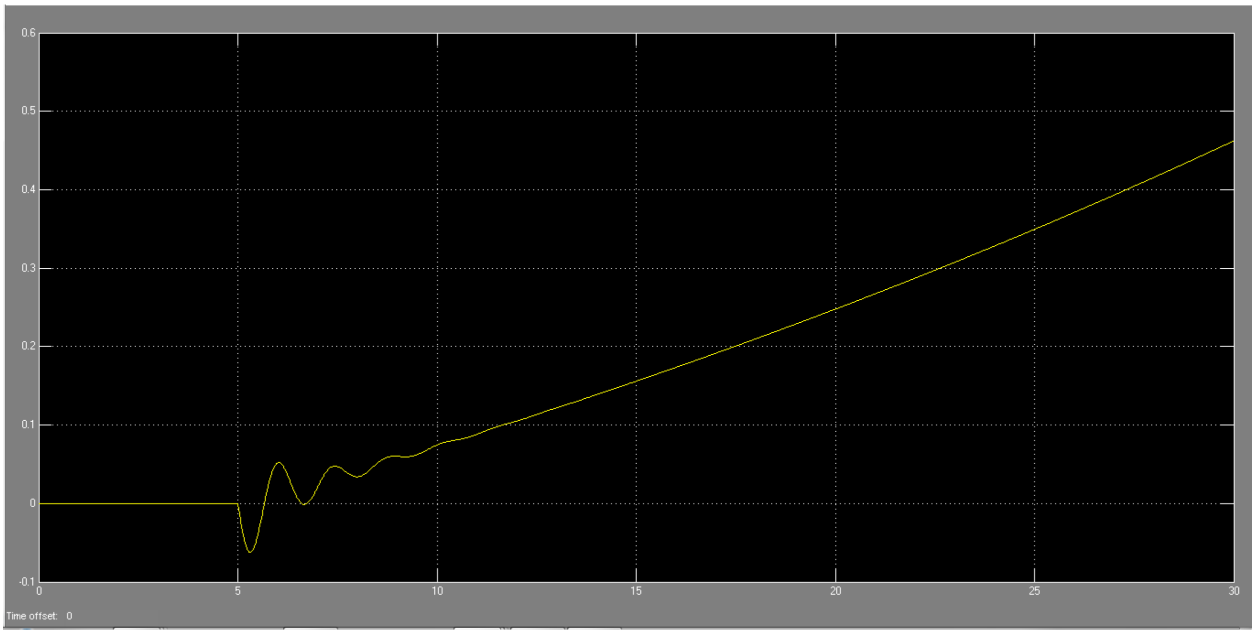

Figure 9-52: Yaw Rate

Rudder Impulse

Beta

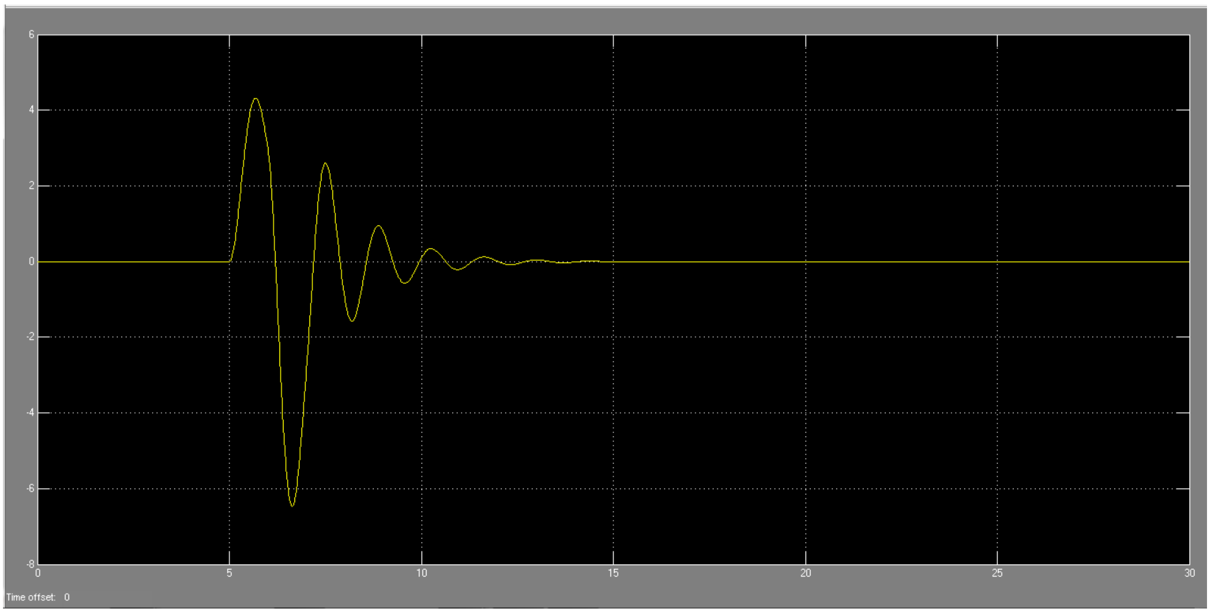

Figure 9-53: Beta

PHI

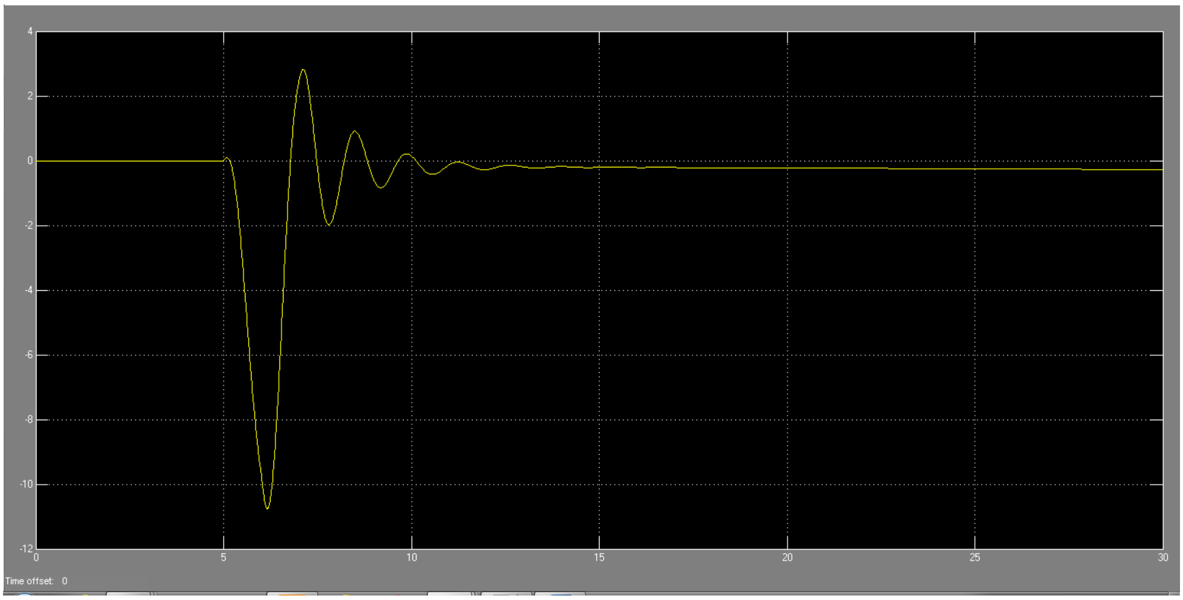

Figure 9-54: phi

Roll Rate

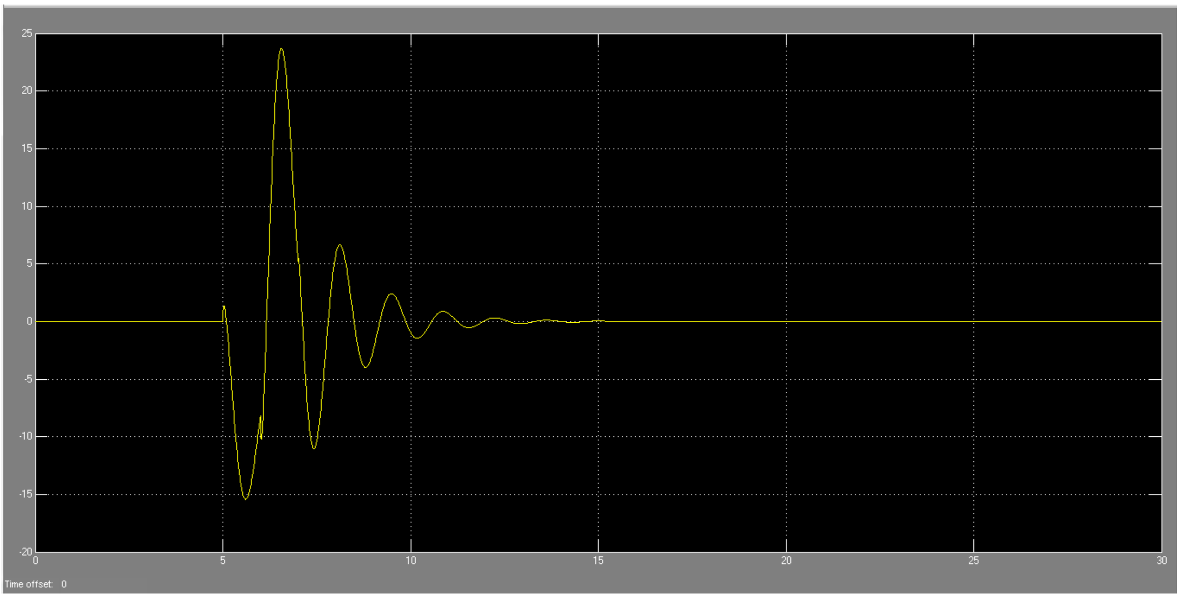

Figure 9-55: Roll Rate

Yaw Rate

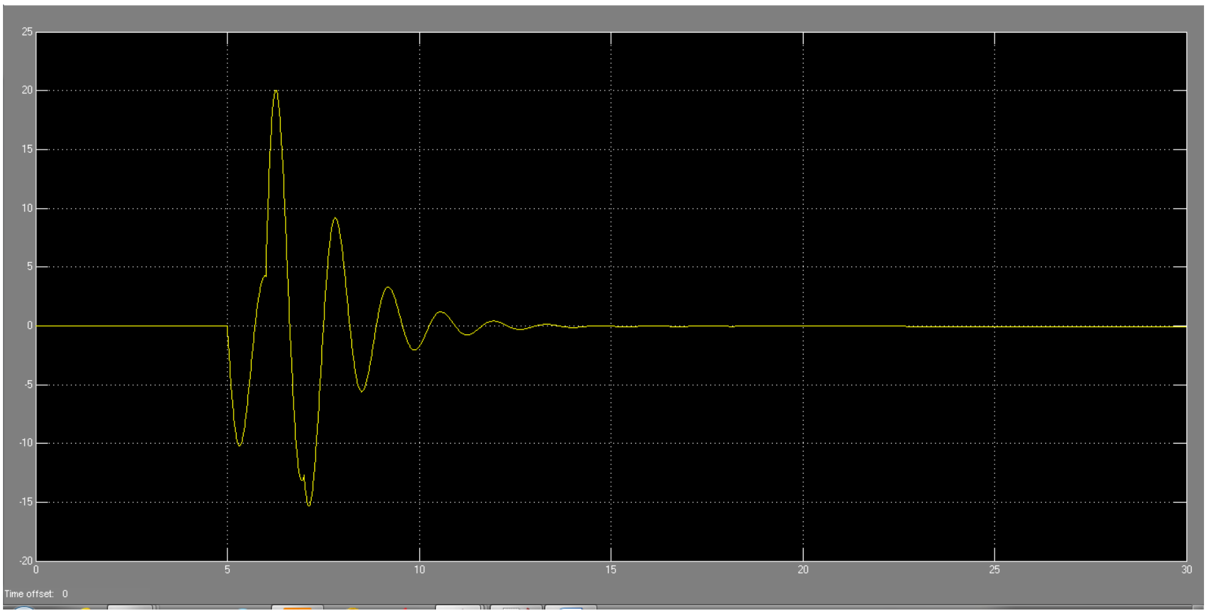

Figure 9-56: Yaw Rate

`

PROPELSION SYSTEM RESULTS:

Diameter calculation:

Equation (7-1) gives D = 1.12 m and the value is too much higher than that calculate from equation (7-2) because it consider only the engine horse power but the value of equation (7-2) is reasonable to avoid tip shock waves

Chord calculation:

The only available equation for calculate the chord is (7-9) but it give unreasonable distribution of chord through root to tip.

.

Propeller model:

The first wooden model of propeller gives weak results such as (lower RPM , lower flow field distribution) . this weak results cured by change the blade angle .the second model give a good results. because that the overall efficiency of a counter-rotating propeller is not seriously affected by changes in rotational speed or small changes in blade angle of the aft propeller disk. These changes did, however, have a moderate effect when the propeller was operated at peak efficiency.

Propeller fabrication:

Due to the lack of welding joints between the rearward propeller and outer shaft on the coaxial system ,propeller separated from the column. This can be solve by using a suitable welding joint ,manufacturing a new column of suitable material, or work to install a good propeller.

Figure 9-57

Practical experimental:

Firstly the air density was taken $1.11 kg/m^3$ because the test base at altitude of 1000 m.

The power source was electrical motor with 2.5 horsepower with 2800 R.P.M and reduced by transmission unit to 1400 R.P.M due to the high load of gearbox.

The propeller static thrust equal to $58.02\ N$ and enhance by using the cascade it clear that thrust increase first with increase of angle of setting but it reduce again due to separation.

When coaxial propeller used, give high thrust compare with single propeller $98.6\ N$ because it almost cancels the swirl and the velocity vector more straight.

Chapter 10 : CONCLUSIONS & RECOMMENDATIONS

Conclusion:

A UAV designed with the roadmap defined at the beginning of the project with exceeding characteristics in performance and stability. The material selected for structure of fuselage has a load factor with a less margin of safety, reserving the integrity of structure.

DATCOM was used to Compute the forces and moments, these values were utilized to calculate the stability coefficients and stability derivatives at a given flight condition. The negative values of $CM_{\alpha}$and$C\ell_{\beta}$and a positiveCn_{β}, demonstrate that the airplane is statically stable.

Dynamic stability was verified using Simulink, results in good dynamic behavior. The longitudinal modes show convergent oscillation.

The derivatives found by DATCOM were validated by AAA, no significant differences were found between the longitudinal static and dynamic stability analysis done by both DATCOM & AAA. Where lateral directional stability were deference.

The dynamic stability characteristics are used to evaluate the flying qualities of the UAV achieving level one flying qualities for short period.

Dutch roll mode and roll mode of the airplane match with damped mode and convergent mode, respectively. However, spiral mode response prediction corresponds to a divergent mode. This means their plane is dynamically unstable for spiral mode, and stable for Dutch roll mode and roll mode.

According to the results from engine, following conclusions are drawn:

- The blade element theory method can be applied to any complicated propeller configuration and determine the characteristics.
- The Cascade and Coaxial system may raise the propeller efficiency around 1-2 percent of design condition for the present system.
- As the difference on thrust increase between the Cascade & Coaxial system is very small, it is prefer logically and practically to avoid the increase in weight and mechanism complexity, used the cascade design.

Recommendations:

- To ensure that a minimum induced drag could be obtained, a further structural arrangement for installation of winglets should be included.
- Aerodynamics data obtained by Raymer is a crude mean of estimation. Therefore, CFD analysis is needed.
- At some point of design, the fuel was selected to be at the wings. This was cancelled since the choice for installation the fuel in fuselage had shown a better alternative. The calculations on wing loads were based on positioning the fuel in it. So, it is needed recalculation on base of being positioned in fuselage.
- The material selected for fuselage structure had a small margin of safety; it should be changed with a stiffer material. Composite materials should be a design alternative with a provided theory to calculate the stresses.
- A stress analysis program such as NASTRAN PATRAN should be used to verify stress analysis on structural components.
- Run flight test to validate stability derivatives & identify the mathematical model.
- Design a control system for the UAV.
- Lateral directional modes had shown middle dynamic behavior, so it needs to be carefully studied.
- Stability augmentation system is required to achieve a good spiral & Dutch roll stability.
- Develop Analysis program for CRPs which is able to capture the thrust/torque characteristics in an averaged sense.
- Use of simulation to observe various parameters that affect propeller interference which can be helpful to optimize propeller performance.
- Use a suitable aerodynamic tool for propeller analysis such as Panel methods and Computational Fluid Dynamics (CFD), etc. to obtain valid animated aerodynamic results.

- ❖ Modifying a new light weight mechanism that satisfying the propeller operation by using suitable engine that give the require power.
- ❖ Make a visualization test to verify that the coaxial propeller system cancel the swirl actually and make a smooth flow.
- ❖ Composition a control system that regulate the engine RPM.
- ❖ Complete the required four tests by using a forward cascade to select wherever it gives a better performance.
- ❖ Reduce the extra noise in the coaxial propeller system by enclose the coaxial propeller in a shroud or by making a new design of the two propellers has different blades (e.g.: use two blades on the forward propeller & three on the aft).

References:

[1] R. Baylis, C. Collins, C. French, E. Pham, and A. Valiyff, "design and development of a tailless fuel cell powered Unmanned Aerial Vehicle," *University of Adelaide*

p. 247, 2009.

[2] D. P. Raymer, *Aircraft design: a conceptual approach*: American Institute of Aeronautics and Astronautics Reston, 2006.

[3] J. Roskam, *Airplane design*: Roskam Aviation and Engineering Corporation, 1990.

[4] J. Vanderover and K. Visser, "Analysis of a Contra-Rotating Propeller Driven Transport Aircraft," *AIAA Student Paper Competition,* 2006.

[5] S. C. Playle, K. Korkan, and E. Von Lavante, "A numerical method for the design and analysis of counter-rotating propellers," *Journal of Propulsion and Power,* vol. 2, pp. 57-63, 1986.

[6] M. S. Farooque, "CFD Grid generation and flow analysis of a counter rotating open rotor propulsion system," The Ohio State University, 2010.

[7] M. H. Sadraey, "Aircraft Design A Systems Engineering Approach," p. 799, 2013.

[8] J. Anderson, "Aircraft Performance And Design

" p. 600.

[9] M. Carley, "Some nots on aircraft and spacecraft stability and control," p. 115.

[10] R. C. Nelson, *Flight stability and automatic control* vol. 2: WCB/McGraw Hill, 1998.

[11] M. A. K. Mark Peters, "The Engineering Analysis and Design of the Aircraft Dynamic Model For the FAA Target Generation Facility," p. 321, 2012.

[12] B. Etkin and L. D. Reid, *Dynamics of flight: stability and control*: Wiley New York, 1996.

[13] B. L. S. a. F. L.Lewis, "Aircraft Control and Simulation," p. 680.

[14] Rankine, "propeller theories," 1885.

[15] F. E. Weick, "Aircraft propeller design," 1930.

[16] K. D. WOODS, "Airplane design."

.

APPENDICIES:

APPENDIX A: WING AIRFOIL DATA

- NACA2412

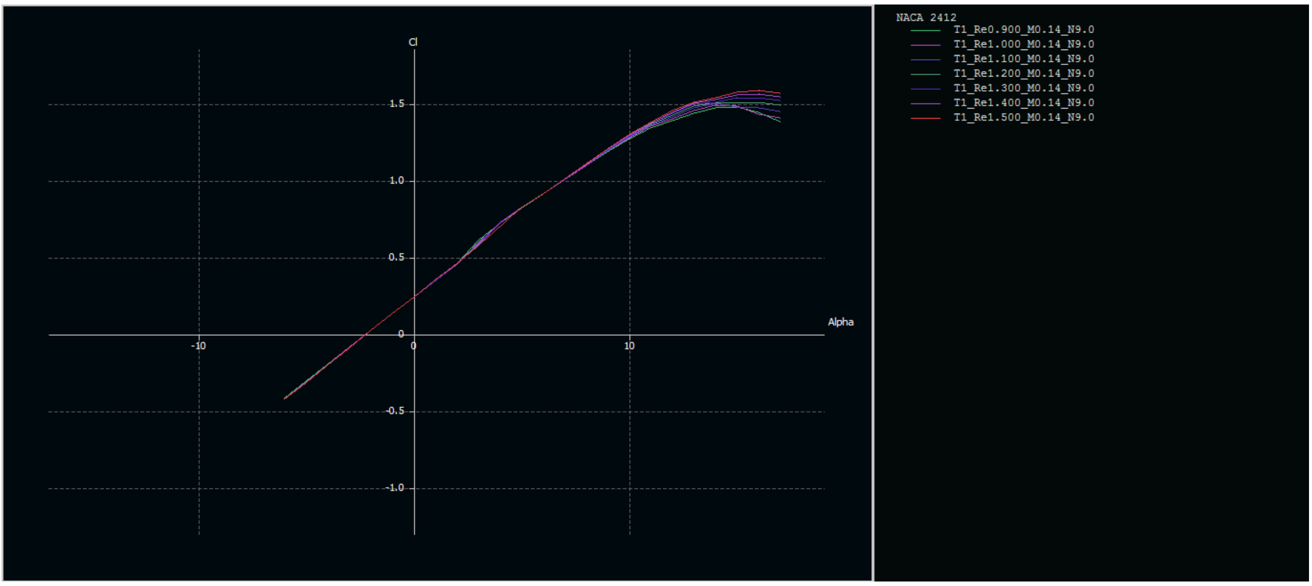

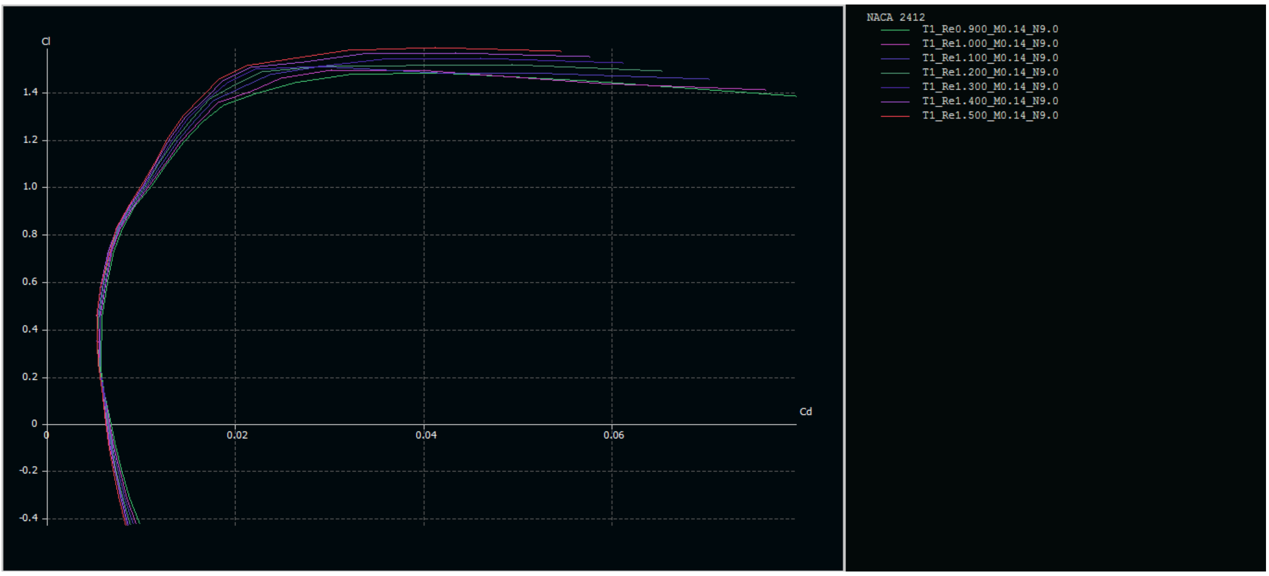

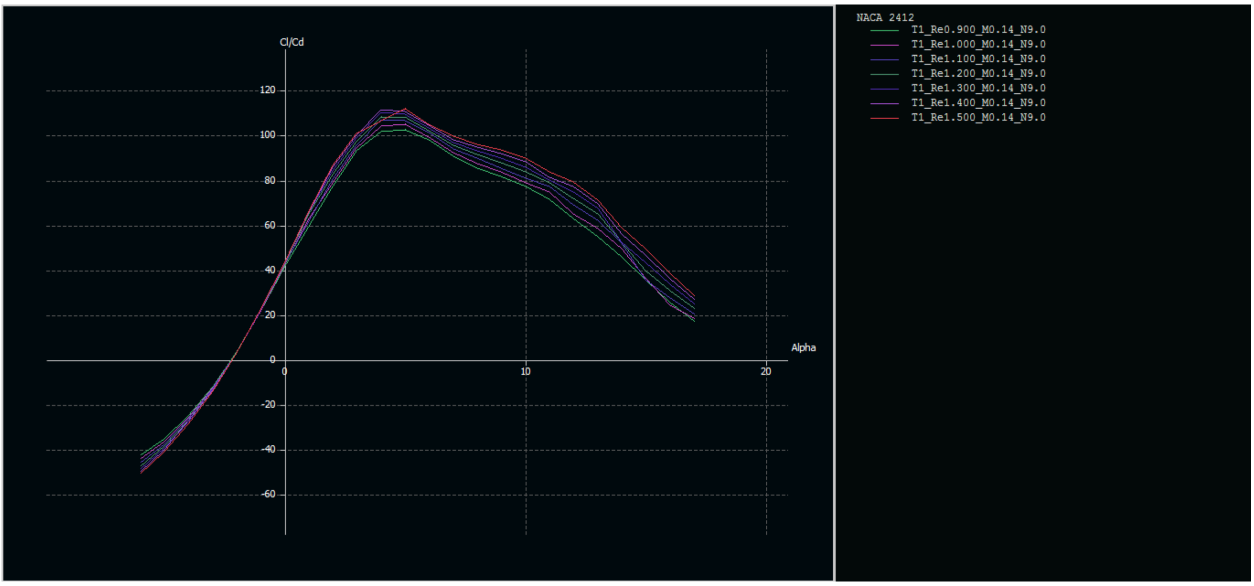

Cl/Cd
Alpha
NACA 2412
T1_Re0.900_M0.14_N9.0
T1_Re1.000_M0.14_N9.0
T1_Re1.100_M0.14_N9.0
T1_Re1.200_M0.14_N9.0
T1_Re1.300_M0.14_N9.0
T1_Re1.400_M0.14_N9.0
T1_Re1.500_M0.14_N9.0

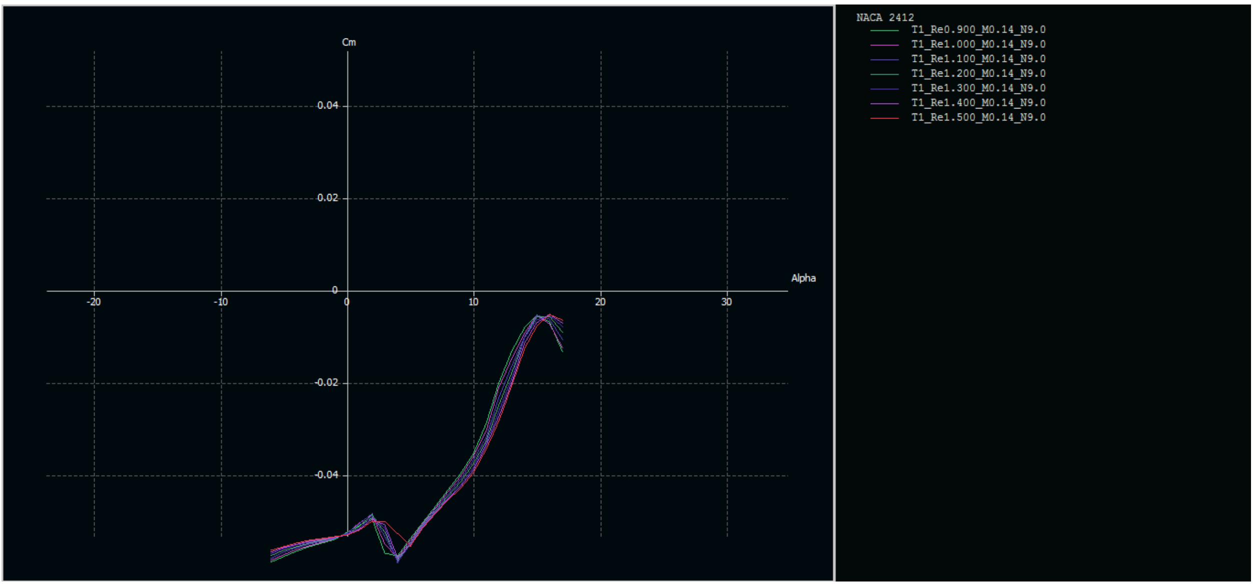

Cm
Alpha
NACA 2412
T1_Re0.900_M0.14_N9.0
T1_Re1.000_M0.14_N9.0
T1_Re1.100_M0.14_N9.0
T1_Re1.200_M0.14_N9.0
T1_Re1.300_M0.14_N9.0
T1_Re1.400_M0.14_N9.0
T1_Re1.500_M0.14_N9.0

- NACA 23012

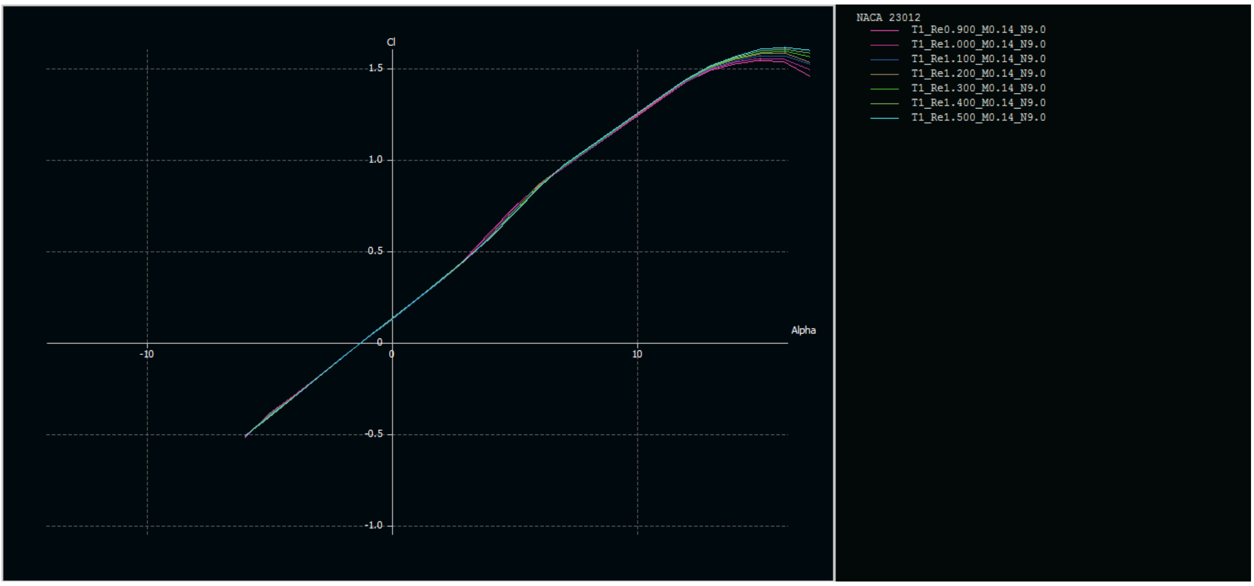

Cl
Alpha
NACA 23012
T1_Re0.900_M0.14_N9.0
T1_Re1.000_M0.14_N9.0
T1_Re1.100_M0.14_N9.0
T1_Re1.200_M0.14_N9.0
T1_Re1.300_M0.14_N9.0
T1_Re1.400_M0.14_N9.0
T1_Re1.500_M0.14_N9.0

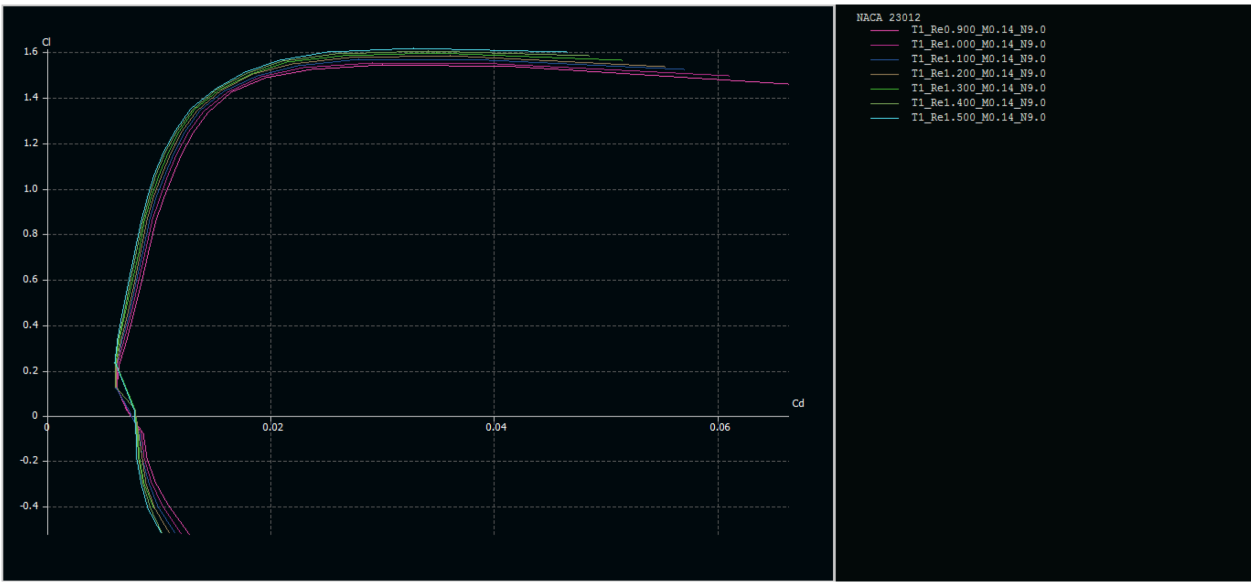

Cl
Cd
NACA 23012
T1_Re0.900_M0.14_N9.0
T1_Re1.000_M0.14_N9.0
T1_Re1.100_M0.14_N9.0
T1_Re1.200_M0.14_N9.0
T1_Re1.300_M0.14_N9.0
T1_Re1.400_M0.14_N9.0
T1_Re1.500_M0.14_N9.0

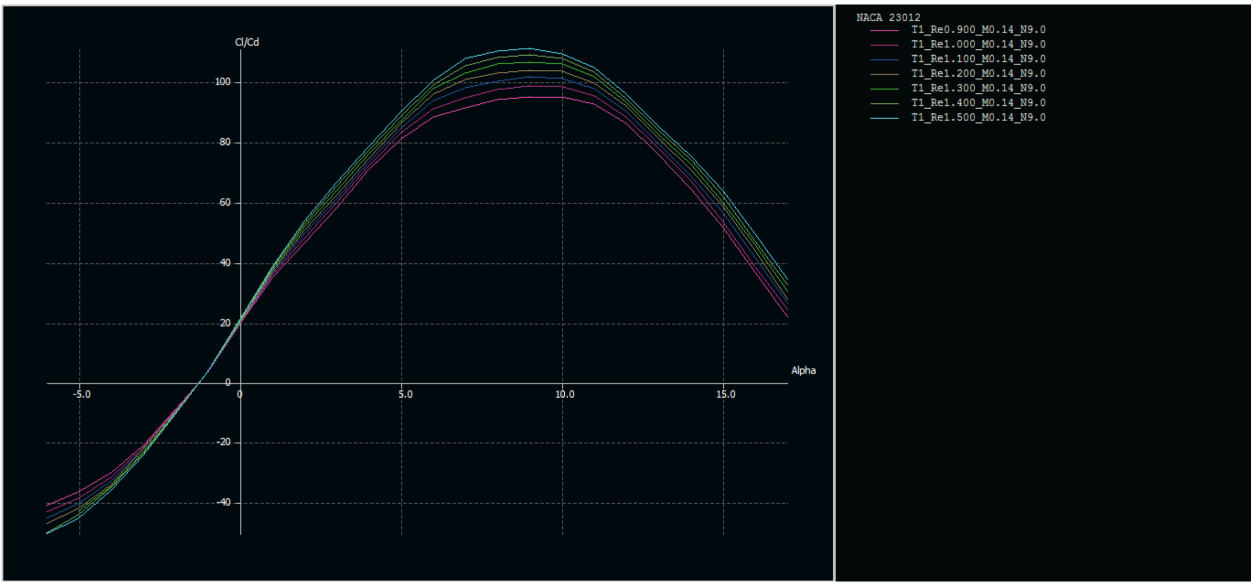
Cl/Cd
Alpha
NACA 23012
T1_Re0.900_M0.14_N9.0
T1_Re1.000_M0.14_N9.0
T1_Re1.100_M0.14_N9.0
T1_Re1.200_M0.14_N9.0
T1_Re1.300_M0.14_N9.0
T1_Re1.400_M0.14_N9.0
T1_Re1.500_M0.14_N9.0

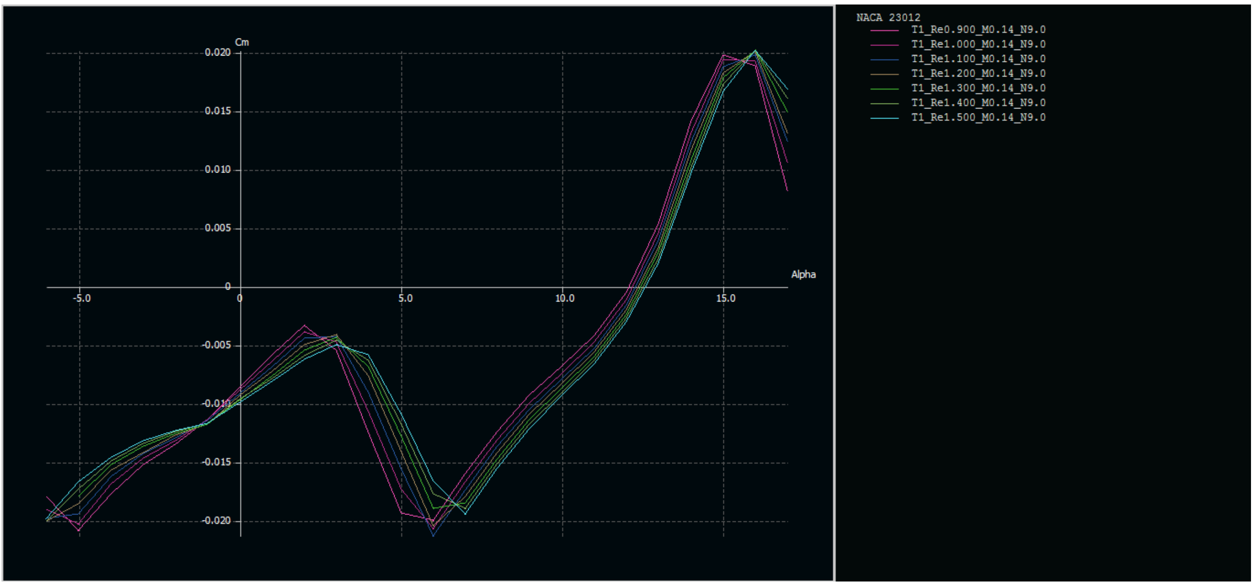
Cm
Alpha
NACA 23012
T1_Re0.900_M0.14_N9.0
T1_Re1.000_M0.14_N9.0
T1_Re1.100_M0.14_N9.0
T1_Re1.200_M0.14_N9.0
T1_Re1.300_M0.14_N9.0
T1_Re1.400_M0.14_N9.0
T1_Re1.500_M0.14_N9.0

- NACA4415

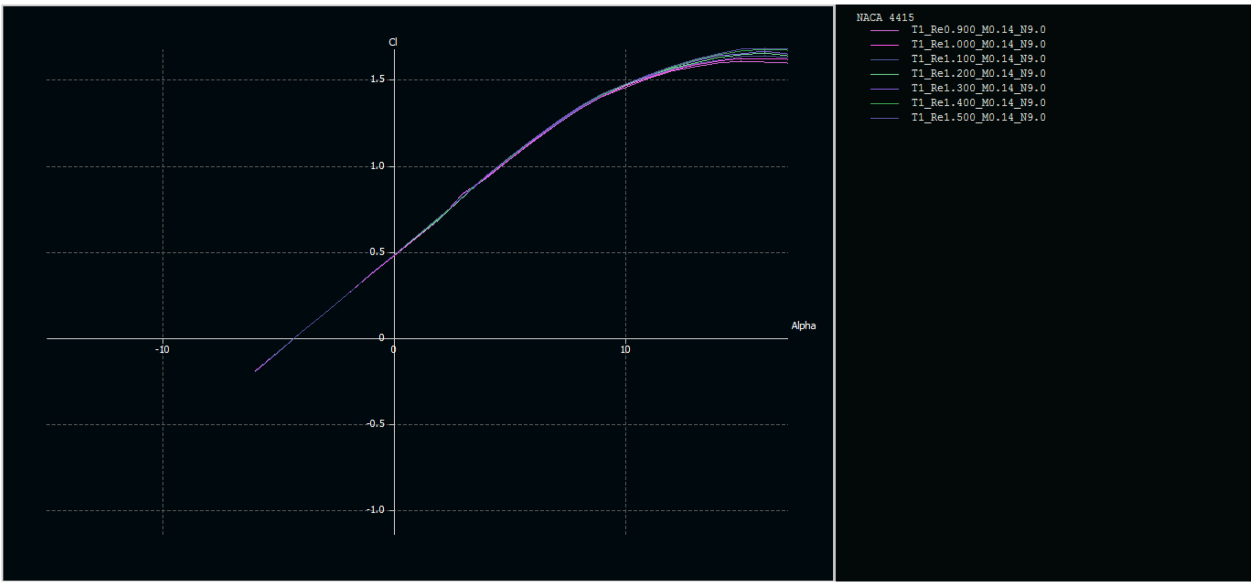
Cl
Alpha
NACA 4415
T1_Re0.900_M0.14_N9.0
T1_Re1.000_M0.14_N9.0
T1_Re1.100_M0.14_N9.0
T1_Re1.200_M0.14_N9.0
T1_Re1.300_M0.14_N9.0
T1_Re1.400_M0.14_N9.0
T1_Re1.500_M0.14_N9.0

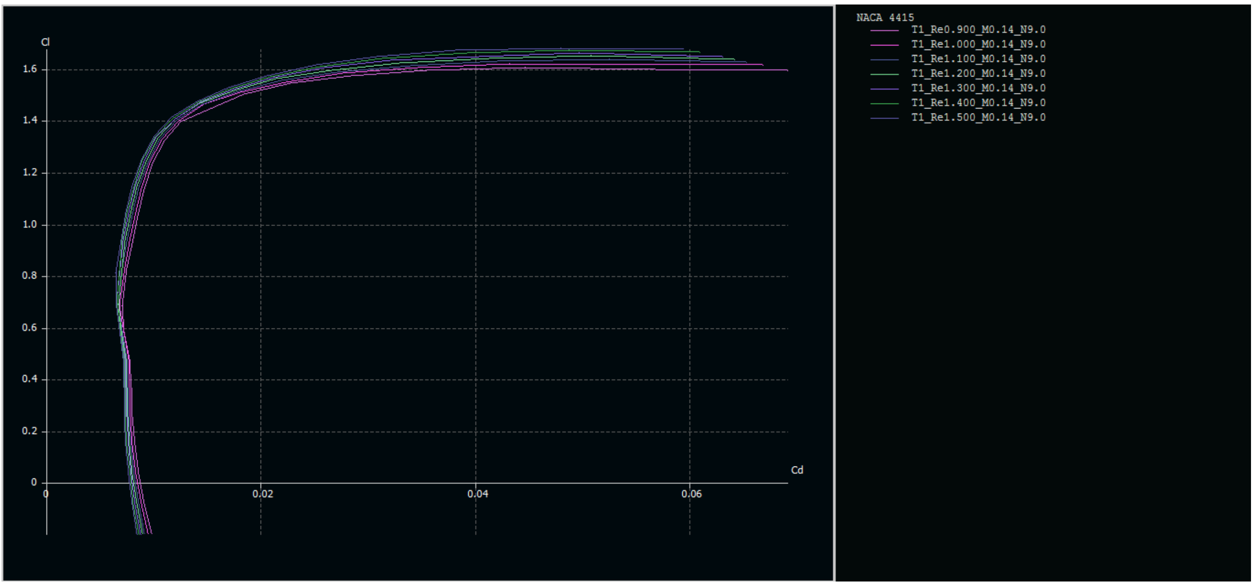
Cl
Cd
NACA 4415
T1_Re0.900_M0.14_N9.0
T1_Re1.000_M0.14_N9.0
T1_Re1.100_M0.14_N9.0
T1_Re1.200_M0.14_N9.0
T1_Re1.300_M0.14_N9.0
T1_Re1.400_M0.14_N9.0
T1_Re1.500_M0.14_N9.0

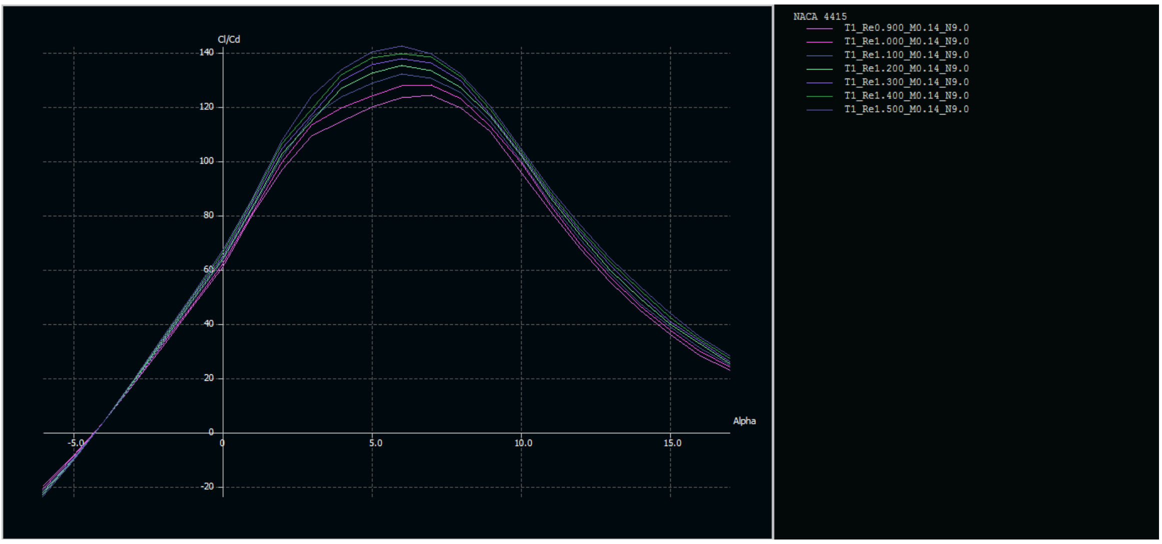
Cl/Cd
Alpha
NACA 4415
T1_Re0.900_M0.14_N9.0
T1_Re1.000_M0.14_N9.0
T1_Re1.100_M0.14_N9.0
T1_Re1.200_M0.14_N9.0
T1_Re1.300_M0.14_N9.0
T1_Re1.400_M0.14_N9.0
T1_Re1.500_M0.14_N9.0

- FX61147

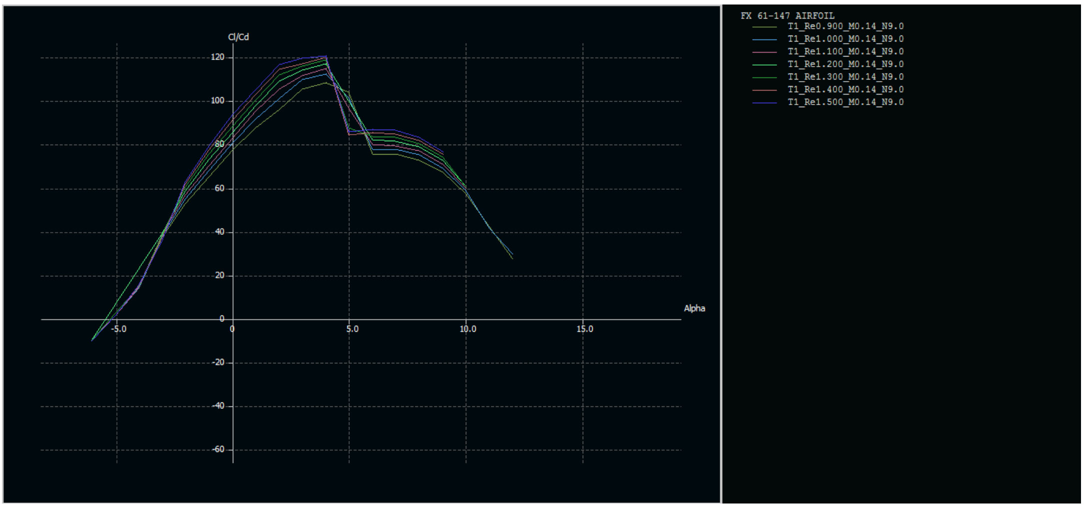
Cl/Cd
Alpha
FX 61-147 AIRFOIL
T1_Re0.900_M0.14_N9.0
T1_Re1.000_M0.14_N9.0
T1_Re1.100_M0.14_N9.0
T1_Re1.200_M0.14_N9.0
T1_Re1.300_M0.14_N9.0
T1_Re1.400_M0.14_N9.0
T1_Re1.500_M0.14_N9.0

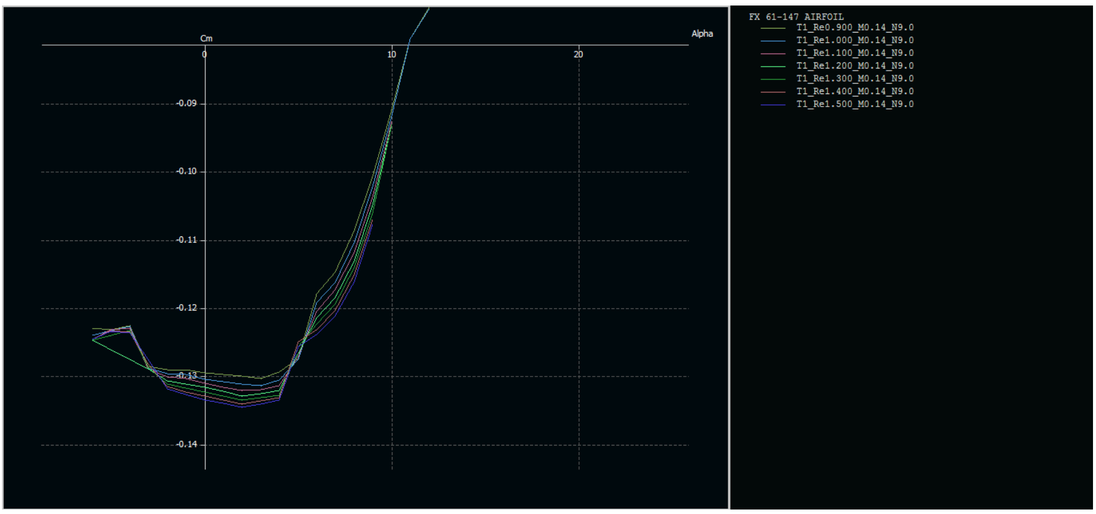
Cm
Alpha
FX 61-147 AIRFOIL
T1_Re0.900_M0.14_N9.0
T1_Re1.000_M0.14_N9.0
T1_Re1.100_M0.14_N9.0
T1_Re1.200_M0.14_N9.0
T1_Re1.300_M0.14_N9.0
T1_Re1.400_M0.14_N9.0
T1_Re1.500_M0.14_N9.0

APPENDIX B: CLARK-Y CHARACTRISTICS

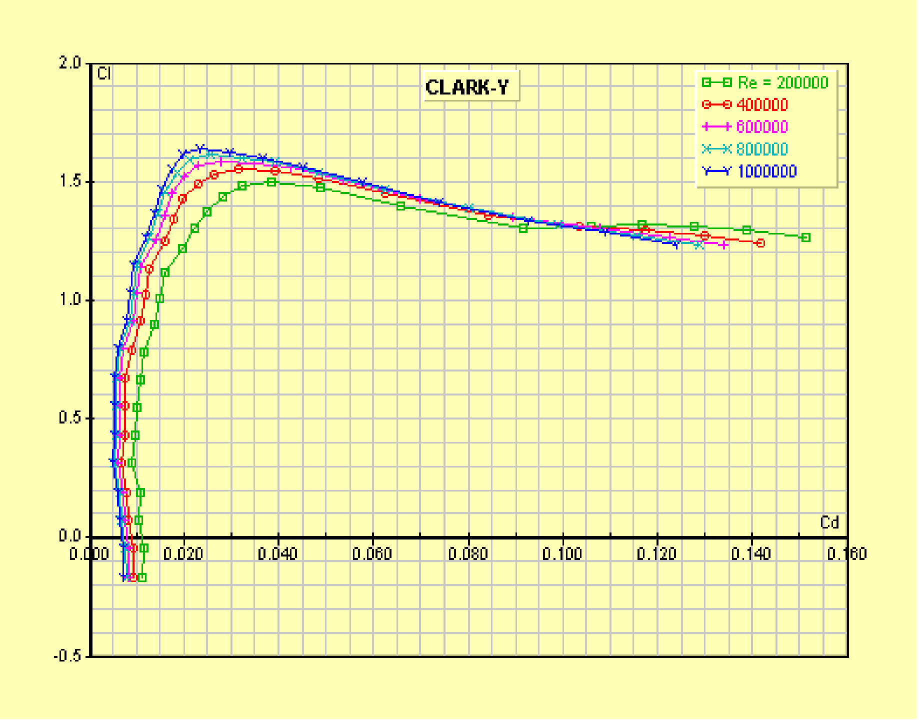

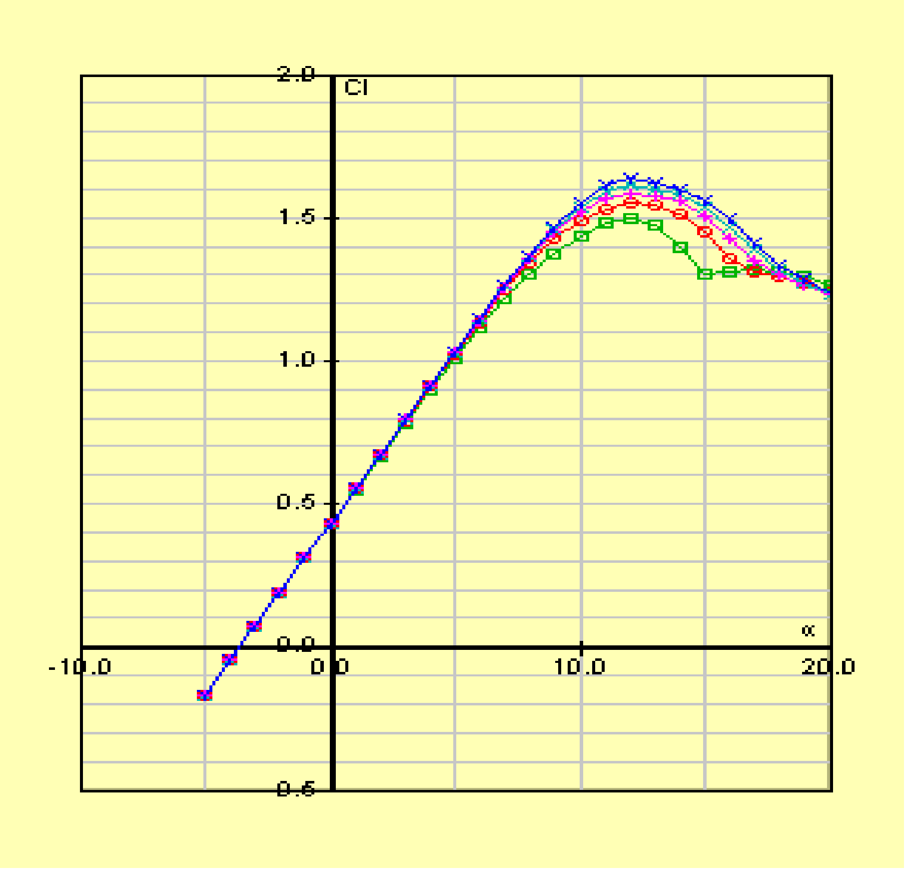

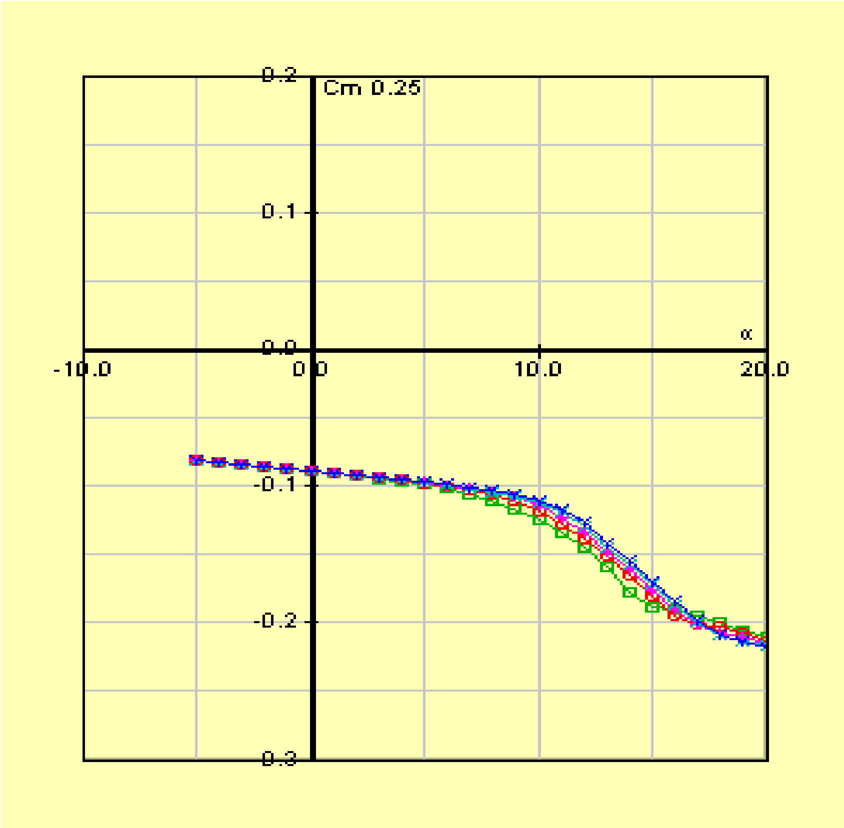

Cm 0.25
0.2
0.1
0.0
-0.1
-0.2
-0.3
-10.0
0.0
10.0
20.0
α

APPEENDIX C: CONISTRAIN DIAGRAM MATLAB CODE

```
m      =  0.04    ;%µ
K      =  0.0401  ;%Drag polar parameter
q      =  0.8     ;%propeller efficiency
g      =  32.2    ;%gravity acceleration
p      =  0.002378;%air density
Vs=  82.0209 ;%stall speed
Vc=  154.2   ;%cruise speed
CLmax =  1.56    ;%maximum lift coefficient
STO    =  492.13  ;%required take-off distance
VTO    =  1.1*Vs  ;%take-off speed
CDoLG=  0.0035  ;%zero landing gear drag
CDoHLD_TO = 0    ;%zero drag for high lift device
CDo=  0.03417 ;%zero lift drag
CLTO   =  1.57    ;%take-off lift coefficient
W_S    =  1 : 1 : 20 ;
%Take off Constraint
CDoTO=  CDo + CDoLG + CDoHLD_TO ;
CDTO   =CDoTO + K .* CLTO^2      ;
CLR    =  CLmax /(1.1*1.1)        ;
CDG    =  CDTO - m * CLTO         ;
Wp     =  ( q ./ VTO ) .* ( 1 - exp( 0.6 .* p .* g .* CDG
.* STO .*( 1 ./ W_S ))) ./( m -( m +( CDG ./ CLR )) .*
(exp(0.6 .* p .* g .* CDG .* STO .*(1 ./  W_S))));
%Maximum Speed Constraint
Vmax=  1.3 * Vc       ;
a     =  0.5 * p  * CDo ;
b     =  2 * K / p      ;
W_P    =  q ./ ( ( a * Vmax^3 ./ W_S ) + ( b / Vmax ) *
W_S ) ;
% Stall Constraint
W_s   =  [ 11.3217 11.3217 11.3217 11.3217  11.3217] ;
W_p   =  [ 0       0.005   0.02    0.045     0.08   ] ;
%Plotting Result
plot(W_S,W_P)
holdon
plot(W_S,Wp)
holdon
plot(W_s,W_p)
title('Constraint Diagram')
xlabel('W/S')
ylabel('W/P')
```

APPENDIX D: PERFORMANCE ANALYSIS CODE

```
%Basic Configuration Parameters
W0 = 167.652     ;
Wf = 9.889176801085958     ;
S  = 14.80812952 ;
P0 = 16.4 ;
g  = 32.2 ;
c  = 2.0202E-07 ;
mr = 0.4  ;%friction coefficient
j  = 1.15 ;
n  = 3    ;
%Aerodynamic Parameters
CLm  = 1.655 ;
Cd0  = 0.034 ;
k    = 0.0401;
Pinf = 0.002577 ;
Pinf1 = 1.225 ;
Palt  = 0.0017556 ;
Eff   = 0.8 ;%Propeller efficiency
theta = 0.0523598775598299 ;%3deg
%Calculating wing loading and power loading
W_S = W0 ./ S  ;
P_W = P0 ./ W0 ;
%Calculating Power Required & Maximum Speed
Vs   = sqrt( W_S ./ ( 0.5 .* Pinf .* CLm ) ) ;
Vinf = 80 : 10 : 380 ;
T_R  = 0.5 .* Pinf .* Vinf.^2 .* S .* Cd0 + 2 .* k .* S
* ( W_S )^2 ./ ( Pinf .* Vinf.^2 )  ;
P_R  = ( W0 ./ G1 ) .* sqrt( 2 .* W0 ./ ( Pinf .* S .*
Vinf.^2 ) ) ;
P_A  = P0 .* ( Pinf ./ Palt ) ;
T_A  =Eff .* P0 ./ 154.2 ;
%Calculating Lift to drag ratios
CL = 2 .* W_S .* g ./( Pinf .* Vinf.^2 ) ;
CD = Cd0 + k .* CL.^2 ;
L_D  = 1 ./ sqrt( 4 .* k .* Cd0 ) ;%lift to drag ratio
max
CL_CD = 0.25 .* ( 3 ./ ( k .* Cd0^( 1 / 3 ) ))^( 3 / 4
);%CL^(1/2)/ CD
CLCD = 0.75 .* ( 1 ./ ( 3 .* k .* Cd0^( 3 ) ))^( 1 ./ 4
);%CL^(3/2)/CD
V1   = sqrt( ( 2 ./ Pinf ) .* sqrt( k ./ Cd0 ) .* W_S  )
;
V2   = 0.76 .* V1 ;%Velocity at CL^(1/2)/ CD is max
V3   = 1.32 .* V1 ;%Velocity at CL^(3/2)/ CD is max
```

```
G  = CL ./ CD ;
G1 = CL.^0.5 ./ CD ;
G2 = CL.^1.5 ./ CD ;
%Calculating RATE OF CLIMB AND CLIMB VELOCITY
h       = 0 : 100 : 10000 ;
Pinf_h = 6.10 .* 10^-19 .* h.^4 - 7.10 .*10^-14 .* h.^3
+ 4.10 .* 10^-9 .* h.^2 - 10^-4 .* h + 1.225 ;
V_RC    = sqrt( ( 2 ./ Pinf_h ) .* ( sqrt( k ./ ( 3 .*
Cd0 ) ) ) .* W_S .* 4.882427636 ) ;
RC      = Eff .* P0 .* 76.04022 .* ( Pinf_h ./ Pinf1 ) ./
( W0 .* 0.45359237 ) - V_RC .* ( 1.155 ./ L_D  ) ;
%Calculating BEST ANGLE AND RATE OF CLIMB
Vv = ( P0 .* Eff ./ ( W0 .* Vinf ) - ( P_R ./ ( W0 ) ) )
.* Vinf ;
R  = ( Eff ./ c ) .* L_D .* log( W0 ./ ( W0 - Wf ) );
E  = ( Eff ./ c ) .* sqrt( 2 .* Pinf .* S ) .* ( CLCD .*
( ( W0 - Wf )^-0.5 - ( W0 )^-0.5 ) ) ;
%Calculating landing distance
Vf   = 1.23 .* Vs ;
R     = Vf^2 ./ ( 0.2 .* g ) ;%Flight Path radius during
flare
hf   = R .* ( 1 - cos( theta ) ) ;%Flare hight
Sa_L = ( 50 - hf ) ./ tan( theta ) ;%Approach distance
to clear 15.24 m obstacle
Sf_L = R .* sin( theta ) ;
Sg_L = j .* n .* sqrt( ( 2 ./ Pinf ) .* W_S .* ( 1 ./
CLm ) ) + j^2 .* ( W_S ) ./ ( g .* Pinf .* CLm .* mr ) ;
L    = Sa_L + Sf_L + Sg_L ;
%Calculating take off distance
V      = 0.77 .* Vs ;
TA     = Eff .* P0 .* 550 ./ V ;
Rt      = 6.96 .* Vs^2 ./ g ;%Flight Path radius during
flare
Theta = acos( 1 - ( 50 ./ R ) ) ;
Sg_T  = 1.21 .* W_S ./ ( g .* Pinf .* CLm .* ( TA ./ W0
) ) ;
Sa_T  =Rt * sin( Theta ) ;
TO    = Sg_T + Sa_T ;
%%Plotting Result
figure(1)
plot(Vinf,P_R)
title('Power Required Curve')
xlabel('Velocity (ft/s)')
ylabel('PR')
%%Plotting Result
figure(1)
plot(Vinf,G)
holdon
plot(Vinf,G1)
holdon
plot(Vinf,G2)
```

```
title('Variation of lift to drag ratio Curves Versus
Velocity')
xlabel('Velocity (ft/s)')
ylabel('Lift to drag ratio Curves')
%%Plotting Result
figure(1)
plot(Vinf,T_R)
holdon
plot(Vinf,T_A)
title('Thrust Required & Thrust available Curve')
xlabel('Velocity (ft/s)')
ylabel('TR & TA')
%%Plotting Result
figure(1)
plot(Vinf,P_R)
holdon
plot(Vinf,P_A)
title('Power Required & Power available Curve')
xlabel('Velocity (ft/s)')
ylabel('PR & PA')
%%Plotting Result
figure(1)
plot(RC,h)
title('Rate of climb Curve')
xlabel('RCmax(ft/s)')
ylabel('Altitude (ft)')
%%Plotting Result
figure(1)
plot(V_RC,h)
title('Rate of climb velocity Curve')
xlabel('V_RC(ft/s)')
ylabel('Altitude (ft)')
%%Plotting Result
figure(1)
plot(Vinf,Vv)
title('Hodograph for climb performance')
xlabel('Vinf(ft/s)')
ylabel('Vv')
```

APPENDIX E: WING OPTMIZATION

```
clc
clear
N = 9;                                              % (number of
segments - 1)
S = 14.80812952;                            % m^2
AR = 11.3;                                  % Aspect ratio
for lambda = 0.4:0.2:0.8
alpha_twist = 0.01;                         % Twist angle (deg)
i_w = 0.515;                                 % wing setting angle
(deg)
a_2d = 5.439;                                  % lift curve slope
(1./rad)
alpha_0 = -4.2;                              % zero-lift angle of
attack (deg)
b = sqrt(AR.*S);                            % wing span (m)
MAC = S./b;                                    % Mean Aerodynamic
Chord (m)
Croot  =  (1.5.*(1+lambda).*MAC)./(1+lambda+lambda.^2);  %
root chord (m)
theta = pi./(2.*N):pi./(2.*N):pi./2;
alpha = i_w+alpha_twist:-alpha_twist./(N-1):i_w;
% segmentâ€™s angle of attack
z = (b./2).*cos(theta);
c  =  Croot  .*  (1  -  (1-lambda).*  cos(theta));%  Mean
Aerodynamics Chord at each segment (m)
mu = c .* a_2d ./ (4 .* b);
LHS = mu .* (alpha-alpha_0)./57.3;  % Left Hand Side
% Solving N equations to find coefficients A(i):
for i=1:N
for j=1:N
B(i,j)  =  sin((2.*j-1)  .*  theta(i))  .*  (1  +  (mu(i)  .*
(2.*j-1)) ./ sin(theta(i)));
end
end
A=B\transpose(LHS);
for i = 1:N
sum1(i) = 0;
sum2(i) = 0;
for j=1:N
sum1(i)   =   sum1(i)   +   (2.*j-1)   .*   A(j).*sin((2.*j-
1).*theta(i));
sum2(i) = sum2(i) + A(j).*sin((2.*j-1).*theta(i));
end
end
```

```
CL = 4.*b.*sum2 ./ c;
CL1=[0 CL(1) CL(2) CL(3) CL(4) CL(5) CL(6) CL(7) CL(8)
CL(9)];
y_s=[b./2 z(1) z(2) z(3) z(4) z(5) z(6) z(7) z(8) z(9)];
plot(y_s,CL1,'-o')
grid
title('Lift distribution');
xlabel('Semi-span location (m)');
ylabel ('Lift coefficient');
holdon
CL_wing = pi .* AR .* A(1);
lambda = lambda + 0.2 ;
end
```

APPENDIX F: V-N DIAGRAM

```
% Define the Variables
S    = 14.8082 ;%Wing areaft^2%
AR   = 11.3    ;          %Aspet ratio
nmax = 3.4     ;          %maximum load factor
nmin =-1.2     ;          %minimum load factor
CLpos= 1.67    ;          %positive lift
CLneg=-1.36    ;          %negative lift
p   =  0.002377;          %air density slugs/ft^3%
W   =  167.6532;          % weight slug*ft/s^2%
V1   = (( nmax *2 * W ) / ( CLpos * p * S) )^(1/2) ;
V2   = (( nmin * 2 * W )/( CLneg * p * S ))^(1/2)  ;
Vpos = [0:V1]                                     ;
Vneg = [0:V2]                                     ;
q    = 50.8                                       ;
n1   = ( CLpos * p * S * Vpos.^2 )/(2*W)          ;
n2   = ( CLneg * p * S * Vneg.^2 )/(2*W)          ;
Vmax = (( 2 * q ) / p)^(1/2);
% PlottingVn diagram
plot(Vpos, n1)
holdon
plot(Vneg, n2)
holdon
plot([V1:.5:Vmax],nmax)
holdon
plot([V2:.5:Vmax],nmin)
holdon
plot(Vmax,[nmin:.01:nmax])


% Labeling Vn Diagram
gtext ('Positive Stall Limit')
gtext ('Negative Stall Limit')
gtext ('Positive Structural Limit')
gtext ('Negative Structural Limit')
xlabel ('Calibrated Airspeed, ft/sec')
ylabel ('Load Factor, n')
```

APPENDIX G: STATE SPACE CALCULATION

```
deltaa =0.0201879968021599;
Cydeltar =-0.0135192662398883;
Cndeltar =0.0567370474494455;
Cldeltar =-0.0m = 167.653 ;%mass of uav
S = 14.80812952 ;%wing refrence area
AR = 11.3;                          % Aspect Ratio
e = 0.9 ;% Oswald efficiency factor
b = 12.9356818;                     %span
Cbar = 1.17691321;                  %mean areodynamic cord
U = 154.2 ;%design cruise speed
p = 0.002378 ;%air density
g = 32.2 ;%gravity constant
Cla =0.09436  ;%aircraft lift curve slope
Cmq =-31.1574  ;%change in pitching moment due to change
in pitch rate
Clq =6.38275  ;%change in lift coefficient due to change
in pitch rate
Cmu = 0.007047 ;%change in pitching moment due to change
in forword speed
Clu = 0 ;%change in lift coefficient due to change in
forward speed
Cdu =0;                              %Drag Change with forward
speed
Cma = -0.7563 ;%pitching moment change with angle of
attack
Cl0 = 0.344 ;%wing zero lift
Cd0 = 0.024 ;%wing zero drag
Clat= 5.4981;                       %tail lift curve slop
Vh = 0.7 ;%volume of the horizontal tail
t =  1 ;                            %tail efficiency
down =0.156  ;                      %downwash
Lt =  5.8  ;                        %tail moment arm
Clai  =  0.142381158  ;%change  in  lift  force  due  to
elevator deflection
Cmai = -0.656325446 ;
CDdeltae = 0.0135;                   %change in MOMENT due to
elevator deflection
Iy=  18.32359572  ;                %inertia
Q = 28.22405;                       %Dynamic pressure
% lateral inputs
Ix      = 2.371494762;
Iz      = 19.26043419;
Cybeta = -1.13319264334939;
Cnbeta = 0.401521483934691;
Clbeta = -0.1347;
Cyp    = -0.000287755824147965;
Cnp    = -0.0479796877158797;
```

```
Clp=  -0.0105;
Cyr    =  0.869496571048604;
Cnr    = -0.3682;
Clr    = 0.2118;
Cydeltaa =   0;
Cndeltaa = -0.00238399695629669;
Cl135192662398883;
theata0  =0;
%calculations for long
Xu = - ( Cdu + 2 .* Cd0 ).* Q .* S ./( m .* U );
Xdeltae=-Q*S*CDdeltae/m;
XdeltaeP=Xdeltae;
Zu = - ( Clu + 2 .* Cl0) .* Q .* S ./( m .* U );
Zw = - ( Cla + 2 .* Cd0) .* Q .* S ./( m .* U );
Za = U .* Zw ;
Czq= -2 .* t .* Clat .* Vh ;
Zq = ( Czq .* Cbar .* Q .* S)./( 2 .* U .* m );
Mu = ( Cmu .* Q .* S .* Cbar )./( U .* Iy );
Mw = (Cma .* Q .* S .* Cbar )./( U .* Iy );
Ma = U .* Mw ;
Mq = ( Cmq .*  Q .* S .* Cbar .* Cbar )/( 2 .* U .* Iy
);
Xw = -( Cd0 - Cl0 ) .* Q .* S / ( m .* U );
Czaa = - 2 .* t .* Clat .* Vh .* down ;
Zww  = ( Czaa .* Q .* S .* Cbar) /( 2 .* U .* m .* U );
Zalphadot = U .* Zww ;
Czai = - Clai ;
Zdeltae = Czai .* Q .* S ./ m ;
Cmaa = - 2 .* t .* Clat .* Vh .* Lt .* down ./ Cbar ;
Mww = Cmaa .* Cbar .* Q .* S .* Cbar ./( 2 .* U .* U .*
Iy ) ;
Malphadot = U .* Mww ;
Mdeltae = Cmai .* Q .* S .* Cbar ./ Iy;
MdeltaeP=Mdeltae+Malphadot*Zdeltae/(U-Zalphadot);
ZdeltaeP=Zdeltae/(U-Zalphadot);
% calculate state space long.
Al = [ XuXw 0 -g ; ZuZw U 0 ; (Mu + Mww * Zu) (Mw + Mww
* Zw) (Mq + Mww * U ) 0 ; 0 0 1 0 ] ;
B = [XdeltaePZdeltaePMdeltaeP 0];
b=eig(Al);
% calculations for lateral directional
Ybeta = Q .* S .* Cybeta / m ;
Nbeta = Q .* S .* b .* Cnbeta / ( Iz ) ;
Lbeta = Q .* S .* b .* Clbeta / ( Ix ) ;
Yp = Q .* S .* b .* Cyp ./( 2 .* m .* U );
Np = Q .* S .* b .* b .* Cnp ./ ( 2 .* Iz .* U );
Lp = Q .* S .* b .* b .* Clp ./ ( 2 .* Ix .* U );
Yr = Q .* S .* b .* Cyr / ( 2 .* m .* U );
Nr = Q .* S .* b .* b .* Cnr / ( 2 .* Iz .* U );
Lr = Q .* S .* b .* b .* Clr / ( 2 .* Ix .* U );
Ydeltaa = Q .* S .* Cydeltaa / m ;
```

```
Ndeltaa = Q .* S .* b * Cndeltaa / Iz ;
Ldeltaa = Q .* S .* b * Cldeltaa / Ix ;
Ydeltar = Q .* S .* Cydeltaa / m ;
Ndeltar = Q .* S .* b * Cndeltar / Iz ;
Ldeltar = Q .* S .* b * Cldeltar / Ix ;
YB = Ybeta ./ U ;
YP = Yp ./ U ;
YR = 1 - ( Yr ./ U ) ;
G  = ( g .* cos(theata0)) ./ U ;
Yu = Ydeltar ./ U ;
% calculate state space lateral
A = [ YB YP -YR G ; LbetaLpLr 0 ; NbetaNp Nr 0 ; 0 1 0 0
] ;
B2 = [ 0 Yu ; LdeltaaLdeltar ; NdeltaaNdeltar ; 0 0 ] ;
B  = [YdeltaaYdeltar -Ybeta 0 1 ; LdeltaaLdeltar -Lbeta
-Lp -Lr ; NdeltaaNdeltar -Nbeta -Np -Nr ; 0 0 0 -1 0];
C = [1 0 0 0 0; 0 1 0 0 0; 0 0 1 0 0;0 0 0 1 0;0 0 0 0
1];
D = [0 0 0 0 0; 0 0 0 0 0; 0 0 0 0 0;0 0 0 0 0;0 0 0 0
0];
lambda = eig(A) ;
```

APPENDIX H: MATLAB CODE FOR PROPELLER DESIGN

```
a=0.1182;                                    % inflow factor
b=0.00013044;                                %inflow factor
b1=2;                                        % number of blades
vinf=47;                                     % inflow velocity
cl=1.1;                                      %lift cofficient
cd=0.075;                                    %drag cofficient
roh=1.225;                                   %air density
omga=1151.33;                                %angular velocity
dr=0.02925;                                    %propeller radius
suction
pi=3.1416;
r=0.2925;                                    %propeller radius
alpha=0.17453;                               %angle of attack
vo=vinf*(1+a);                               %airflow Velocity
v2=omga*r*(1-b);                             %outlet velocity
v1=sqrt(vo^2+v2^2);                           %resultant velocity
vector
phai=atan(vo/v2);                            %flow angle
theta=alpha+phai;                            %blade angle
lamdar=v2/vo;                                %Veolocity fraction
c=(8*pi*r*sin(phai))/(3*b1*lamdar);          %propeller chord
dt=0.5*roh*v1^2*c*(cl*cos(phai)-
cd*sin(phai))*b1*dr;%Element thrust
dq=0.5*roh*v1^2*c*(cl*sin(phai)-
cd*cos(phai))*b1*dr*r;%Element  torque
z=dt/(4*pi*roh*vinf^2*dr);%
x=[1 1 -z];
an=roots(x);                                 %new inflow factor
bn=dq/(4*pi*r^3*vinf^2*(1+a)*omga*dr);           %new    inflow
factor
```

APPENDIX I: PROPELLER BLADE SECTIONS CAD DRAWING

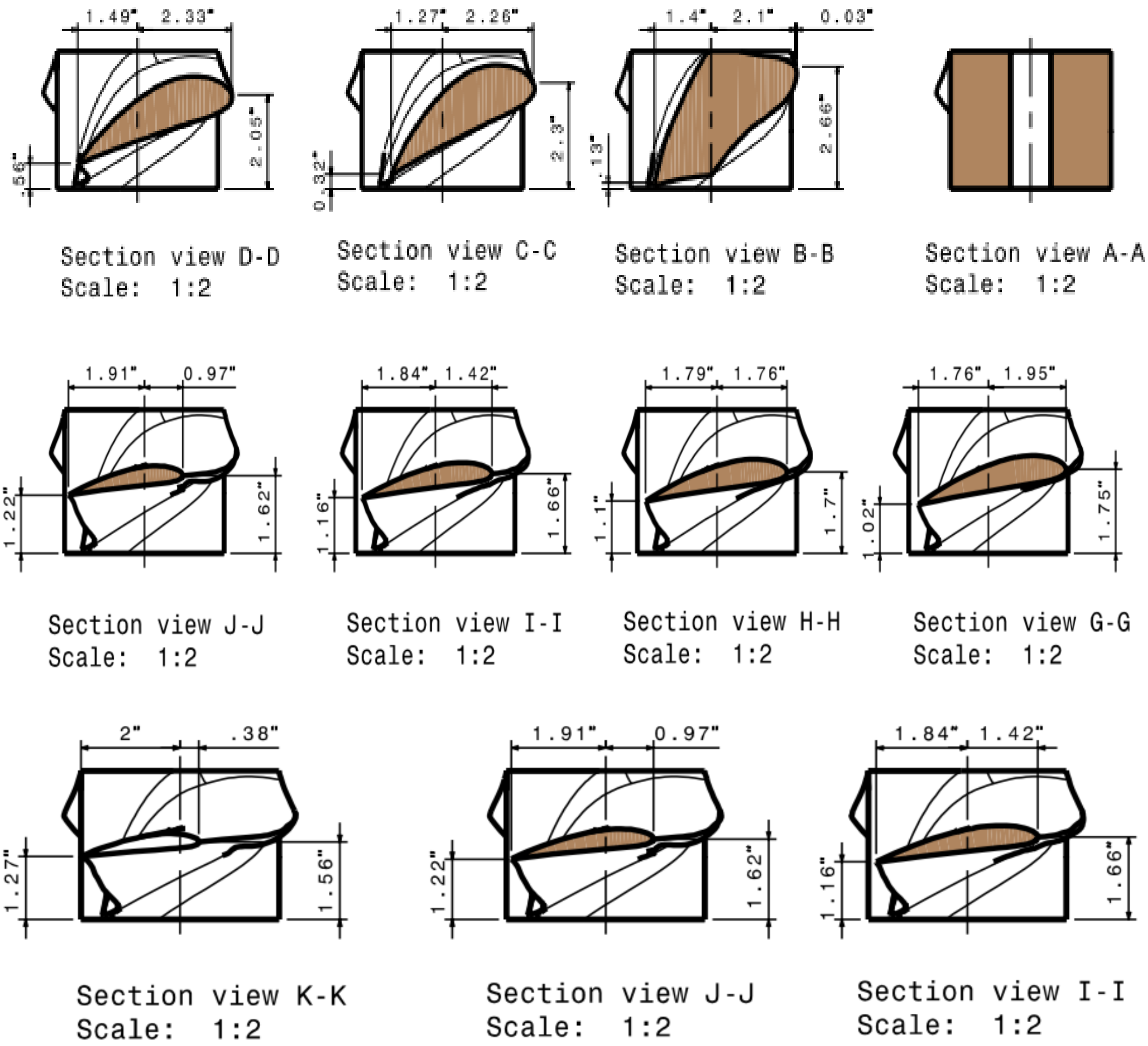

APPENDIX J: PROPELLER PROJECTED VIEWS

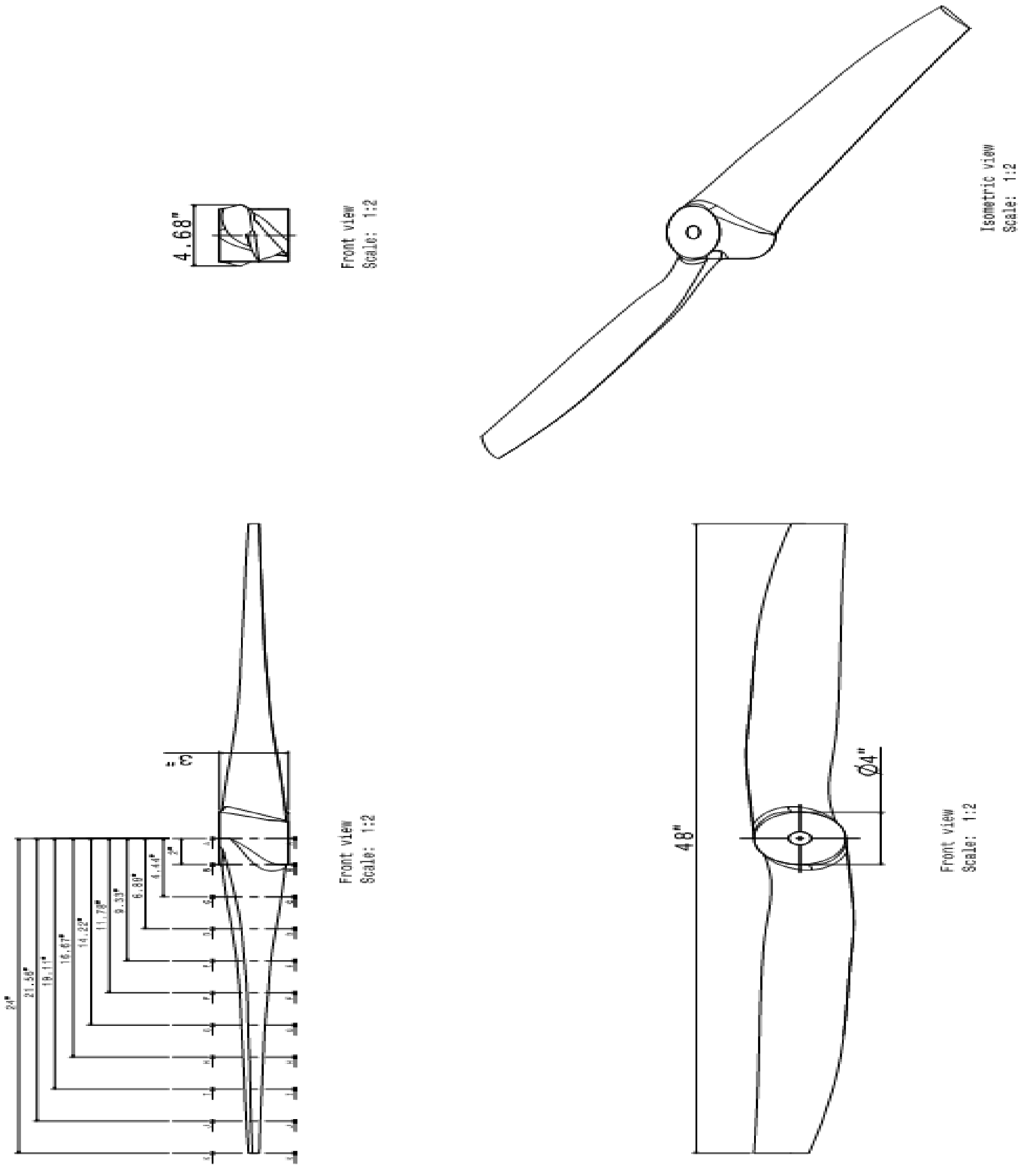

APPENDIX K: UAV CAD DRAWING

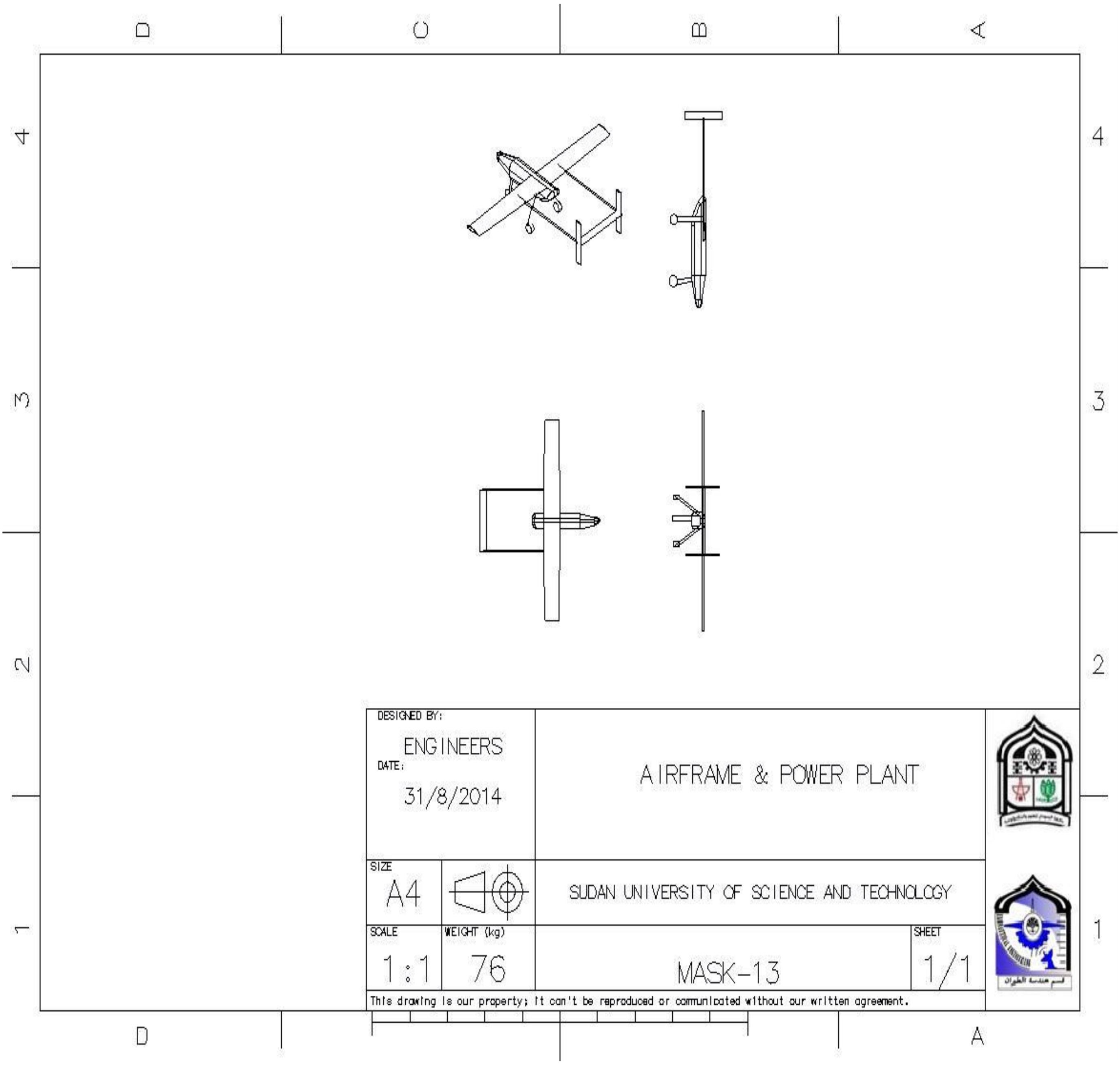

APPENDIX L: SNAP SHOT (DATCOM)

```

DIM FT
DAMP
DERIV RAD
PART
 $FLTCON NMACH=1.0, MACH(1)=0.138,
        NALT=1.0, ALT(1)=0.0,
        NALPHA=20.0,
        ALSCHD(1)= -8.0, -6.0, -4.0, -3.6550, -2.0, -1.0, 0.0, 1.0, 2.0, 3.0,
        4.0, 6.0, 8.0, 9.0,10.0, 12.0, 14.0, 16.0, 18.0, 19.0$
 $OPTINS SREF=14.80812952, CBARR=1.149461509, BLREF=12.9356818$

 $SYNTHS XCG=4.060148926,ZCG=0.0,
        XW=3.356177089,ZW=0.327580774,ALIW=0.51514,
        XH=9.789982219,ZH=0.327580774,ALIH=0.90,
        XV=9.789982219,ZV=-0.585897284$

 $BODY NX=9.0,
        X(1)=0.0,0.174,0.348,0.696,1.044,1.392,1.74,4.8,5.8,
        R(1)=0.0,0.217944947,0.3,0.4,0.458257569,0.489897949,0.5,0.5,0.3,
        ZU(1)=0.0,0.217944947,0.3,0.4,0.458257569,0.489897949,0.5,0.5,0.5,
        ZL(1)=0.0,-0.217944947,-0.3,-0.4,-0.458257569,-0.489897949,-0.5,-0.5,-0.1,
        ITYPE=1.0, METHOD=1.0$

NACA W 4 4415
NACA H 4 0012

 $WGPLNF CHRDR=1.271945113,CHRDTP=1.01755609,
        SSPN=6.31604247,SAVSI=2.941529472,
        SSPNE=6.467840899
        DHDADI=2.0$


```

```
           ZL(1)=0.0,-0.217944947,-0.3,-0.4,-0.458257569,-0.489897949,-0.5,-0.5,-0.1,
           ITYPE=1.0, METHOD=1.0$

NACA W 4 4415
NACA H 4 0012

 $WGPLNF CHRDR=1.271945113,CHRDTP=1.01755609,
         SSPN=6.31604247,SAVSI=2.941529472,
         SSPNE=6.467840899
         DHDADI=2.0$


 $HTPLNF CHRDTP=0.527950079,CHRDR=0.527950079,
         SSPNE=1.988611877,SSPN=1.988611877,
         TYPE=1.0$
 $SYMFLP FTYPE=1.0,
         NDELTA=9.0, DELTA(1)=-25.0,-15.0,-10.0,-5.0,0.0,5.0,10.0,16.0,25.0,
         CHRDFI=0.26397504,  CHRDFO=0.26397504,
         SPANFI=0.0,    SPANFO=0.39553347,
         NTYPE=1.0$
NACA V 4 0012

 $VTPLNF CHRDR=0.646710129,CHRDTP=0.646710129,
         SSPN=1.826956116,SSPNE=1.826956116,
         TYPE=1.0$


CASEID TOTAL: UAV
```

```
 CASEID TOTAL: TOTAL: UAV
0 INPUT DIMENSIONS ARE IN FT, SCALE FACTOR IS 1.0000

1                              AUTOMATED STABILITY AND CONTROL METHODS PER APRIL 1976 VERSION OF DATCOM
                                                          WING SECTION DEFINITION
                                                                  NACA 4415
     UPPER ABSCISSA     UPPER ORDINATE     LOWER ABSCISSA     LOWER ORDINATE      X-FRACTION CHORD    MEAN LINE    THICKNESS
          .00000             .00000             .00000             .00000              .00000          .00000       .00000
         -.00036             .00701             .00236            -.00661              .00100          .00020       .01389
          .00009             .00998             .00391            -.00918              .00200          .00040       .01954
          .00068             .01228             .00532            -.01108              .00300          .00060       .02382
          .00134             .01424             .00666            -.01264              .00400          .00080       .02740
          .00204             .01597             .00796            -.01398              .00500          .00099       .03053
          .00278             .01755             .00922            -.01517              .00600          .00119       .03334
          .00354             .01901             .01046            -.01623              .00700          .00139       .03591
          .00432             .02037             .01168            -.01720              .00800          .00158       .03829
          .00511             .02166             .01289            -.01810              .00900          .00178       .04051
          .00592             .02288             .01408            -.01893              .01000          .00198       .04259
          .01449             .03288             .02551            -.02508              .02000          .00390       .05899
          .02354             .04068             .03646            -.02913              .03000          .00577       .07100
          .03285             .04731             .04715            -.03211              .04000          .00760       .08069
          .04234             .05314             .05766            -.03439              .05000          .00937       .08887
          .05196             .05839             .06804            -.03619              .06000          .01110       .09594
          .06168             .06317             .07832            -.03762              .07000          .01277       .10216
          .07149             .06756             .08851            -.03876              .08000          .01440       .10768
          .08137             .07162             .09863            -.03967              .09000          .01597       .11262
          .09132             .07539             .10868            -.04039              .10000          .01750       .11707
          .10131             .07889             .11869            -.04094              .11000          .01897       .12108
          .11135             .08215             .12864            -.04135              .12000          .02040       .12470
          .12144             .08519             .13856            -.04164              .13000          .02177       .12798
          .13156             .08803             .14844            -.04183              .14000          .02310       .13095
          .14171             .09067             .15829            -.04192              .15000          .02437       .13363
          .15190             .09314             .16810            -.04194              .16000          .02560       .13605
          .16210             .09543             .17790            -.04188              .17000          .02677       .13822
```

```
          .88225          .03545          .87775          -.00665            .88000          .01440        .04235
          .90200          .03021          .89800          -.00576            .90000          .01222        .03619
          .92172          .02480          .91828          -.00489            .92000          .00996        .02989
          .94140          .01924          .93860          -.00404            .94000          .00760        .02345
          .96104          .01351          .95896          -.00320            .96000          .00516        .01684
          .98064          .00762          .97936          -.00238            .98000          .00262        .01008
         1.00000          .00000         1.00000           .00000           1.00000          .00000        .00000
1                            AUTOMATED STABILITY AND CONTROL METHODS PER APRIL 1976 VERSION OF DATCOM
                                                    WING SECTION DEFINITION
0                                IDEAL ANGLE OF ATTACK =    .51514 DEG.

                             ZERO LIFT ANGLE OF ATTACK =  -3.65530 DEG.

                                IDEAL LIFT COEFFICIENT =    .51204

                 ZERO LIFT PITCHING MOMENT COEFFICIENT =   -.10050

                            MACH ZERO LIFT-CURVE-SLOPE =    .09436 /DEG.

                                   LEADING EDGE RADIUS =    .02479 FRACTION CHORD

                             MAXIMUM AIRFOIL THICKNESS =    .15000 FRACTION CHORD

                                               DELTA-Y =   3.96122 PERCENT CHORD


0                         MACH=  .1380 LIFT-CURVE-SLOPE =    .09493 /DEG.      XAC =    .25883
1                            AUTOMATED STABILITY AND CONTROL METHODS PER APRIL 1976 VERSION OF DATCOM
                                                HORIZONTAL TAIL SECTION DEFINITION
                                                          NACA 0012
     UPPER ABSCISSA     UPPER ORDINATE     LOWER ABSCISSA     LOWER ORDINATE       X-FRACTION CHORD    MEAN LINE    THICKNESS
          .00000          .00000          .00000           .00000            .00000          .00000        .00000
          .00100          .00556          .00100          -.00556            .00100          .00000        .01111
          .00200          .00781          .00200          -.00781            .00200          .00000        .01563
```

```


0                         MACH=  .1380 LIFT-CURVE-SLOPE =    .09673 /DEG.      XAC =    .25862
1                             AUTOMATED STABILITY AND CONTROL METHODS PER APRIL 1976 VERSION OF DATCOM
                                       CHARACTERISTICS AT ANGLE OF ATTACK AND IN SIDESLIP
                                      WING-BODY-VERTICAL TAIL-HORIZONTAL TAIL CONFIGURATION
                                                     TOTAL: TOTAL: UAV

 ----------------------  FLIGHT CONDITIONS  ------------------------           --------------  REFERENCE DIMENSIONS  ------------
  MACH     ALTITUDE   VELOCITY    PRESSURE    TEMPERATURE     REYNOLDS              REF.      REFERENCE LENGTH   MOMENT REF. CENTER
 NUMBER                                                        NUMBER               AREA       LONG.     LAT.      HORIZ      VERT
             FT        FT/SEC     LB/FT**2      DEG R          1/FT                FT**2       FT        FT         FT         FT
0  .138        .00     154.05   2.1162E+03    518.670     9.7542E+05              14.808      1.149    12.936      4.060      .000
0                                                                   -------------------DERIVATIVE (PER RADIAN)-------------------
0 ALPHA     CD       CL       CM       CN       CA       XCP        CLA          CMA          CYB          CNB          CLB
0
   -8.0    .031    -.410    .1682   -.411    -.026    -.409    5.533E+00   -3.793E-01   -4.060E-01    5.872E-02   -2.631E-02
   -6.0    .026    -.219    .1368   -.220     .003    -.621    5.415E+00   -9.738E-01                             -3.185E-02
   -4.0    .024    -.032    .1002   -.034     .021   -2.957    5.292E+00   -1.054E+00                             -3.710E-02
   -3.7    .023     .000    .0939   -.002     .023   ******    5.302E+00   -1.043E+00                             -3.799E-02
   -2.0    .023     .155    .0654    .154     .029     .425    5.470E+00   -9.917E-01                             -4.240E-02
   -1.0    .024     .251    .0480    .251     .029     .191    5.564E+00   -9.820E-01                             -4.517E-02
     .0    .026     .349    .0312    .349     .026     .089    5.634E+00   -9.167E-01                             -4.802E-02
    1.0    .028     .448    .0160    .448     .020     .036    5.699E+00   -8.863E-01                             -5.094E-02
    2.0    .031     .548    .0002    .549     .012     .000    5.788E+00   -1.032E+00                             -5.392E-02
    3.0    .035     .650   -.0200    .651     .001    -.031    5.871E+00   -1.215E+00                             -5.695E-02
    4.0    .040     .753   -.0422    .754    -.013    -.056    5.917E+00   -1.280E+00                             -6.002E-02
    6.0    .051     .961   -.0874    .961    -.050    -.091    5.965E+00   -1.372E+00                             -6.627E-02
    8.0    .065    1.170   -.1380   1.167    -.098    -.118    5.354E+00   -1.605E+00                             -7.256E-02
    9.0    .072    1.257   -.1674   1.253    -.125    -.134    4.829E+00   -1.836E+00                             -7.495E-02
   10.0    .079    1.338   -.2021   1.332    -.154    -.152    4.438E+00   -2.071E+00                             -7.696E-02
   12.0    .094    1.480   -.2800   1.467    -.216    -.191    3.638E+00   -2.365E+00                             -8.005E-02
   14.0    .107    1.592   -.3672   1.571    -.282    -.234    2.506E+00   -2.628E+00                             -8.157E-02
   16.0    .117    1.655     NA     1.623    -.344     NA     -6.148E-01      NA                                   -8.072E-02
```

```
                                  14.0      1.000      4.416         .073
                                  16.0      1.000      4.462        -.107
                                  18.0      1.000      3.990        -.330
                                  19.0      1.000      3.613        -.377
0*** NA PRINTED WHEN METHOD NOT APPLICABLE
1                               AUTOMATED STABILITY AND CONTROL METHODS PER APRIL 1976 VERSION OF DATCOM
                                                   DYNAMIC DERIVATIVES
                                   WING-BODY-VERTICAL TAIL-HORIZONTAL TAIL CONFIGURATION
                                                   TOTAL: TOTAL: UAV

 ----------------------- FLIGHT CONDITIONS ------------------------           -------------- REFERENCE DIMENSIONS ------------
  MACH    ALTITUDE   VELOCITY    PRESSURE    TEMPERATURE     REYNOLDS             REF.      REFERENCE LENGTH    MOMENT REF. CENTER
 NUMBER                                                       NUMBER              AREA       LONG.     LAT.      HORIZ      VERT
             FT       FT/SEC     LB/FT**2      DEG R           1/FT               FT**2       FT        FT        FT         FT
0  .138        .00     154.05   2.1162E+03    518.670     9.7542E+05             14.808      1.149    12.936     4.060      .000
                                                  DYNAMIC DERIVATIVES (PER RADIAN)
0          -------PITCHING-------    -----ACCELERATION------    --------------ROLLING--------------    --------YAWING--------
0   ALPHA       CLQ          CMQ           CLAD         CMAD         CLP          CYP          CNP          CNR          CLR
0
    -8.00    6.671E+00   -3.305E+01    1.755E+00   -8.955E+00   -4.878E-01   -7.918E-02    4.803E-02   -8.393E-02   -7.485E-02
    -6.00                              1.754E+00   -8.954E+00   -4.703E-01   -6.975E-02    2.575E-02   -8.358E-02   -2.940E-02
    -4.00                              1.768E+00   -9.024E+00   -4.581E-01   -6.040E-02    4.067E-03   -8.401E-02    1.435E-02
    -3.65                              1.780E+00   -9.083E+00   -4.594E-01   -5.879E-02    3.490E-04   -8.416E-02    2.183E-02
    -2.00                              1.824E+00   -9.310E+00   -4.766E-01   -5.099E-02   -1.787E-02   -8.517E-02    5.859E-02
    -1.00                              1.822E+00   -9.297E+00   -4.860E-01   -4.622E-02   -2.916E-02   -8.604E-02    8.148E-02
      .00                              1.784E+00   -9.104E+00   -4.946E-01   -4.142E-02   -4.064E-02   -8.713E-02    1.048E-01
     1.00                              1.741E+00   -8.884E+00   -5.024E-01   -3.659E-02   -5.228E-02   -8.844E-02    1.285E-01
     2.00                              1.739E+00   -8.878E+00   -5.091E-01   -3.173E-02   -6.406E-02   -8.999E-02    1.526E-01
     3.00                              1.779E+00   -9.082E+00   -5.149E-01   -2.685E-02   -7.596E-02   -9.179E-02    1.770E-01
     4.00                              1.794E+00   -9.155E+00   -5.196E-01   -2.196E-02   -8.795E-02   -9.383E-02    2.016E-01
     6.00                              1.724E+00   -8.800E+00   -5.259E-01   -1.214E-02   -1.121E-01   -9.866E-02    2.512E-01
     8.00                              1.620E+00   -8.266E+00   -4.694E-01   -2.306E-03   -1.367E-01   -1.045E-01    3.012E-01
     9.00                              1.407E+00   -7.179E+00   -4.184E-01    2.304E-03   -1.472E-01   -1.071E-01    3.216E-01
    10.00                              1.141E+00   -5.824E+00   -3.777E-01    6.756E-03   -1.567E-01   -1.096E-01    3.397E-01
```

```
 THIS SOFTWARE AND ANY ACCOMPANYING DOCUMENTATION
 IS RELEASED "AS IS".  THE U.S. GOVERNMENT MAKES NO
 WARRANTY OF ANY KIND, EXPRESS OR IMPLIED, CONCERNING
 THIS SOFTWARE AND ANY ACCOMPANYING DOCUMENTATION,
 INCLUDING, WITHOUT LIMITATION, ANY WARRANTIES OF
 MERCHANTABILITY OR FITNESS FOR A PARTICULAR PURPOSE.
 IN NO EVENT WILL THE U.S. GOVERNMENT BE LIABLE FOR ANY
 DAMAGES, INCLUDING LOST PROFITS, LOST SAVINGS OR OTHER
 INCIDENTAL OR CONSEQUENTIAL DAMAGES ARISING OUT OF THE
 USE, OR INABILITY TO USE, THIS SOFTWARE OR ANY
 ACCOMPANYING DOCUMENTATION, EVEN IF INFORMED IN ADVANCE
 OF THE POSSIBILITY OF SUCH DAMAGES.








                                    ****************************************************
                                    *    USAF STABILITY AND CONTROL  DIGITAL DATCOM    *
                                    *    PROGRAM REV. JAN 96   DIRECT INQUIRIES TO:    *
                                    *   WRIGHT LABORATORY  (WL/FIGC)  ATTN: W. BLAKE   *
                                    *         WRIGHT PATTERSON AFB, OHIO  45433        *
                                    *    PHONE (513) 255-6764,   FAX (513) 258-4054    *
                                    ****************************************************
1                         CONERR - INPUT ERROR CHECKING
0 ERROR CODES - N* DENOTES THE NUMBER OF OCCURENCES OF EACH ERROR
0 A - UNKNOWN VARIABLE NAME
0 B - MISSING EQUAL SIGN FOLLOWING VARIABLE NAME
0 C - NON-ARRAY VARIABLE HAS AN ARRAY ELEMENT DESIGNATION - (N)
0 D - NON-ARRAY VARIABLE HAS MULTIPLE VALUES ASSIGNED
0 E - ASSIGNED VALUES EXCEED ARRAY DIMENSION
```

APPENDIX M: SNAP SHOT (AAA)

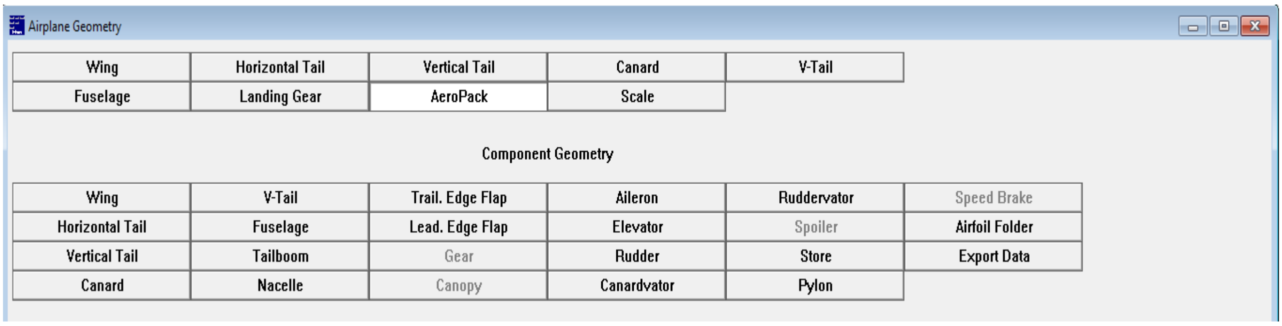

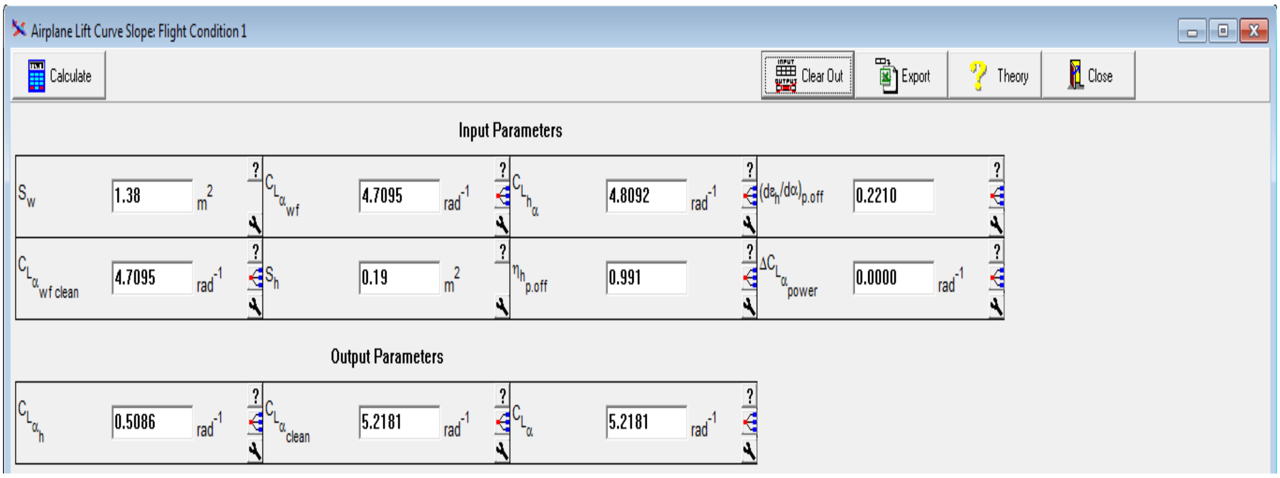

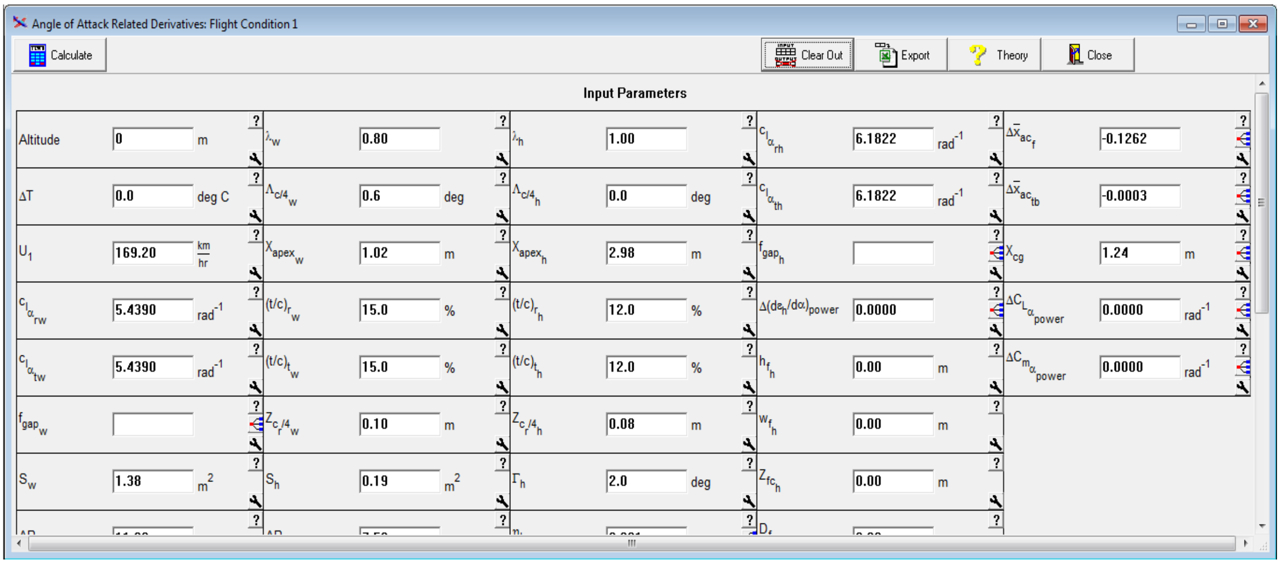

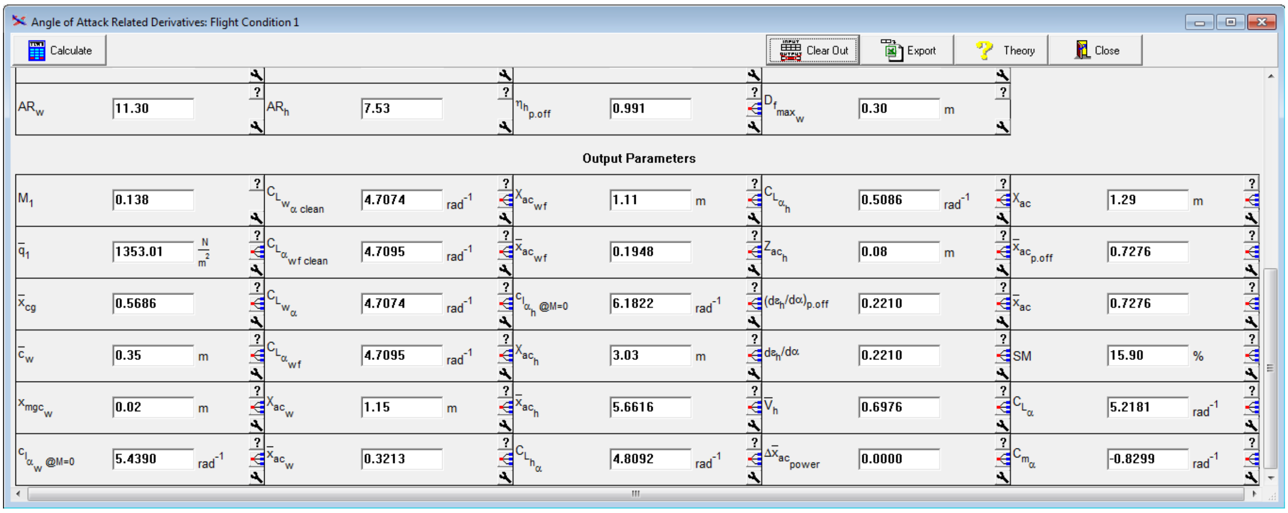

Angle of Attack Related Derivatives: Flight Condition 1
Calculate
Clear Out
Export
Theory
Close
ARw 11.30
ARh 7.53
ηh p.off 0.991
Dfmax w 0.30 m
Output Parameters
M1 0.138
q1 1353.01 N/m2
xcg 0.5686
cw 0.35 m
xmgc w 0.02 m
clα w @M=0 5.4390 rad-1
CLwα clean 4.7074 rad-1
CLα wf clean 4.7095 rad-1
CLwα 4.7074 rad-1
CLα wf 4.7095 rad-1
Xac w 1.15 m
xac w 0.3213
Xac wf 1.11 m
xac wf 0.1948
clα h @M=0 6.1822 rad-1
Xac h 3.03 m
xac h 5.6616
CLhα 4.8092 rad-1
CLαh 0.5086 rad-1
Zac h 0.08 m
(dεh/dα)p.off 0.2210
dεh/dα 0.2210
Vh 0.6976
Δxac power 0.0000
Xac 1.29 m
xac p.off 0.7276
xac 0.7276
SM 15.90 %
CLα 5.2181 rad-1
Cmα -0.8299 rad-1

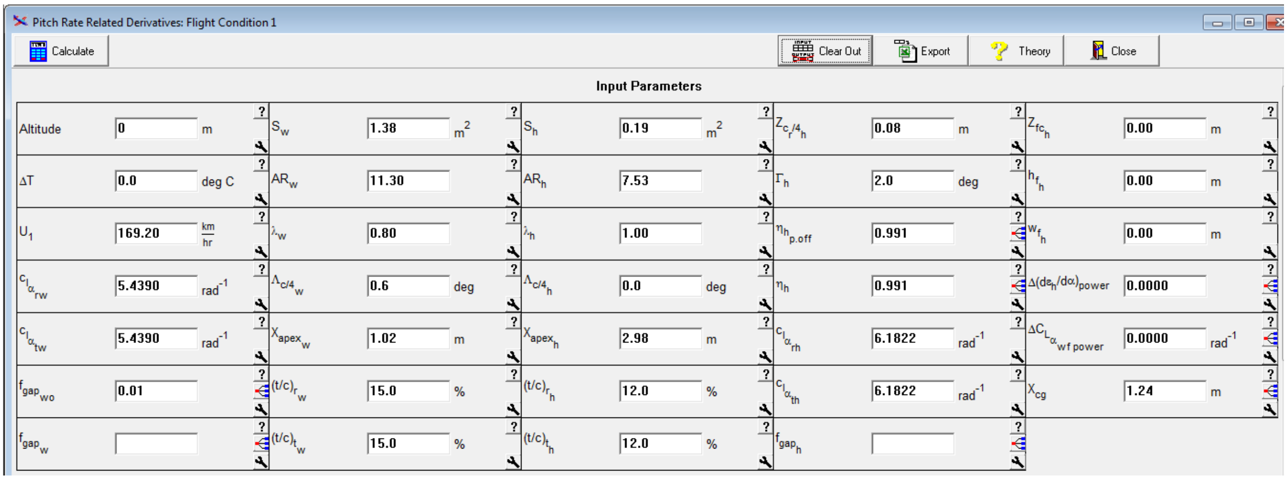

Pitch Rate Related Derivatives: Flight Condition 1
Calculate
Clear Out
Export
Theory
Close
Input Parameters
Altitude 0 m
ΔT 0.0 deg C
U1 169.20 km/hr
clα rw 5.4390 rad-1
clα tw 5.4390 rad-1
fgap wo 0.01
fgap w
Sw 1.38 m2
ARw 11.30
λw 0.80
Λc/4 w 0.6 deg
Xapex w 1.02 m
(t/c)r w 15.0 %
(t/c)t w 15.0 %
Sh 0.19 m2
ARh 7.53
λh 1.00
Λc/4 h 0.0 deg
Xapex h 2.98 m
(t/c)r h 12.0 %
(t/c)t h 12.0 %
Zcr/4 h 0.08 m
Γh 2.0 deg
ηh p.off 0.991
ηh 0.991
clα rh 6.1822 rad-1
clα th 6.1822 rad-1
fgap h
Zfc h 0.00 m
hf h 0.00 m
wf h 0.00 m
Δ(dεh/dα)power 0.0000
ΔCLα wf power 0.0000 rad-1
Xcg 1.24 m

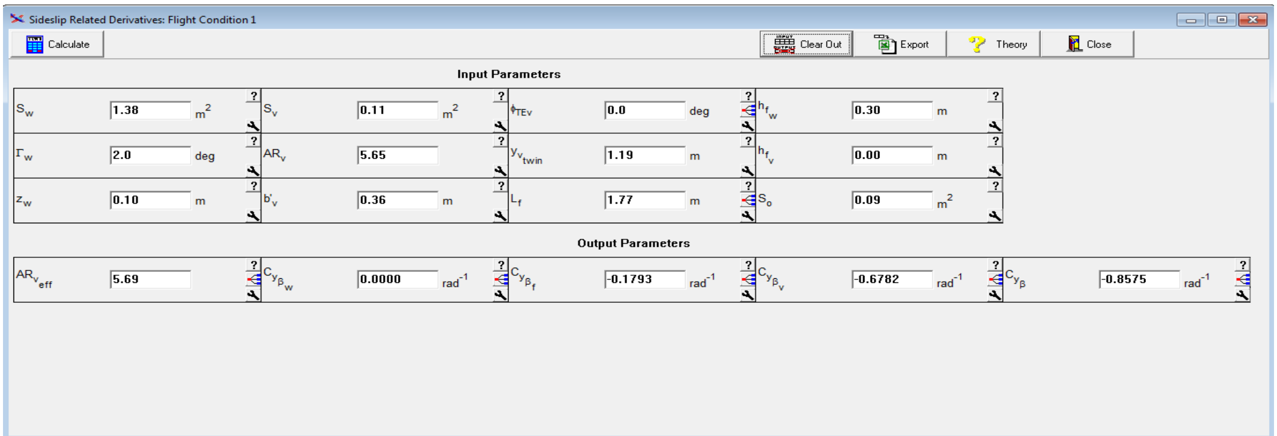

Sideslip Related Derivatives: Flight Condition 1
Calculate
Clear Out
Export
Theory
Close
Input Parameters
Sw 1.38 m2
Γw 2.0 deg
zw 0.10 m
Sv 0.11 m2
ARv 5.65
b'v 0.36 m
φTEv 0.0 deg
yv twin 1.19 m
Lf 1.77 m
hf w 0.30 m
hf v 0.00 m
So 0.09 m2
Output Parameters
ARv eff 5.69
Cyβ w 0.0000 rad-1
Cyβ f -0.1793 rad-1
Cyβ v -0.6782 rad-1
Cyβ -0.8575 rad-1

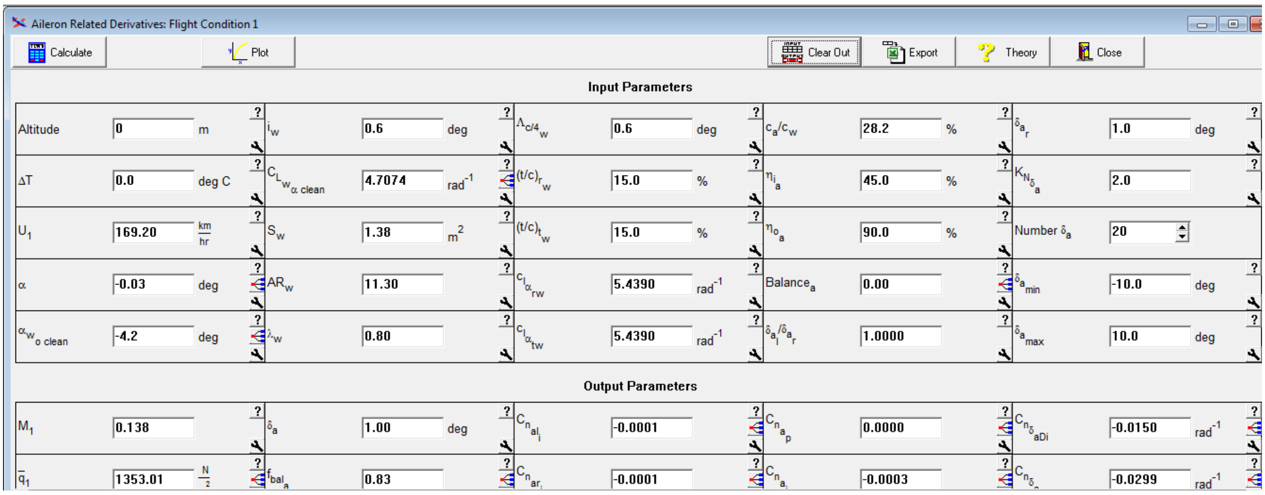

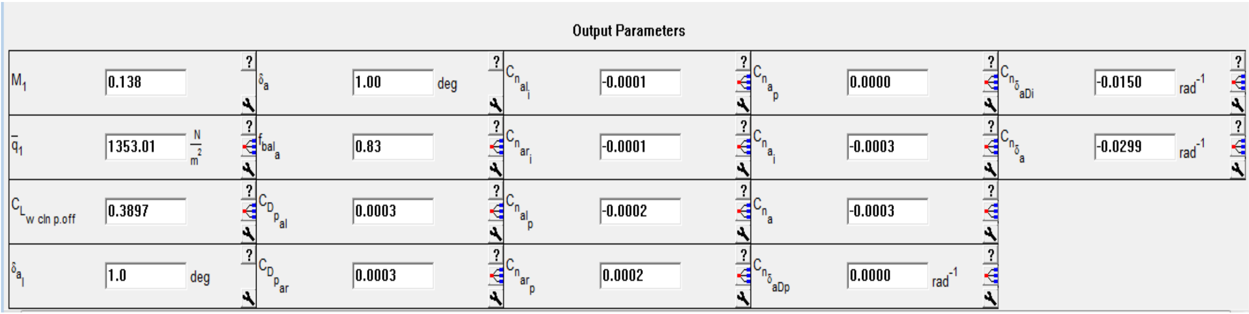

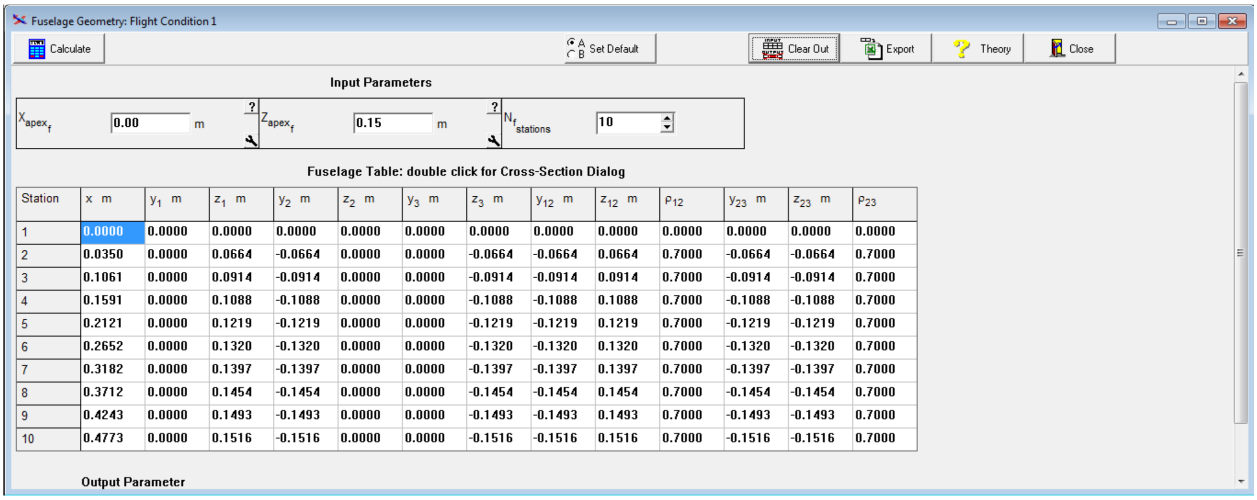

Station	x m	y_1 m	z_1 m	y_2 m	z_2 m	y_3 m	z_3 m	y_{12} m	z_{12} m	ρ_{12}	y_{23} m	z_{23} m	ρ_{23}
1	0.0000	0.0000	0.0000	0.0000	0.0000	0.0000	0.0000	0.0000	0.0000	0.0000	0.0000	0.0000	0.0000
2	0.0350	0.0000	0.0664	-0.0664	0.0000	0.0000	-0.0664	-0.0664	0.0664	0.7000	-0.0664	-0.0664	0.7000
3	0.1061	0.0000	0.0914	-0.0914	0.0000	0.0000	-0.0914	-0.0914	0.0914	0.7000	-0.0914	-0.0914	0.7000
4	0.1591	0.0000	0.1088	-0.1088	0.0000	0.0000	-0.1088	-0.1088	0.1088	0.7000	-0.1088	-0.1088	0.7000
5	0.2121	0.0000	0.1219	-0.1219	0.0000	0.0000	-0.1219	-0.1219	0.1219	0.7000	-0.1219	-0.1219	0.7000
6	0.2652	0.0000	0.1320	-0.1320	0.0000	0.0000	-0.1320	-0.1320	0.1320	0.7000	-0.1320	-0.1320	0.7000
7	0.3182	0.0000	0.1397	-0.1397	0.0000	0.0000	-0.1397	-0.1397	0.1397	0.7000	-0.1397	-0.1397	0.7000
8	0.3712	0.0000	0.1454	-0.1454	0.0000	0.0000	-0.1454	-0.1454	0.1454	0.7000	-0.1454	-0.1454	0.7000
9	0.4243	0.0000	0.1493	-0.1493	0.0000	0.0000	-0.1493	-0.1493	0.1493	0.7000	-0.1493	-0.1493	0.7000
10	0.4773	0.0000	0.1516	-0.1516	0.0000	0.0000	-0.1516	-0.1516	0.1516	0.7000	-0.1516	-0.1516	0.7000

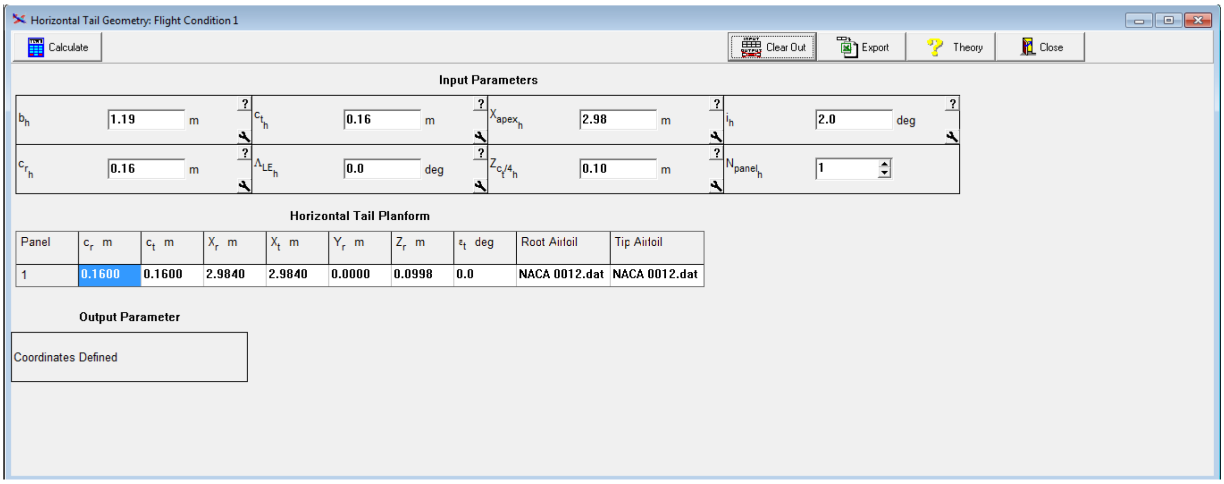

Horizontal Tail Geometry: Flight Condition 1

Calculate | Clear Out | Export | Theory | Close

Input Parameters

b_h	1.19 m	c_{t_h}	0.16 m	X_{apex_h}	2.98 m	i_h	2.0 deg
c_{r_h}	0.16 m	Λ_{LE_h}	0.0 deg	$Z_{c/4_h}$	0.10 m	N_{panel_h}	1

Horizontal Tail Planform

Panel	c_r m	c_t m	X_r m	X_t m	Y_r m	Z_r m	ε_t deg	Root Airfoil	Tip Airfoil
1	0.1600	0.1600	2.9840	2.9840	0.0000	0.0998	0.0	NACA 0012.dat	NACA 0012.dat

Output Parameter

Coordinates Defined

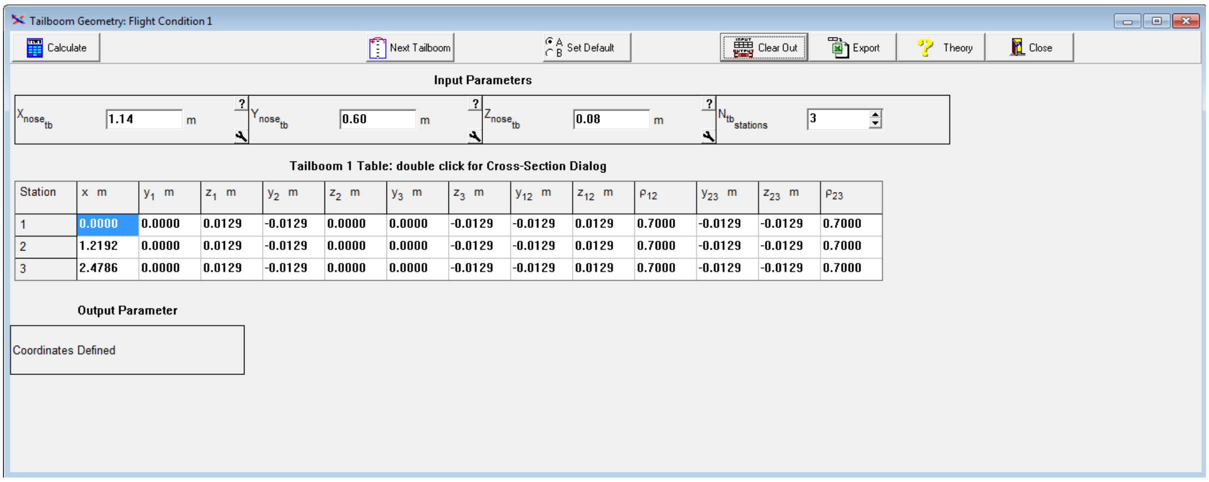

Tailboom Geometry: Flight Condition 1

Calculate | Next Tailboom | Set Default | Clear Out | Export | Theory | Close

Input Parameters

$X_{nose_{tb}}$	1.14 m	$Y_{nose_{tb}}$	0.60 m	$Z_{nose_{tb}}$	0.08 m	$N_{tb_{stations}}$	3

Tailboom 1 Table: double click for Cross-Section Dialog

Station	x m	y_1 m	z_1 m	y_2 m	z_2 m	y_3 m	z_3 m	y_{12} m	z_{12} m	ρ_{12}	y_{23} m	z_{23} m	ρ_{23}
1	0.0000	0.0000	0.0129	-0.0129	0.0000	0.0000	-0.0129	-0.0129	0.0129	0.7000	-0.0129	-0.0129	0.7000
2	1.2192	0.0000	0.0129	-0.0129	0.0000	0.0000	-0.0129	-0.0129	0.0129	0.7000	-0.0129	-0.0129	0.7000
3	2.4786	0.0000	0.0129	-0.0129	0.0000	0.0000	-0.0129	-0.0129	0.0129	0.7000	-0.0129	-0.0129	0.7000

Output Parameter

Coordinates Defined

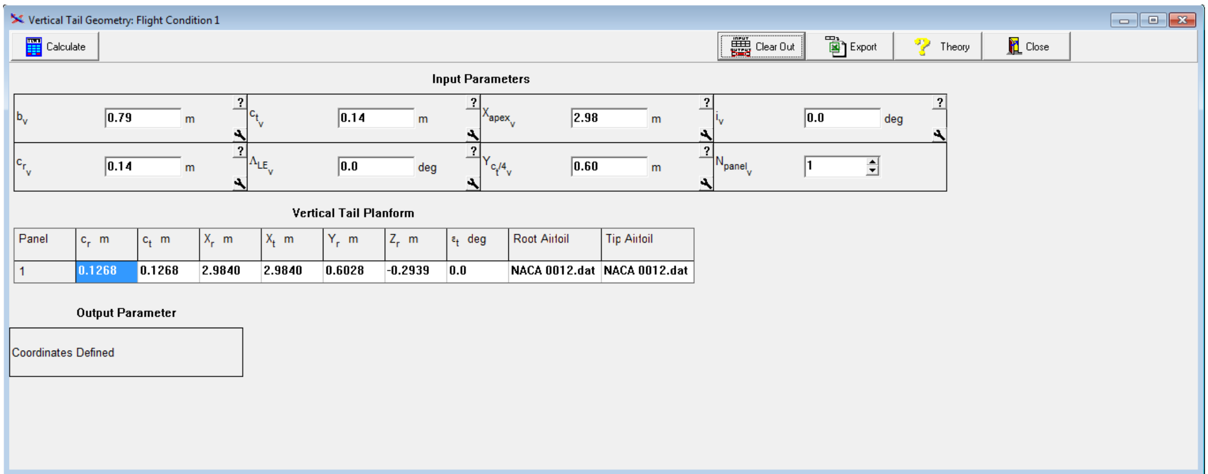

Vertical Tail Geometry: Flight Condition 1

Calculate | Clear Out | Export | Theory | Close

Input Parameters

b_v	0.79 m	c_{t_v}	0.14 m	X_{apex_v}	2.98 m	i_v	0.0 deg
c_{r_v}	0.14 m	Λ_{LE_v}	0.0 deg	$Y_{c/4_v}$	0.60 m	N_{panel_v}	1

Vertical Tail Planform

Panel	c_r m	c_t m	X_r m	X_t m	Y_r m	Z_r m	ε_t deg	Root Airfoil	Tip Airfoil
1	0.1268	0.1268	2.9840	2.9840	0.6028	-0.2939	0.0	NACA 0012.dat	NACA 0012.dat

Output Parameter

Coordinates Defined

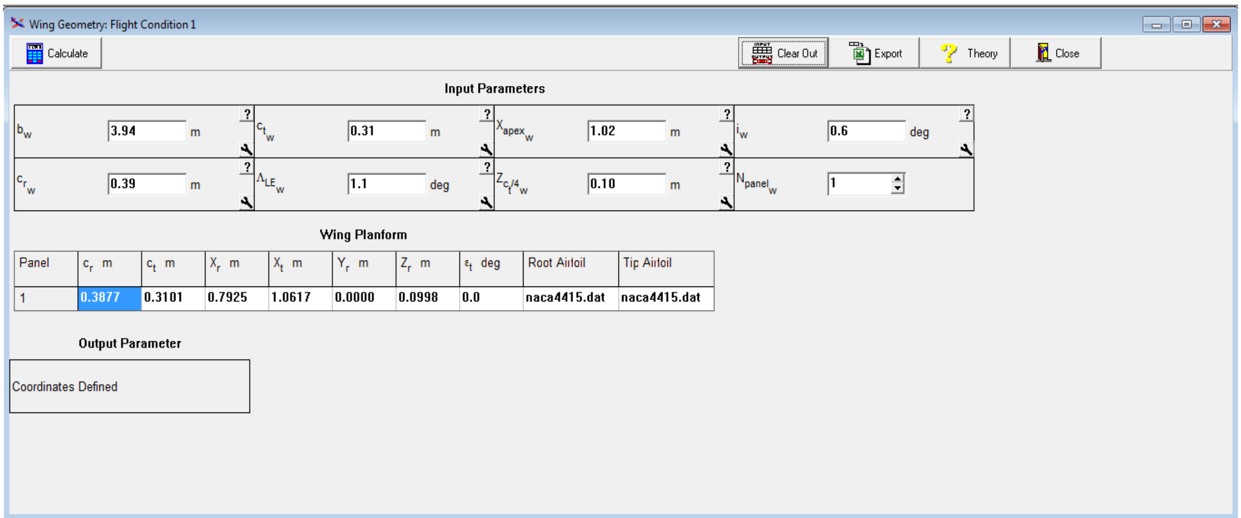
Wing Geometry: Flight Condition 1
Calculate
Clear Out
Export
Theory
Close
Input Parameters
b w 3.94 m
c t w 0.31 m
X apex w 1.02 m
i w 0.6 deg
c r w 0.39 m
Λ LE w 1.1 deg
Z c t/4 w 0.10 m
N panel w 1
Wing Planform
Panel
c r m
c t m
X r m
X t m
Y r m
Z r m
ε t deg
Root Airfoil
Tip Airfoil
1
0.3877
0.3101
0.7925
1.0617
0.0000
0.0998
0.0
naca4415.dat
naca4415.dat
Output Parameter
Coordinates Defined

APPENDIX N: JAVAFOIL PROGRAM OUUTPUT

- Design card after a design has been performed.

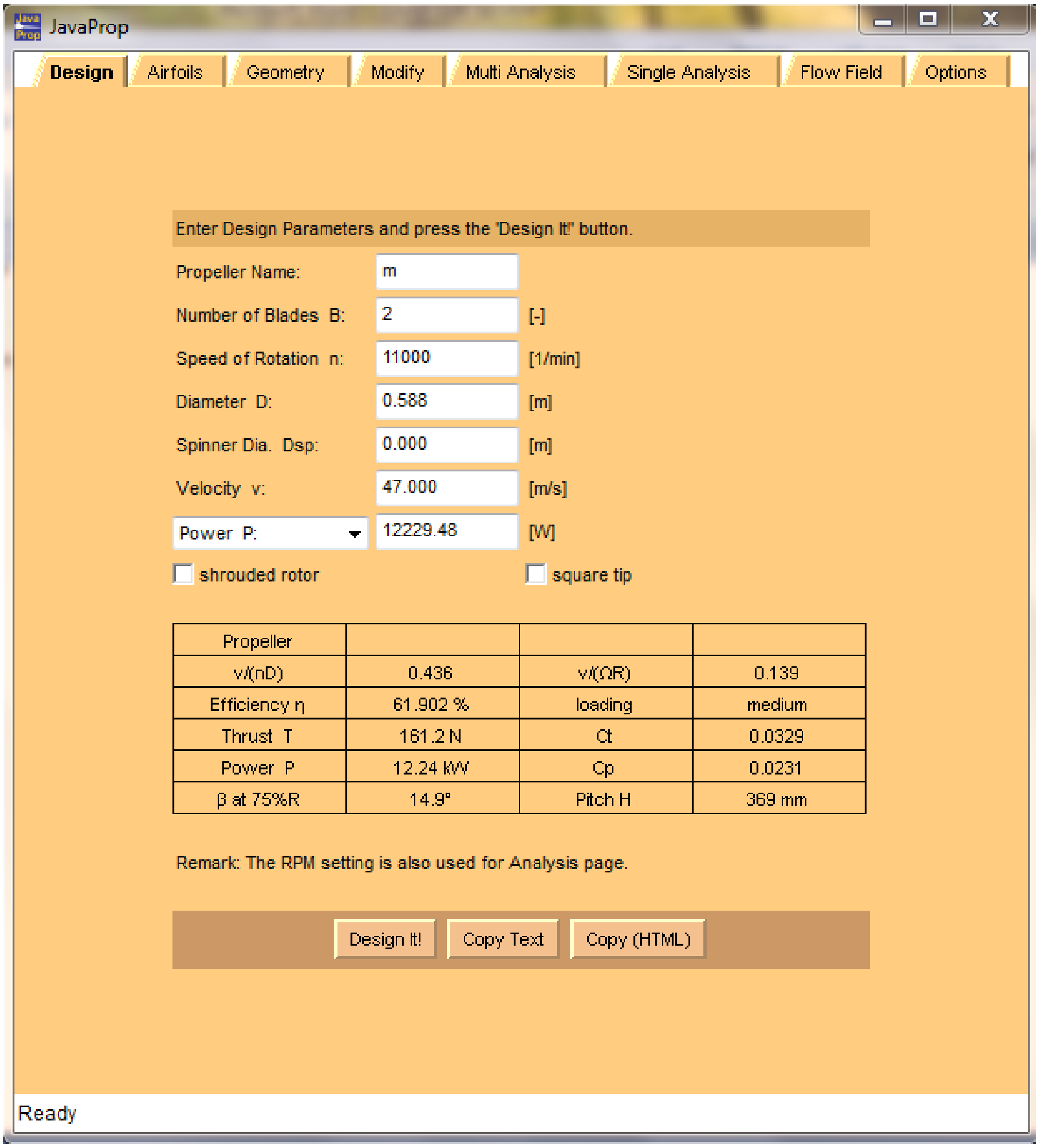

- Airfoils card with four design sections and a graph of the lift and drag coefficients Versus angle of attack

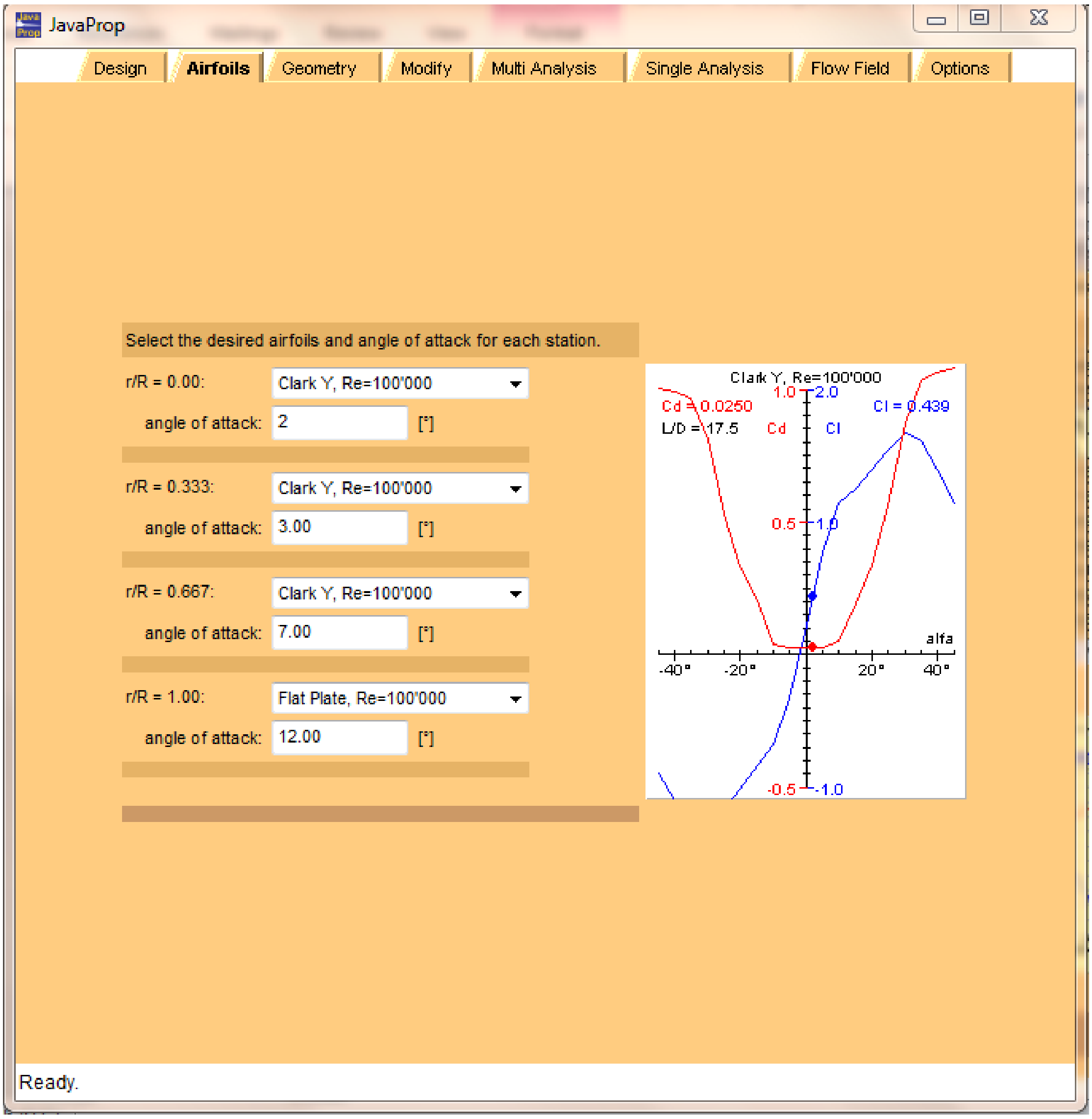

- Geometry card with current propeller.

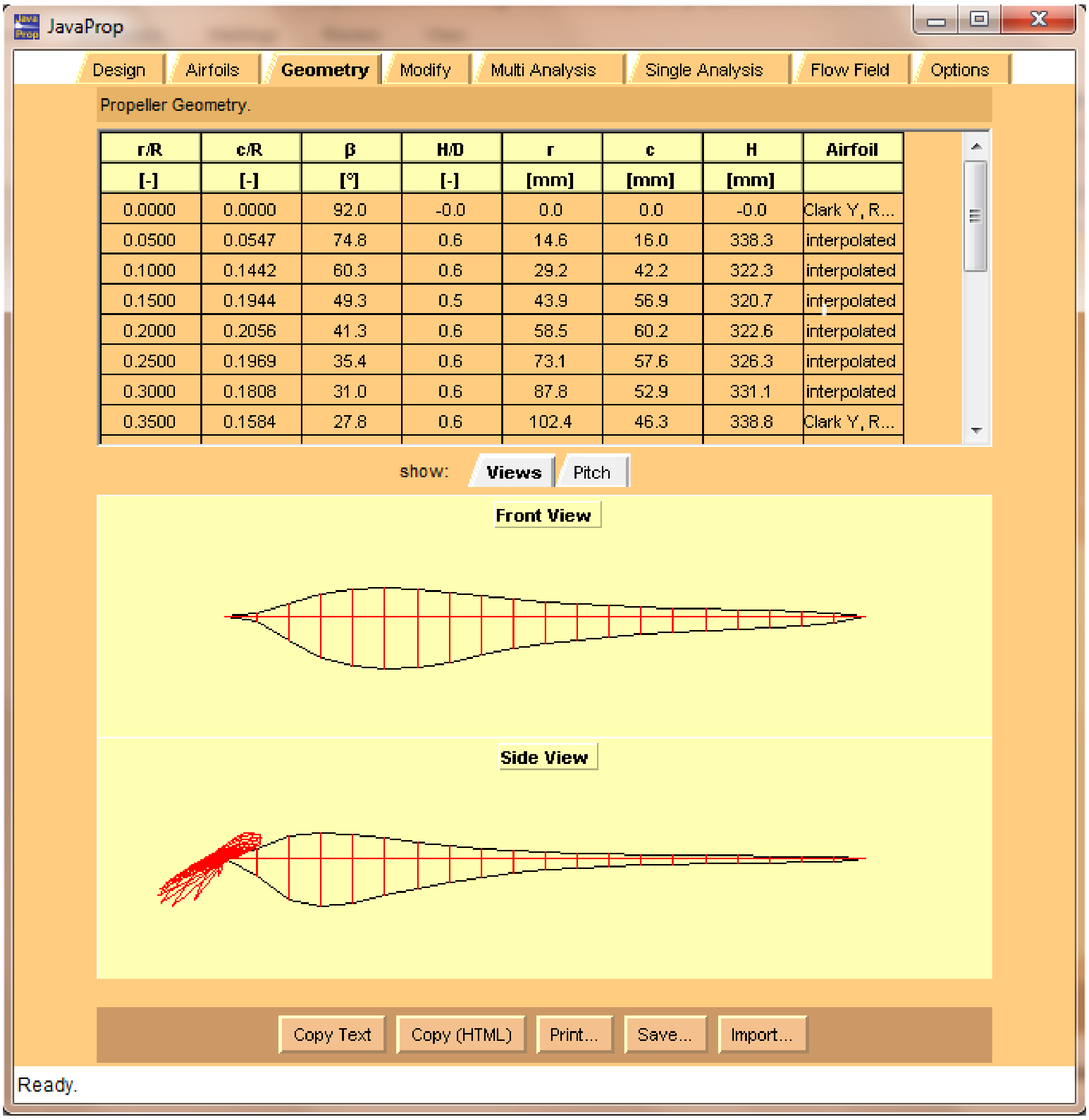

- Propeller pitch distribution

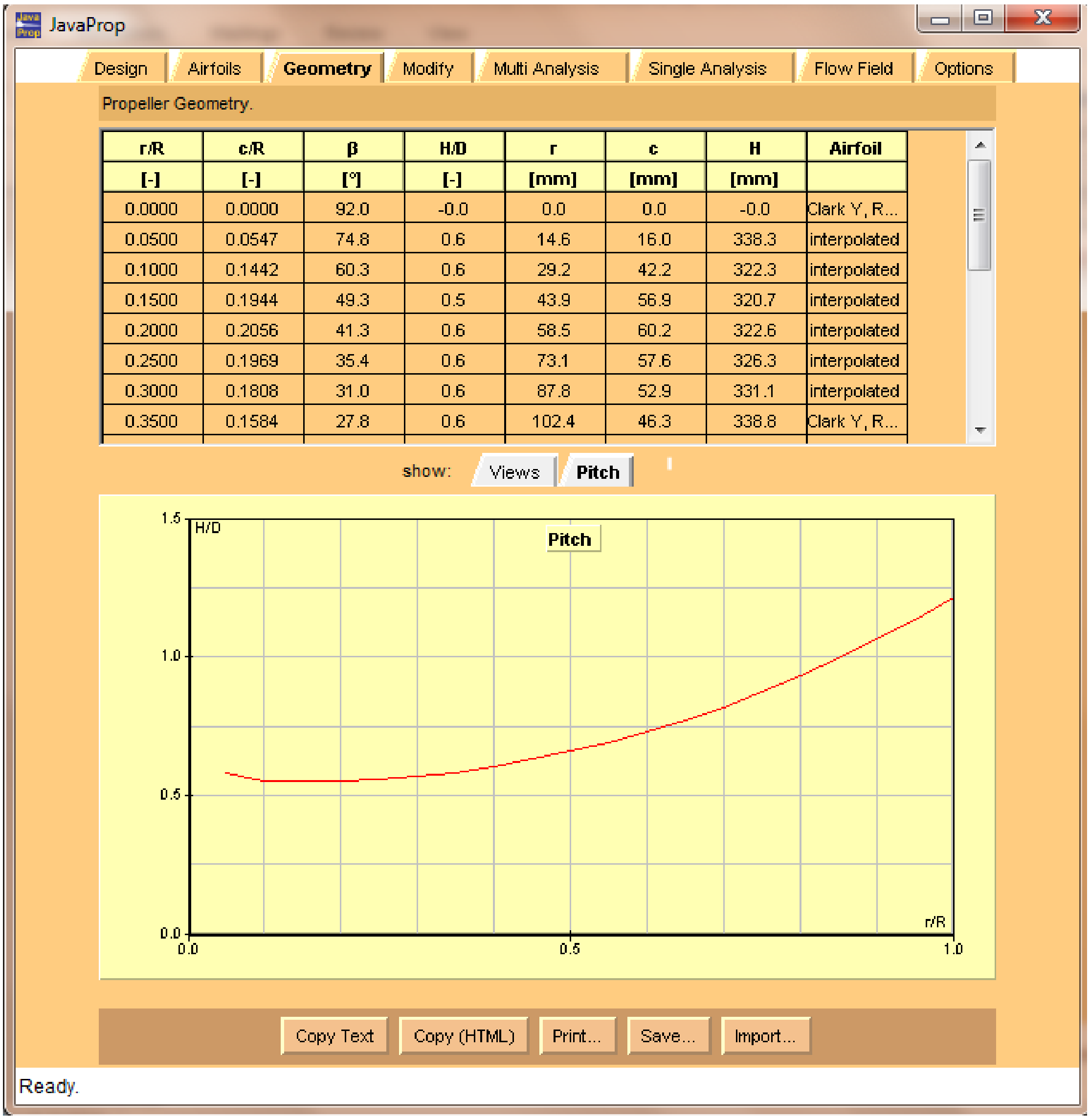

- The Multi-Analysis card produces global propeller coefficients over a range of Operating conditions.

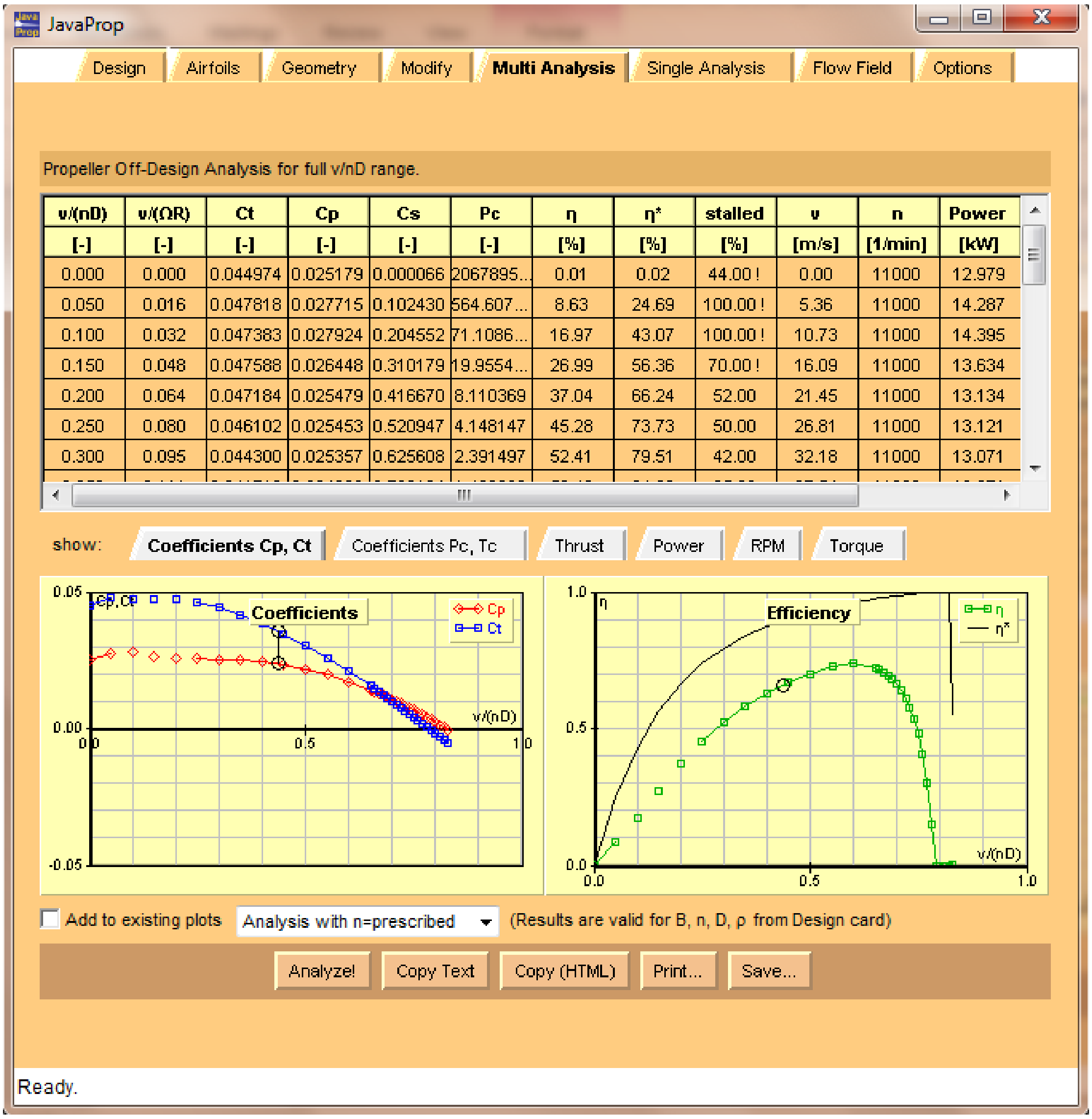

v/(nD)	v/(ΩR)	Ct	Cp	Cs	Pc	η	η*	stalled	v	n	Power
[-]	[-]	[-]	[-]	[-]	[-]	[%]	[%]	[%]	[m/s]	[1/min]	[kW]
0.000	0.000	0.044974	0.025179	0.000066	2067895...	0.01	0.02	44.00 !	0.00	11000	12.979
0.050	0.016	0.047818	0.027715	0.102430	564.607...	8.63	24.69	100.00 !	5.36	11000	14.287
0.100	0.032	0.047383	0.027924	0.204552	71.1086...	16.97	43.07	100.00 !	10.73	11000	14.395
0.150	0.048	0.047588	0.026448	0.310179	19.9554...	26.99	56.36	70.00 !	16.09	11000	13.634
0.200	0.064	0.047184	0.025479	0.416670	8.110369	37.04	66.24	52.00	21.45	11000	13.134
0.250	0.080	0.046102	0.025453	0.520947	4.148147	45.28	73.73	50.00	26.81	11000	13.121
0.300	0.095	0.044300	0.025357	0.625608	2.391497	52.41	79.51	42.00	32.18	11000	13.071

- The individual graphs on the Multi-Analysis card present thrust, power, RPM and Torque versus flight speed for the selected operating mode (in this case RPM=constant).

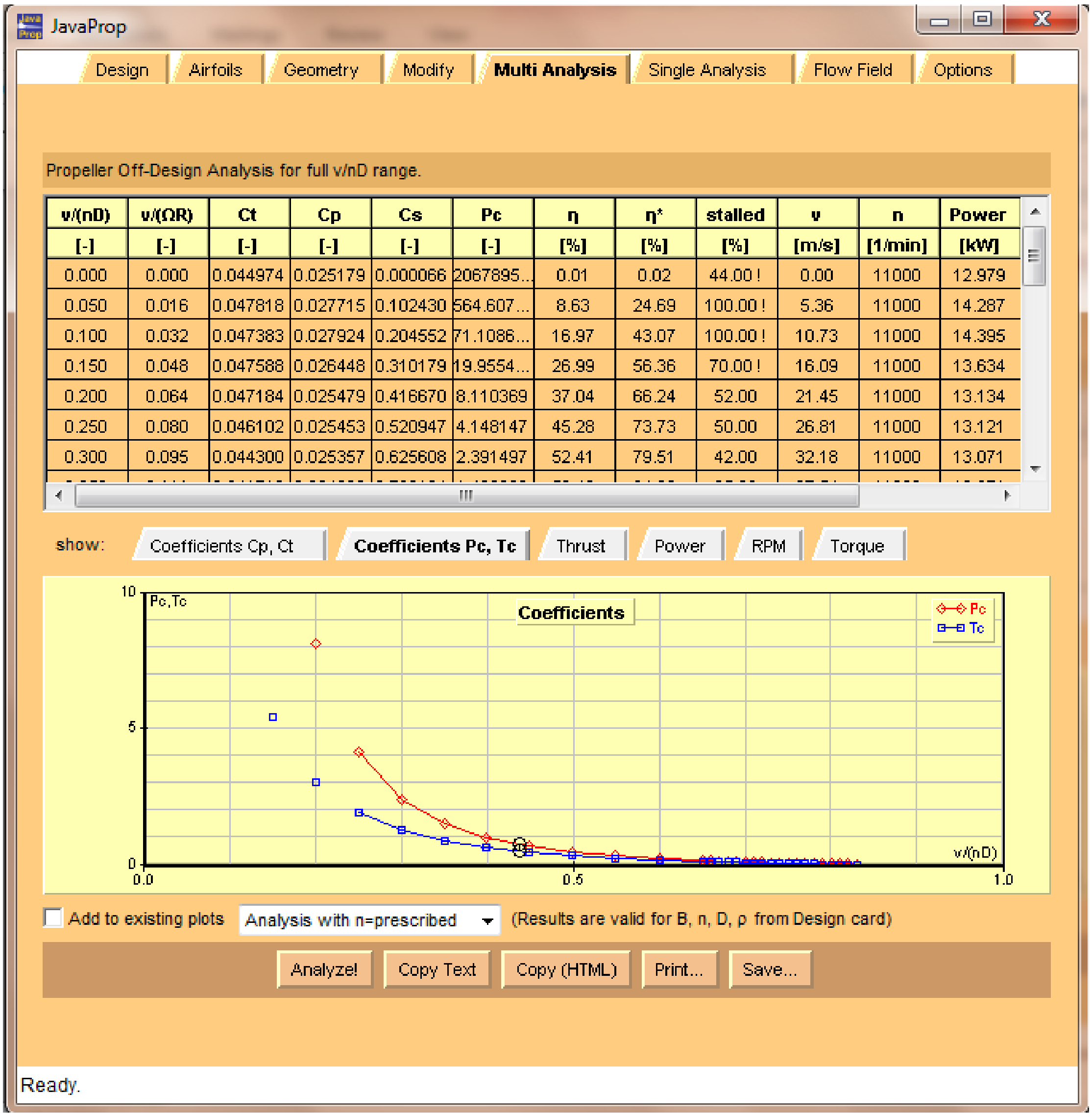

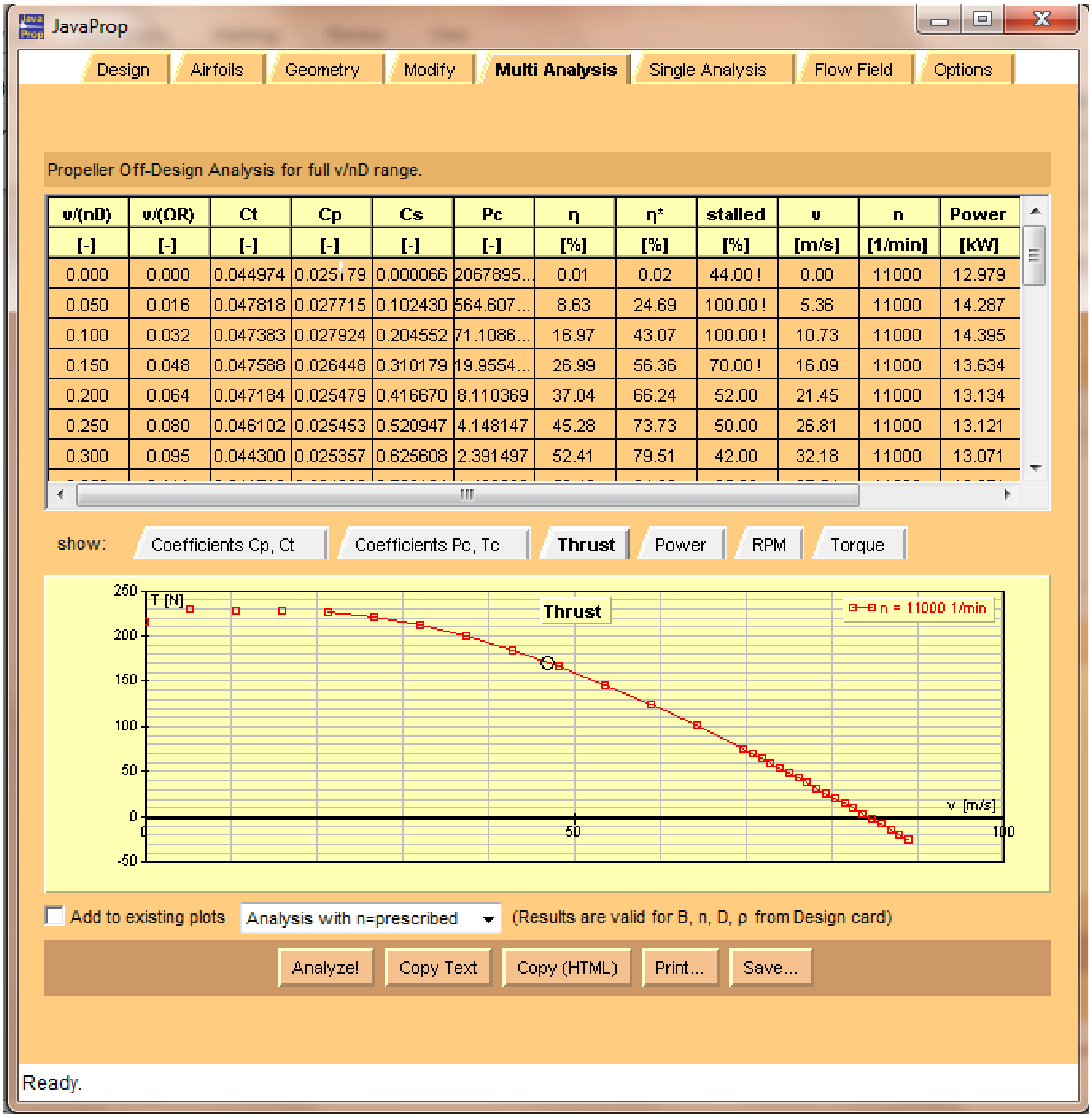

v/(nD)	v/(ΩR)	Ct	Cp	Cs	Pc	η	η*	stalled	v	n	Power
[-]	[-]	[-]	[-]	[-]	[-]	[%]	[%]	[%]	[m/s]	[1/min]	[kW]
0.000	0.000	0.044974	0.025179	0.000066	2067895...	0.01	0.02	44.00 !	0.00	11000	12.979
0.050	0.016	0.047818	0.027715	0.102430	564.607...	8.63	24.69	100.00 !	5.36	11000	14.287
0.100	0.032	0.047383	0.027924	0.204552	71.1086...	16.97	43.07	100.00 !	10.73	11000	14.395
0.150	0.048	0.047588	0.026448	0.310179	19.9554...	26.99	56.36	70.00 !	16.09	11000	13.634
0.200	0.064	0.047184	0.025479	0.416670	8.110369	37.04	66.24	52.00	21.45	11000	13.134
0.250	0.080	0.046102	0.025453	0.520947	4.148147	45.28	73.73	50.00	26.81	11000	13.121
0.300	0.095	0.044300	0.025357	0.625608	2.391497	52.41	79.51	42.00	32.18	11000	13.071

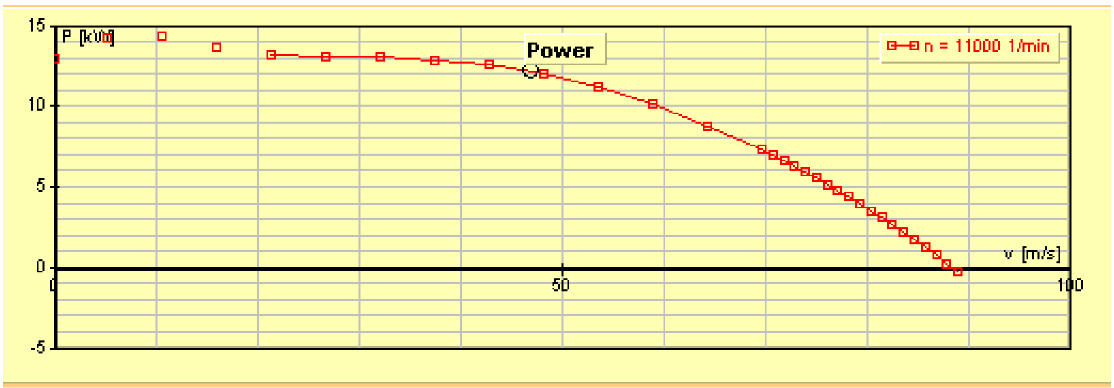

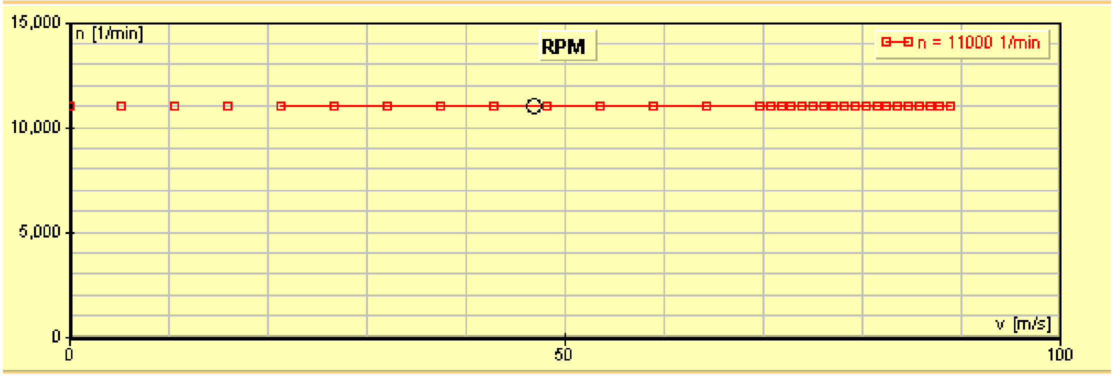
15,000
n [1/min]
RPM
n = 11000 1/min
10,000
5,000
0
v [m/s]
0
50
100

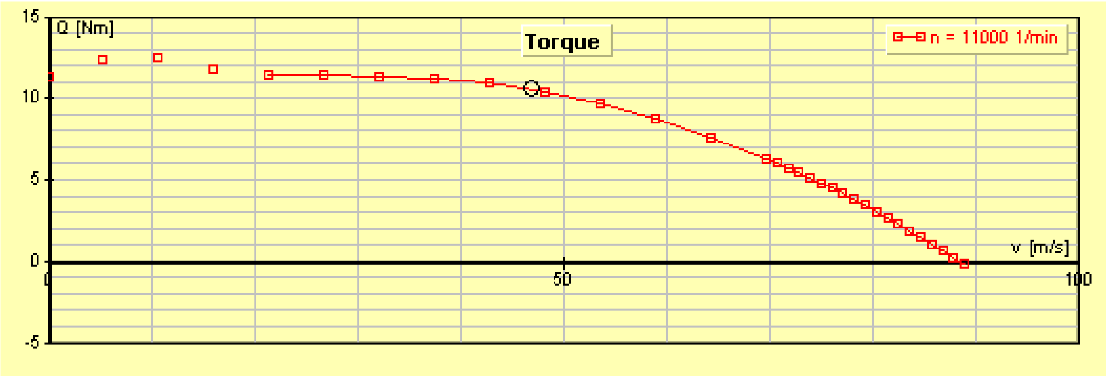
15
Q [Nm]
Torque
n = 11000 1/min
10
5
0
v [m/s]
0
50
100
-5

- The Single-Analysis card shows detailed results for a single operating condition. The first set of graphs contains parameters related to airfoil section aerodynamics.

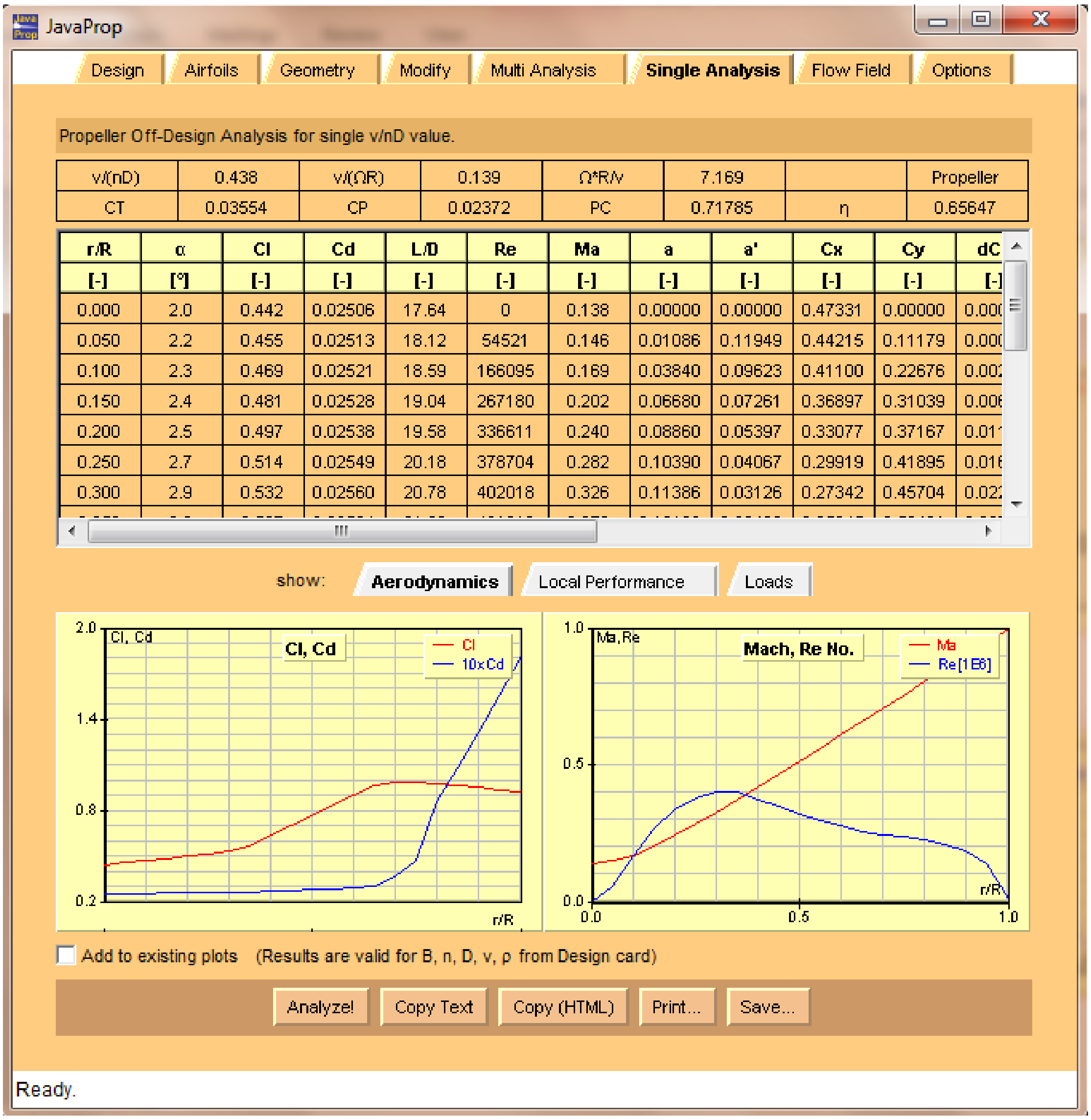

- The second set of graphs contains local power and thrust coefficients as well as the local efficiency.

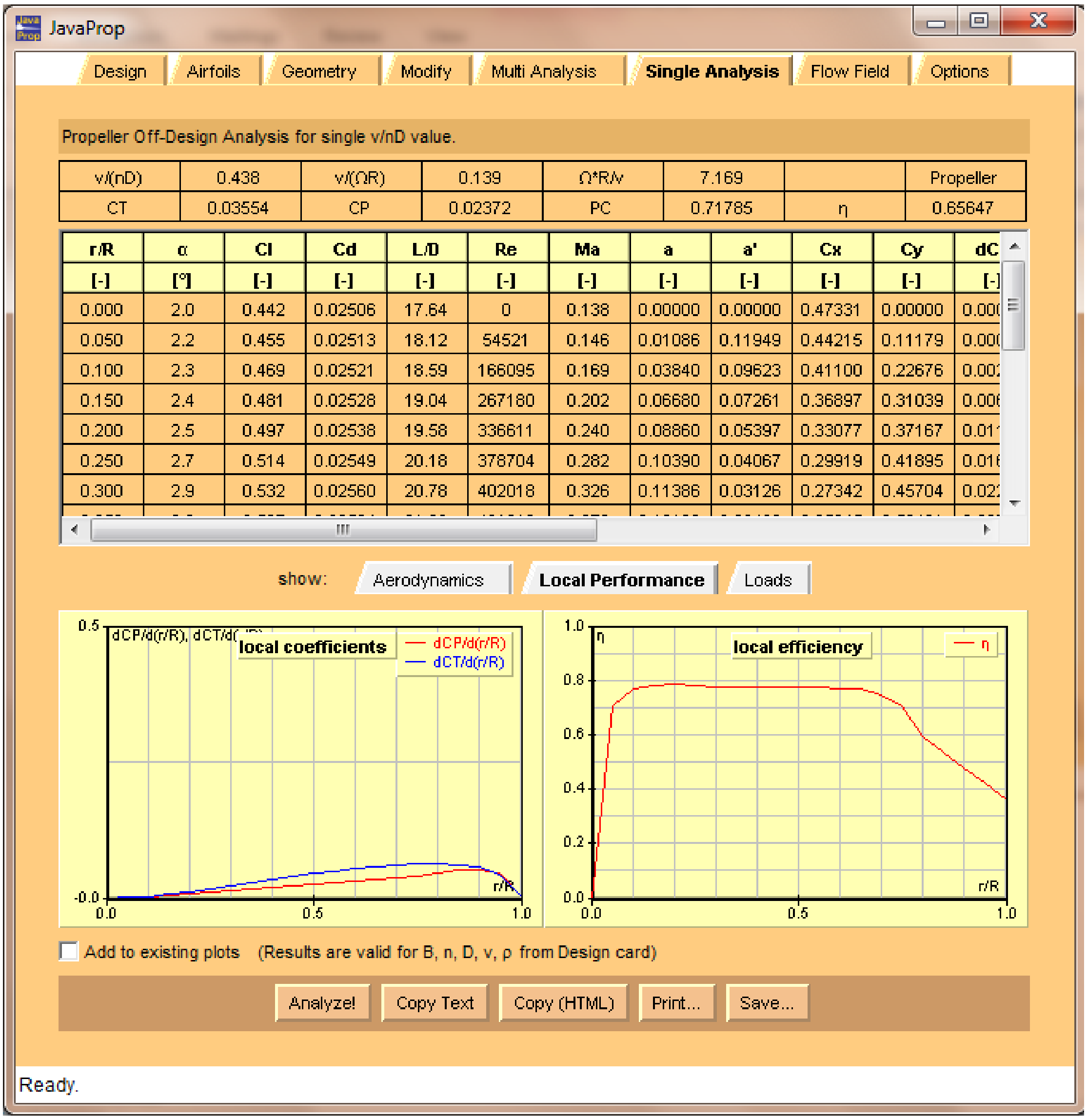

- The third set of graphs shows shear force and bending moment.

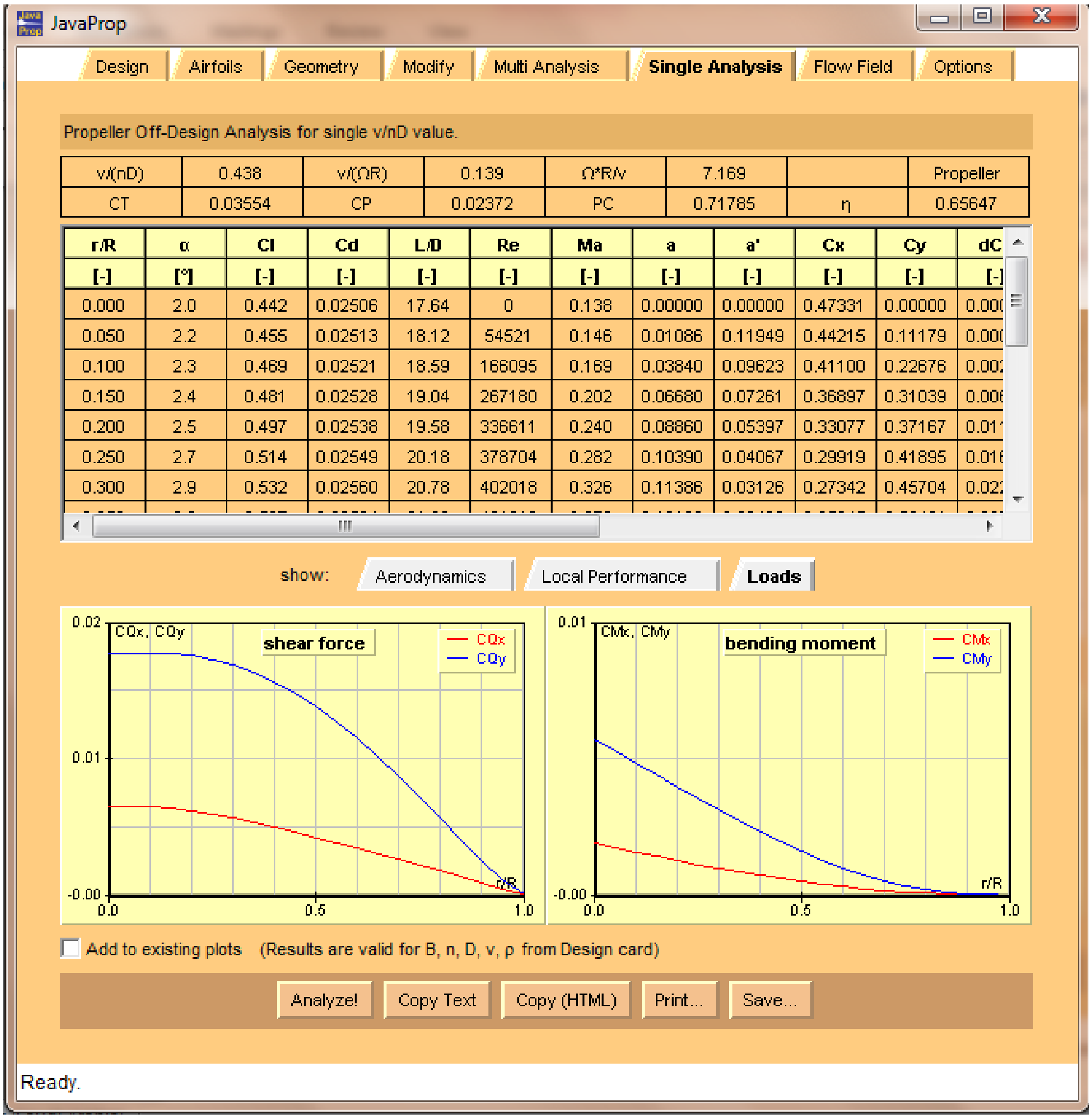

- The third set of graphs shows shear force and bending moment

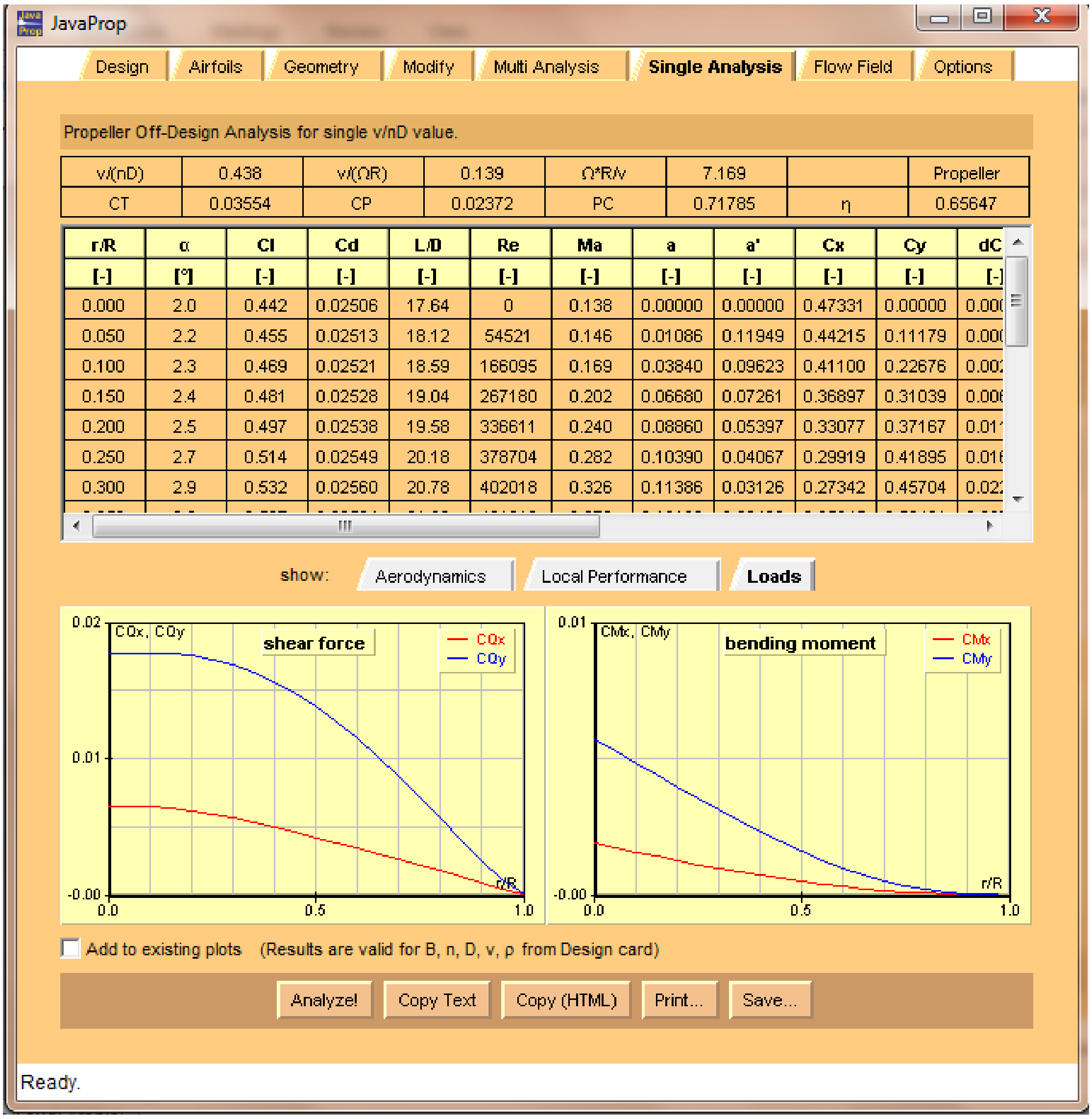

- Flow field

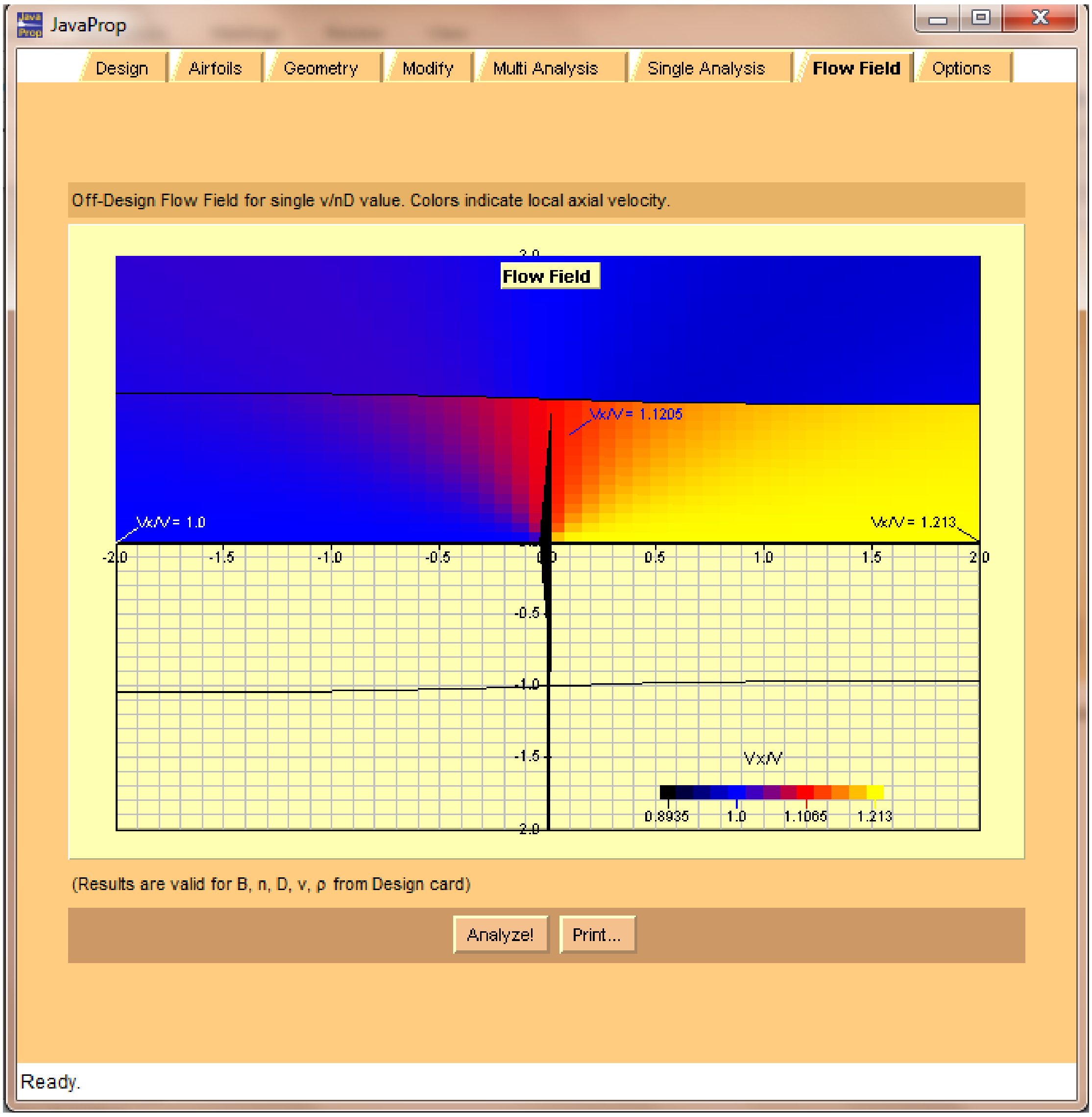

JavaProp
Design
Airfoils
Geometry
Modify
Multi Analysis
Single Analysis
Flow Field
Options
Off-Design Flow Field for single v/nD value. Colors indicate local axial velocity.
Flow Field
Vx/V = 1.1205
Vx/V = 1.0
Vx/V = 1.213
Vx/V
0.8935
1.0
1.1065
1.213
(Results are valid for B, n, D, v, ρ from Design card)
Analyze!
Print...
Ready.

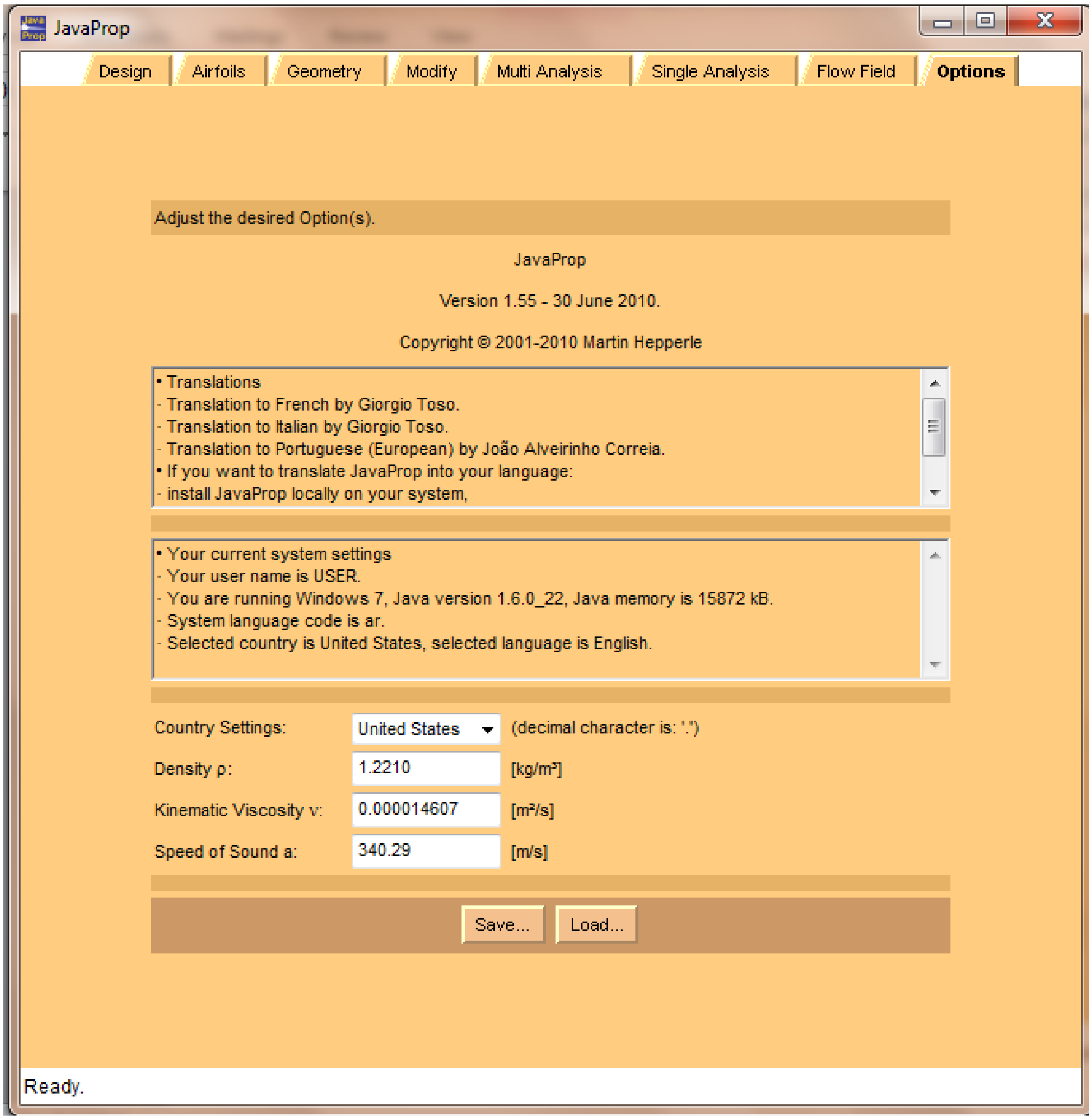
JavaProp
Design
Airfoils
Geometry
Modify
Multi Analysis
Single Analysis
Flow Field
Options
Adjust the desired Option(s).
JavaProp
Version 1.55 - 30 June 2010.
Copyright © 2001-2010 Martin Hepperle
• Translations
· Translation to French by Giorgio Toso.
· Translation to Italian by Giorgio Toso.
· Translation to Portuguese (European) by João Alveirinho Correia.
• If you want to translate JavaProp into your language:
· install JavaProp locally on your system,
• Your current system settings
· Your user name is USER.
· You are running Windows 7, Java version 1.6.0_22, Java memory is 15872 kB.
· System language code is ar.
· Selected country is United States, selected language is English.
Country Settings:
United States
(decimal character is: '.')
Density ρ:
1.2210
[kg/m³]
Kinematic Viscosity ν:
0.000014607
[m²/s]
Speed of Sound a:
340.29
[m/s]
Save...
Load...
Ready.

APPENDIX O: UAV WEIGHT AND BALANCE

One of the primary concerns during the aircraft design process, even during the conceptual design phase, is the aircraft weight distribution. The distribution of aircraft weight (sometimes referred to as weight and balance) will greatly influence airworthiness as well as aircraft performance. The distribution of aircraft weight will influence the airworthiness and performance via two aircraft parameters: (i) aircraft center of gravity (cg) and (ii) aircraft mass moment of inertia.

Weight Distribution

Aircraft weights are usually divided into two categories; internal weight (payload, control, engine, fuel tank…) and external weight (wing weight, tail boom and tails).the position of this weight must be derived with considering achieving acceptable C.G location.by taking this into account and by carful looking at the trends the following weight distribution is found:

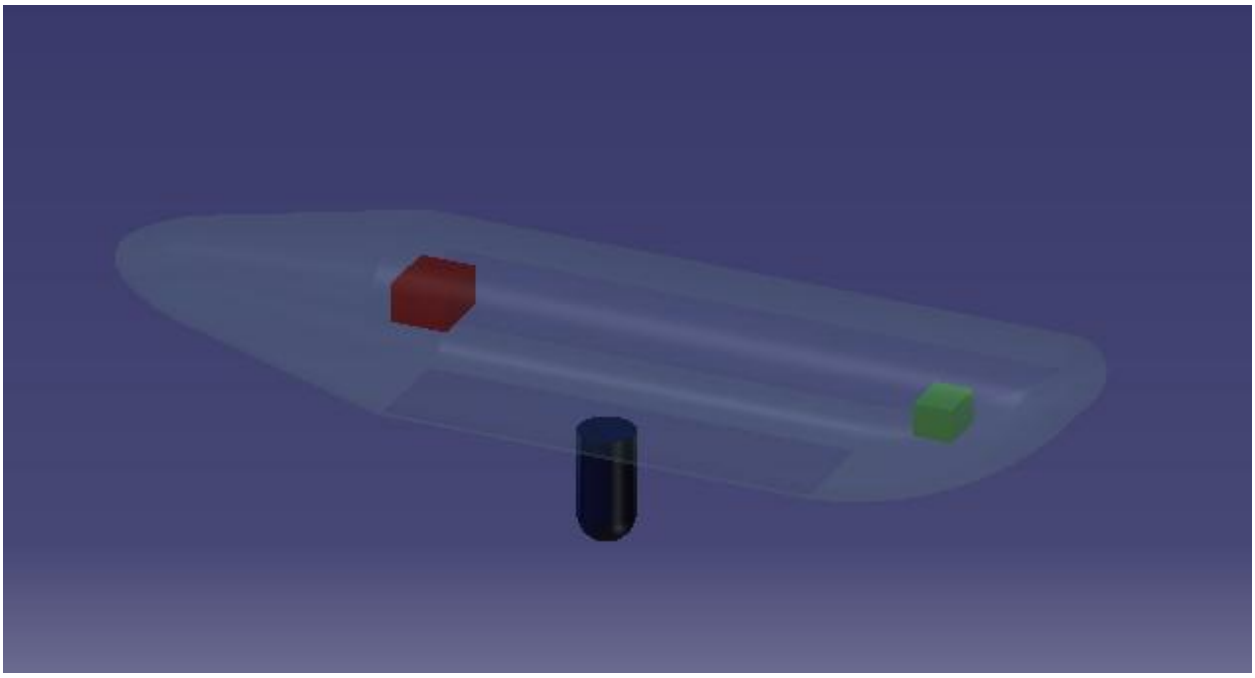

Second C.G estimation

The C.G position affects UAV stability, controllability and performance. The position of C.G determined with assumption that's the C.G is fixed, latter in this chapter a Longitudinal C.G rang will be determined.

The following formula used to calculate C.G location (saddrey) :

$$X_{cg} = \frac{W_w * X_w + W_{ht} * X_{ht} + W_{vt} * X_{vt} + W_f * X_f + W_p * X_p + W_e * X_e + W_{fuel} * X_{fuel}}{W_w + W_{ht} + W_{vt} + W_p + W_e + W_{fuel}}$$

And the table below shows the result of weight distribution, C.G and inertia estimation.

component	w	Xcgi	Xcgi-Xcg	Ycgi-Ycg	Zcgi-Zcg			
fuselage	33.6	2.9	-1.1704	0	0	0	46.02641	46.0
wing	37.02032	4.028563	-0.04184	0.243456	0.389218	7.802457	5.673018	2.25
payload	33.1	3.123	-0.9474	0	0	0	29.70939	29.7
engine	12.593	5.7	1.629601	0	0	0	33.44197	33.4
vertical	6.195549	10	5.929601	1.977667	0.389218	25.1704	218.7751	242
hori	4.153453	10	5.929601	0	0.389218	0.629208	146.6653	146
boom	2.896	6.4	2.329601	1.977667	0.389218	11.76546	16.15543	27.0
fuel	11.77263	5.411	1.340601	0	0	0	21.1579	21.
avionix	16.76535	2	-2.0704	0	0	0	71.86554	71.8
N L.G	3.185417	1.8	-2.2704	-1.1979	-1.3294	10.20056	22.0495	20.9
M L.G	6.370833	4.56	0.489601	1.2188	-1.3294	20.7229	12.78635	10.9

Moment of inertia calculation

Aircraft controllability and maneuverability is a function of several factors, including aircraft mass moment of inertia. In contrast, the weight distribution will greatly influence the aircraft mass moment of inertia.

The mass moment of inertia provides information on how easy or difficult it is (how much inertia there is) to rotate an object around a given axis. The mass moment of inertia is one measure of the distribution of the mass of an object relative to a given axis.

Since an aircraft has three rotational axes, namely x, y, and z, there are generally three moments of inertia. Weight distribution along the x-axis affects the mass moment of inertia about the y-and z-axes, and consequently influences the aircraft pitch (longitudinal) and yaw (directional) control. Weight distribution along the y-axis affects the mass moment of inertia about the x-and z-axes, and consequently influences the aircraft roll (lateral) and yaw (directional) control. Weight distribution along the z-axis affects the mass moment of inertia about the x-and z-axes, and consequently influences the aircraft pitch (longitudinal) and roll (lateral) control.

Longitudinal C.G Range:

The aircraft longitudinal cg range is defined as the distance between the most forward and the most aft cg locations. The aircraft center of gravity is a function of two major elements: (i) center of gravity of aircraft components such as wing, fuselage, tail, fuel, engine, etc. and (ii) rate of change of location of movable or removable components.